This is to certify that the

dissertation entitled

New Approaches to Highly Sterically
Encumbered Porphyrins as Heme Active Sites

presented by

Chen-Yu Yeh

has been accepted towards fulfillment
of the requirements for

Ph.D. degree in Chemistry

Chi-Chang
Major professor

Date Sep 14, 1999

DATE DUE	DATE DUE	DATE DUE

NEW APPROACHES TO HIGHLY STERICALLY ENCUMBERED PORPHYRINS AS HEME ACTIVE SITES

By

Chen-Yu Yeh

A DISSERTATION

Submitted to
Michigan State University
in partial fulfillment of the requirements
for the degree of

DOCTOR OF PHILOSOPHY

Department of Chemistry

1999

ABSTRACT

NEW APPROACHES TO HIGHLY STERICALLY ENCUMBERED PORPHYRINS AS ACTIVE SITES

By

Chen-Yu Yeh

A series of highly hindered β-substituted bis-pocket porphyrins in which both sides of the porphyrin plane are protected to provide a nonpolar environment have been synthesized. The iron(II) complexes of these porphyrins are capable of binding dioxygen irreversibly at room temperature, indicating that the hindered substituents can prevent the irreversible oxidation of the coordination site via the formation of the μ-oxo dimer. Compared to other model porphyrins, the decreased O_2 affinities of our system are ascribed to the nonpolar nature of the binding sites. This can be confirmed by the observation that increasing the polarity of solvents increases the O_2 affinity. The results are consistent with the fact that in hemoproteins, the polar environments about the active site can stabilize the oxygenated adduct and result in a higher O_2 affinity. We have also observed that the polarity of the pockets has little effect on CO binding.

The manganese complexes of these sterically hindered bis-pocket porphyrins have also been used as catalysts for shape selective epoxidation of alkenes. The sizes of the substituents at the periphery of porphyrins are responsible for the shape selectivity. The high selectivity of our system is ascribed to increased steric crowding on both face and side ways of the porphyrins. The porphyrin with intramolecular hydrogen bonding shows the highest shape-selectivity since the top way is blocked and the opening of the side way is constrained. In our system, the steric protection of the active site by the substituents at

β-positions also increases the stability of catalysts during the oxidation reactions.

The β-substituted zinc porphyrins show shape-selectivity on ligation with various amines having different sizes and shapes. The hydrophobic pockets of the porphyrins can stabilize the bound ligand, thus showing higher binding constants than Zn(TPP). The size of the pocket of the porphyrin reflects on the selectivity on ligation to small and bulky ligands. In addition to the size of the pocket, some other attractive interactions such as π-π stacking also play an important role on the shape selectivity of ligation.

A new highly steric β-substituted water-soluble porphyrin has also been synthesized. The spectophotometric data of the iron(III) complex support the absence of μ-oxo dimeric species in the whole range of pH due to the added steric hindered substituents at β-positions. The pKa of the iron complex was estimated to be 8.11 which is the highest of the sulfonated iron porphyrins due to the electron-donating nature of the substituents at β-positions. It is unlikely that the ligated water molecule on the iron center can be replaced by anions such as SO_4^{2-}, NO_2^-, ClO_4^-, and PO_4^{3-}. However, the ligated water molecule can be replaced by neutral ligands such as imidazole and nitric oxide. These coordination studies demonstrated that the hydrophobic pockets prohibited the coordination of anionic ligands.

The syntheis of fully substituted xanthene-bridged chiral porphyrins and their circular dichroism profiles have also been described. The (R) and (S) enantiomers of this series of chiral porphyrins, exhibit a positive and negative split Cotton effect at longer wavelengths in the Soret region, respectively. The CD spectra of the (R) and (S) forms are perfect mirror images of each other. Based on the CD spectra and the X-ray crystal structure, the conformations of this series of single armed fully substituted porphyrins can be assigned and the conformation-circular dichroism relationship can be established.

This thesis is dedicated to my family for their support, patience, and love.

ACKNOWLEDGMENTS

I would like to thank Dr. Chi K. Chang for his help, and advice during the course of my graduate work. I would also like to thank Drs. Gregory L. Baker, Rawle I. Hollingsworth, and Joan B. Broderick for serving on my guidance committee.

I am also thankful to Dr. Shi M. Peng, Dr. Sheung S. Chern, and Baixin Qian for their help in obtaining X-ray crystal structures. Dr. Yu Oliver Su's helpful advice on electrochemistry is also appreciated. Dr. Chang's students in Hong Kong and Dr. Suslick's group are also acknowledged for the performing catalytic epoxidation experiments. Thanks also go out to Dr. Eugene LeGoff for providing me with lab space, and Dr. Muraleedharan Nair for allowing me to use his CD spectropolarimeter.

I would also like to thank the members of Dr. Chang's group. I give special thanks to Craig M. Shiner, Yongqi Deng, Ying Liang, Baoming Guo, and Nilkamal Bag for their friendship and helpful discussion. In addition, I would like to acknowledge my friends: Kuei-Ho Hsieh, Ya-Szu Lin, Jian-Yang Cho, Yu-Shang Lu, Shin-Yi Huang, Shu-Wen Yang, Shu-Ting Yang and many others for their friendship throughout these years. Words are not enough to express how grateful I am to them. I am equally thankful to my friends across the Pacific that have been in my heart.

Last, but by no means least, I want to thank my family. Without them, all of this would have never been possible. Special appreciation goes to my mother for her priceless love.

TABLE OF CONTENTS

LIST OF TABLES

LIST OF FIGURES

Chapter 1

INTRODUCTION

Oxygen Binding

Most creatures require molecular oxygen in order to survive. For some small animals and for plants, where the surface-to-volume ratio is large, simple diffusion can provide a sufficient amount of dioxygen to the interior cells. For other organisms, diffusion does not supply sufficient dioxygen for respiration. In order to facilitate dioxygen transport, a delicate system has evolved to transport dioxygen from regions of high abundance to those of relatively low abundance and high need. The key component is a dioxygen carrier protein. In invertebrates the dioxygen carrier is either a copper-containing protein, hemocyanin,[1] or a iron-containing protein, hemerythrin.[2] In most organisms the most widely distributed family of dioxygen carriers are hemoglobins.[3,4] In many organisms an additional dioxygen-binding protein which stores dioxygen has been found. For the hemoglobin family the dioxygen storage protein is called myoglobin. Myoglobin (Mb), is a relatively simple protein found primarily in the muscles of vertebrates, especially in the muscles of aquatic diving mammals such as seals, porpoises and whales which must store dioxygen for relatively long periods. The first X-ray crystal structure of myoglobin obtained from a sperm whale, was reported by Kendrew.[5] Myoglobin has two components, the heme cofactor which is an iron protoporphyrinate IX complex and the protein with about 150 amino acid residues. The protein consists of eight α-helices labeled A through H and six interhelix bends identified by double letters of the helices that they connect. The remarkable feature of the myoglobin structure is that the protein forms a pocket for the heme. The heme is completely surrounded by protein and held in position by a large number of nonpolar and hydrogen-bonding interactions at its periphery except for the edge that contains two

propionic acid side groups, which are positioned out of the pocket into the surrounding water. Both ferric and ferrous irons generally prefer to be coordinated by six ligands. In myoglobin, four ligands are provided by a square-planar tetradentate ligand, the protoporphyrin IX dianion, and one ligand comes from the imidazole group of the proximal histidine residue (Figure 1-1). The sixth position is a binding site for an exogenous ligand, e.g., dioxygen or carbon monoxide. Near the sixth coordination site of the iron center, the distal amino acid residues are responsible for controlling the binding environment. They can induce dipole-dipole, hydrogen-bonding, or steric interactions which help regulate the affinities of the binding ligands. If the heme cofactor is isolated from the protein and exposed to oxygen, the iron(II) is irreversibly oxidized to its iron(III) complex and it does not bind dioxygen.[6,7]

The dioxygen binding to myoglobin shows a simple equilibrium with 1:1 association between the heme and dioxygen.

$$Mb + O_2 = MbO_2 \qquad K=[MbO_2]/[Mb][O_2] \tag{1-1}$$

This is often expressed in terms of the fraction of the heme oxygenated.

$$y = [MbO_2]/([Mb] + [MbO_2]) \tag{1-2}$$

then

$$\ln (y/1-y) = \ln KO_2 + \ln PO_2 \tag{1-3}$$

The above expression is known as the Hill equation. The equilibrium constants can be determined by Hill plots.

It is very convenient to express the equilibrium constant with the dioxygen partial pressure ($P_{1/2}$) at which half-saturation occurs. Under such a condition, we obtain $P_{1/2} = K^{-1}$. In general, the $P_{1/2}$ for myoglobin is about 1 torr.[8]

Hemoglobin, which is a protein in the blood cells, transports dioxygen from the lungs to the tissues and assists the transport of carbon dioxide from the tissues back to the lungs where the CO_2 is exhaled. Among all the heme proteins, hemoglobin has been the most intensive studied system and has played a very important role in the history of

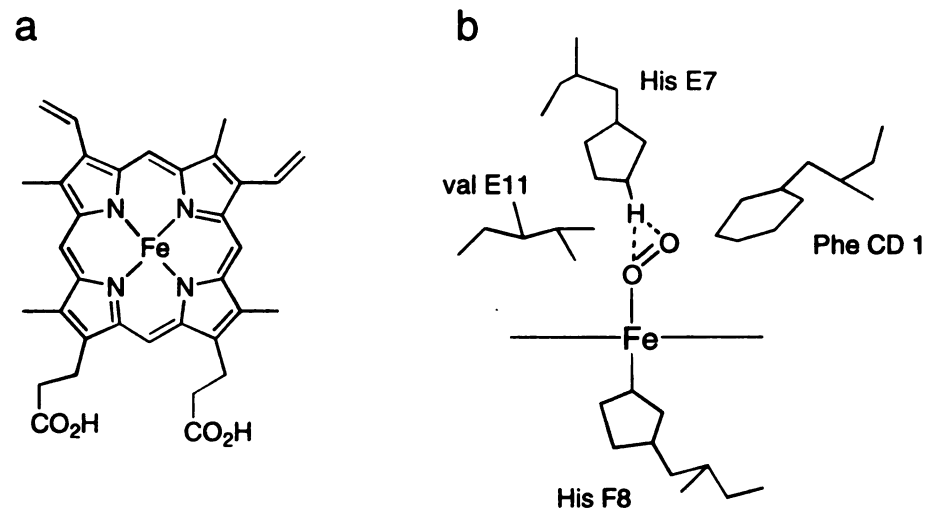

Figure 1-1. (a) Iron Protoporphyrinate IX; (b) Heme and its environment.

protein research. It was one of the first proteins to be purified and its molecular weight determined accurately, the first protein to be crystallized, the first to have its amino acid sequences determined, the first protein whose specific physiological function was known, and the first associated with genetic disease.[9]

Human hemoglobin is a tetramer made up of two identical chains labeled α, with 141 amino acid residues of 15126 dalton each, and two identical β chains with 146 residues (15867 dalton each). The α-chains have seven and the β-chains eight helices, interrupted by nonhelical segments. The packing of the chains in the hemoglobin molecule is close; interlocking contact of the chains exists between subunits α and β, but there is only a little contact between the same chains α and α, or β and β. Each of these subunits has one heme group responsible for binding one molecule of dioxygen. On the exterior of the molecule, the polar side chains are exposed to aqueous surroundings, but nonpolar side chains are buried in contact with each other and form nonpolar hydrophobic environments for the heme groups. The proximal histidine bound to the heme iron is tilted about 10° away from being perpendicular to the heme plane. The sixth position is empty in deoxyhemoglobin or has a dioxygen molecule attached in oxyhemoglobin. On the distal side around the sixth coordinate site, there is another histidine which is in van der Waals contact with the porphyrin. Recent studies on the X-ray structure of oxyhemoglobin show that the distal histidine provides strong hydrogen bonding with the dioxygen. In the deoxy form, the iron atom of each heme is five-coordinated and in a high-spin Fe(II) state and lies about 0.5 Å out of the mean plane of the porphyrin nitrogens and carbons. This out-of-plane iron atom in a domed porphyrin ring is in an unfavorable position for dioxygen binding on the opposite side of the heme plane. Upon dioxygen binding, the oxygenated heme has a low-spin six-coordinate state, the iron atom moves toward the porphyrin plane, and dioxygen binds to the heme in an end-on bent-bond fashion. Furthermore, the histidine bound to the iron atom straightens and the off-axis tilt is reduced.

Unlike myoglobin, hemoglobin has four dioxygen binding sites. The binding of dioxygen to myoglobin and to isolated α or β monomeric subunits has similar behavior. However, the dioxygen binding to the tetrameric hemoglobin molecule is much more complicated. The active sites in hemoglobin do not function independently. Instead, the four subunits operate in a cooperative manner. The interactions between the subunits are known as allosteric properties and are physiologically important. Based on X-ray structural data of deoxy and oxy forms of hemoglobin, Perutz[3,10] proposed a stereochemical mechanism for the cooperative interactions on the basis of the two-state allosteric model proposed by Monod et al.[11] In this model, two quarternary structures are in equilibrium with each other during the ligation process. These two structures are T (tense) and R (relaxed) states as shown in Figure 1-2, corresponding to those found in oxygenated and deoxygenated molecules, respectively. These two states differ both in the tertiary structure of each subunit and the quarternary structure between the subunits in the tetramer. The structural difference between T and R states is reflected in the dioxygen binding affinities of hemoglobin. The dioxygen binding affinities of these two categories are quite different. The $P_{1/2}$ for the T state (low affinity) is much larger than that of isolated, monomeric subunits or simple myoglobin whereas the $P_{1/2}$ for the R state (high affinity) is slightly smaller. The greater stability of the T state relative to the R state in the absence of dioxygen is because of larger contact area and the presence of more salt bridges and hydrogen bonds between the dimers in the T form. On going from deoxy to oxy hemoglobin, strain is produced and this strain is transmitted to the salt bridges and hydrogen bonds. Consequently, this strain alters the heme environments, heme positions, electrostatic interactions, nonpolar interactions and hydrogen bonding between the subunits inducing tertiary structure changes in other subunits. The intrinsic cooperative interaction is homotropic (not dependent on other effectors) and is fundamental to efficient dioxygen transport.

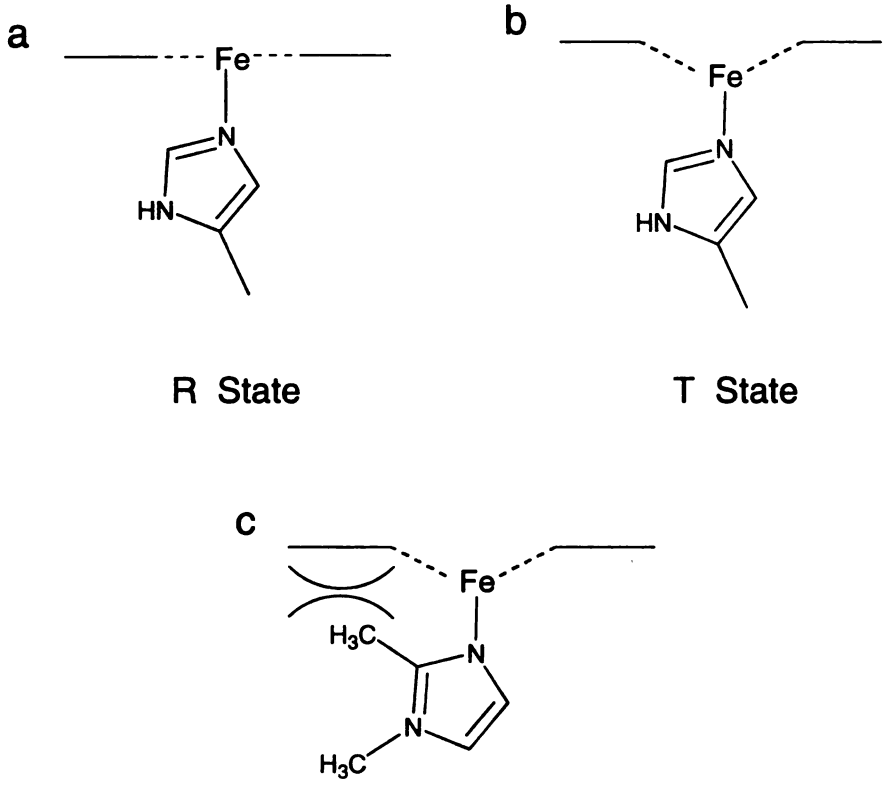

Figure 1-2. (a) R state; (b) T state; (c) Model to mimic T state of the active site in hemoglobin.

Similar to myoglobin, the O_2 affinity constants can also be determined by Hill plots.

$$K=[Hb(O_2)_n]/[Hb][O_2]^n \quad (1\text{-}4)$$

This can also be expressed in terms of the fraction of the heme oxygenated.

$$y = [Hb(O_2)_n]/([Hb] + [Hb(O_2)_n]) \quad (1\text{-}5)$$

then

$$\ln (y/1\text{-}y) = \ln KO_2 + n \ln PO_2 \quad (1\text{-}6)$$

Where n is the cooperative parameter. The Hill plot for Hb shows an indication of an interaction between the subunits. At intermediate pressures of O_2, n is observed to be about 3 rather than 1 as for myoglobin.

The first heme in hemoglobin binds dioxygen poorer than myoglobin and isolated α and β subunits. However, the last heme has a slightly higher dioxygen affinity than myoglobin or isolated hemoglobin subunits. Hence the hemoglobin tetramer functions by decreasing the binding tendency of the first heme, but not by increasing the binding of the last dioxygen. The high pressure in lungs ensures the full saturation of hemoglobin tetramer. When a fully oxygenated hemoglobin molecule (R state) arrives at the tissues, its tendency to bind or lose the first dioxygen is about the same as that of myoglobin. Once the first dioxygen is transferred to myoglobin, the remaining ones are more easily lost. This guarantees complete transfer of dioxygen to the tissues. Hemoglobin is also able to regulate the efficiency of dioxygen transport to give large amounts of dioxygen to some organs and small amounts to others as needed. This capacity is achieved by heterotropic interactions between hemolglobin and effectors. Among these effectors which influence the dioxygen affinity curve is the pH. The deoxyhemoglobin has a higher affinity for protons than does oxyhemoglobin. Hence, under acidic conditions the equilibrium between deoxy- and oxyhemoglobin is shifted in favor of deoxyhemoglobin. This is the Bohr effect, and is physiologically important since hemoglobin can release dioxyen to muscle when its acidity indicates that dioxygen is most needed. Three other

naturally occurring substances are known to stabilize the deoxyhemoglobin over the oxyhemoglobin by preferentially interacting with the T state. These are carbon dioxide, chloride ions, and 2,3-diphosphoglycerate (DPG) because each binds to deoxyhemoglobin better than to oxyhemoglobin. For example, in the T state, DPG can enter the cavity between the two β subunits which contains some positively charged groups and is able to bind DPG with a number of salt bridges. In the R state, however, the cavity is closed and the binding with DPG is impossible. Carbon dioxide influences the dioxygen affinity in two ways. It can bind to the amino group at the beginning of each subunit and forms carbamates ($-NH_2 + CO_2 \rightarrow -NH-CO_2^- + H^+$). When the hemoglobin is reoxgenated at the lungs, it releases protons. These protons shift the equilibrium to the left, converting bicarbonate ions to the less soluble CO_2 which is exhaled. In addition, when carbon dioxide dissolves in water, it produces bicarbonates and protons. The protons are picked up by deoxyhemoglobin and bicarbonate ions are carried back to the lungs as the counterions.

The microenvironment of the heme which controls the ligand binding is a fascinating research topic. Dioxygen affinities ($P_{1/2}$ of dioxygen binding) of various hemoproteins at room temperature may range from 0.002 torr for Ascaris hemoglobin to 2.5 torr for Aplysia hemoglobin.[12,13] Furthermore, the presence of carbon monoxide, an intrinsicly toxic ligand produced when one molecule of heme is catabolized by heme oxygenase, complicates dioxygen transport and storage.[14] The heme proteins are capable of discriminating between dioxygen and carbon monoxide. The relative CO/O_2 affinity is described by "M" (partition coefficient). The M values in hemoproteins range from 6000 for glycera Hb, to 20-40 for Mb, to 0.02 for Ascaris Hb, and are thought to be related to the nature of the Fe-CO geometry regulated by protein residues.[15,16] The assessment of the factors is frequently difficult in the protein system. The studies of model compounds which are structurally and functionally similar to the active sites of the metallproteins can provide a detailed understanding of the structure and function of the

active site which can not be obtained by studying the protein itself. Thus a model compound similar to the active sites in hemoglobin can be assembled from an iron porphyrin and a ligand. In the past three decades numerous model compounds have been synthesized to mimic the functions of hemoproteins and elucidate the factors which influence the dioxygen affinities. One of requirements for the synthetic model compounds is their ability to bind oxygen reversibly. However, unhindered ferrous hemes are oxidized rapidly and irreversibly in the presence of oxygen. Two general autoxidation pathways have been proposed: (1) μ–oxo dimer formation and (2) H^+ (H_2O) catalyzed autoxidation.

$$Fe^{II}(O_2)(P)(B) + Fe^{II}(P)(B) \rightarrow\rightarrow (B)(P)Fe^{III}OFe^{III}(P)(B) \quad (1\text{-}7)$$

$$Fe^{II}(O_2)(P)(B) + H^+ \rightarrow Fe^{III}(P)(B) + HO_2^- \quad (1\text{-}8)$$

Where P is porphyrin dianion and B the axial ligand. In order to thwart μ–oxo dimer formation that leads to irreversible oxidation, the approaches which have been employed successfully are low-temperature stabilization,[17] immobilization of porphyrins into polymers,[18,19] and construction of heme models with sterically hindered substituents.[20-22]

It has been known that the iron-dioxygen complexes are relatively stable at low temperature. Chang and Traylor[17] reported the reversible oxygenation of a chelated Fe(II) porphyrin in which an imidazole is covalently attached to a pyrrolic position. The $P_{1/2}$ was estimated to be 0.2 torr in dichloromethane solution at –45 °C. A similar system with a covalently linked pyridine showed rapid oxidation at –45 °C. After the report by Chang and Traylor, many papers described the reactions of dioxygen with flat hemes and chelated hemes.[23-26] In the presence of axial ligands such as alkyl imidazoles, pyridine, simple amine-type ligands, and DMF, these systems can reversibly bind dioxygen at temperatures below –45 °C. In summary, imidazole appears to be the best ligand and dioxygen affinities are higher in solvents of high dielectric constant.

In hemoproteins, globins provide hydrophobic environments to prevent the active sites from irreversible oxidation and suppress proton-driven oxidation in the presence of dioxygen. Synthetic polymers can fill the roles of proteins. Wang was the first to report a polymer-encapsulated heme system in which dioxygen binds to the heme reversibly.[27] The results suggested that the hydrophobic environments provided by polystyrene matrix excluded water molecules and the isolation of the hemes from each other prevented the oxidation by dimerization. Chang and Traylor reported a similar system in which a porphyrin with a built-in imidazole was embedded in a polystyrene film.[28] A reversible oxygenation was observed by spectrophotometry.

Oxygen-binding to the iron(II) porphyrin attached to a modified silica gel was also reported.[29] In this system, an imidazole group was covalently linked on the surface of silica gel and Fe(II)TPP was coordinated to the imidazole. The active sites are capable of binding molecular oxygen reversibly. The spectrum of the oxygen adduct of a water soluble complex of poly(1-vinyl-2-methylimidazole) (PMI) and protoporphinatoiron IX agreed with that of oxyheme when its aqueous solution was exposed to oxygen at –10 °C to –30 °C. The oxyheme returned to the deoxyheme upon flushing the solution with nitrogen, and the oxy-deoxy cycle was repeated several times at low temperature. The results suggest that the water soluble but hydrophobic polymer created a hydrophobic environments for oxygen-binding to the five-coordinate protoheme complex in cold aqueous media and the proton-driven irreversible oxidation was suppressed.

Another class of stable heme complexes is when the heme itself is attached to a polymer. Fuhrhop was the first to employ this approach.[30] He incorporated the vinyl side chains of iron protoporphyrin IX dimethyl ester into the back-bone of a polymer. The solid polymers with <10% imidazole reacted with dioxygen reversibly. In solution the heme was oxidized by oxygen rapidly. A similar approach was taken by Tsuchida. A picket-fence iron porphyrin was covalently bound to the central hydrophobic block of a triblock copolymer: poly(ethylene oxide)/polystyrene/poly(ethylene oxide). This system

showed reversible oxygenation at room temperature and the half-life of the oxygen adduct was estimated to be half a day, although the oxygen association and dissociation occurred slowly. This is the first report that dioxygen binds to the heme reversibly in aqueous solution at room temperature. The use of *meso*-tetraphenylporphyrin (TPP) derivatives, however, resulted in somewhat different spectral features from that of protoporphyrin IX. However, the use of biological porphyrin (e.g. protoporphyrin IX) often leads to irreversible oxidation due to a π-π stacked aggregate which induces an unfavorable electron transfer. Tsuchida has recently reported the reversible oxygenation of a lipid/protoporphyrin having three long alkyl chains and an axial imidazole embeded into the bilayer membrane of the phospholipid vesicle.[31] He also found that the oxygen-binding affinity was affected by the phase transition of the membrane.[19 32] The oxygen-binding affinity is higher below the gel-(liguid crystal) phase transition temperature (Tc) of the bilayer membrane and lower above the Tc. That is, the T- and R-states of hemoglobin were mimicked by the phase transition behavior of the phospholipid vesicle.

In order to inhibit the irreversible oxidation of iron(II) porphyrins via dimerization, many steric hindered porphyrins have been constructed. Modified porphyrins for modeling hemoproteins can be divided into two categories: systems in which one face of the porphyrin is protected by sterically hindered groups (Figure 1-3), and systems in which both faces of the porphyrin are protected by sterically hindered groups (Figure 1-4). The first attempted synthesis of a single-face-hindered porphyrin, in which one face of the porphyrin was protected by a cyclophane strap, was reported by Traylor.[33] However, this porphyrin was prepared in very poor yield and no chemical studies were reported. The earliest successful iron porphyrin model for Hb and Mb active sites was reported by Collman.[34,35] He described the reversible dioxygen-binding of a "picket-fence" model compound having four pivalamido groups on one side of porphyrin plane and leaving the other side unencumbered for axial ligand coordination. The four bulky groups provide a hydrophobic pocket for complexation of dioxygen. In the presence of

excess axial ligand, the oxygenation-deoxygenation was repeated several times at room temperature without appreciable decomposition.

In order to mimic the T state of hemoglobin, the sterically hindered axial ligand, 1,2-dimethylimidazole was employed.[22] In the presence of 1,2-Me_2Im, the 5-coordinate complex was formed and the iron(II) was pulled out of porphyrin plane due to the steric interactions of methyl group and the π electrons on porphyrin ring (Figure 1-2). It is interesting that the use of this hindered imidazole can effectively reduce the oxygen affinity to the level found in T-state Hb. After the picket fence porphyrin, a series of tailed picket fence porphyrins were prepared.[36-38] In this system, the axial ligand, either imidazole or pyridine was built into the porphyrin. In addition to the picket fence model compounds, many types of sterically protected model systems have been synthesized and their binding properties have also been reported. These include strapped,[39,40] capped,[41,42] pocket,[16,43] picnic basket,[36,44] crowned,[45] and cofacial porphyrins[21] as well as hybrids[46] of these classifications. Some examples are shown in Figure 1-3. Most of the model compounds can bind dioxygen reversibly in aprotic organic solvents at room temperature in the presence of a high concentration of the axial ligand. However, in the absence or at low concentrations of the axial ligand, the iron center oxidizes irreversibly via the formation of μ-oxo dimer from the unprotected side.

Another attempt to prevent μ-oxo dimer formation is to introduce sterically encumbered groups to both sides of the heme. Figure 1-4 shows some of double-sided porphyrins with or without built-in nitrogenous base. The "bis-pocket",[47] "bis-fenced",[48] "basket-handle",[49,50] and "doubly-bridged"[51] porphyrins are suitable model compounds for dioxygen binding. The stability of the oxyhemes to oxidation is related to the degree of steric hindrance.

By studying the O_2 binding to hemoproteins and iron(II) porphyrin synthetic model compounds, it has been shown that the heme reactivity is governed by the microenvironment near the active sites. As noted, the $P_{1/2}$ of dioxygen binding and the

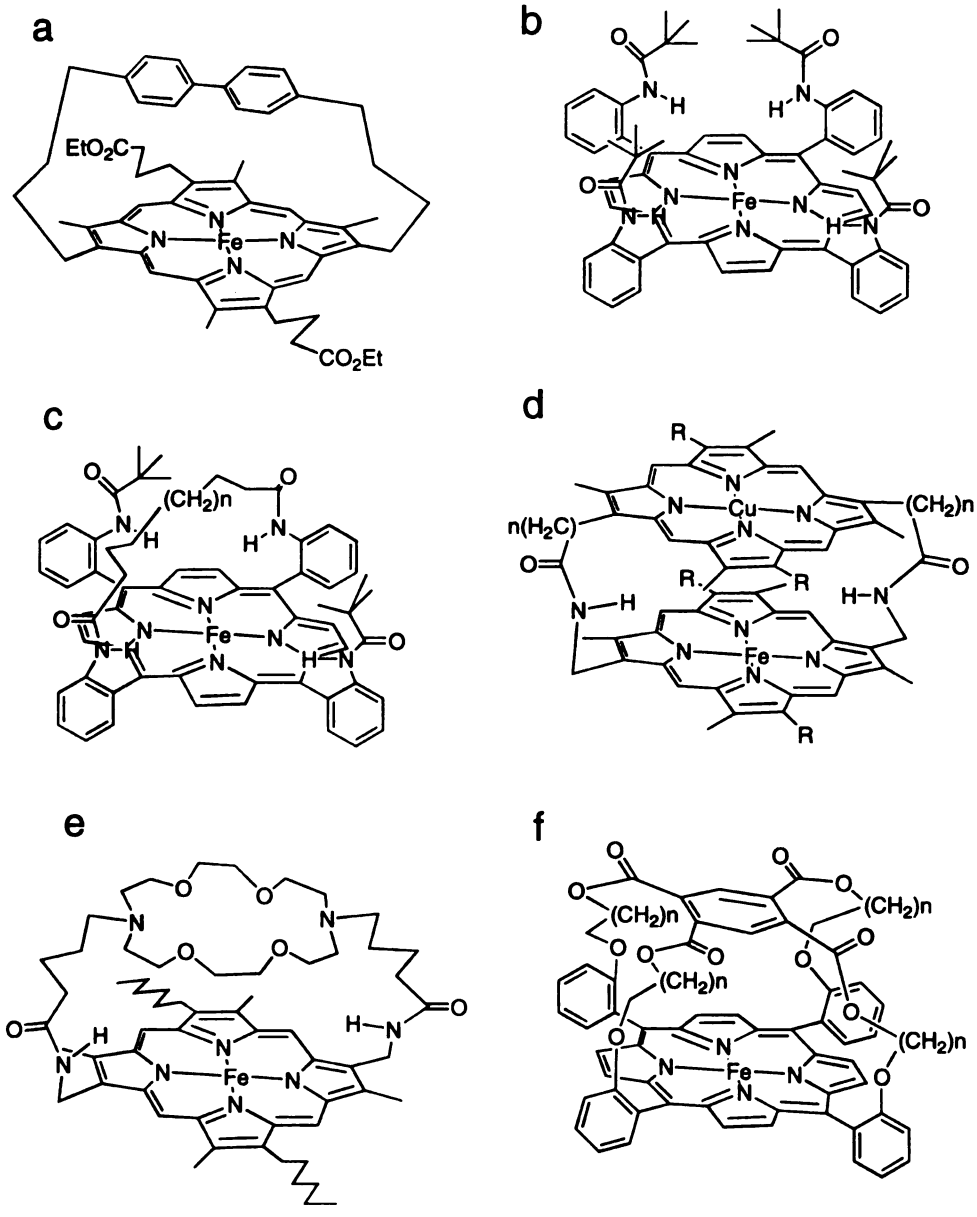

Figure 1-3. Some examples of single-sided heme model compounds. (a) cyclophane; (b) picket fence; (c) hybrid; (d) cofacial; (e)crowned; (f) capped porphyrins.

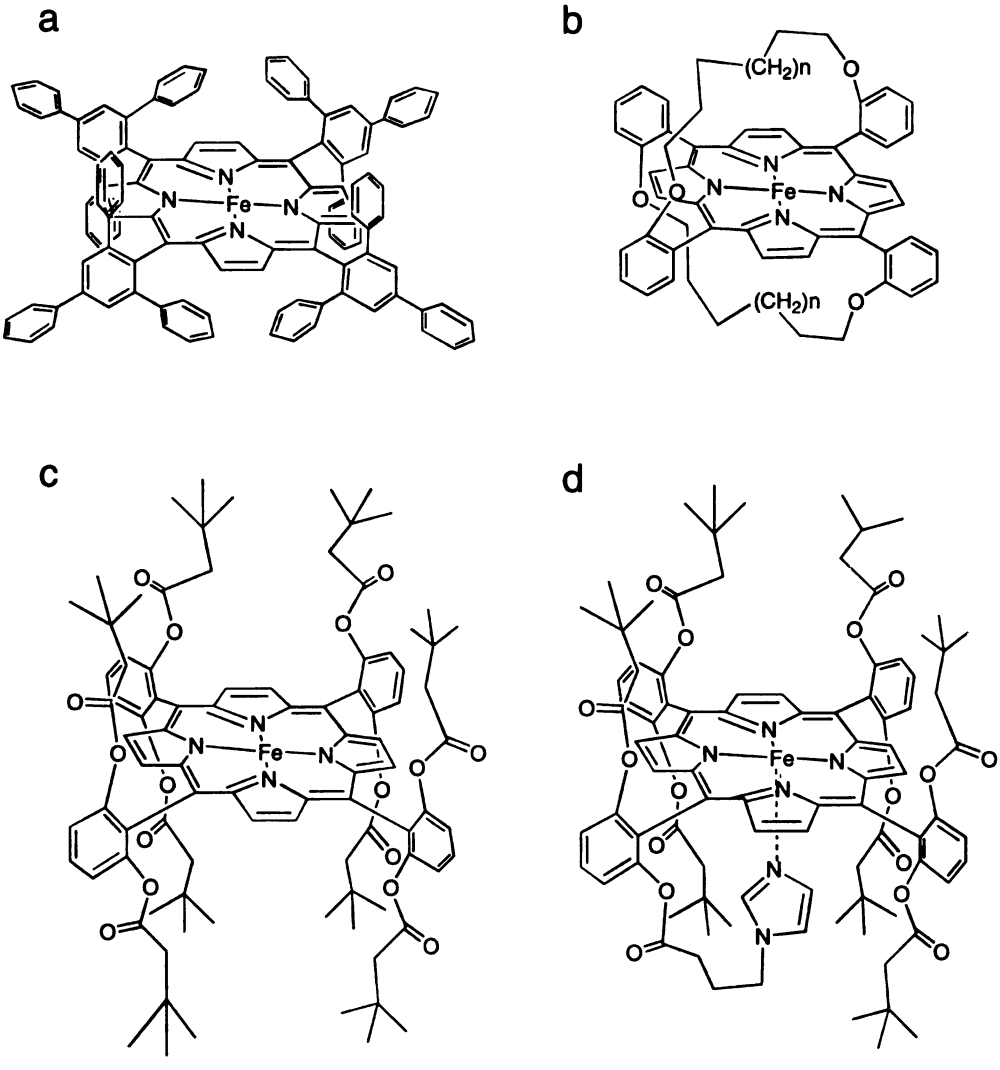

Figure 1-4. Some examples of double-sided heme model compounds. (a) bis-pocket; (b) basket-handle; (c) bis-fenced; (d) integrated porphyrins.

relative CO/O_2 affinity to the hemes vary from system to system. The factors that affect the small molecule binding to the heme include the nature of axial ligand, solvent effects, distal steric interactions, dipole-dipole interactions, and hydrogen bonding.

Fe(II) porphyrins can bind to dioxygen in the presence of a variety of axial ligands such as imidazoles, pyridine, simple amines, and some donor solvents. The effects of the axial ligand on the gasous ligand binding to ferrous porphyrins have been an interest. There are major electronic changes at the iron center upon O_2 binding. Therefore, electronic effects in axial ligand coordination influence the small molecule affinities to iron(II) porphyrins. Chang and Traylor reported that the oxygen affinity of an imidazole-chelated iron(II) porphyrin is about 20-fold higher than the pyridine-chelated analogue.[52] Kinetic studies show that the effects of axial ligands reflect on the dissociation (off) rates. This is consistent with the fact that imidazole can donate more electron density to the iron for π back-bonding than pyridine. Similar results from O_2 and CO binding to three "hanging base" ferrous porphyrins were also reported by Momenteau.[53] A reduction of the dissociation rate for oxygen was observed when imidazole was replaced by pyridine. This appears to be consistent with the greater basicity of the imidazole. In addition to electronic effects of axial ligands, steric effects are appreciable as well. The studies on O_2 and CO binding to pocket Fe(II) porphyrin show that the O_2 affinity is about 35 times lower using 1,2-dimethylimidazole as the axial ligand than using 1-methylimidazole.[36] The reduction in O_2 affinity can be ascribed to the severe steric interaction between the 2-methyl group of imidazole and the porphyrin plane. Traylor and coworker studied O_2 affinities of a series of appended-base porphyrins. In this system, increasing the rigidity, or shortening the length of the covalent linkage results in a decrease in O_2 binding affinities.[54]

The heme protein crystal structures suggest that hydrogen bonding to the N-H of the proximal imidazole, by releasing electron density to the heme iron, should increase dioxygen affinity. From this point of view, Traylor et al. studied the O_2 and CO binding

affinities of caped iron(II) porphyrins in the presence of internally hydrogen-bonded imidazole.[55] However, they found that proximal hydrogen bonding has little effect upon O_2 or CO binding affinity.

The picket-fence iron porphyrin forms a very stable oxyheme in toluene at room temperature and has a long lifetime compared to those of the others. The high stability of the oxygen adduct was ascribed to the amides in the pickets. The roles of the amide groups for stabilizing the oxyheme have been debated for two decades. The hydrogen bonding between the terminal oxygen and the hydrogens of the amide residues, or the dipole-dipole interactions are known to contribute to the high dioxygen binding affinity.[56] In order to quantify the effects of dipole-dipole interctions on heme ligand binding, Chang and coworkers reported the kinetics of O_2 and CO binding to heme model compounds equipped with a range of groups of varying dipole moments positioned near the acitve site.[57] They have found that the dipolar forces can play a significant role in regulating oxygen affinities of the hemes. Tsuchida et al. synthesized the iron complexes of double-sided porphyrins having four ester groups on each side of the porphyrin plane, and reported the kinetics of O_2 binding (Figure 1-4c and 1-4d).[52] This model compound exhibits good stability to oxidation when exposed to oxygen at room temperature. The $P_{1/2}$ of this bis-fenced iron(II) porphyrin with ester bulky groups was estimated to be 866 torr at room temperature using 1,2-dimethylimidazole as the axial ligand. Under the same conditions, the oxygen affinity of this model compound is lower than that of the picket-fence iron porphyrin having a more polar environment. Another factor, which causes the reduced dioxygen affinity, is a decrease in the basicity of the axial ligand. It has been reported that decreasing the basicity of the axial ligand results in a reduction in oxygen affinity. In this case, it appears that the unfavorable steric interaction between the axial base and the ester fence, as evidenced from small formation constants of the base and the heme, must play an important role in the reduced oxygen affinity. This is further confirmed by the oxygen-binding affinity of a later version of the double-sided iron

porphyrin in which a covalently linked imidazole was built into the porphyrin as the axial ligand.[58] In this system, a $P_{1/2}$ of 13 torr was reported, which is slightly higher than that of the tailed picket-fence heme of Collman. The O_2 binding behavior of double-sided iron(II) porphyrin complexes modified by amide residues was also reported by Tsuchida.[59] They demonstrated that increasing the local polarity of the binding site results in an increase in the O_2 binding affinity, as reflected by the reduced dissociation rate.

The hydrogen bonding between bound oxygen and the distal histidine residue in hemoproteins has been a focal point of interest. The first successful synthetic model compound which showed hydrogen bonding between the terminal oxygen and amide groups was reported by Momenteau and Lavalette (Figure 1-5a).[53,60] The amide-linked basket handle porphyrin has a 10-fold higher oxygen binding affinity than its ether-linked analogue. The interaction was further confirmed by ^1H and ^{17}O NMR of the Fe-O_2 moiety. Chang designed a series of Co(II) 1-naphthyl porphyrins substituted with amido, carboxy, and hydroxymethyl groups at the 8-naphthyl position and demonstrated their O_2 binding behavior (Figure 1-5b).[61] Thermodynamic results show that the presence of a protic group near the dioxygen binding site significantly increases the O_2 adduct formation constant. The large gain in enthalpy, -22 kcal/mol and –13 kcal/mol for carboxylate and hydroxyl groups, respectively, indicates that intramolecular hydrogen bonding occurred upon the coordination of O_2 to the active center. The large negative entropy is also consistent with the loss of rotational degree of freedom of the bound O_2. Chang et al. also reported the O_2 binding affinities of series tailed hemes equipped with appended polar groups near the coordination site.[57] For models with protic groups, the O_2 off rate is substantially reduced due to the hydrogen bonding with the bound O_2. The stabilization energy of the hydrogen bonding was estimated to be 0.7 and 1.6 kcal/mol for an alcohol and a secondary amide, respectively. Another study of H-bonded oxyheme models was provided by Reed and coworkers (Figure 1-5c).[62] The synthesis of a

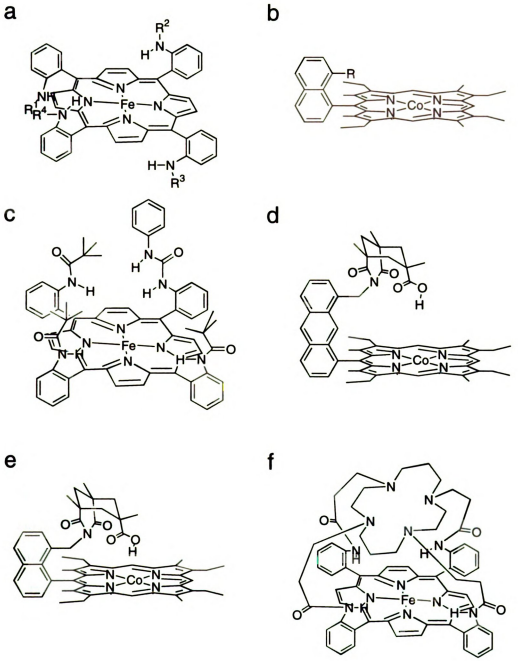

Figure 1-5. Some examples of heme model compounds.

variety of picket fence porphyrins having one of the four pickets replaced by passive and protic groups and the thermodynamic and kinetic results of their O_2 affinities were reported. A 9-fold increase, corresponding to a free energy difference of 1.3 kcal/mol, in O_2 affinity of the phenylurea analogue compared to picket-fence porphyrin was observed.

The studies on the synthetic model compounds having intramolecular hydrogen bonding with bound oxygen have provided us informative data. However, the geometry and orientation of the bound oxygen and the protic group near the active site are well understood. The X-ray crystal structures and neutron diffraction data of oxyhemoproteins showed that the N-H bond of the distal histidine is in fact restrained from optimal alignment for strong hydrogen bonding and is not coplanar with the Fe-O-O moiety. Rather, it is located off to the side so that the hydrogen bonding between the distal histidine and Fe-O_2 is an oblique interaction.[62] This indicates that the histidine residue can interact with both the iron-bound oxygen and the terminal oxygen. Recently, Chang et al. have prepared anthracene and naphthalene Kemp's acid porphyrins and reported the oxygen binding behavior of the cobalt(II) complexes (Figure 1-5d and 1-5e).[63] In the naphthalene case, a 10^4-fold enhancement of the O_2 affinity from the ester to the acid was observed. Furthermore, ΔH and ΔS are relatively small in naphthalene Kemp's acid model compared to those in the naphthoic acid model, in which it has coplanar and inflexible Fe-O-O...H resulting in the highest gain in ΔH and the highest loss in ΔS. The high O_2 affinity and small ΔH and ΔS demonstrate that a high O_2 affinity does not necessarily come from a maximum Fe-O-O...H interaction since the smaller loss in entropy is obviously more than enough to compensate for the loss in enthalpy.

As noted, one molecule of carbon monoxide is produced when one molecule of heme is catabolized by heme oxygenase. The heme proteins are capable of discriminating between dioxygen and carbon monoxide. In contrast, simple heme models are unable to mimic the O_2/CO discrimination of hemoproteins and bind to CO with a much higher affinity than hemoproteins. Structural determinations and neutron

diffraction studies of the CO adducts of hemoproteins showed that the Fe-C-O unit was either tilted or bent by as much as 120-140°,[64-66] whereas CO preferentially binds to the Fe(II) center of simple heme models in a linear fashion.[67,68] However, recent high resolution x-ray crystal structures for the CO adducts of some sterically constrained porphyrins and hemoproteins showed that there are only small degrees of tilting and bending for the Fe-C-O unit.[69,70] Recent spectroscopic studies also support this conclusion.[71] The Fe-C-O bond in Mb was found to be oriented < 7° from the heme normal. It is widely accepted that the distorted binding of CO resulted from close contacts with distal residues in the proteins. These interactions are referred to as distal steric effects. The FeCO unit is forced to adopt a nonlinear geometry by steric interactions whereas the bound oxygen, being naturally bent, does not suffer these interactions, resulting in a discrimination between the binding of CO and O_2 in hemoproteins. To mimic the steric discrimination of hemoproteins against the binding of CO many types of sterically hindered porphyrins have been synthesized. These include "cofacial" diporphyrin,[21] and "strapped",[39,72,73] "picnic basket",[44,56] "pocket",[16,74] and "capped"[75-77] porphyrins. The cofacial diporphyrin was first synthesized by Chang (Figure 1-3d).[21] The O_2 and CO binding to the diporphyrinatocopper-iron was studied in benzene solution containing excess N-alkylimidazoles. It was considered that the inert porphinato copper, covalently attached to the porphinato iron, protects the iron-oxygen adduct. Indeed, the oxyheme complex formed in the Cu-Fe dimers was so stable that the $P_{1/2}$ values can be measured directly by gas titration. The most striking result is that distal steric hindrance can affect ligand binding. The CO-binding affinity of the Cu-Fe dimer was suppressed and was similar to that of Mb. The Fe-Fe dimer showed the same reduced CO-binding affinity, but it bound two CO molecules due to two binding sites. It also showed a strong cooperativity in the binding reaction. The cooperative parameter, n, was estimated for CO-binding to the Fe-Fe dimer to be 3.4. The studies on the CO and O_2 binding of picket fence and pocket iron(II) porphyrins reported by Collman showed

that decreasing the cavity size of the iron(II) pocket porphyrin series suppressed the CO affinities without substantially affecting O_2 affinities.[36] In the R state, the most encumbered pocket porphyrin has 60-fold lower CO affinity than that of picket fence complex. The kinetic data suggested that the reduced CO affinities were almost entirely reflected in the decreased association rates. In the case of O_2 binding, both association and dissociation rates are reduced in similar extent resulting unchanged O_2 affinities. This allows the model iron(II) porphyrins to discriminate between CO and O_2 binding. Momenteau designed a series of strapped porphyrins in which the amount of central steric hindrance is modulated by means of an aliphatic chain of various length attached to the pyrrole carbons.[39] The CO affinities in this system are reduced by several orders of magnitude. Kinetic studies showed that the reduction of CO affinties could be ascribed to the central steric interactions. Ibers and coworkers reported the binding behavior of 1,2,4,5-linked capped model hemes having a cavity very near the limit to hold a linear Fe-C-O linkage (Figure 1-3f).[41] They found that the $P_{1/2}$ values of O_2 and CO binding at room temperature are 100 and 200 torr, respectively. The resultant M value is among the lowest obtained in model hemes and indicates that steric interactions inhibit CO binding. The C=O stretching frequency of 2014 cm-1, greater than those in other model compounds, is a clear indication of significantly reduced Fe back-bonding and hence of a stronger C=O bond. Recently Collman et al. synthesized a series of aza-crown-capped heme models and studied their steric interactions of gas binding (Figure 1-5f).[75,78] The most striking result is that the Fe(II) complex of the "cyclam" capped porphyrin exhibits a normal O_2 affinity and does not bind CO at all (at 1 atm); the M value is estimated to be less than 0.007! The x-ray structure of the Zn complex showed that each amide nitrogen is coplanar with the three atoms covalently attached to it as well as the hydrogen-bonded cyclam nitrogen. The hydrogen bonding between amide hydrogen atoms and cyclam nitrogen atoms results in a less flexible cap, and the distance which the cap can span is reduced. Furthermore, the methylene groups just over the metal core have hydrogen

atoms positioned right at the axis perpendicular to the porphyrin and passing through the metal center. The naturally bent O_2 ligand does not suffer the unfavored steric interactions, whereas the CO ligand is strongly distorted and hence destabilized.

Catalytic Oxidation

Dioxygen is both a terminal electron acceptor and a source of biosynthesis of various molecules in metabolic pathways. The four-electron reduction of dioxygen to give two molecules of water per dioxygen molecule represents the major source of energy in aerobic organisms. The use of dioxygen in biosynthesis involves the enzyme-catalyzed incorporation of one or both of the oxygen atoms of dioxygen into substrate. The enzymes involved in the activation of dioxygen are either monooxygenase or dioxygenase enzymes, depending on whether one or both oxygen atoms from dioxygen are incorporated into the substrate. The reactions of dioxygen with organic substrates are thermodynamically favorable, i.e., exothermic. However, direct reactions of dioxygen with organic substrates at ambient temperature are intrinsically slow, unless the substrate is a good reducing agent. If this were not the case, dioxygen would spontaneously react with organic substrates and would be harmful or fatal rather than useful for living organisms. To understand the sluggishness of dioxygen reactions with organic compounds, we must consider the kinetic barrier to these reactions. The low kinetic reactivity of dioxygen to organic compounds arises from its triplet ground state, i.e., it contains two unpaired electrons. Typical organic substrates have singlet ground states (no unpaired electrons) and the resulting products from their oxidation reactions also have singlet ground states. The reaction of triplet dioxygen with singlet organic compounds to give singlet products is a spin-forbidden process.[79,80] One way of circumventing this barrier is via the spin allowed, but energy-demanding formation of an unstable triplet intermediate followed by a spin conversion to a singlet product. However, this reaction is highly endothermic for most organic compounds and occurs

only with easily oxidizable singlet organic molecules, such as reduced flavins.

$$XH_2 + O_2 \rightarrow [XH^{\cdot} + HO_2^{\cdot}] \rightarrow XH\text{-}O_2H \qquad (1\text{-}9)$$

The reaction involves the formation of a caged radical pair, followed by spin inversion to singlet products.

Another way to overcome the kinetic barrier for the reactions of triplet dioxygen is to include a transition metal ion such as iron or copper. Transition metals in appropriate oxidation states can react with dioxygen to form the corresponding dioxygen adducts which can participate in reaction pathways that result in the oxidation of organic substrates. In biological systems, the activation of dioxygen is achieved by utilizing metalloenzymes, many of which are heme-containing enzymes.[81] Understanding how these metalloenzymes work and the design of synthetic model compounds has been a major research area in bioinorganic chemistry. In this respect monooxygenases, in particular, cytochrome P450 monooxygenases have attracted much attention in recent years.

In late 1950s, it was shown that liver microsomes contained a CO-binding pigment which exhibited an unusual absorption band at 450 nm.[82] A particularly important breakthrough for understanding the role of the CO-binding pigment was made by Estabrook and coworkers.[83] They described the catalytic role for the pigment in microsomal drug and steroid hydroxylation and showed that the photochemical spectrum has a maximum absorption at 450 nm. In 1964, Omura and Sato demonstrated that the CO-binding pigment was a heme protein containing protoheme IX and assigned it the name "cytochrome P450".[84] The term cytochrome P450 was then widely adopted for this class of monooxygenases having a maximum absorption near 450 nm in the presence of carbon monoxide. Cytochrome P450 monooxygenases are now known to exist ubiquitously in nature. A great number of P450 monooxygenases have been isolated from a variety of mammalian tissues and organs as well as in plants, insects, yeasts, bacteria, and so on. These monooxygenases have been shown to play the central role in

the catalysis of a variety of important biosynthetic pathways, such as steroid hormone and prostaglandin biosynthesis, and detoxification of a wide range of drugs and xenobiotics.[85] Examples of such reactions include hydroxylation of aliphatic and aromatic compounds, epoxidation of alkenes and arenes, amine oxidation, sulfide oxidation, and oxidative dealkylation of heteroatoms. Many of the P450 enzymes have been difficult to characterize because they are tightly bound to membranes in mammalian systems and consequently are relatively insoluble in aqueous solutions. Initial efforts to release the membrane-bound P450s from the membrane by detergent solubilization resulted in deactivation of these monooxygenases. However, a soluble bacterial P450 monooxygenase (P450cam) has been isolated from *Pseudomonas putida*.[86] P450cam has been the model system from which many mechanistic, catalytic, and spectroscopic studies have been carried out including an X-ray structure determination. Much of our knowledge and current concepts of the mechanism of P450 catalysis are derived from P450cam. The first X-ray crystal structure of P450cam was reported by Poulos and coworkers in 1985.[87] This enzyme consists of a single polypeptide chain having a triangular shape and a Fe-protoporphyrin IX nearly parallel to the plane of the triangle. The heme prosthetic group is deeply embedded in the hydrophobic environments with no covalent attachments between the porphyrin ring and the protein. One axial ligand bound to the iron is a cysteinyl thiolate, and there are no close contacts between the heme and amino acids in the distal site. In the resting state without bound substrate, the iron is predominently low-spin Fe(III), and a hydrogen-bonded network of six water molecules occupies the active site probably having a water molecule as the sixth coordination ligand.[88]

The starting point in the catalytic cycle of cytochrome P450 involves the binding of camphor to ferric P450, which results in the displacement of all of the water molecules from the active site as shown in Figure 1-6. The heme becomes five-coordinate which

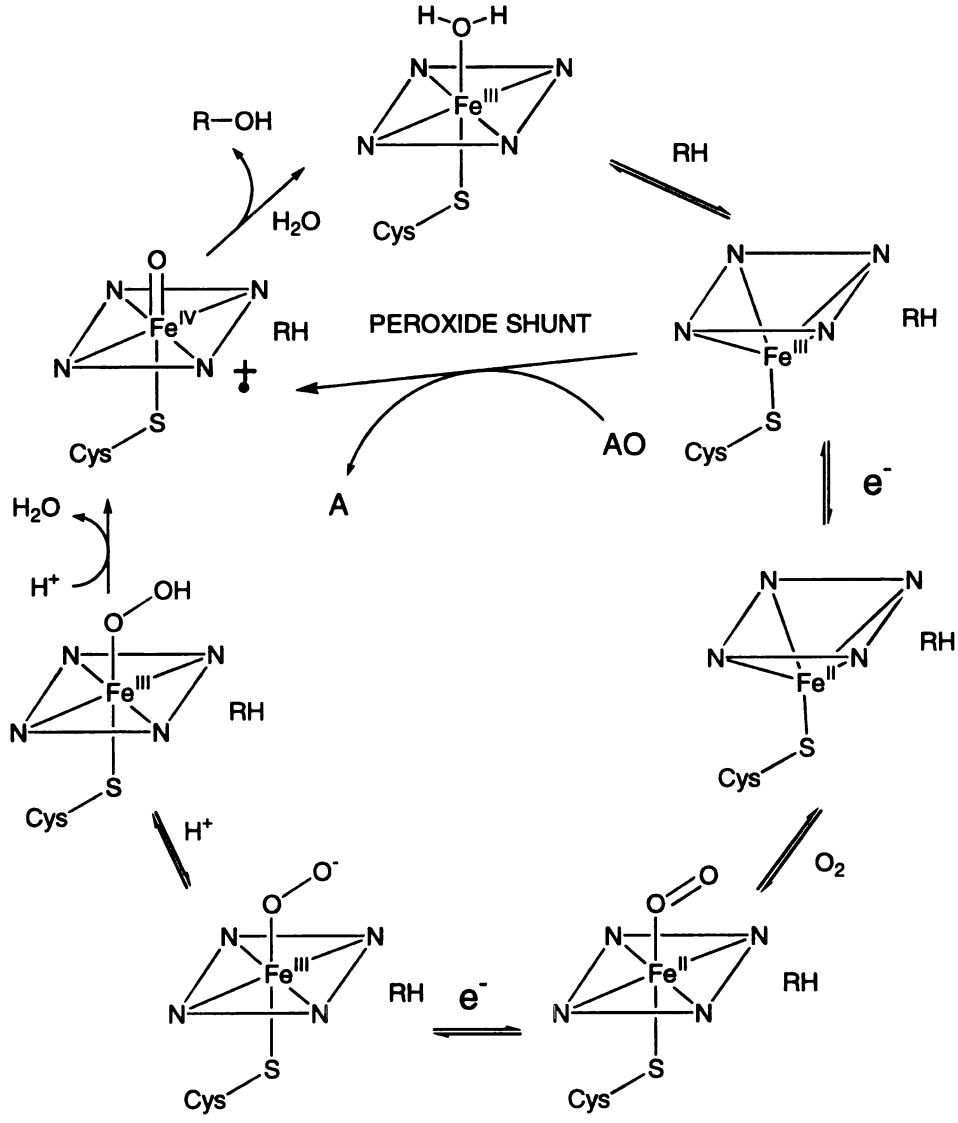

Figure 1-6. Catalytic cycle of cytochrome P450.

has a vacant coordination site that ultimately will be available for dioxygen binding. Furthermore, when the substrate binds to the resting enzyme the spin state of the iron(III) center changes to high spin from low spin resulting in a significant increase in the redox potential of the heme (from approx. -330 mV to -170 mV vs. NHE).[89] Thus the redox potential shift permits one-electron reduction by reduced putidaredoxin (E° = -190 mV) to generate the five-coordinate high spin deoxyferrous state. Dioxygen then binds to the ferrous heme iron, forming a low spin six-coordinate Fe(II) complex which differs from oxyhemoglobin by the nature of its axial ligand trans to O_2.[90] The oxy complex is then reduced by another electron to yield a ferric peroxide adduct, which can be protonated to give a hydroperoxide. A second protonation leads to heterolytic O-O bond cleavage, releasing a water and giving the proposed oxo-ferryl ($O=Fe^{IV}$) porphyrin radical cation, which is the most likely active oxidant. This species then transfers the oxygen atom to the bound substrate giving a ferric enzyme-product complex. Dissociation of the oxidized product regenerates the resting form of the enzyme. In such a system, dioxygen and electron donors (NADH or NAPDH) are required for the normal catalytic cycle.[91] It has been shown that numerous oxygen atom donors can replace dioxygen and electron donors and react with liver microsomal P450 to catalyze the hydroxylation of hydrocarbon substrates. These oxygen atom donors include hydrogen peroxide, alkyl peroxides, peracids, chlorite, periodate, and iodosylbenzene. This pathway became known as the "peroxide shunt". It is believed that the same high-valent iron-oxo intermediate is generated in these types of reactions via the peroxide shunt.[92]

Similar to cytochrome P450, chloroperoxidase is also a heme enzyme that functions as a peroxidase, a catalase, or halogenation catalyst. Extensive spectroscopic similarities to P450 and X-ray crystal structure reported by Poulos and coworkers confirmed that chloroperoxidase also has a cysteinate proximal ligand.[93,94] It has been shown that chloroperoxidase can form a spectroscopically detectable and isolable compound I intermediate, a thiolate-ligated oxo-ferryl porphyrin radical cation.[95] Thus,

chloroperoxidase compound I seems to be a good model for the P450 active oxygen intermediate. In the catalytic cycle of cytochrome P450, the electrophilic nature of the active oxygen intermediate is well known. Many efforts have been devoted to the search for the identity of the P450 reactive oxygen intermediate in the O_2-dependent cycle. None of the results are supportive of postulated compound I-type intermediate of P450. However, evidence of an oxoiron(IV) porphyrin radical cation (compound I like) in the peroxide-shunt pathway has been reported by Ishimura.[96] It is now generally accepted that oxidations of substrates in the P450 catalytic cycle are performed by the high-valent iron-oxo intermediate.

As noted, various oxidation reactions of organic substrates can be performed by the P450 active oxygen complex. One of the most interesting properties of cytochrome P450 is the ability to hydroxylate unactivated C-H bonds in hydrocarbons. The mechanism of cytochrome P450 catalyzed hydroxylation is widely considered to proceed through a "rebound mechanism".[97-99] The rebound mechanism involves an initial hydrogen abstraction from the alkane (R-H) by the P450 active oxygen intermediate to generate an alkyl radical R•, which then combines with metal-bound OH group. The rebound mechanism is supported by the large intra- and intermolecular isotope effect, a partial loss of stereochemistry observed during the hydroxylation, and the observation of rearranged hydroxylated products. The existence and the lifetime of the proposed carbon radical intermediate in the P450 cycle can be estimated using 'radical clock' substrates.[100,101] Ortiz de Montellano and coworkers reported methylcyclopropane yielded only unrearranged alcohol, whereas bicyclo[2.1.0]pentane gave a mixture of the unrearranged and rearranged hydroxylated products.[102] The hydroxyl radical recombination rate was calculated to be 1.4×10^{10} s^{-1}. Despite accumulated data, recent attempts using faster radical clock substrates to quantify the rate constants (k_r) for rearrangements of the putative radical and the amounts of rearranged products have challenged the rebound mechanism. A linear correlation between the rate constants and the amounts of

rearranged products would be expected because higher k_r values would produce more rearranged hydroxylated products. Actually, much less rearranged product was found for the substrate with high k_r while the opposite is true for the substrate with low k_r. To explain these inconsistencies, Newcomb and co-workers have argued that the hydroxylation primarily follows a nonsynchronous concerted mechanism along with minor pathways that involve radicals and carbocations.[103-105] Another possible mechanism involves a reversible formation of a complex between the substrate and the P450 iron leading to a P450 "α-alkyl complex" followed by a reductive elimination of theα-alkyl and OH ligands in *cis* position on the iron center. Collman and coworkers reported that hydrocarbon hydroxylation reactions by models of cytochrome P450 are inhibited by hydrogen and methane.[106] Thus, the results support the proposed mechanism.

The second main reaction catalyzed by cytochrome P450 is the epoxidation of alkenes. Many mechanisms have been proposed for this reaction. Most of the experimental and theoretical evidence accumulated to date supports a concerted mechanism.[107,108] The concerted mechanism proposed by Bruice and coworkers involves rate-limiting formation of a charge transfer complex between alkene and iron(IV)-oxo porphyrin radical cation, followed by a very fast change of spin state, and concerted oxygen insertion into the alkene double bond to form the epoxide product. After the rate-limiting step and change of spin state, electrophilic attack of the metal-bound oxygen on the double bond of the alkene produces a carbocation intermediate that gives the rearrangement products. The ratio of the epoxidation product and rearrangement product is dependent on the oxidation potentials of reactants, the electronic and steric structure of alkene and the active oxidant, along with the structure of the substrate.

Because of its ability to activate molecular oxygen, understanding and successfully mimicking the catalytic cycle of cytochrome P450 has become extremely important in

constructing less expensive catalysts for hydroxylation of alkanes and epoxidation of alkenes, both of which are industrially important reactions. Groves and coworkers were the first to demonstrate that Fe(III) 5,10,15,20-tetraphenylporphyrin chloride, Fe(TPP)(Cl), can catalyze the hydroxylation and epoxidation of hydrocarbons using iodosylbenzene as an oxygen source.[109] This system mimicked the short catalytic cycle of cytochrome P450, suggesting the generation of the high-valent intermediate. Using Fe(TPP)(Cl) as the catalyst and cyclohexene as the substrate, the major product is cyclohexene oxide (55%), but the allylic oxidation product, cyclohexenol (15%), is also detected. Shortly after the first report, the manganese and chromium complexes of TPP were also shown to be able to catalyze alkene epoxidation and alkane hydroxylation using iodosylbenzene or *m*-CPBA as the oxygen source under the similar reaction conditions.[110-112] In contrast with Fe(TPP)(Cl), Mn(TPP)(Cl) gives a mixture of *cis* and *trans* epoxides in the epoxidation of alkenes. The loss of stereospecificity suggested that a long-lived radical is involved during the oxidation reaction. However, it has been shown that manganese porphyrins are more efficient catalysts than the corresponding chromium or iron complexes. Unlike in the enzyme system where the active unit is bound to protein and protected, metalloporphyrins have a propensity for self-destruction under the strong oxidizing conditions. These metal complexes of TPP are called first generation catalysts.

In order to prevent oxidative self-destruction, bulky *ortho* substituents have been introduced to the phenyl groups in the TPP system. Groves et al. demonstrated that the active high-valent oxoiron species could be observed with Fe(III) 5,10,15,20-tetramesitylporphyrin chloride, Fe(TMP)(Cl).[113] Meunier and Bortolini also reported that Mn(TMP)(Cl) has a better catalytic activity compared to Mn(TPP)(Cl) by using NaOCl as the oxygen donor in a biphasic solution in the presence of phase transfer agent.[114] The stability of catalysts can also be increased by decreasing the electron density of the porphyrin ring. In 1981, Chang and Ebina discovered that the use of

fluorinated porphyrins such as Fe(III) 5,10,15,20-tetrakis-(pentafluorophenyl) porphyrin chloride ($FeTF_{20}PPCl$) greatly enhanced the stability and also increase the reactivity to the substrate since the electron-deficient porphyrin presumably would generate a more electrophilic oxoiron intermediate.[115] In 1984, Traylor and Dolphin described that high turnovers and good yields of epoxides were obtained using Fe(III) 5,10,15,20,-tetrakis-(dichlorophenyl)porphyrin chloride (FeTDCPPCl) as the catalyst.[116] This high efficiency catalyst has both electron withdrawing and steric substituents incorporated into the phenyl groups at *meso*-positions. An 85% yield of epoxynorbornene was detected in 20 min. This yield indicated that 1 mol of catalyst catalyzed 10,000 mol of norbornene (eight turnovers per second). If the metal complexes of TPP constitute the first generation of catalysts then the more robust TMP, $TF_{20}PP$, and TDCPP systems described above can be regarded as the second generation of oxidation catalysts for mimicking the catalytic cycle of cytochrome P450. Because second generation of catalysts still have oxidative-vulnerable C-H bonds in the pyrrole rings, the more robust third generation of catalysts has been developed.

The development of the third generation of catalysts involves the introduction of electron-withdrawing group into the β-positions of the pyrrole rings to create greater electrophilic deficiency in the systems. Several research groups promoted β-halogenated porphyrins as much more active catalysts and significantly more resistant to oxidative degradation than their β-unsubstituted analogous. In 1987, Traylor and Tsuchiya were the first to report the preparation and catalytic property of a β-halogenated porphyrin. They brominated the β-positions of Zn(TDCPP) with NBS and ultimately formed Fe(TDCPPβ-Br_8)(Cl) after removal of zinc and insertion of iron.[117,118] In the study of the catalytic oxidation of nobornane using pentafluoroiodosylbenzene as the oxygen donor, Fe(TDCPPβ-Br_8)(Cl) gave a 75% yield of norborneols with no hemin loss, whereas Fe(TDCPP)(Cl) afforded about a 40% yield of norborneols accompanied by about 75% hemin destruction. The same group also demonstrated that

Fe(TDCPCl$_8$P)(Cl) can be prepared by chlorination of Fe(TDCPP)(Cl). The yield obtained for hydroxylation of heptane was much higher using Fe(TDCPCl$_8$P)(Cl) (80%) than using Fe(TDCPP)(Cl). Mn(TDCPCl$_8$P)(Cl) also has higher activity than Mn(TDCPP)(Cl) for hydroxylation of heptane using iodosylbenzene.[119] However, Johnstone observed that Mn(TDCPCl$_8$P)(Cl) was in fact more rapidly destroyed and less efficient than Mn(TDCPP)(Cl) for the alkane hydroxylation by H_2O_2.[120] The electron-withdrawing groups such as chloro and bromo groups attached to β-positions of the porphyrin rings can stabilize the porphyrin HOMO. On the other hand, nonplanar distortions of the porphyrin ring caused by the added bulky substituents increase the HOMO energy, partially counteracting the gains made by the additional substitution. Moreover, substituents having π-electrons can interact with the porphyrin ring and function as π-donors. This effect becomes more important when the porphyrin is increasingly electron-deficient. Electochemical and theoretical studies show that the β-chlorinated and β-brominated porphyrins have first oxidation potentials which are not much different from those of the corresponding non-β-halogenated complexes.[121,122] Contrary to the β-chlorinated and β-brominated porphyrins, the β-fluorinated porphyrin has strong electronic withdrawing effect and does not suffer from the stereochemical crowding. Tsuchiya and Seno reported the synthesis of a new perfluoronated iron porphyrin, Fe(TPPF$_{28}$)Cl, and the catalytic oxidation of benzene.[123] They were able to convert benzene to phenol with hydrogen peroxide catalyzed by this "Teflon" porphyrin without destruction of the catalyst during the catalytic reaction. However, having no characterization data available for the porphyrin made these results questionable. In 1997, Dimagno et al. reported the synthesis and characterization of the perfluoronated porphyrin and the zinc complex.[124] The preparation of the free base is based on Lindsey's method[125] involving the condensation of 3,4-difluoropyrrole and pentafluorobenzaldehyde. The first reliable results on the catalytic activity and the stability to oxidation of the iron complex were reported by Leroy and coworkers.[126]

Quite recently, Mansuy and coworkers found that nitration of Zn(TDCPP) with fuming nitric acid led to Mn(II)(TDCP(NO_2)$_7$P) after removal of zinc and insertion of manganese.[127,128] This complex catalyzed the epoxidation of cyclooctene by iodosylbenzene with a nearly quantitative yield. It was also quite efficient for the hydroxylation of cyclohexane.

The ability of cytochrome P450 enzymes to catalyze regioselective reactions originates from discrimination based on the shape and size of the substrates, i.e., shape-selectivity.[129,130] In order to mimic the selectivity of P450 enzymes, many metalloporphyrins have been employed as catalysts for a variety of oxidation reactions, including epoxidation of alkenes and hydroxylation of alkanes.[131-133] Suslick et al. reported good regioselective hydroxylation of *n*-alkanes and remarkable shape selective hydroxylation of substituted alkanes catalyzed by the sterically crowded manganese and iron complexes of the bis-pocket porphyrin, TTPPP, bearing four 2,4,6-triphenylphenyl groups at *meso* positions.[134] The steric hindrance greatly increases the yield of the primary alcohol and also dramatically enhances the oxidative stability of the catalyst compared to the catalysts without steric hindered substituents at *meso*-positions. Collman and coworkers designed the picnic basket system to effect catalytic, shape-selective oxidation reactions and thus to mimic cytochrome P450 enzymes.[132,135] Their early attempts to epoxidize olefins using manganese derivatives and iodosylbenzene failed to achieve shape selectivity since the open side of the porphyrin could not be blocked by bulky neutral axial ligands such as 3,5-disubstituted imidazoles. Therefore, the alkenes were epoxidized on the open face of the porphyrin. However, shape selectivity that reflects the interplay between the shape of the substrate and the environments of the active site has been achieved by the use of anionic axial ligands such as 3,5-di-*t*-butylphenoxide. The manganese porphyrin bearing a rigid *para*-xylyl group near the active site, shows dramatic shape selectivity for the epoxidation of cis-2-octene versus tub-shaped *cis*-cyclooctene, whereas Mn(TMP)Cl bearing no steric hindered substituents

close to the active site gives inverted selectivity. Recent reports by Suslick et.al. described the synthesis and shape-selective catalysis of a new class of metalloporphyrin-dendrimers in which bulky cascade dendrimers have been attached at the periphery of the porphyrin.[136,137] Both intermolecular and intramolecular selecitivities of epoxidation reactions were investigated. Dendrimer catalysts showed two to three times higher selectivity than the parent Mn(TPP)Cl. Cumputer-generated molecular modeling studies suggest that the alkene substrate can approach the active site from the sideways rather than from the face of dentritic porphyrin. The relatively lower selectivity observed for the porphyrin-dendrimers compared to bis-pocket porphyrin is consistent with the larger pockets in the porphyrin-dendrimers.

Cytochrome P-450 enzymes perform intrinsically difficult oxidations such as hydroxylation of alkanes and epoxidation of alkenes often with high stereoselectivity.[138] Recently the use of model compounds to mimic the asymmetric catalytic oxidations of these enzymes has been active.[139] In 1983 Groves et al. first reported asymmetric epoxidation catalyzed by model porphyrins prepared by the reaction of an chiral acid chloride with 5,10,15,20-tetrakis(2-aminophenyl)porphyrin.[140] The epoxidation of styrene catalyzed by the iron complex gave an ee of 31%. The same group used the same strategy to prepare a porphyrin having a binaphthyl group attached to each side of the porphyrin core.[141] The iron complex catalyzed epoxidation of substituted styrene using iodosylbenzene as the oxygen donor afforded epoxides in 20% and 73% yields and enantiomeric excesses between 30% and 73%. Both the iron and manganese complexes catalyzed benzylic hydroxylation reactions with high efficiency. But only the iron catalyst yielded a remarkable asymmetric induction, up to 72%, in what is the first reported asymmetric hydroxylation of a simple alkane catalyzed by metalloporphyrins. Although many modified chiral porphyrins have been synthesized and their catalytic enantioselectivities have also been reported, a detailed analysis of asymmetric induction has not been described and only empirical steric interaction between the substrate and

chiral auxiliaries of catalysts was proposed. To analyze the detailed catalytic mechanism of these asymmetric oxidation reactions, Maruyama and Naruta synthesized "twin-coronet" porphyrins, bearing four chiral bitetralin (Bitet) or binaphthalene (Binap) auxiliaries on both sides of the porphyrin plane through eight ethereal linkages (Figure 1-7a).[142,143] These chiral catalysts showed excellent ee's in the epoxidation reactions of electron-deficient substituted styrenes: 76% for 2,4-dinitrostyrene, 89% for 2-nitrostyrene, 96% for 3,5-dinitrostyrene. These are the highest ee values ever reported with metalloporphyrin-based catalysts. The detailed analysis of the substrate LUMO and the chiral auxiliary HOMO suggests that the enantioselectivity is controlled by the interaction of their frontier orbitals at the oxo transfer arrangement to the substrate. Since this interaction is tunable by introducing appropriate substituents into the porphyrin and predictable by considering their frontier orbitals it will give a useful guideline for the design of the asymmetric catalyst.

In 1997, Halterman and coworker reported the catalytic epoxidation results obtained with a manganese complex of a D_4-symmetric dinorbornabenzene-derivatized tetraarylporphyrin (Figure 1-7b) and NaOCl.[144] A high rapid turnovers (200 to 7200) and complete conversion of aryl-substituted alkenes to epoxides were observed with most substrate and the catalyst was capable of recycling. A similar D_4-symmetric terpene-derived porphyrin (Figure 1-7c) was also synthesized by Kodadek and the catalytic asymmetric epoxidation of terminal alkenes by the manganese complex showed ee's of 70-85% and thousands of turnovers.[145] Recently, Collman et al. showed that the iron complex of a C_2 symmetric binaphthyl strapped porphyrin (Figure 1-7d) catalyzed epoxidation of alkene in good yields with high enantioselectivities: 82% for *m*-chlorostyrene, 83% for styrene, 88% for pentafluorostyrene.[146] It was also shown that this system afforded high enantioselectivities for nonconjugated terminal olefins such as 3,3-dimethylbutene (>90%) and vinyltrimethylsilane (82%). The ee's obtained for these two olefins exceed the highest values from any previously reported catalytic systems,

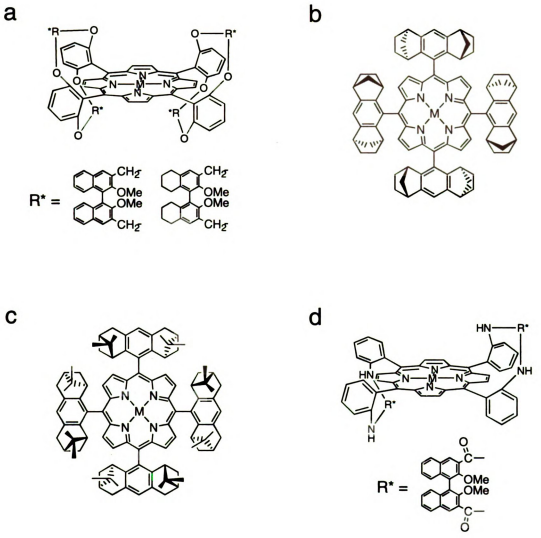

Figure 1-7. Some examples of chiral metalloporphyrins.

including the remarkable Mn(salen) derivatives.

Results and Presentation

Numerous sterically hindered iron(II) porphyrins have been synthesized. Each of these sterically hindered porphyrins is encumbered on at least one side of the heme. By studying hemoproteins and various model compounds, it has been shown that dipole-dipole interaction and hydrogen bonding of the bound dioxygen and the residues around the active sites strongly affect the oxygen affinity of the hemes. In view of this point, it is interesting to design a new type of model compound having nonpolar protected pockets on both sides of the porphyrin plane. Recently, Barton and Zard developed a convenient method for the synthesis of α-free pyrroles by the reaction of nitroalkenes and isocyanoacetates. In chapter 2, we describe the synthesis of a series of sterically hindered β-substituted bis-pocket porphyrins by using the methods of Barton-Zard and of Ono-Maruyama, and also the oxygen binding of the iron complexes.

In spite of extensive studies on the oxidations of organic substrates catalyzed by metalloporphyrins, their use in shape-selective catalysis has been less explored. In chapter 3, the shape selectvities of epoxidation reactions catalyzed by the manganese complexes including a rigid porphyrin and the selective-ligation of the zinc complexes are described. In catalytic epoxidation and ligation, the substrate can approach the active site from the top or the side of the porphyrin plane. Only a limited number of β-substituted water-soluble porphyrins have been synthesized to date. Chapter 4 describes the synthesis of a water-soluble β-substituted porphyrin, and the electrochemical and ligation properites of its iron complex. Most chiral porphyrins prepared for assymmetric oxidations of alkanes and alkenes are planar. In Chapter 5, we describe the synthesis of nonplanar chiral porphyrins, and the correlation of the absolute conformation of the nickel complexes and their circular dichroism patterns. The manganese complexes of these chiral nonplanar porphyrins can be used as chiral catalysts.

Chapter 2

SYNTHESIS OF β-SUBSTITUTED BIS-POCKET PORPHYRIN AND OXYGEN BINDING OF THEIR IRON(II) COMPLEXES

Introduction

The oxygen transport and storage functions of hemoproteins continue to be a topic of considerable interest. In order to elucidate the factors that influence the oxygen affinity, model compounds have been used extensively.[51,63,72,147,148] One essential requirement for the synthetic models is their ability to bind oxygen reversibly. However, unhindered ferrous hemes are irreversibly oxidized rapidly in the presence of oxygen. Two general autoxidation pathways have been proposed: (1) μ-oxo dimer formation and (2) H^+ (H_2O) catalyzed autoxidation as discussed in Chapter 1.[23]

In order to thwart μ-oxo dimer formation leading to irreversible oxidation, Numerous sterically hindered iron(II) porphyrins have been synthesized, with either one face or both faces of the heme protected. As the single-face hindered hemes can still be oxidized when low concentration of axial base is used,[72] attempts have been made to prepare doubly-shielded porphyrin complexes such as bis-pocket porphyrins,[47] bis-fenced porphyrins,[59,149] and basket-handle porphyrins.[150] These model compounds have played an important role to increase our knowledge on hemoglobin. However, most such model complexes are based on *meso*-substituted TPP. Only limited cases involve β-substituted cyclophane porphyrins because of the synthetic difficulties and poor yield.[151] We have now developed a general method to synthesize a series of sterically hindered β-substituted bis-pocket hemes that bind oxygen reversibly. Our approach gave a much higher yield than a previously reported *meso*-substituted bis-pocket TTPPP.[47]

Results and Discussion

Synthesis

The structures of a series of β-substituted bis-pocket porphyrins are shown in Figure 2-1. The synthesis of intermediate pyrrole is shown in Scheme 2-1. Aniline **1** was converted to the corresponding diazonium salt by reaction with sodium nitrite under acidic conditions. The diazonium solution was then treated with potassium cyanide in the presence of CuCN as the catalyst under alkaline conditions to give nitrile **2** in 71% yield. Nitrile **2** was reduced to aldehyde **3** in 90% yield by reacting with DIBAL-H. Aldehyde **3** was then condensed with nitroethane in the presence of NH_4OAc to afford nitropropene **4** in an excellent yield. ^1H NMR of the singlet vinylogous proton at δ 8.08 ppm showed that the only product obtained had the nitro group *trans* to the aryl group. Empolying the method developed by Barton and Zard for the condensation of nitroalkene and isocyanoacetates,[152,153] nitropropene **4** was treated with ethyl isocyanoacetate in the presence of excess DBU in THF at room temperature to give pyrrole **5** in 93% yield after addition of $HCl_{(aq)}$. Pyrrole **5** contains two bromine substituents, which can be replaced by aryl groups using Suzuki cross-coupling with boronic acids.[154] The aryl boronic acids used for Suzuki cross coupling reactions were prepared by the typical Grignard method (Scheme 2-2).[155] The aryl bromides were first converted to Grignard reagents, and the reaction with trimethyl borate afforded arylboronic acids in excellent yields after hydrolyzing with 10% $HCl_{(aq)}$. The Suzuki coupling reactions were carried out in gently refluxing DMF with K_2CO_3 as base and $Pd(PPh_3)_4$ as catalyst under argon for 2 days to give the doubly coupled pyrrole as the major product in good yields (Scheme 2-3). A mono-coupled pyrrole was also obtained as the minor product, in which one bromine was substituted by an aryl group and the other bromine was replaced by hydrogen. The use of 4 instead of 2.5 equivalents of the boronic acid had little effect on the yield of the expected di-coupled product and did not suppress the formation of mono-coupled product. The TLC R_f's of the di- and mono-coupled products are close to each

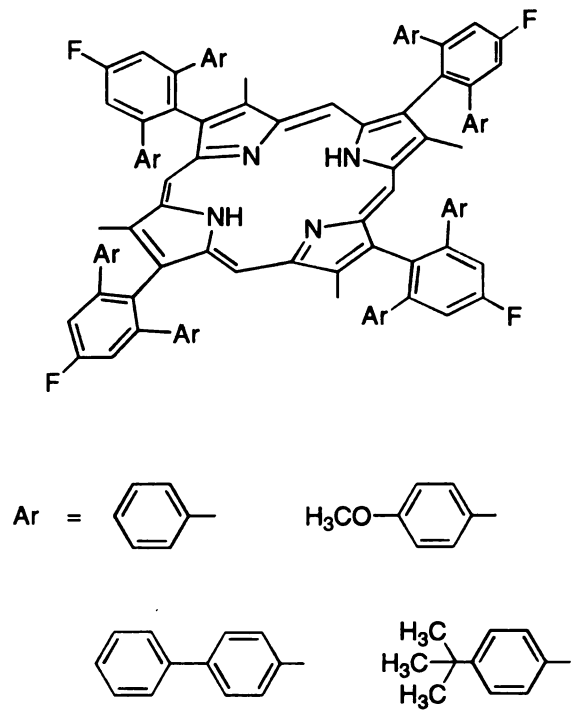

Figure 2-1. Structures of sterically hindered β-substituted bis-pockets porphyrins.

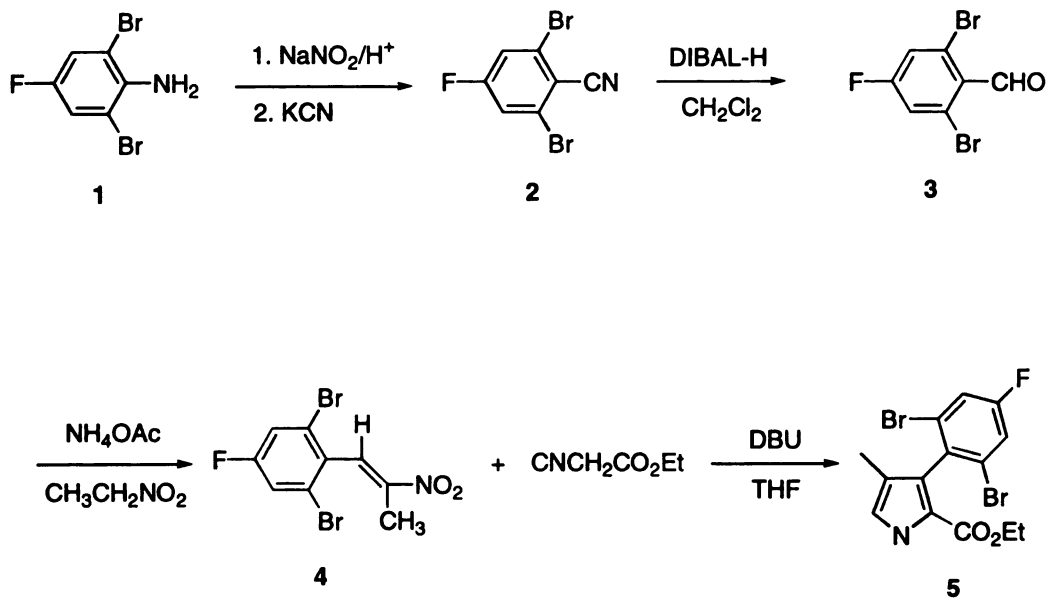

Scheme 2-1

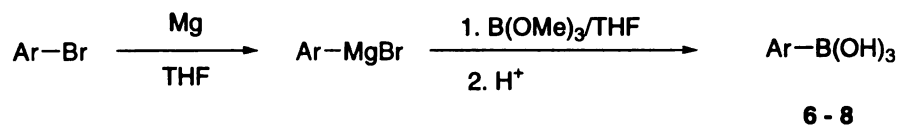

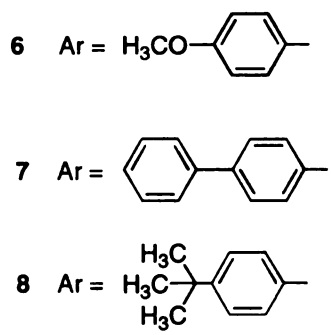

Scheme 2-2

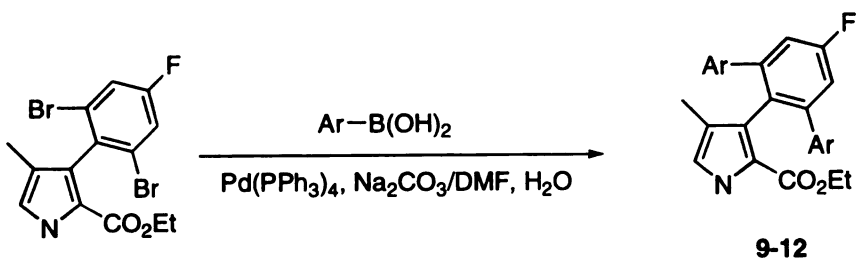

5

9-12

9 Ar =

10 Ar = H_3CO

11 Ar =

12 Ar = H_3C, H_3C, H_3C

Scheme 2-3

other. After column chromatography, recrystallization was necessary to separate the desired di-coupled product.

As shown in Scheme 2-4, an alternative route for the synthesis of pyrroles with bulky groups was also tested. The bromine substituents of nitropropene **4** was converted to aryl groups using Suzuki cross coupling. Pyrrole **14**, however, could not be obtained by the same procedure of condensation using DBU as base. We found no evidence for pyrrole formation even after 2 days of reaction in reluxing THF, and only recovered mostly unreacted starting material **13**. The problem was partially solved by using a much stronger and expensive non-nucleophilic base than DBU to promote the condensation. Thus, in the presence of stoichiometric amount of phosphazene base P_4-*t*-Bu, pyrrole **14** was obtained in about 35% yield.[156]

For the synthesis of porphyrin from pyrroles such as **9**, we started with the reduction of the pyrrole ester to a very reactive 2-hydroxymethylpyrrole followed by cyclization and oxidation. Initially, the pyrrole ester was reduced by $LiAlH_4$ in THF;[157] after quenching with water and extracting with ether, the mixture was evaporated to dryness. We found that some of pyrrole ester was overreduced to 2-methylpyrrole with $LiAlH_4$ even when the reduction was carried out at low temperature. This resulted in a low yield on the cyclization. Therefore, we employed milder reductants such as DIBAL-H and Red-Al for the reduction of pyrrole ester. The use of 10 equivalents of Red-Al converted the pyrrole ester to the corresponding pyrrole alcohol as shown in Scheme 2-5. The conversion was tested under various conditions, and the best yield was obtained if the reaction was performed in ether for an hour at room temperature. Longer reaction times led to overreduction of the ester. The work-up step involved the slow addition of minimum amount of water at 0 °C to quench the excess Red-Al and then extraction of the product with CH_2Cl_2 or ether. The use of excess water made it difficult to separate the organic and water layers during the extraction step. In general, the reduction of the pyrrole ester to the pyrrole alcohol by Red-Al afforded a quantitative yield. Without

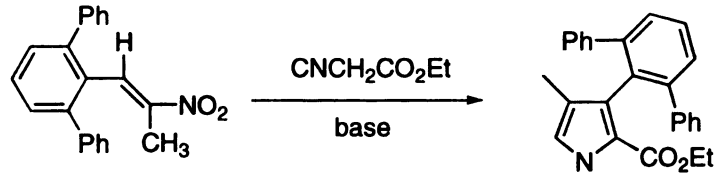

13 14

Scheme 2-4

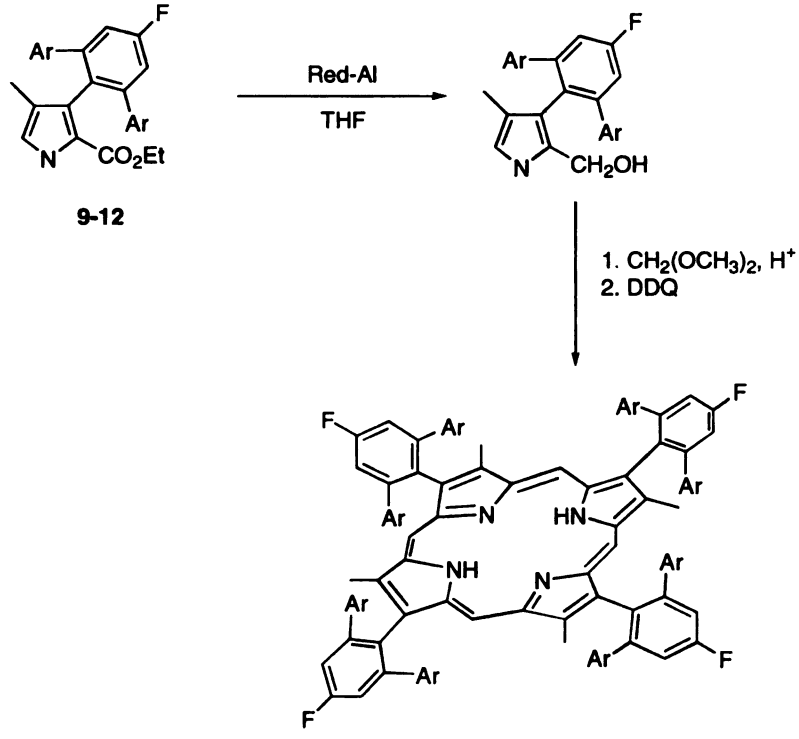

9-12

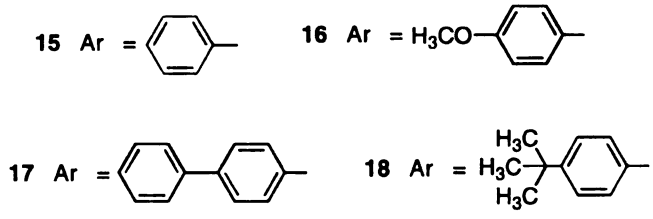

Scheme 2-5

further purification, acetic acid was added to the pyrrole alcohol and the mixture was heated on steam bath in open air for 12 h. Under the reaction conditions, the porphyrinogen intermediate was converted to porphyrin without the use of oxidant such as *p*-chloranil. This approach can only be employed satisfactorily to give about 20% yields for less hindered porphyrins **15** and **16**. However, the conversions of pyrrole **11** and **12** to porphyrin **17** and **18** respectively, were not successful under the same conditions.

Recently, Ono et al. have reported the preparation of β-substituted porphyrins by the reduction of pyrrole esters with $LiAlH_4$ followed by treatment with an acid catalyst and oxidation with chloranil or oxygen.[157] They found that the hydroxymethyl group at the pyrrole α-position was eliminated as formaldehyde by an acid catalyst. Additional formaldehyde is required to obtain a good yield. Alternatively, they used dimethoxymethane as an equivalent of formaldehyde.

A procedure similar to Ono's method was employed for the synthesis of our highly hindered porphyrins (Scheme 2-5). The general procedure involved the reduction of the pyrrole ester to the pyrrole alcohol with Red-Al instead of $LiAlH_4$ in ether for 1 h at room temperature followed by extraction. Without further purification, the reactive pyrrole alcohol was immediately cyclized in CH_2Cl_2 in the presence of 3 equivalent of dimethoxymethane for 12 h using *p*-TsOH as catalyst and then oxidized by DDQ. The use of *p*-chloranil as the oxidant resulted in partial oxidation even after 12h at elevated temperatures. By employing this procedure, the yields for porphyrins **15** and **16** were 48% and 45%, respectively. Suslick et al. reported the synthesis of a *meso*-substituted "bis-pocket" porphyrin, TTPPP, by the condensation of 2,4,6-triphenylbenzaldehyde with pyrrole in refluxing propionic acid. Under the best conditions, they obtained only 1% of the product.[47] Our synthesis, obviously, is a much more practical approach to highly hindered porphyrin molecules.

Encouraged by this success using Ono's method, the same strategy was employed to synthesize porphyrins **17** and **18**, which could not be obtained under acetic acid conditions. The yields for porphyrins **17** and **18** were 21% and 11%, respectively. In our system, the yield of porphyrin is related to the steric hindrance of the substituents on the terphenyl groups. For example, porphyrin **18** has the most crowded substituents and gives the lowest yield. The good solubility of these sterically hindered porphyrins in organic solvents, except for porphyrin **17**, allowed us to easily purify and characterize them. The purification of these porphyrins involved chromatography and then recrystallization from CH_2Cl_2 and methanol. In general, porphyrins insoluble in most organic solvents became soluble upon treatment with CF_3CO_2H to convert the free bases to their protonated forms. However, this was not the case for porphyrin **17**. As long as it precipitates it does not dissolve in organic solvents even in 30% CF_3CO_2H in CH_2Cl_2. Fortunately, porphyrin **17** is soluble in a solution of CH_2Cl_2 previously washed with concentrated $HCl_{(aq)}$. This allowed us to purify porphyrin **17** by recrystallizing it several times from CH_2Cl_2 containing HCl, and methanol.

In general, the chemical cyclization of monopyrroles substituted with the 2-hydroxymethyl group or other active methylene groups results in a mixture of the four possible regioisomeric porphyrins (Type I-IV) due to the scambling of dipyrrylmethane intermediates during the cyclization step.[158] Indeed, on the basis of proton NMR spectra of the porphyrins whose *meso*-protons appeared as a multiplet, scrambling produced a trace amount of a mixture of isomers. However, the undesired isomers can be removed by recrystallizing the products from CH_2Cl_2 and methanol as evidenced by a sharp singlet for *meso*-protons. The amount of undesired isomers were somewhat dependent on the bulkiness of the pyrrole. This suggested that the steric bulk of the aryl group has a major influence in directing the pyrrole cyclization as less hindered aryl substitutents invariably result in a mixture of substitution patterns.

The conversion of a pyrrole ester into the corresponding porphyrin was also tested by other means. For example, the pyrrole ester was hydrolyzed and decarboxylated under alkaline condition, and then treated with formaldehyde in refluxing benzene in the presence of acid followed by oxidation with DDQ. However, the expected porphyrins could not be obtained in good yields by this procedure.

As shown in Sheme 2-6, iron was inserted into porphyrins **15**, **16**, and **18** by treatment with $FeBr_2$ in refluxing DMF overnight followed by column chromatography and washing with 5-10% HCl(aq) until the axial ligand was substituted by chloride as evidenced by UV-vis. The preparation of the iron complex of porphyrin **17** can not be accomplished by this method, but can be achieved with $Fe(CO)_5$ and I_2 in refluxing toluene followed by chromatography, washing with 10% HCl(aq) gave 78% of the iron porphyrin chloride.

Using the synthetic strategy described, we successfully introduced various substituted terphenyl groups into porphyrins. These substituents fine-tune the porphyrin properties and influence the oxygen binding affinity. The preparation of ferrous porphyrins could not be achieved by the usual method with $Na_2S_2O_4$ in water-toluene solution under anaerobic atmosphere,[159] but was successful with Red-Al (scheme 2-7). However, when a large excess Red-Al was employed, ring reduction took place as evidenced by UV-vis spectra. In order to prevent ring reduction, benzophenone was chosen to quench excess Red-Al. The UV-vis spectra of the 1-MeIm-iron(II) porphyrin complexes obtained by treatment with Red-Al were identical to that obtained by spectroelectrochemical method.

The equilibria between iron(II) prophyrins and axial ligands are as follows:

$$FeP + B \overset{K_B}{\rightleftharpoons} FeP(B) \qquad (2\text{-}1)$$

$$FeP(B) + B \overset{K_B{}^B}{\rightleftharpoons} FeP(B)_2 \qquad (2\text{-}2)$$

where P represents the porphyrinato ligand, and B is an axial ligand. In this study, 1-

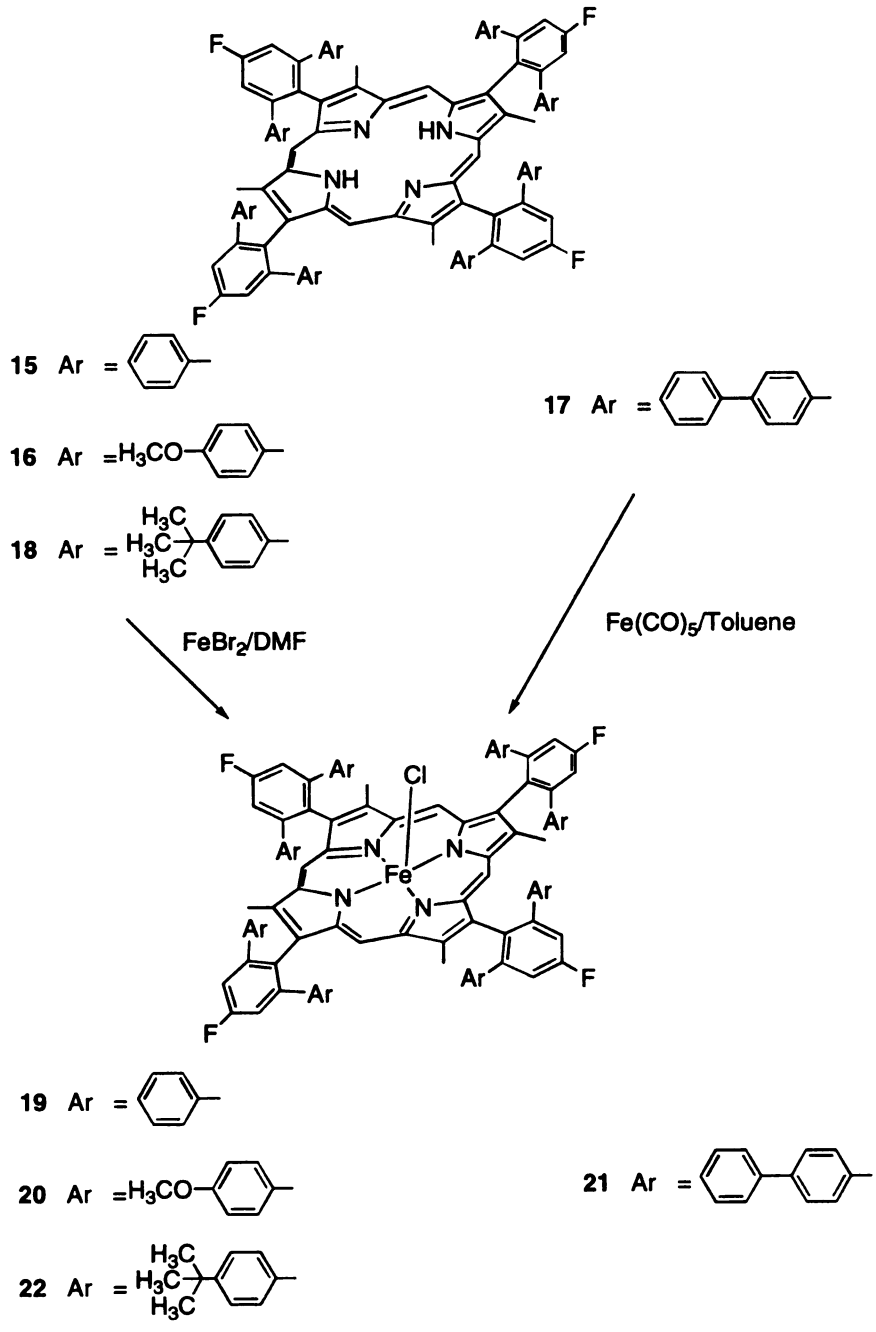
15 Ar =
16 Ar =H3CO
18 Ar =
17 Ar =
FeBr2/DMF
Fe(CO)5/Toluene
19 Ar =
20 Ar =H3CO
22 Ar =
21 Ar =

Scheme 2-6

methylimidazole (1-MeIm) and 1,2-dimethylimidazole (1,2-Me_2Im) were chosen as axial ligands. Previous work has shown that for unhindered imidazoles iron(II) porphyrin complexes bind the second axial ligand more strongly than the first one ($K_B^B > K_B$) for unhindered imidazoles.[37,160,161] In the case of the sterically hindered base 1,2-Me_2Im, iron(II) porphyrins form five-coordinate adducts cleanly ($K_B^B << K_B$) due to the repulsive interactions between 2-methyl group on the axial ligand and the electrons of the porphyrin ring. Therefore, 1,2-dimethylimidazole has been used to mimic T-state hemoglobin.[162] Suslick et al. showed that the equilibrium constant, $K_BK_B^B$, for binding two 1-methylimidazoles is about 5 x 10^9 M^{-2} for Fe^{II}TTPPP.[47] Attempts to obtain the equilibrium constants by spectrophotomeric titration with 1-MeIm for our iron(II) porphyrins were not successful. Therefore, we switched to electrochemistry for the investigation of 1-MeIm binding affinity in this system.

Electrochemistry of Iron Porphyrin 20

In order to investigate the binding ability of the iron(II) porphyrins to 1-MeIm, cyclic voltammetry was employed. Figure 2-2 shows the cyclic voltammograms of iron porphyrin **20** in CH_2Cl_2 in the presence of various concentrations of 1-MeIm. In the absence of 1-MeIm an irreversible reductive peak of $Fe^{II/II}$ at -0.55 V was observed. When the concentration of 1-MeIm increased, a new redox couple at -0.29 V formed and the reductive current at -0.55 V decreased. When the ratio of porphyrin **20** and 1-MeIm was more than 2, the irreversible reductive current for $Fe^{II/II}$ disappears. The CV's of iron porphyrin **20** remain unchanged as the concentration of 1-MeIm reaches 0.1 M. The results are consistent with $K_B^B > K_B$, in that we did not observe two separate steps of 1-MeIm ligation to the iron(II) porphyrin. In the presence of oxygen the oxidative peak of Fe(II) at -0.28 V separated to two peaks as shown in Figure 2-2. The first, with $E_{a,p}$ at -0.23 V involved the oxidation of iron(II) center, the other one with $E_{a,p}$ at -0.08 V is assigned to the oxidation of the oxygen iron(II) porphyrin adduct. Compared to the first

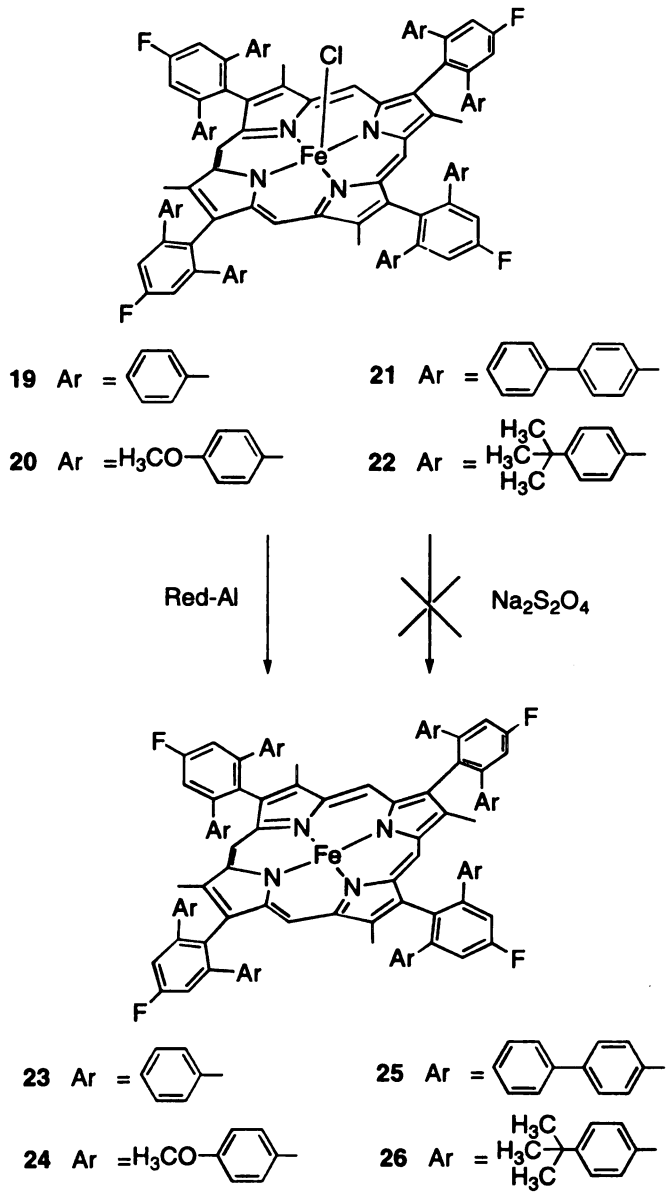
F
Ar
Cl
Ar
F
Ar
Ar
N
N
Fe
N
N
Ar
Ar
Ar
Ar
F
Ar
F
19 Ar =
21 Ar =
20 Ar =H3CO
22 Ar =
H3C
H3C
H3C
Red-Al
Na2S2O4
23 Ar =
25 Ar =
24 Ar =H3CO
26 Ar =

Scheme 2-7

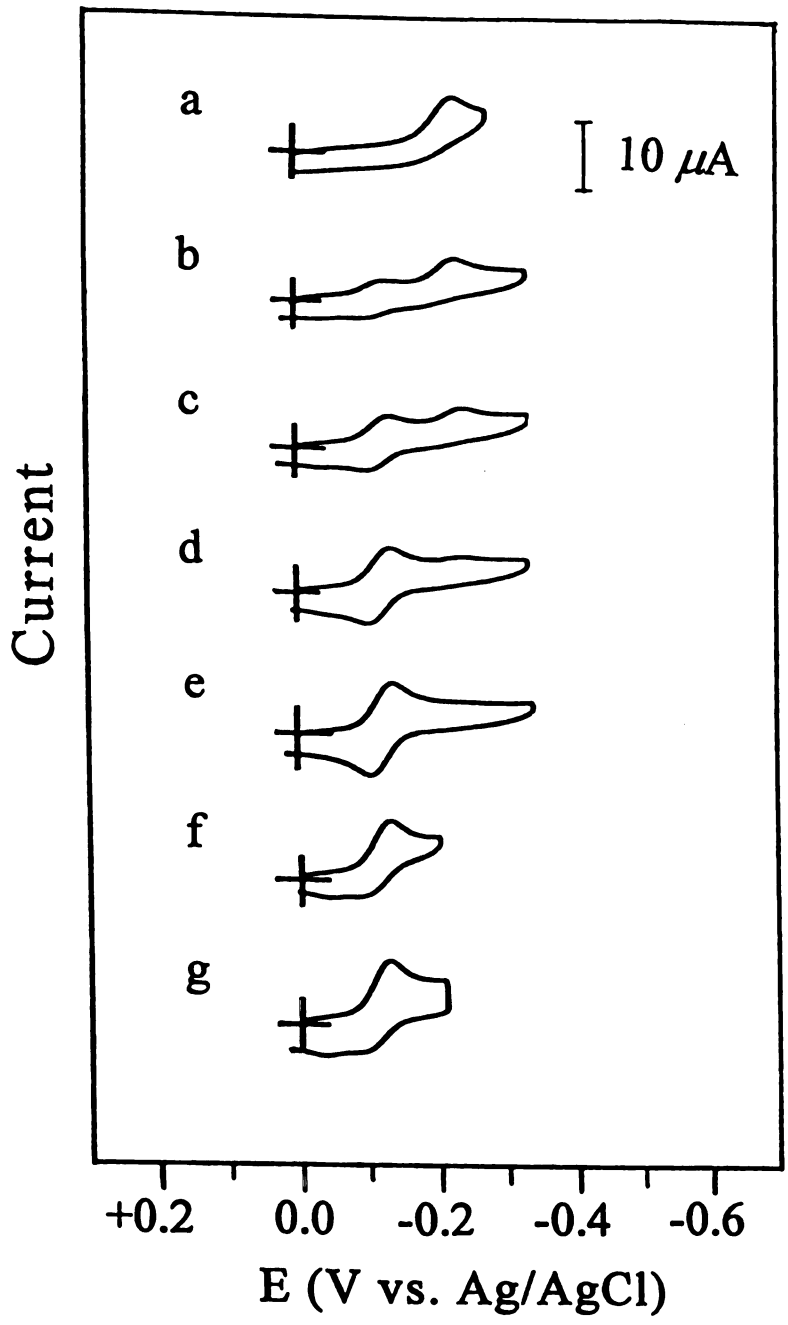

Figure 2-2. Cyclic voltammograms of iron porphyrin **20** in 0.1 M solution of TBAP in CH_2Cl_2. [**20**]:[1-MeIm] = (a) 1:0; under N_2; (b) 1:0.5; under N_2; (c) 1:1; under N_2; (d) 1:1.5; under N_2; (e) 1:2; under N_2; (f) 1:2; under O_2; (g) 1:2; after holding the potential at –0.5 V for 2 min under O_2.

oxidative current, the second one is more pronounced when the potential is held at -0.55 V for 2 minutes. Based on CV's of iron porphyrin **20** in O_2-saturated and N_2- saturated CH_2Cl_2 solutions, the electrochemical reactions of iron porphyrin **20** can be expressed by the following equations:

$$Fe^{III}P(1\text{-MeIm})_2 + e^- \rightleftharpoons Fe^{II}P(1\text{-MeIm})_2 \quad E^{o'} = -0.28\ V \tag{2-3}$$

$$Fe^{II}P(1\text{-MeIm})_2 + O_2 \overset{KO_2}{\rightleftharpoons} Fe^{II}P(1\text{-MeIm})(O_2) \tag{2-4}$$

$$Fe^{II}P(1\text{-MeIm})(O_2) + 1\text{-MeIm} \rightleftharpoons Fe^{III}P(1\text{-MeIm})_2 + O_2 + e^- \quad E_{a,p} = -0.08\ V \tag{2-5}$$

where P is the dianion of porphyrin **16**. The results also indicate that a stable oxygen iron(II) porphyrin adduct can be obtained.

O_2 Binding

All of the iron(II) porphyrins used for O_2 binding studies were prepared in *situ* by reduction of the corresponding iron(III) porphyrins with a minimum amount of Red-Al. When a large excess Red-Al was present, porphyrin ring reduction sometimes was evidenced by UV-vis spectra. In order to prevent ring reduction benzophenone was chosen to quench excess Red-Al. In the presence of 1-MeIm or 1,2-Me_2Im the UV-vis spectra of the iron(II) porphyrins obtained by this method were identical with that obtained in electrochemical cells. Oxygenation at 25 °C were achieved by all the iron(II) porphyrins with 1-MeIm or 1,2-Me_2Im as the axial ligand. The stability of the oxygen adducts and oxygen affinities of the iron porphyrins were dependent on the concentration of the axial ligands. When 2.5 equivalents of 1-MeIm were used, no clean isosbestic points were observed. An increase in the concentration of 1-MeIm resulted in a decrease in oxygen affinity. Therefore, 5 equivalents of 1-MeIm were chosen as the optimum ligand-to-heme ratio to achieve reproducible Im-Fe-O_2 formation and to maximize oxygen affinity. With 1,2-Me_2Im as the axial ligand, high concentrations of the base must be employed. When the concentration of 1,2-Me_2Im is less than 0.1 M, no well-defined

isosbestic points were observed. Figure 2-3 shows the spectral change in the Q band of iron(II) porphyrin **25** in toluene solution in the presence of 5 equivalents of 1-MeIm upon exposure to dioxygen. When the O_2 pressure increases, the peaks at 534 and 562 nm shift to 548 and 580 nm with isosbestic points at 512, 540, 554 and 570 nm. With 1,2-Me_2Im as the axial ligand, the Soret band at 444 nm shifts to 426 nm upon addition of O_2 as shown in Figure 2-4. The oxygen adducts readily changed to the corresponding CO adducts upon bubbling carbon monoxide gas in the solution. Removing O_2 with freeze-pump-thaw cycles restored about 90 % of the deoxy adducts. The stability of the O_2 adducts of these highly shielded hemes is quite remarkable with the half-life of heme **23** more than 2 h at the half-saturation O_2 pressure, and much longer for the more bulky **24**, **25** and **26**. Table 2-1 shows the $P_{1/2}^{O_2}$ for these iron(II) complexes under various titration conditions. The oxygen affinities of these hemes are necessarily low in comparison with myoglobin and its model compounds because of the hydrophobic nature of the heme center created by the nonpolar shielding wings. The oxygen affinity of heme **23** using 1,2-Me_2Im as base ($P_{1/2}^{O_2}$ = 467 torr) is close to that of the *meso*-substituted bis-pocket porphyrin, Fe(II)TTPPP, reported by Suslick, in which $P_{1/2}^{O_2}$ is 508 torr.[47] Previously, it was established that Fe-O_2 binding is enhanced by H-bonding or dipolar interactions present near the heme center and that increased solvent polarity results in higher O_2 affinities of model compounds due to the stabilization of the expected charge separation in such complexes.[57,163] Indeed, solvent effects were also observed in our heavily shielded iron porphyrins: as solvent polarity increases, O_2 affinity increases.

The fact that solvent may play a role in governing the O_2 affinity can be seen in another way. Among our hemes, the order of oxygen affinity is **26** > **25** > **24** > **23**, suggesting that the size, or the degree of shielding, has an effect on the O_2 binding. Since the polarity at the heme micro-environment cannot differ too greatly, the higher oxygen affinity associated with the bulkier wings is potentially due to two factors: the planarity effect and the solvation effect. The planarity effect was suggested for certain *ortho*-

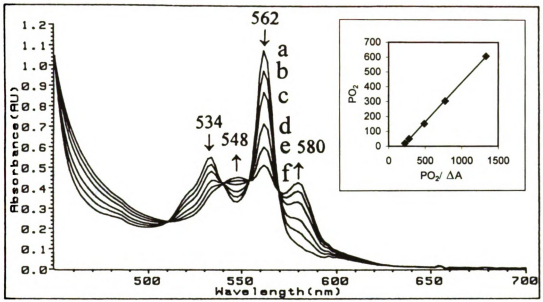

Figure 2-3. Spectral changes of iron(II) porphyrin **25** at 25 °C in toluene in the presence of 1- MeIm upon addition of O_2. [**25**]:[1-MeIm] = 1:5, PO_2 = (a) 0; (b) 20.3; (c) 50.7; (d) 152; (e) 304; (f) 608 torr. Inset: Plot of PO_2 versus $PO_2/\Delta A$ at 562 nm.

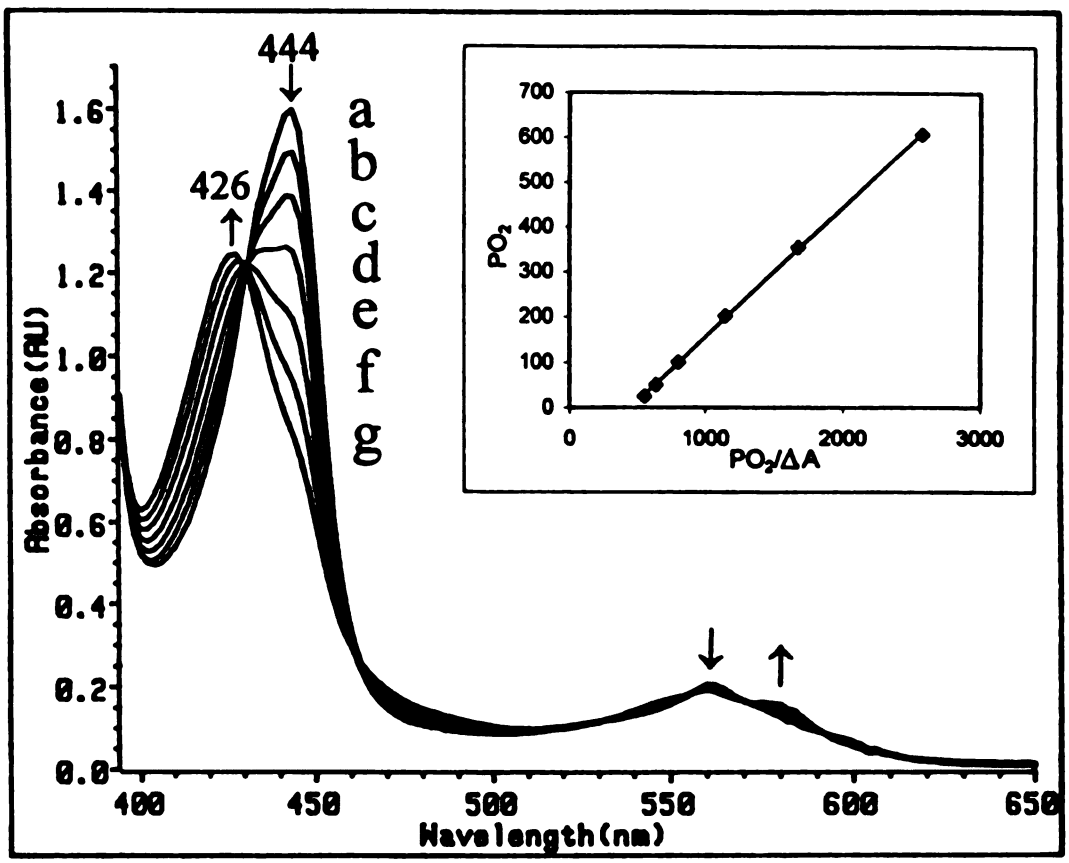

Figure 2-4. Spectral changes of iron(II) porphyrin **25** at 25 °C in toluene in the presence of 0.3 M 1,2-Me_2Im upon addition of O_2. PO_2 = (a) 0; (b) 10.1; (c) 25.3; (d) 50.7; (e) 101.3; (f) 202.7; (g) 354.7; (h) 608 torr. Inset: Plot of PO_2 versus $PO_2/\Delta A$ at 426 nm.

Table 2-1. $P_{1/2}$ of dioxygen-binding for iron(II) porphyrin complexes

Fe(II) porphyrin	Solvent	Ligand[a]	$P_{1/2}^{O}2$ (torr)	$P_{1/2}^{CO}$ (torr)
23	Toluene	1-MeIm	583	
	Toluene	1,2-Me_2Im	467	0.050
	Chlorobenzene	1-MeIm	200	
24	Toluene	1-MeIm	214	
	Toluene	1,2-Me_2Im	304	0.045
	Chlorobenzene	1-MeIm	56	
25	Toluene	1-MeIm	98	
	Toluene	1,2-Me_2Im	144	0.026
	Chlorobenzene	1-MeIm	20	
26	Toluene	1,2-Me_2Im	10.3	0.008

[a] [FeP]:[1-MeIm] = 1:5; [1,2-Me_2Im] = 0.3 M.

substituted tetraphenylporphyrin (TPP) in which the *ortho* groups, by virtue of steric interactions with the porphyrin plane, hinder the porphyrin ring doming or deformation.[164] The result is an increase in ligand binding at the sixth site. Since porphyrin **26** shows steric interactions among the shielding wings and produces a tighter enclosure above and below the plane, the porphyrin ring therefore could be more resistant to doming as compared with the other three. Collman et al., on the other hand, proposed that with "flat" iron(II) porphyrins (e.g., FeTPP or "chelated mesoheme"), the unligated five-coordinate species might be subject to a stronger solvation stabilization than the protected "picket-fence" complexes (Figure 2-5), thus extra solvent reorganization energy is required for flat hemes changing from five-coordination to six-coordination, resulting in lower oxygen affinities.[43] The higher oxygen affinities for **25** and **26**, compared to **23** and **24** could be similarly due to the more effective disruption of the solvent shell by the bulky wings surrounding the heme micro-enviroment. Judging from the X-ray structures as described below, it seems that these β-substituted shielding wings still have some degree of flexibility to rotate, the planarity effect therefore cannot play a major role to influence the ligand binding affinity.

Previous work has shown that more than a 10-fold decrease in oxygen affinity was observed when the axial ligand changed from 1-MeIm to 1,2-Me_2Im.[36,52] However, the oxygen affinities using 1-MeIm and 1,2-Me_2Im as bases in our case are in the same order since the binding of dioxygen molecules must compete with that of 1-MeIm when using 1-Me-Im as the base. Therefore, the use of a low 1-MeIm concentration would minimize the competition with dioxygen ligand and increase the dioxygen affinities.

CO binding

The conditions used for CO binding affinities of these iron(II) porphyrins were similar to those for O_2 binding studies. The values of $P_{1/2}^{CO}$ binding were measured spectrophotometrically by the addition of various quantities of 1% CO in N_2 using 1,2-

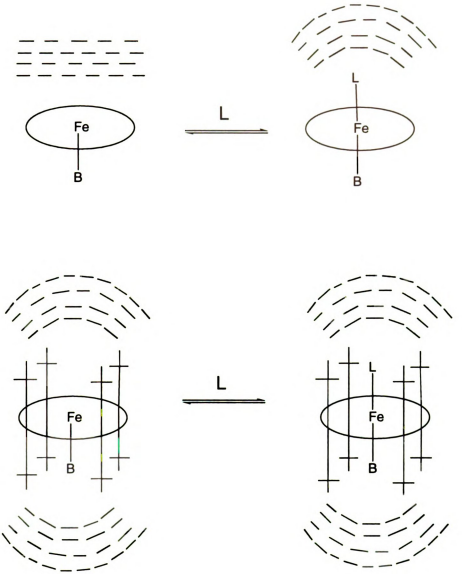

Figure 2-5. Schematic representation of solvation effects of iron(II) porphyrins. Upper scheme, simple porphyrins; lower scheme, protected porphyrins.

Me_2Im as base. Figure 2-6 shows the Soret band change of **25** in toluene solution in the presence of 0.3 M 1,2-Me_2Im upon exposure to CO. When the CO pressure increases, the peak at 442 nm shifts to 426 nm with isosbestic points at 432 and 464 nm. Table 2-1 contains the values of $P_{1/2}^{CO}$ of the iron(II) porphyrins. As noted, the nonpolar nature of the binding site of our bis-pocket porphyrins resulted in lower oxygen affinities compared to the porphyrins having a polar active site. In contrast, the CO affinities are not decreased related to other iron(II) porphyrins indicating little charge separation for Fe-CO binding. For example, the $P_{1/2}^{CO}$ of FeTTPPP(1,2-Me_2Im) with a nonpolar binding site is 9.1 x 10^{-3} torr and the $P_{1/2}^{CO}$ of FeTpivPP(1,2-Me_2Im) with a polar binding site is 8.9 x 10^{-3} torr.[37,47] The data in table 2-1 show that increasing the steric hindrance in the bis-pocket porphyrin series increases CO affinities. This can also be explained by planarity and solvation effects encountered in the case of O_2 binding affinity studies.

X-ray Crystal Structures

The crystal structure of porphyrin **16** is shown in Figure 2-7. Table 2-2 shows the crystal data and refinement parameters. Table 2-3 lists the average out-of-plane displacements, bond lengths, and bond angles. As Figure 2-7 shows, the macrocycle of pophyrin **16** is basically planar. The average displacement from the 24-atom mean plane is only 0.021 Å for nitrogen, 0.051 Å for C_{meso}, 0.043 Å for C_α, and 0.047 Å for C_β atoms. The core size (defined as half of the average distance between opposite nitrogens) is 2.028 Å, which is slightly shorter than those of H_2TPP (2.099 Å) and H_2OEP (2.098 Å).[165] In 1995, Chang and coworkers reported the synthesis and the structure of a bis-pocket porphyrin without *meso*-substituents.[156] The 2,6-isopropylphenyl groups at β-positions are nearly perpendicular to the porphyrin plane. For porphyrin **16**, the phenyl groups at β-positions rotate toward porphyrin plane. The average dihedral angle of the porphyrin plane and the phenyl groups is 66.3°. The dihedral angles between adjacent phenyl groups range from 49 to 54° and the two *ortho*-

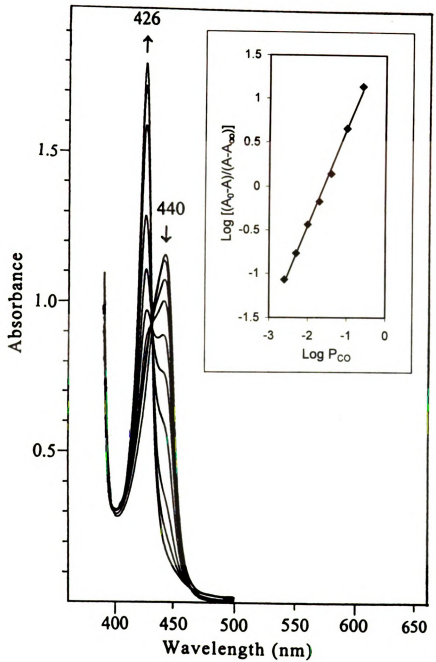

Figure 2-6. Spectral changes of iron(II) porphyrin **25** in toluene in the presence of 0.3 M 1,2-Me_2Im upon addition of CO. The following pressures of CO were used: 0, 0.001, 0.0025, 0.005, 0.01, 0.02, 0.04, 0.10, 0.25, 2.5 torr. Inset: Plot of Log $[(A_0\text{-}A)/(A\text{-}A_\infty)]$ versus Log P_{CO} at 440 nm.

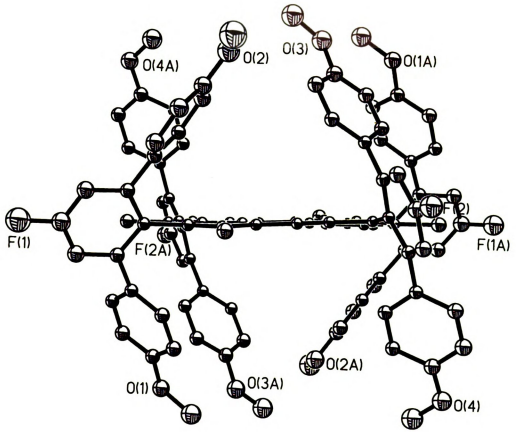

Figure 2-7. X-ray crystal structure of porphyrin **16**. Hydrogen atoms have been omitted for Clarity.

Table 2-2. Crystal data, Intensity Measurements, and Refinement Parameters for Porphyrins **16** and **21**.

	Porphyrin **16**	Porphyrin **21**
Formula	$C_{110}H_{88}N_4O_8F_4Cl_{12}$	$FeC_{144}H_{96}N_4O_4F_4Cl$
Formula Weight	2095034	2113.66
Crystal System	Monoclinic	Monoclinic
Space Group	$P2_1/n$	Cc
Temperature, K	298	298
a, Å	14.352(3)	25.800(5)
b, Å	18.684(3)	21.447(4)
c, Å	20.259(5)	21.936(4)
β, deg	97.333(23)	103.33(1)
V, Å^3	5,388.1(19)	11,811(3)
Z	2	4
Crystal Dimensions, mm	0.4 x 0.5 x 0.5	0.05 x 0.1 x 0.2
D_{calcd}, g cm^{-1}	1.292	1.189
μ, cm^{-1}	0.784	17.37
F(000)	2,164	4,396
2θ(max), deg	45	120.2
Scan Type	$\theta/2\theta$	ω
Scan Width, deg	(0.65 + 0.35 tan θ)	(1.21 + 0.3 tan θ)
No. of Unique Reflections	7,026	9,059
No. of Reflections Observed	2,770	5,114
No. of Parameters	641	1,247
R; Rw[a]	0.100; 0.079	0.108;0.069
S	2.34	5.16

[a] $R = \Sigma||Fo|-|Fc||/\Sigma|Fo|$, $Rw = [\Sigma w(||Fo|-|Fc||)^2/\Sigma wFo^2]^{1/2}$.

Table 2-3. Average Out-of-Plane Displacements, Bond Lengths, and Bond Angles for porphyrins **16** and **21**.

	Porphyrin **16**	Porphyrin **21**
	Displacement (Å)[a]	
Fe		0.5272
N	0.021	0.038
C_α	0.043	0.075
C_β	0.047	0.126
C_m	0.051	0.059
	Bond Length (Å)	
Fe-Cl		2.181
Fe-N		2.125
C_α-C_β	1.444	1.410
C_α-C_m	1.389	1.387
N-C_α	1.362	1.358
C_β-C_β	1.363	1.356
	Bond Angle (deg)	
N-Fe-N		86.5
N-C_α-C_β	110.4	108.9
C_α-N-C_α	106.3	107.3
C_m-C_α-C_β	124.9	126.9
N-C_α-C_m	124.6	123.8
C_α-C_β-C_β	106.4	107.0
C_α-C_m-C_α	126.9	129.1

[a] From the least-square plane of the 24 atoms.

groups are approximately perpendicular to each other. The terphenyl group is about 6.4 Å tall (from the porphyrin plane), which is sufficient to prevent the formation of μ-oxo iron(III) dimer. This has been confirmed by the dioxygen binding experiments described above.

Figure 2-8 shows the X-ray crystal structure of porphyrin **21**. The crystallographic data and structural summary are given in Tables 2-2 and 2-3, respectively. Surprisingly, in the presence of highly hindered substituents at β-positions the porphyrin macrocycle is only slightly distorted. The average deviation from the 24-atom mean plane is 0.038 Å for nitrogen, 0.059 Å for C_{meso}, 0.075 Å for C_{α}, and 0.126 Å for C_{β} atoms. The core size is 2.058 Å. The out-of-plane distance of iron is 0.527 Å and the distance of Fe-Cl is 2.181 Å. As expected, the phenyl groups directly attached to porphyrin macrocycle rotate toward the ring to prevent the steric interactions between the highly hindered substituents. The average dihedral angle of the phenyl and the macrocycle planes is 62.4°, which is smaller than that for porphyrin **16**. The dihedral angles between the adjacent phenyl groups range from 25 to 51° with an average of 40.5°. The hindered substituents at β-positions are about 7.9 Å tall and the pockets are better protected than those in the case of porphyrin **16**. Therefore, the iron(II) complex porphyrin **21** is more stable than that of porphyrin **16** upon dioxygenation.

Conclusions

We have described the synthesis of highly hindered β-substituted bis-pocket porphyrins in which both sides of the porphyrin plane are protected to provide a nonpolar environment. The iron(II) complexes of these porphyrins are capable of binding dioxygen irreversibly at room temperature, indicating that the hindered substituents can prevent the irreversible oxidation of the coordination site via the formation of the μ-oxo dimer. The decreased O_2 affinities of these iron complexes are ascribed to the nonpolar nature of the binding site. This can be confirmed by the observation that increasing the

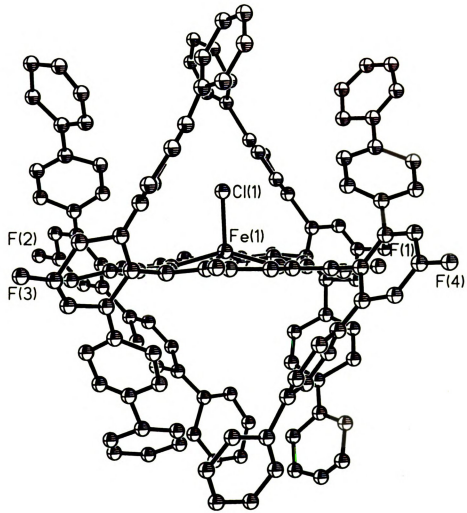

Figure 2-8. X-ray crystal structure of porphyrin **21**. Hydrogen atoms have been omitted for clarity.

polarity of solvents increases the O_2 affinity. The results described here are consistent with the fact that in hemoproteins the polar environments near the active site can stabilize the oxygenated adduct and result in a higher O_2 affinity.

Experimental

Materials

All reagents and solvents were obtained from commercial sources and were used without further purification unless otherwise noted. Dry dichloromethane and chlorobenzene were obtained by refluxing and distilling over CaH_2. Dry toluene and THF were obtained by refluxing and distilling over sodium/benzophenone. 1,2-Dimethylimidazole and 1-methylimidazole were distilled over sodium under reduced pressure. Silica gel for flash chromatography was 60-200 mesh, manufactured by Fisher Scientific. Analytical TLC was performed by using Eastman Kodak 13181 silica gel sheets. Compositions of solvent mixtures are quoted as ratios of volume.

Instrumentation

^1H NMR (300 MHz) spectra were recorded on a Varian Gemini spectrometer. Chemical shifts were reported in ppm relative to the residual proton in deuterated chloroform (7.24 ppm). Absorption spectra were recorded on a Shimadzu UV-160, Varian Carry 219, or HP 8452A spectrometer. Mass spetra were obtained on a benchtop VG Trio-1 mass spectrometer. FAB-MS mass spectra were obtained on a JEOL HX-110 HF double focusing spectrometer operating in the positive ion detection mode.

Oxygen Affinity Measurements

A solution of porphyrin Fe(III)Cl in solvent containing the appropriate concentration of 1-methylimidazole or 1,2-dimethylimidazole was introduced to a three-armed tonometer previously flushed with argon. A small amount of Red-Al in toluene

was introduced to one arm by a syringe and benzophenone was placed into the other arm of the tonometer. After deaeration by freeze-pump-thaw cycle, iron(III) was reduced to iron(II) by mixing with Red-Al. Excess Red-Al was then quenched by benzophenone when the reduction of iron(III) was complete. Spectral changes were recorded, with isosbestic points, by the addition of aliquots of oxygen from a gas manifold via a gas-tight valve to the solution. After equilibrium measurements were made, reversibility was checked by vacuum removal of oxygen; in all cases >90% reversibility was achieved. Oxygen partial pressures were determined from injections of known volumes of gas into the tonometer of known volume. The data from the spectrophotometric titrations were fitted to the equation described as follows.

Oxygen binding of iron(II) porphyrins can be expressed by the following equation:[22,52]

$$FeP(B) + O_2 \overset{K_{O_2}}{\rightleftharpoons} FeP(B)(O_2) \qquad (2\text{-}6)$$

The data from the spectrophotometric titrations can be determined in two ways. (1) When the absorbance of the completely oxygenated adduct can be obtained, the data are fitted to the Hill equation:

$$\log[y/(1-y)] = \log P_{O_2} - \log P_{1/2} \qquad (2\text{-}7)$$

where y equals the fraction of the total oxygenated adduct. Values for $P_{1/2}$ were determined from the x intercept of the regression line for a plot of log [y/(1-y)] vs. log P_{O_2}. (2) When only partial dioxygenation occurred at the highest O_2 pressure that we used, the data were fitted by equation (2-7) employed by Collman et al.[22]

$$P_{O_2} = [Fe(P)]_T b\Delta\varepsilon(P_{O_2}/\Delta A) - P_{1/2} \qquad (2\text{-}8)$$

where $P_{1/2}$ is equal to $1/K_{O_2}$ and is defined as the pressure of dioxygen at which one-half of the available bonding sites are oxygenated. Fe(P) is the total concentration of iron porphyrin, b is the cell path length, $\Delta\varepsilon$ is the difference in molar extinction coefficient between the oxy and the deoxy complexes, ΔA is the difference between the absorbance

at the particular P_{O_2} and the absorbance of deoxy complex at the same wavelength. Because $[Fe(P)]_T b\Delta\varepsilon$ is a constant, a plot of P_{O_2} vs. $P_{O_2}/\Delta A$ gives a straight line with slope $[Fe(P)]_T b\Delta\varepsilon$ and intercept $P_{1/2}$. $P_{1/2}$ values were determined at various wavelengths with large spectral changes. The deviation within each titration is less than 10 %. In all cases of oxygen titrations, well-defined isosbestic points were observed.

Carbon Monoxide Affinity Measurements

The experimental procedures used for these studies were similar to those described above for oxygen affinity measurements. Partial pressures of CO were continuously varied from 1 x 10^{-3} to 7.6 torr by the injections of 1% of CO in N_2. The data from the spectrophotometric titrations were treated in one of two ways described above.

Crystallography

Crystals of porphyrins **16** and **21** were grown from the CH_2Cl_2/MeOH mixture and benzene, respectively, by slow evaporation. To prevent solvent evaporation, the chosen crystals were coated with hydrocarbon oil and mounted on glass fibers. The diffraction data of porphyrins **16** were collected on a Nonius CAD4 diffractometer with graphite-monochromated Mo Kα radiation. The diffraction data of porphyrins **21** were collected on a Rigaku AFC5R diffractometer with graphite-monochromated Mo Kα radiation. The crystal structures were solved by direct methods and refined by full matrix least-squares using NRCVAX program. All non-hydrogen atoms were refined anisotropically, while hydrogen atoms were refined isotropically. Crystallographic details for the structures are given in Table 2-2.

2,6-Dibromo-4-fluorobenzonitrile (2)

Sodium nitrite (15.18 g, 0.22 mmol) was added portionwise to a magnetically stirred concentrated sulfuric acid (100 ml) at 0 °C. The resulting mixture was allowed to warm

to 55 °C and then held at room temperature. This nitrosyl sulfuric acid was then added dropwise to an acetic acid (110 ml) solution of 2,6-dibromo-4-fluoroaniline (53.6 g, 0.2 mmol) at 20 °C. After stirring for 1 h the diazonium solution was added dropwise to a mechanically stirred solution containing KCN (65.12 g, 1 mol), CuCN (21.49, 240 mmol), and Na_2CO_3 (340 g, 3.2 mol) in 1 l of water at 0 °C. When the addition was complete, the mixture was stirred at room temperature for 1 h. The mixture was then filtered, washed with water and dried. The resulting crude product was dissolved in benzene and insoluble solid was removed by filtration. Benzene was removed under reduced pressure and the solid was chromatographed on silica gel eluting with CH_2Cl_2 and hexanes (1:1) to afford 35.9 g (71%) of nitrile **2**. m.p. 103-105 °C; ^1H NMR (300 MHz, $CDCl_3$): δ 7.41 (2H, d); MS found m/e 278.8, cacld. 276.85 for $C_7H_2Br_2FN$.

2,6-Dibromo-4-fluorobenzaldehyde (3)

To a solution of aniline **1** (2.78 g, 10 mmol) in 20 ml CH_2Cl_2 was added DIBAL-H (1 M solution in hexane, 12 ml, 12 mmol) at 0 °C under argon. The solution was stirred at room temperature for 4 h and then poured into 30 ml 6 N $HCl_{(aq)}$ in an ice bath. After stirring for 1h, the mixture was extracted with CH_2Cl_2. The dichloromethane solution was dried over anhydrous sodium sulfate and then the solvent was removed under reduced pressure. The crude product was purified by flash chromatography on silica gel eluting with CH_2Cl_2 and hexanes (1:1) to give 2.54 g (90%) of aldehyde **3**. m.p. 85-86 °C; 1H NMR (300 MHz, $CDCl_3$): δ 10.20 (1H, s, CHO), 7.43 (2H, s, phenyl); MS found m/e 282, cacld. 279.85 for $C_7H_3Br_2FO$.

Ethyl 4-methyl-3-(2,6-dibromo-4-fluorophenyl)-2-pyrrolecarboxylate (5)

The mixture of aldehyde **3** (2.8 g, 10 mmol) and NH_4OAc (1.1 g, 14 mmol) in 12 ml nitroethane was refluxed under argon for 12 h. The solution was cooled to 20 °C and then the salt was filtered. Excess nitroethane was removed in *vacuo*. The crude product

was purified by flash chromatography on silica gel, eluting with CH_2Cl_2 and hexanes (3:7) to give orange-yellow oil of nitropropene **4** (2.6 g, 76%). Ethyl isocyanoacetate (0.95 g, 8.4 mmol) was added to a THF solution (10 ml) of nitropropene **4** (2.6 g, 7.6 mmol) cooled in an ice bath under argon. To the solution was added dropwise DBU (2.1g, 15.2 mmol) in 10 ml THF. The mixture was stirred at room temperature for 24 h, and then poured into 100 ml of 6 N HCl(aq). The solution was stirred for 5 min, filtered, washed with water, and then dried under reduced pressure to give 2.86 g (93%) of pyrrole **5**. m.p. 161-162 °C; ^{1}H NMR (300 MHz, $CDCl_3$): δ 9.05 (1H, br s, NH), 7.37 (2H, d, phenyl), 6.82 (1H, d, pyrryl), 4.09 (2H, q, CH_2), 1.85 (3H, s, CH_3), 1.04 (3H, t, CH_3); MS found m/e 405, cacld. 402.92 for $C_{14}H_{12}Br_2FNO_2$.

4-Methoxyphenylboronic acid (6)

Mg (2.67 g, 0.11 mmol) was placed in a 500 ml three-necked round-bottomed flask equipped with a reflux condenser. The system was flushed with argon for 20 min while the Mg and flask were heated with a heating mantle. The apparatus was cooled and a solution of 4-bromoanisole (18.7 g, 0.1 mol) in THF (200 ml) was added from an additional funnel. The mixture was heated to initiate the reaction. The remaining solution of 4-bromoanisole was added rapidly enough to maintain a gentle reflux. The solution was refluxed for 4 h and then transfer to an additional funnel. To a solution of trimethyl borate (10.39 g, 0.1 mol) in THF (50 ml) cooled at –78 °C was slowly added the Grignard reagent under argon. The solution was stirred overnight while warming up to room temperature slowly. After acidified with 100 ml of 10% $HCl_{(aq)}$, the product was extracted with 200 ml of ether three times, and dried over anhydrous Na_2SO_4. The solvent was removed under reduced pressure. The solid was then precipitated from actone and water to give 8.05 g (53%) of boronic acid **6**. ^{1}H NMR (300 MHz, $CDCl_3$): δ 8.18 (2H, d, phenyl), 7.02 (2H, d, phenyl), 3.90 (3H, s, CH_3).

Biphenylboronic acid (7)

A procedure similar to that used for the synthesis of boronic acid **6** was followed to give the product in 70% yield. m.p. 255-257 °C; ^{1}H NMR (300 MHz, $CDCl_3$): δ8.33 (2H, d), 7.75 (2H, d), 7.82-7.58 (4H, m), 7.52-7.34 (3H, m).

4-(t-butyl)phenylboronic acid (8)

A procedure similar to that used for the synthesis of boronic acid **6** was followed to give the product in 58% yield. m.p. 202-203 °C ; ^{1}H NMR (300 MHz, $CDCl_3$): δ8.19 (2H, d, phenyl), 7.55 (2H, d, phenyl), 1.40 (3H, s, CH_3):

Ethyl 4-methyl-3-(2,6-diphenyl-4-fluorophenyl)-2-pyrrolecarboxylate (9)

The mixture of pyrrole **5** (1g, 2.47 mmol), phenylboronic acid (750 mg, 6.18 mmol), and $Pd(PPh_3)_4$ (200 mg, 0.17 mmol) in 25 ml of DMF containing 5 ml of 2 M $Na_2CO_{3(aq)}$ was purged with argon for 10 min. The solution was gently refluxed under argon for 2 d. The reaction mixture was then cooled to room temperature and inorganic solids were removed by filtration. The filtrate was concentrated in *vacuo*, and then extrated with CH_2Cl_2. The solvent was dried over anhydrous Na_2SO_4 and removed under reduced pressure. The product was purified by column chromatography on silica gel eluting with CH_2Cl_2 and hexanes (4:6). The crude product was recrystallized from methanol to give 620 mg (63%) of pyrrole **9**. m.p. 180-181 °C; ^{1}H NMR (300 MHz, $CDCl_3$): δ8.53 (1H, br s, NH), 7.18-7.04 (12H, m, phenyl), 6.41 (1H, d, pyrryl), 4.01 (2H, q, CH_2), 1.52 (3H, t, CH_3); MS found m/e 399.3, cacld. 399.16 for $C_{26}H_{22}FNO_2$.

Ethyl 4-methyl-3-(2,6-bis-(4-methoxylphenyl)-4-fluorophenyl)-2-pyrrolecarboxylate (10)

A procedure similar to that used for the synthesis of pyrrole **9** was followed to give the product in 68% yield. m.p. 158-160 °C; ^{1}H NMR (300 MHz, $CDCl_3$): δ8.90 (1H, br s,

NH), 7.03 (2H, d, phenyl), 6.98 (4H, d, phenyl), 6.68 (4H, d, phenyl), 6.44 (1H, d, pyrryl), 4.01 (2H, q, CH_3), 3.74 (6H, s, CH_3), 1.52 (3H, s, CH_3), 1.05 (3H, t, CH_3); MS found m/e 459.3, cacld. 459.18 for $C_{28}H_{26}FNO_4$.

Ethyl 4-methyl-3-(2,6-bis-(4-biphenyl)-4-fluorophenyl)-2-pyrrolecarboxylate (11)

A procedure similar to that used for the synthesis of pyrrole **9** was followed to give the product in 92% yield. m.p. 230-232 °C; ^1H NMR (300 MHz, $CDCl_3$): δ 8.59 (1H, br s, NH), 7.56 (4H, d, phenyl), 7.46-7.35 (8H, m, phenyl), 7.34-7.26 (2H, m, phenyl), 7.16 (4H, d, phenyl), 7.15 (2H, d, phenyl), 6.45 (1H, d, pyrryl), 4.05 (2H, q, CH_2), 1.58 (3H, s, CH_3), 1.09 (3H, t, CH_3); MS found m/e 551.4, cacld. 551.23 for $C_{38}H_{30}FNO_2$.

Ethyl 4-methyl-3-(2,6-bis-(4-t-butylphenyl)-4-fluorophenyl)-2-pyrrolecarboxylate (12)

A procedure similar to that used for the synthesis of pyrrole **9** was followed to give the product in 74% yield. m.p. 190-192 °C; ^1H NMR (300 MHz, $CDCl_3$): δ 8.53 (1H,br s, NH), 7.13 (4H, d, phenyl), 7.06 (2H, d, phenyl), 6.99 (4H, d, phenyl), 6.42 (1H, d, pyrryl), 3.99 (2H, q, CH_2), 1.51 (3H, s, CH_3), 1.24 (18H, s, CH_3), 1.09 (3H, t, CH_3); MS found m/e 511.5, cacld. 511.29 for $C_{34}H_{38}FNO_2$.

2,7,12,17-Tetramethyl-3,8,13,18-tetrakis(2,6-diphenyl-4-fluorophenyl)porphyrin (15)

Method a:

To a 30 ml ether solution of pyrrole (399 mg, 1 mmol) was added Red-Al (3 ml, 65% in toluene, 10 mmol) dropwise at 0 °C under argon. When the addition of Red-Al was complete, the mixture was returned to room temperature and stirred for 1 h. The excess Red-Al was destroyed by the addition of ice at 0 °C, follow by 5 ml water. The resulting mixture was extracted with 30 ml CH_2Cl_2 twice. The combined organic portions were washed with water, dried over Na_2SO_4, and concentrated under reduced pressure to give

yellow an oily residue. The crude product, without any purification, was dissolved in 20 ml acetic acid and heated over a steam bath in open air overnight. Solvent was removed in *vacuo* and then the residue was taken into dichloromethane, washed with water and purified by silica gel column chromatography eluting with CH_2Cl_2 to give the product as a purple solid. The solid was recrystalized from CH_2Cl_2 and methanol to afford 71 mg (21%) of porphyrin **15**. ^{1}H NMR (300 MHz, $CDCl_3$): δ 9.23 (4H, s, *meso*), 7.44 (8H, d, phenyl), 7.01 (16H, d, phenyl), 6.65 (8H, t, phenyl), 6.55 (16H, t, phenyl), 2.85 (12H, s, CH_3), -4.24 (2H, br s, NH); UV-vis (toluene, λ_{max} nm (ε)): 636 (6,400), 580 (9,000), 546 (14,800), 509 (19,200), 418 (162,200) ; MS (FAB): found m/e 1351.8, cacld. 1350.52 for $C_{96}H_{66}F_4N_4$.

Method b:

The same reduction procedure in **method a** was followed to obtain the alcohol which was then dissolved in 40 ml CH_2Cl_2. To the solution was added dimethoxymethane (0.28 ml, 3 mmol) and *p*-toluenesulfonic acid monohydrate (38 mg, 0.2 mmol). After stirring the mixture overnight under argon, DDQ (227 mg, 1 mmol) was added and the solution was stirred for a further hour. The solvent was removed in *vacuo* to give a dark residue. The residue was chromatoghraphed on silica gel eluting with CH_2Cl_2. The purple fraction was collected and recrystallized from CH_2Cl_2 and methanol to give 162 mg (48%) of porphyrin **15**.

2,7,12,17-Tetramethyl-3,8,13,18-tetra(2,6-bis-(4-methoxyphenyl)-4-fluorophenyl) porphyrin (16)

Method b was employed to give the product in 45% yield. ^{1}H NMR (300 MHz, $CDCl_3$): δ 9.32 (4H, s, *meso*), 7.38 (8H, d, phenyl), 6.92 (16H, d, phenyl), 6.15 (16H, d, phenyl), 3.31 (24H, s, CH_3), 2.87 (12H, s, CH_3), -4.21 (2H, br s, NH); UV-vis (toluene, λ_{max} nm

(rel intens)): 638 (0.07), 582 (0.08), 549 (0.12), 512 (0.14), 421 (1.00); MS (FAB): found m/e 1591.3, cacld. 1590.61 for $C_{104}H_{82}F_4N_4O_8$.

2,7,12,17-Tetramethyl-3,8,13,18-tetra(2,6-bis-(4-biphenyl)-4-fluorophenyl)porphyrin (17)

Method b was employed. After oxidation with DDQ, the mixture was passed through a short silica gel column eluting with CH_2Cl_2. The purple fraction was collected and evaporated in *vacuo*. The crude product was consecutively recrystallized from CH_2Cl_2, which had been washed with concentrated $HCl_{(aq)}$, and methanol to give the product in 21% yield. ^{1}H NMR (300 MHz, $CDCl_3$): δ9.33 (4H, s, *meso*), 7.47 (8H, d, phenyl), 7.05 (16H, d, phenyl), 7.0-6.8 (40H, m, phenyl), 6.69 (16H, d, phenyl), 2.92 (12H, s, CH_3), -4.03 (2H, br s, NH); UV-vis (toluene, λ_{max} nm (ε)): 637 (7,300), 582 (8,700), 549 (14,300), 513 (17,200), 422 (135,400); MS (FAB): found m/e 1962.4, cacld. 1958.77 for $C_{144}H_{98}F_4N_4$.

2,7,12,17-Tetramethyl-3,8,13,18-tetra(2,6-bis-(4-t-butylphenyl)-4-fluorophenyl) porphyrin (18)

Method b was employed to give the product in 11% yield. ^{1}H NMR (300 MHz, CDCl3): δ9.30 (4H, s, *meso*), 7.40 (8H, d, phenyl), 6.92 (16H, d, phenyl), 6.59 (16H, d, phenyl), 2.87 (12H, s, CH_3), 0.78 (72H, s, CH_3), -4.18 (2H, br s, NH); UV-vis (Toluene, λ_{max} nm (ε)): 637 (5,800), 582 (7,200), 547 (12,600), 512 (16,000), 421 (152,000); MS (FAB): found m/e 1800.6, cacld. 1799.02 for $C_{128}H_{130}F_4N_4$.

Fe(III) 2,7,12,17-tetramethyl-3,8,13,18-tetrakis(2,6-diphenyl-4-fluorophenyl) porphyrin chloride (19)

Free base **15** (27 mg, 0.02 mmol), anhydrous $FeBr_2$ (86 mg, 0.4 mmol), and 0.5 ml of pyridine were added to 20 ml of DMF and refluxed under argon. After 12 h, the reaction

was completed as monitored by the UV-vis spectrum. The solvent was evaporated to a minimum amount in *vacuo* and the iron porphyrin was purified over silica gel column eluting with CH_2Cl_2 and methanol (97:3). The collected iron porphyrin was washed twice with 5-10% $HCl_{(aq)}$ and dried with Na_2SO_4, and the solvent was evaporated under reduced pressure, yielding 20 mg (83%) of **19**. UV-vis (toluene, λ_{max} nm (rel intens)): 641 (0.08), 546 (0.14), 513 (0.13), 418 (1.00), 393 (0.89); MS (FAB): found m/e 1405.5, cacld. 1404.44 for $C_{96}H_{64}F_4N_4Fe$.

Fe(III) 2,7,12,17-tetramethyl-3,8,13,18-tetrakis(2,6-bis(4-methoxyphenyl)-4-fluorophenyl)porphyrin chloride (20)

A procedure similar to that of **19** was employed to give **20** in 78% yield. UV-vis(toluene, λ_{max} nm (ε)): 643 (5,700), 546 (11,700), 512 (11,800), 416 (75,000); MS (FAB): found m/e 1645.7, cacld.1644.53 for $C_{104}H_{80}F_4N_4O_8Fe$.

Fe(III) 2,7,12,17-tetramethyl-3,8,13,18-tetrakis(2,6-bis(4-t-butylphenyl)-4-fluorophenyl)porphyrin chloride (22)

A procedure similar to that used for the synthesis of **19** was employed to give **22** in 76% yield. UV-vis(toluene, λ_{max} nm (ε)): 644 (4,600), 511 (11,400), 415 (86,400); MS (FAB): found m/e 1854.4, cacld. 1852.94 for $C_{128}H_{128}F_4N_4Fe$.

Fe(III) 2,7,12,17-tetramethyl-3,8,13,18-tetrakis(2,6-bis(4-biphenyl)-4-fluorophenyl) porphyrin chloride (21)

To a solution of the free base **17** (20 mg, 0.01 mmol) and iodine (5 mg, 0.02 mmol) in 20 ml of toluene was added iron pentacarbonyl (118 mg, 0.6 mmol) and the mixture was refluxed under argon. After 2 h, the reaction was completed as monitored by the visible spectrum. The solvent was evaporated in *vacuo* and the iron porphyrin was purified over silica gel column eluting with CH_2Cl_2 and methanol (95:5). The collected iron porphyrin

was washed twice with 5-10% $HCl_{(aq)}$ and dried over anhydrous Na_2SO_4, and the solvent was evaporated under reduced pressure, yielding 16 mg (78%) of iron porphyrin. UV-vis (toluene, λ_{max} nm (ε)): 643 (5,700), 546 (11,600), 514 (11,700), 421 (80,200); MS (FAB): found m/e 2014.4, cacld. 2012.69 for $C_{144}H_{96}F_4N_4Fe$.

Chapter 3

SHAPE-SELECTIVE EPOXIDATION AND LIGATION OF β-SUBSTITUTED PORPHYRINS

Introduction

Many sterically hindered metalloporphyrins, such as bis-pocket,[47] basket handle,[132,139] dendritic,[137] steroidal,[166] and others[142,145,167,168] have been used to mimic the selective epoxidation of cytochrome P450 enzymes. The synthesis of such sterically encumbered metal centers for shape- or regio-selective catalysis continues to be of great interest. However, synthetic difficulty limits the use of sterically hindered *meso*-substituted metalloporphyrins as shape-selective catalysts, although the presence of bulky substituents at the *ortho*-positions of *meso*-phenyl groups exhibits high stability during the catalytic reaction.[116] In Chapter 2, we have described the synthesis of sterically hindered *β*-substituted porphyrins. This new class of porphyrins that we employed for dioxygen binding is also used for shape-selective epoxidation catalysis.

Figure 3-1 gives examples of selective oxidations. For example, under thermodynamic control, the internal C=C bond is more reactive than the external C=C bond when reacted with simple oxidants such as peracids. In contract, under the influence of catalysts, the selectivity of the catalysts may be controlled by the steric interactions and van der Waals contact between the substrate and the substituents at the periphery of the porphyrin. Therefore, these catalysts can selectively epoxidize the external C=C bond (Figure 3-2). In the catalytic reaction, the substrate might approach the active site from the top or the sides of the porphyrin plane. The selectivity is basically controlled by the accessibility to the active site or the cavity size of the steric superstructure which can be varied by synthesis.

HYDROXYLATION: allylic, benzylic > 3^{o} > 2^{o} > 1^{o}

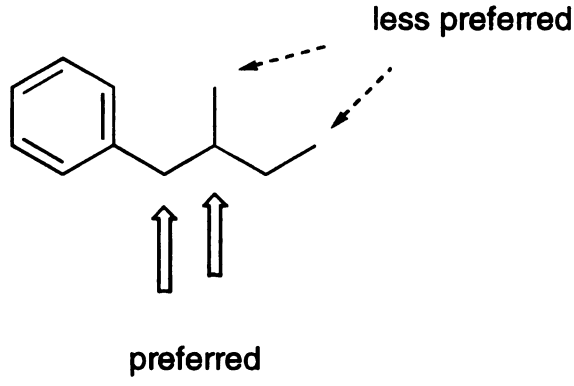

EPOXIDATION: more substituted > less substituted

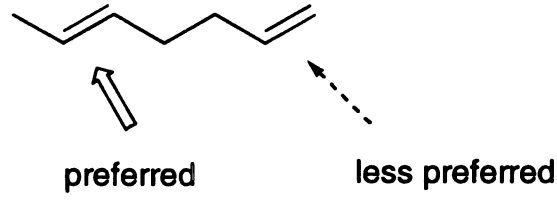

Figure 3-1. The preferred oxidation sites of hydrocarbons under thermodynamic control.

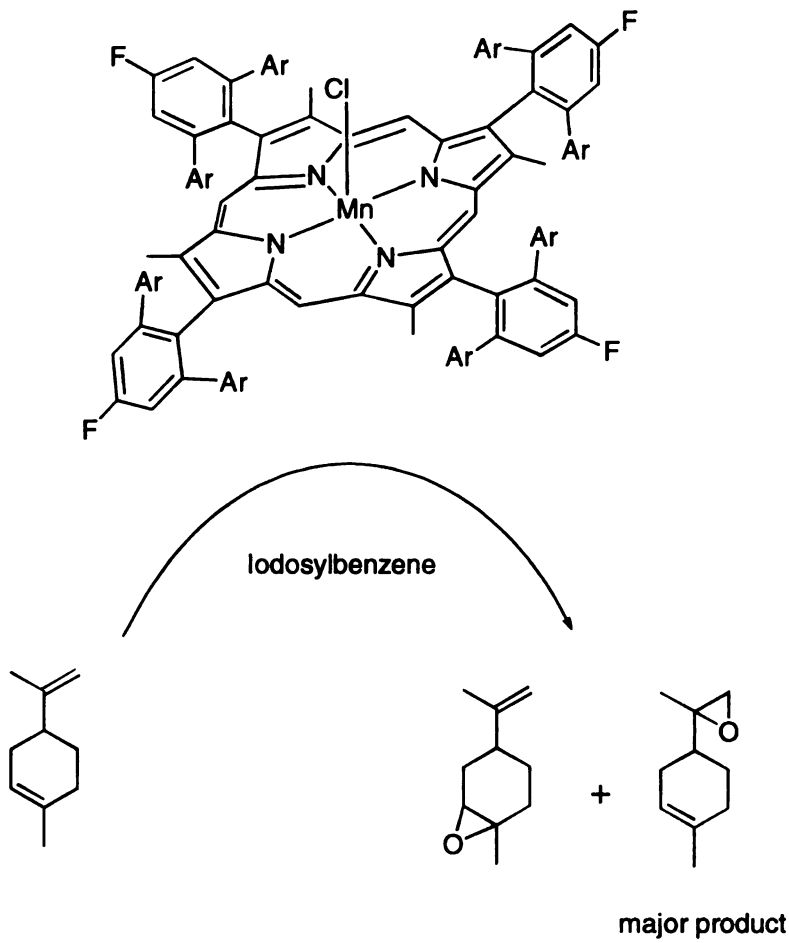

Figure 3-2. Intra-molecular shape-selective epoxidation.

The introduction of different substituents should allow us to modify the structures of the sterically hindered β-substituted porphyrins, thus regulating their properties. However, the structures of the porphyrins are flexible due to the rotation or vibration of the substituents. To better control the micro-environment of the active site of the metalloporphyrin, it is necessary to reduce the flexibility of the porphyrin structure. In view of this point, it would be interesting to examine the activities of these catalysts as a function of the rigidity of the superstructure. We therefore designed and synthesized a rigid porphyrin in which the shielding wings are locked by intramolecular hydrogen bonding, thereby blocking the top entrance of the channel as well as limiting access via the sideway wings.

In addition to the regioselective epoxidation reactions that can be demonstrated by using these hindered porphyrins as catalysts, their unique structure also proves to be useful as an example of molecular recognition. Molecular recognition of neutral molecules that control or initiate specific interactions is the essence of biological chemistry. In addition to their biological importance, porphyrins provide a potentially useful framework for artificial acceptors since they have a well-defined binding pocket, can be functionalized at the *meso*- and β-positions, and can be inserted with a number of metals. Thus, metalloporphyrins have been constructed as the acceptors for the recognition of small molecules such as carbohydrates,[169] amino acid derivatives,[170-172] and quinone derivatives.[173,174] However, shape-selective ligation has been less examined.[175,176]

In this chapter, we describe the synthesis, characterization, and utilization of this new class of sterically hindered metalloporphyrins as catalysts for shape-selective epoxidation reactions. We also report the shape-selective ligation of the zinc porphyrins to substituted pyridines and alkyl amines.

Results and Discussion

Synthesis

Unlike *meso*-phenyl bis-pocket porphyrin synthesized by Suslick et al., our β-substituted porphyrins can be prepared in good yields as described in Chapter 2 and substituents with different hindrance can be easily introduced to the periphery of the porphyrins to control the cavity size. In this chapter, the synthetic efforts are focused on a system in which intramolecular hydrogen bonding can take place among the shielding terphenyl groups. Initially, we tried to synthesize porphyrins **27** and **28**, having carboxylic acids and amides on the terphenyl groups, respectively, as shown in Figure 3-3. Porphyrin **27** could be converted to porphyrin **28** by treatment with thionyl chloride followed by NH_3 gas. The key step for the formation of pyrrole **31** involves Suzuki cross-coupling of pyrrole **5** and commercially available boronic acid **30** (Scheme 3-1). However, the Suzuki coupling gave a low yield and a mixture of mono- and di-substituted pyrroles, which could not be separated with chromatography. The use of ester **32** instead of acid **30** did not improve the yield. Therefore, an alternative preparation of pyrrole **31** is necessary. Miyaura[177] and Giroux[178] have reported a modified Suzuki coupling which involved the use of $PdCl_2$(dppf), pinacol ester of diboron, and arylhalides. The modified coupling reaction employing the method as shown in Scheme 3-2 also gave a mixture of mono-, di-substituted, and debrominated pyrroles in low yields for which the separation was tedious.

We then switched to the preparation of porphyrin **29** (Figure 3-3). The key feature for the preparation of porphyrin **29** is the synthesis of a pyrrole having an amine substituted terphenyl group at β-position, which can be easily converted to the desired amide group. Boronic acid **37**, in which the amine group was protected by two benzyl groups, was prepared by the route shown in Scheme 3-3. Dibenzylaniline **34** was brominated with Br_2 in $CHCl_3$ at 0 °C to give bromide **35**, which was then reacted with 10 equivalent of Mg to give Grignard reagent **36**. The use of excess Mg was necessary

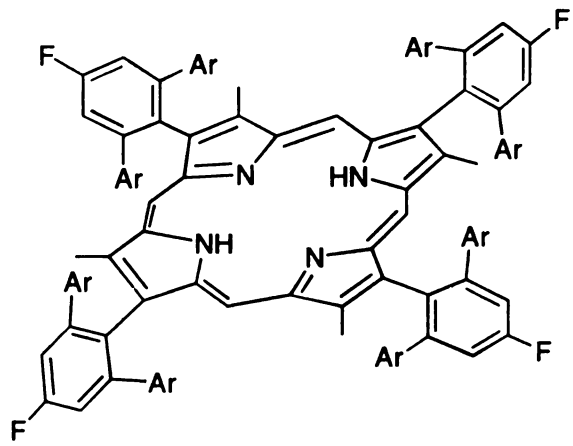

27 Ar = 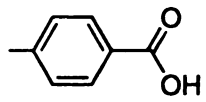

28 Ar = 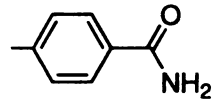

29 Ar = 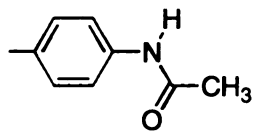

Figure 3-3. Structures of porphyrins with intramolecular hydrogen bonding.

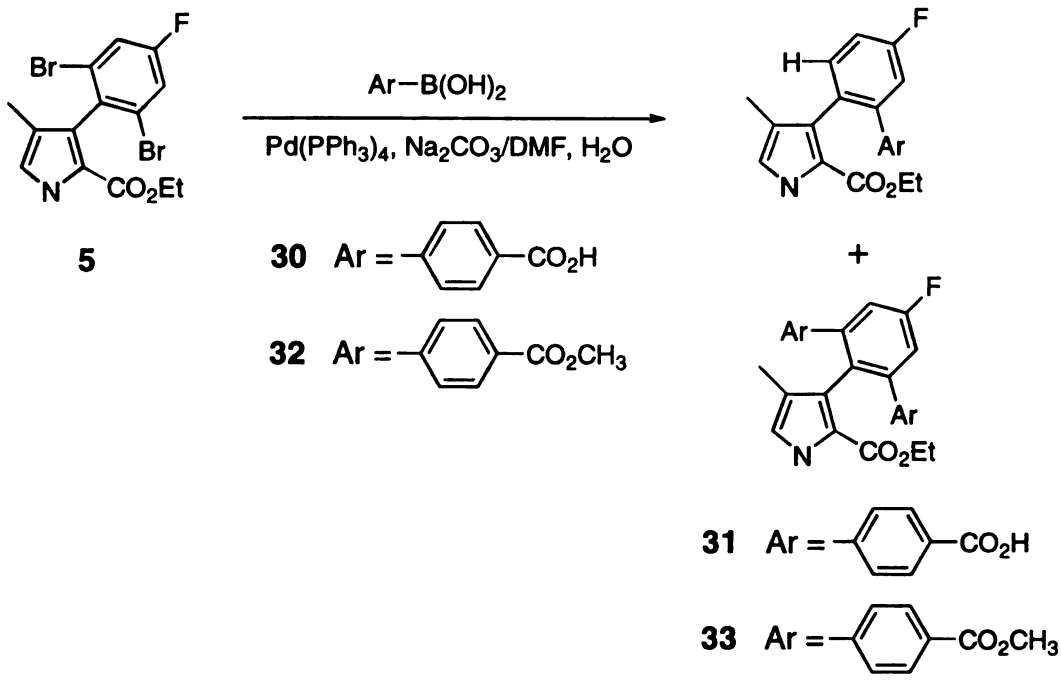

Scheme 3-1

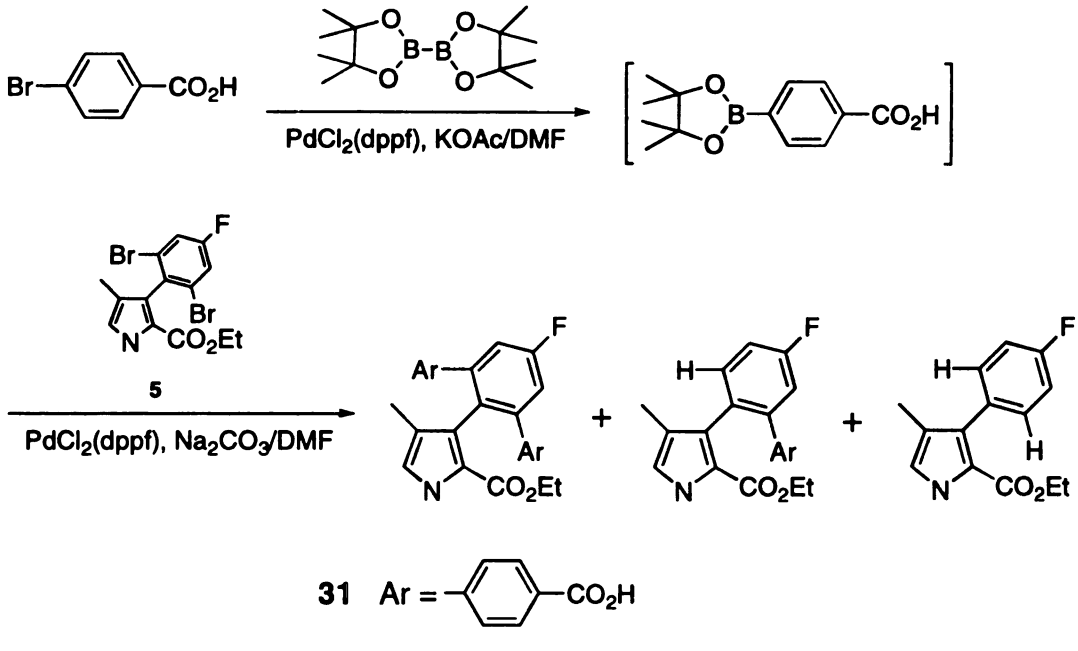

Scheme 3-2

for the preparation of Grignard reagent **36** since the reaction proceeded much slower than most of Grignard reactions and the use of 1.1 equivalent of Mg resulted in a low yield of the boronic acid. The reaction of Grignard reagent **36** and trimethyl borate gave the desired boronic acid **37** after hydrolysis with 10% $HCl_{(aq)}$. The work-up step for boronic acid **37** must be carried out carefully since the amphoteric product can dissolve in both acidic and alkaline solutions. We obtained crude boronic acid **37** after hydrolysis with 10% $HCl_{(aq)}$ and separation of organic layer from the reaction mixture followed by the removal of THF. The crude product, containing the protonated form of boronic acid **37**, was washed with saturated $NaHCO_{3(aq)}$ using ether as the solvent. After the removal of solvent, CH_2Cl_2 was added to the oily residue and the pure boronic acid was obtained in 44% yield upon heating on steam bath followed by filtration.

Several routes have been examined for the preparation of porphyrin **29**. In Scheme 3-4, pyrrole **38** was first prepared in 70% by Suzuki cross-coupling of pyrrole **5** and 2.5 equivalent of boronic acid **37** in the presence of $Pd(PPh_3)_4$ as catalyst. Porphyrin **40** was obtained in about 5 % yield from pyrrole **38**, after being reduced by Red-Al to give pyrrole **39**. Unfortunately, attempts to convert porphyrin **40** to porphyrin **41** with hydrogenation over Pd/C were unsuccessful. Thus, an alternative method was tested as shown in Scheme 3-5. Hydrogenation of pyrrole **38** in the presence of catalytic amount of Pd/C gave pyrrole **42**. Reduction of pyrrole **42** with Red-Al followed by cyclization gave only a small amount of porphyrin **41**, presumably due to the unprotected amine group. It was hoped that the protection of amine group by the reaction with acetic anhydride would result in an increase in the yield of the desired porphyrin. To test this idea, pyrrole **42** was converted to pyrrole **44** quantitatively by reacting with acetic anhydride (Scheme 3-6). Pyrrole ester **44** was then reduced to the corresponding pyrrole alcohol with Red-Al in THF. Unfortunately, under the reduction condition, the acetamide groups were readily reduced to the amine groups. After reacting with acetic anhydride and followed by cyclization, pyrrole **45** afforded the secondary acetamido

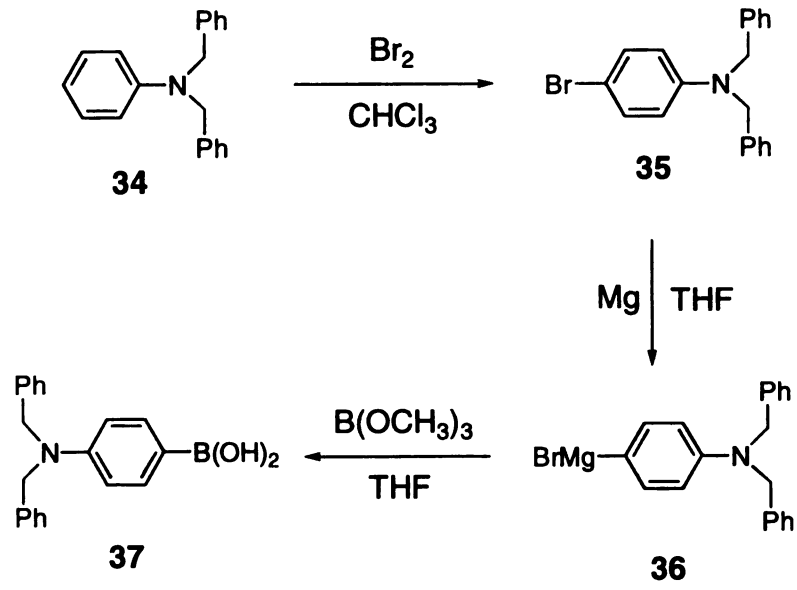
Ph
N
Ph
34
Br2
CHCl3
Br
N
Ph
Ph
35
Mg
THF
Ph
N
B(OH)2
Ph
37
B(OCH3)3
THF
BrMg
N
Ph
Ph
36

Scheme 3-3

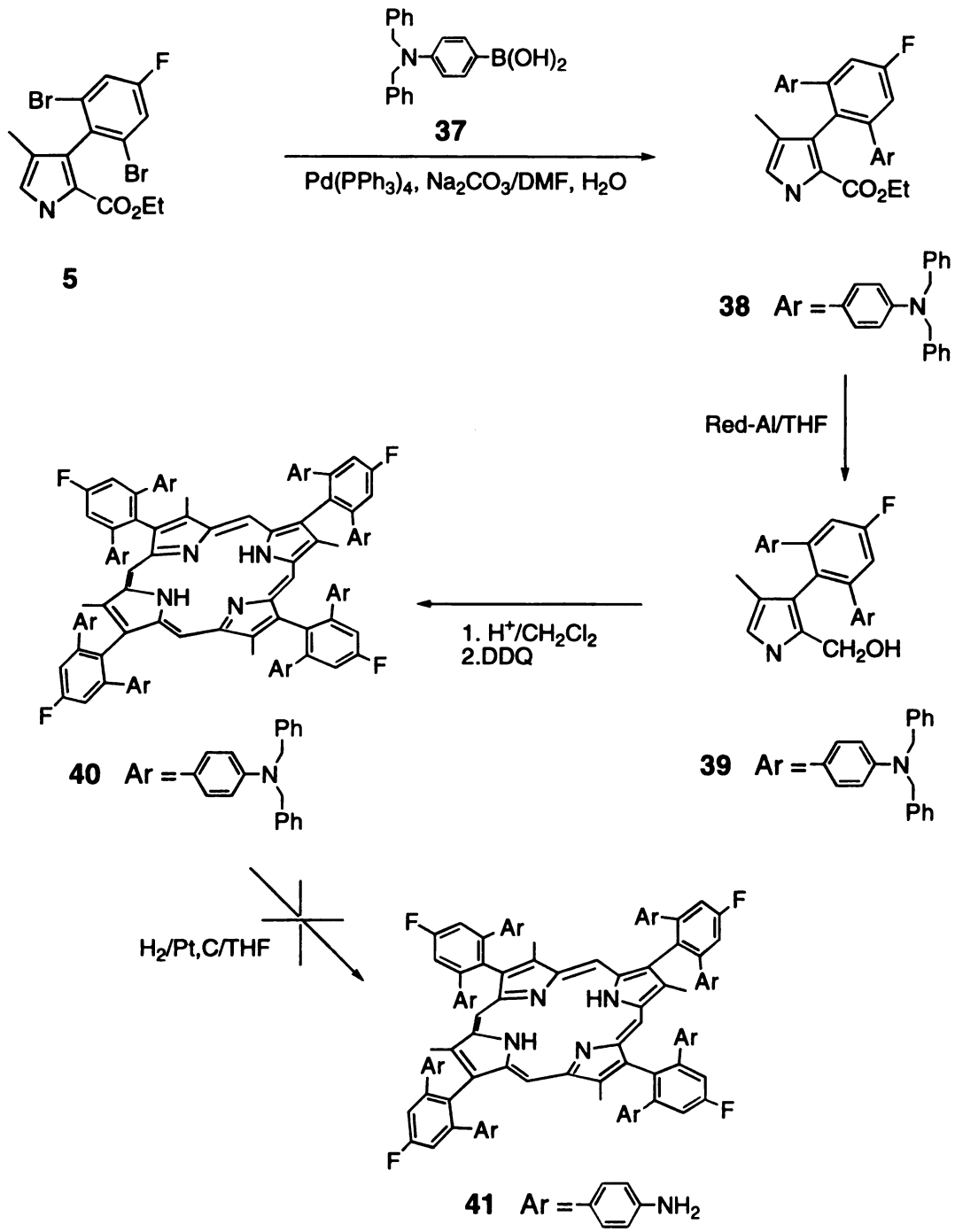
Ph
N
B(OH)2
Ph
37
Pd(PPh3)4, Na2CO3/DMF, H2O
Br
F
Br
N
CO2Et
5
Ar
F
Ar
N
CO2Et
38 Ar =
Ph
N
Ph
Red-Al/THF
Ar
F
Ar
N
CH2OH
39 Ar =
Ph
N
Ph
1. H+/CH2Cl2
2.DDQ
F
Ar
Ar
F
Ar
N
HN
Ar
NH
N
Ar
Ar
Ar
F
Ar
F
40 Ar =
Ph
N
Ph
H2/Pt,C/THF
F
Ar
Ar
F
Ar
N
HN
Ar
NH
N
Ar
Ar
Ar
F
Ar
F
41 Ar =
NH2

Scheme 3-4

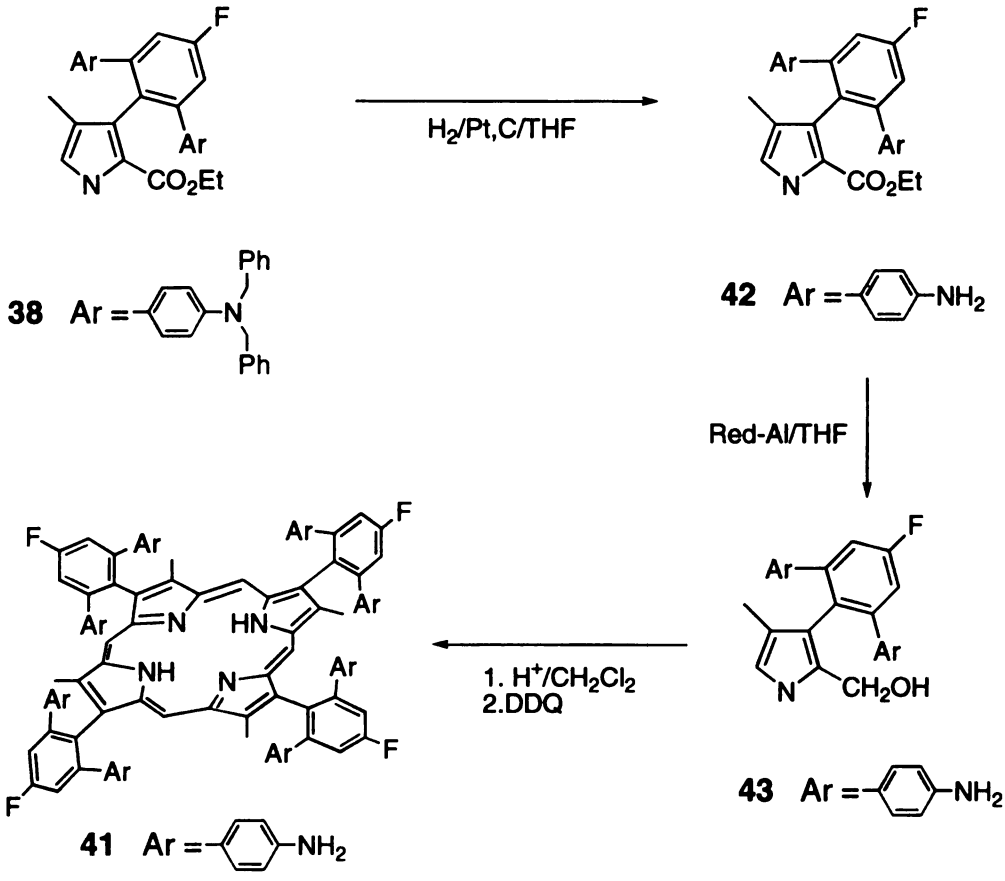
F
Ar
Ar
N
CO2Et
H2/Pt,C/THF
38 Ar =
Ph
N
Ph
42 Ar =
NH2
Red-Al/THF
43 Ar =
CH2OH
1. H+/CH2Cl2
2.DDQ
41 Ar =
NH2
HN
NH

Scheme 3-5

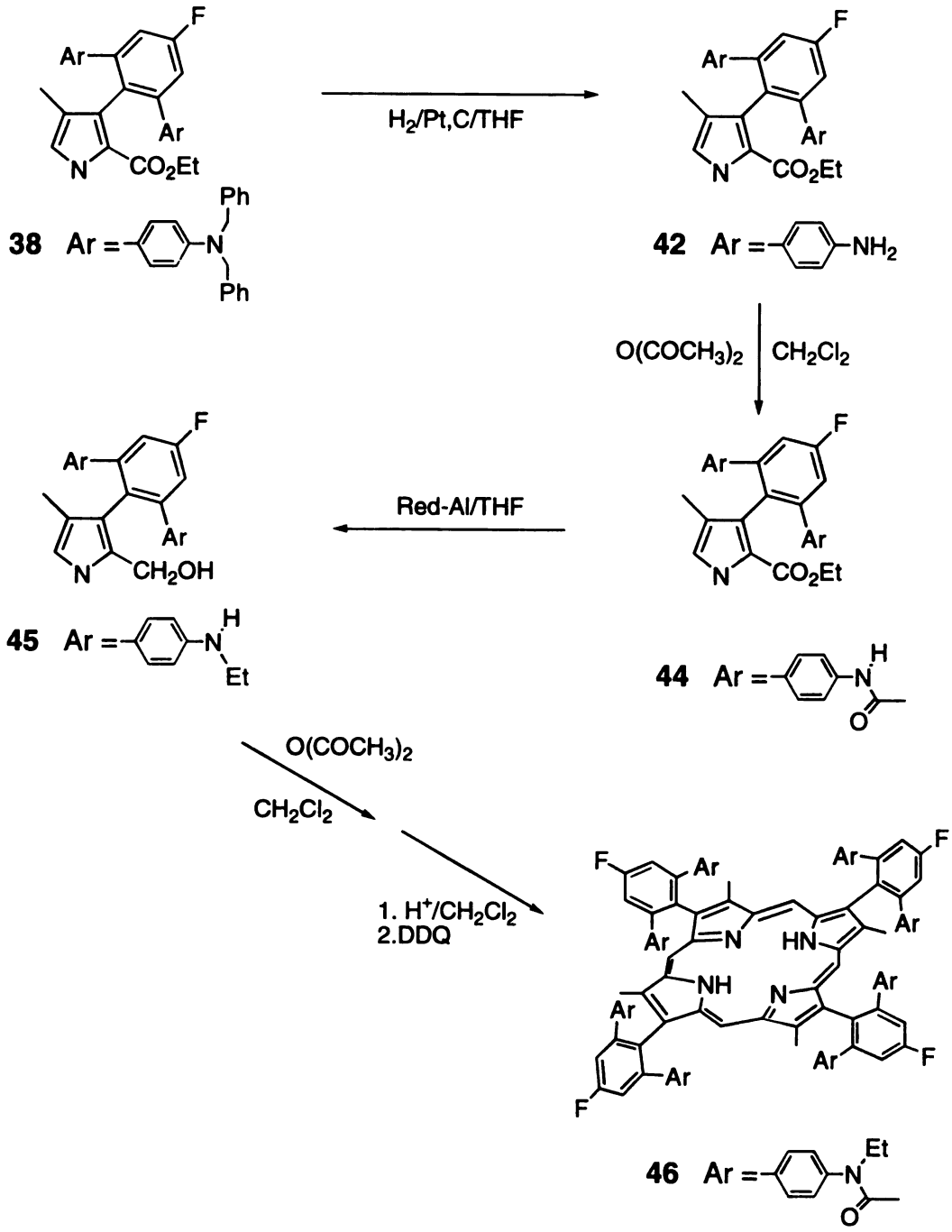
F
Ar
Ar
N
CO2Et
H2/Pt,C/THF
38 Ar =
Ph
N
Ph
42 Ar = NH2
O(COCH3)2
CH2Cl2
CH2OH
Red-Al/THF
45 Ar =
H
N
Et
44 Ar =
H
N
O
O(COCH3)2
CH2Cl2
1. H+/CH2Cl2
2.DDQ
NH
HN
N
46 Ar =
Et
N
O

Scheme 3-6

porphyrin **46** in 8% yield. Evidence supporting the formation of porphyrin **46** was given by mass and ^{1}H NMR spectra.

To counteract the unwanted reduction on amide groups, we therefore reduced pyrrole ester **42** to pyrrole alcohol **43** with Red-Al without the protection of amine groups (Scheme 3-7). As mentioned above, the presence of unprotected amine groups during the cyclization reaction resulted in an unsatisfactory yield of porphyrin. The protection of amines with acetyl groups was necessary for pyrrole alcohol **43** before cyclization. Pyrrole alcohol **47** was produced in *situ* by the treatment of pyrrole alcohol **43** with acetic anhydride in CH_2Cl_2 followed by cyclization in the presence of 3 equivalent of trimethoxymethane and a catalytic amount of trifluoroacetic acid gave about 6% of porphyrin **29** after oxidation with DDQ. Because the rather low yield of porphyrin **29** could be due to the low solubility of the intermediates formed during the cyclization reaction, we decided to change the solvent system to a 5:1 mixture of CH_2Cl_2 and acetic acid instead of CH_2Cl_2. With the new solvent system, the cyclization of pyrrole alcohol **47** employing Ono's method followed by oxidation with DDQ, column chromatography, and recrystallization afforded porphyrin **29** in 37% yield. The higher yield for porphyrin **29** compared to the most hindered porphyrins described in Chapter 2 could be ascribed to the presence of intramolecular hydrogen bonding among the amide groups. The solubility of porphyrin **29** is not good in organic solvents. However, in the presence of trifluoroacetic acid porphyrin **29** can be protonated as evidenced by UV-vis spectra, and thus dissolved in polar solvents such as CH_2Cl_2, $CHCl_3$, DMF, and methanol. Porphyrin **29** was characterized by mass, ^{1}H NMR, and IR spectroscopies. The ^{1}H NMR spectrum of **29** in $CDCl_3$ containing 1% TFA showed that the signal for the methyl groups of amides shifted upfield due to shielding of the porphyrin ring current. In the mass spectrum, consecutive cleavages of CH_3 and $HNCOCH_3$ was observed. The IR spectrum exhibited N-H and C=O stretching.

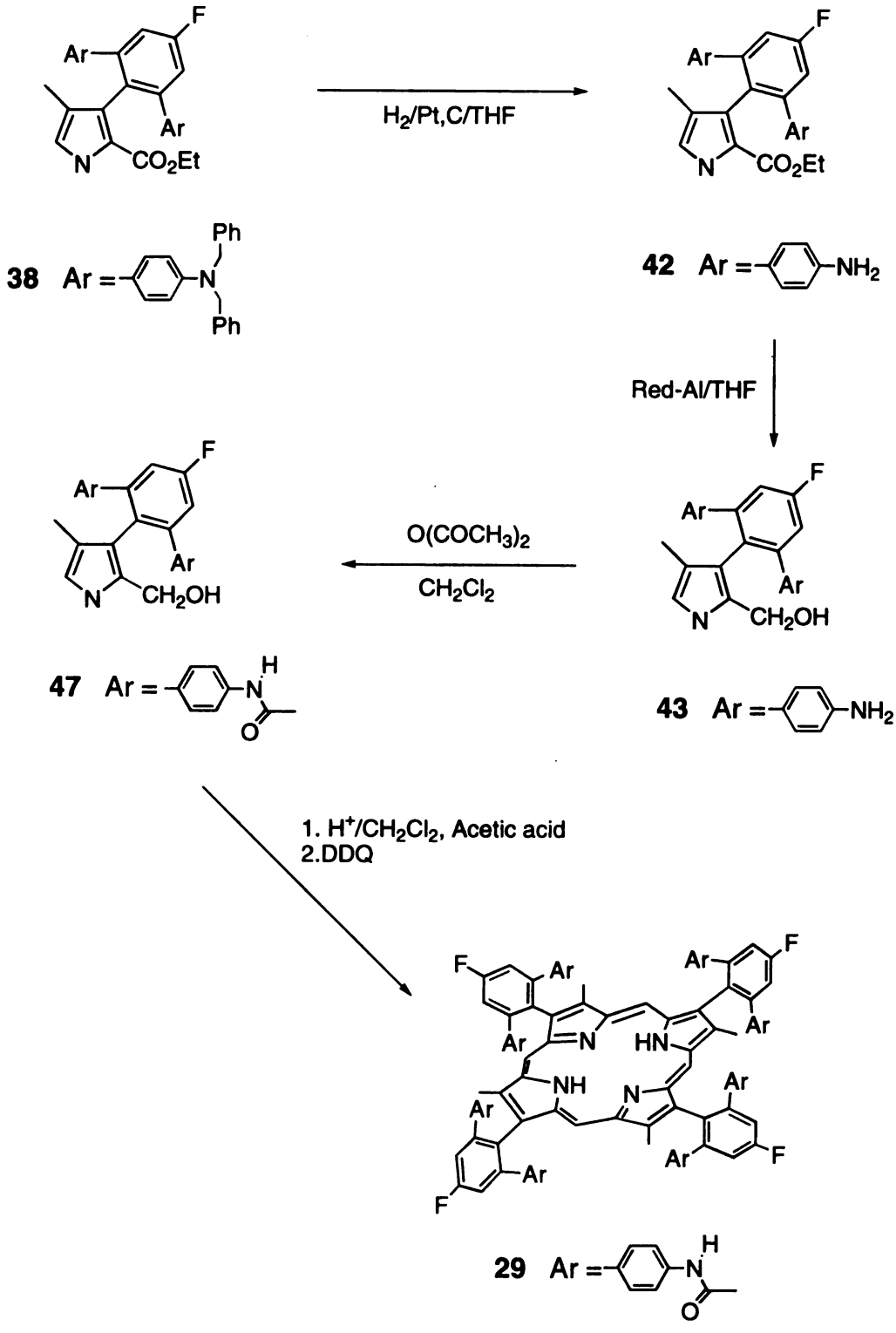
F
Ar
Ar
N
CO2Et
H2/Pt,C/THF
38 Ar =
Ph
N
Ph
42 Ar =
NH2
Red-Al/THF
CH2OH
O(COCH3)2
CH2Cl2
47 Ar =
H
N
O
43 Ar =
1. H+/CH2Cl2, Acetic acid
2.DDQ
HN
NH
29 Ar =

Scheme 3-7

The metallation of porphyrin **29** carried out with the typical method in DMF was unsuccessful since the rigid pockets created by the intramolecular hydrogen bonding did not allow the metal ions to approach the porphyrin center. Therefore, the removal of the amine protecting groups was necessary and it could be achieved by hydrolysis in a refluxing mixture of methanol and water in the presence of H_2SO_4 for 3 days (Scheme 3-8). After hydrolysis, the metal was inserted into the porphyrin in refluxing dry DMF in the presence of excess metal salt and pyridine. Without work-up, excess acetic anhydride was added to the reaction mixture and stirred for 2 hours at room temperature under a nitrogen atmosphere. The metalloporphyrin was purified by flash chromatography of Al_2O_3 eluting with a mixture of CH_2Cl_2 and methanol. The zinc and iron complexes of porphyrin **29** were recrystalized from CH_2Cl_2 and methanol and the manganese complex was recrystalized from CH_2Cl_2, methanol, and toluene. These metal complexes showed low solubility in organic solvent. However, the solubility increased when mixtures of solvents such as CH_2Cl_2 and methanol were used. The mass spectra of the metal complexes of porphyrin **29** also showed consecutive cleavages of CH_3 and $HNCOCH_3$ as observed for free base.

The insertion of Mn(III)Cl to the other β-substituted porphyrins for shape selective epoxidation was achieved by the reaction with $MnCl_2 \cdot 4H_2O$ in refluxing DMF. These manganese complexes showed considerable solubility in polar and nonpolar solvents and exhibited less solubility in alkanes.

X-ray Crystal Structure of Porphyrin 49

The crystal structure of porphyrin **49** consists of an independent porphyrin molecule, two solvated CH_3OH, and two solvated H_2O. Figure 3-4 shows the crystal structure of porphyrin **49**. Some of the solvated molecules are omitted for clarity. Table 3-1 shows the crystal data and refinement parameters. As shown in Figure 3-4, the macrocycle of pophyrin **16** is basically planar. Table 3-2 lists the average out-of-plane

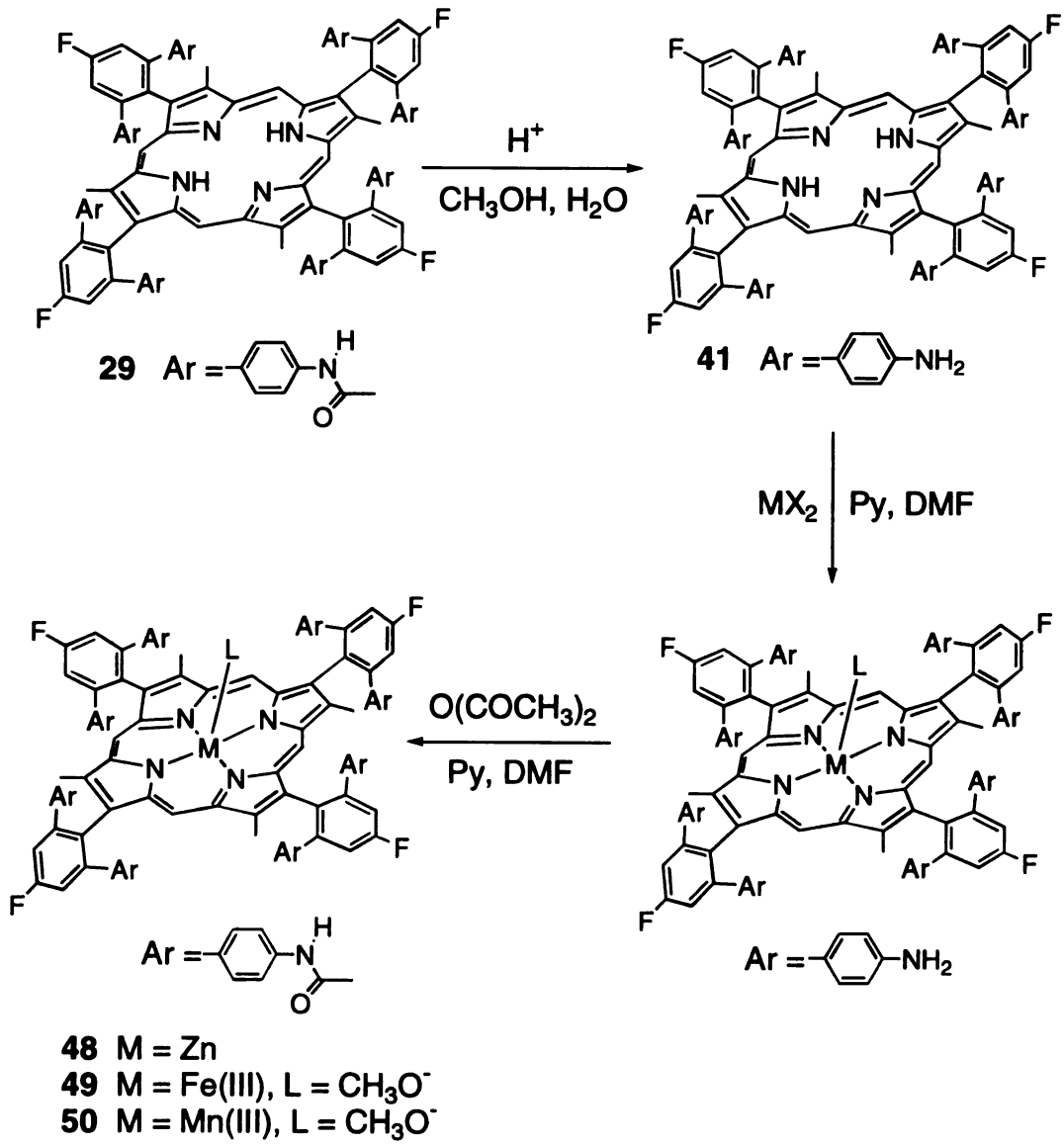
H+
CH3OH, H2O
29 Ar =
41 Ar = NH2
MX2 | Py, DMF
O(COCH3)2
Py, DMF
Ar =
Ar = NH2
48 M = Zn
49 M = Fe(III), L = CH3O-
50 M = Mn(III), L = CH3O-

Scheme 3-8

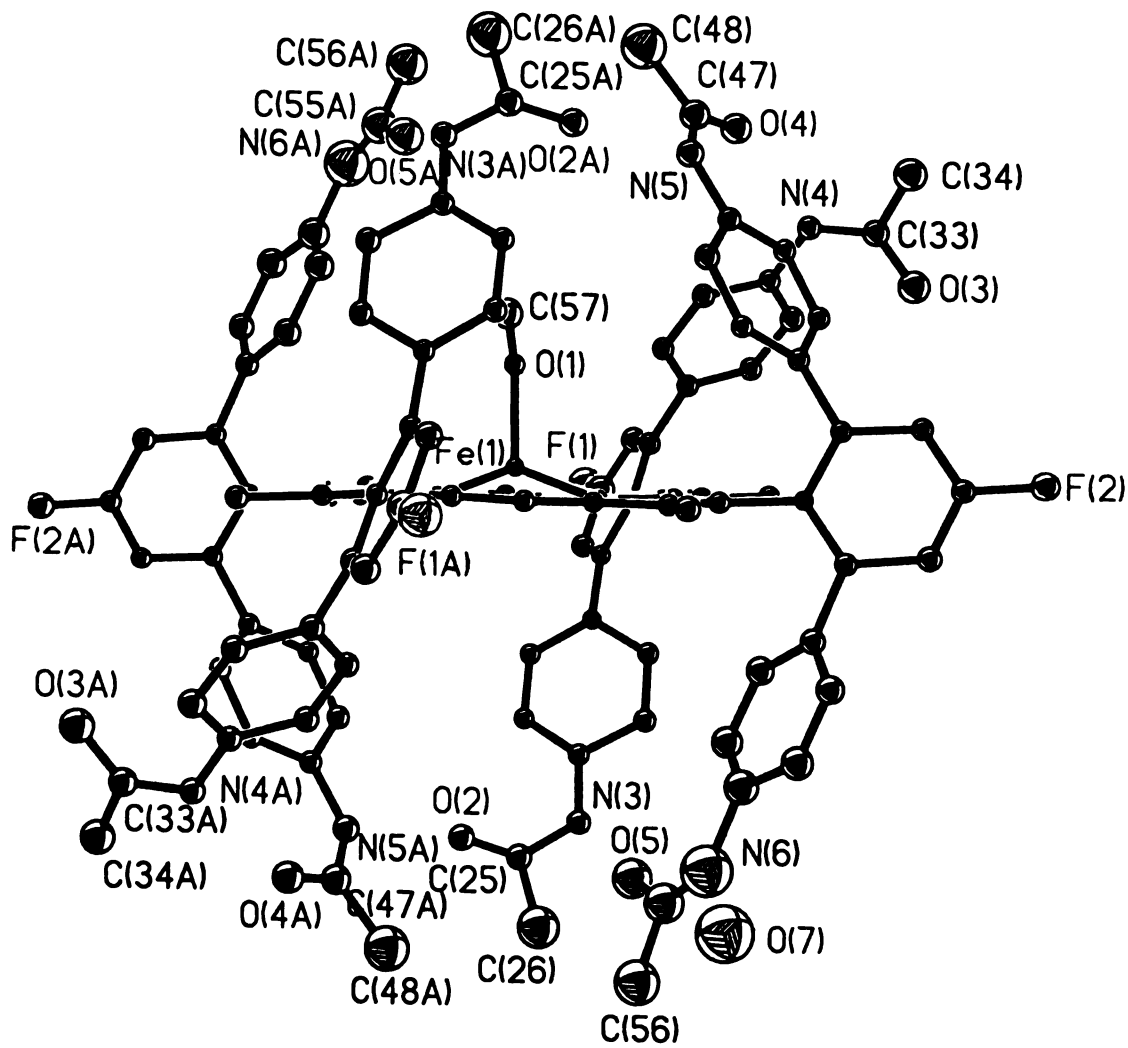

Figure 3-4. X-ray crystal structure of porphyrin **49**. Hydrogen atoms and some of the solvated molecules have been omitted for clarity.

Table 3-1. Crystal data, Intensity Measurements, and Refinement parameters for Porphyrin **49**.

Formula	$FeC_{115}H_{103}F_4N_{12}O_{13}$
Formula Weight	1,992.94
Crystal System	Triclinic
Space Group	$P2_1$
Temperature, K	120
a, Å	112.7762(5)
b, Å	13.7811(6)
c, Å	14.4907(5)
α	90.994(2)
β, deg	99.156(1)
γ	90.280(2)
V, Å^3	2,518.42(12)
Z	1
Crystal Dimensions, mm	0.2 x 0.07 x 0.06
D_{calcd}, g cm^{-1}	1.314
F(000)	1,043
θ range, deg	1.42 – 22.50
Transm Range	0.6891 – 0.9280
Reflection collected	16,490
No. of Unique Reflections	6,473
No. of Parameters	618
R; Rw[a]	0.1284; 0.3143
S	1.062

[a] $R = \Sigma||Fo|-|Fc||/\Sigma|Fo|$, $Rw = [\Sigma w (||Fo|-|Fc||)^2/\Sigma wFo^2]^{1/2}$.

Table 3-2. Average Out-of-Plane Displacements, Bond Lengths, and Bond Angles for Porphyrin **49**.

		Displacement (Å)[a]	
Fe	0.557	C_m	0.037
N	0.005	C_β	0.030
C_α	0.031		
		Bond Length (Å)	
Fe-O1	1.845	C_α-C_m	1.375
Fe-N	2.086	N-C_α	1.389
C_α-C_β	1.457	C_β-C_β	1.375
		Bond Angle (deg)	
Fe-O1-C57	129.2	C_m-C_α-C_β	125.5
N-Fe-N	85.9	N-C_α-C_m	124.0
N-C_α-C_β	110.5	C_α-C_β-C_β	106.7
C_α-N-C_α	105.6	C_α-C_m-C_α	127.6

[a] From the least-square plane of the 24 atoms.

displacements, bond lengths, and bond angles. The X-ray structure shows the occurrence of the intramolecular hydrogen bonding among the anilides, but they fall short of forming a circular lock. On each side of the porphyrin plane, one of the four amide groups rotates out to break the interlock, with the dihedral angle between the amide plane and the attached phenyl plane being about 43°. The reason for the tilting of the amide may be ascribed to the interference of the solvated molecules and/or the crystal packing forces. The X-ray structure shows that there is intermolecular hydrogen bonding between an amide and a solvated water, in which the distance of O7(H_2O)-N6(amide) is 2.794 Å. Even though the expected interlocking amide circle is interrupted, intramolecular hydrogen bonding interactions among the other amides are present. For example, the distances for O2-N5A and O4A-N4A are 2.894 and 2.957 Å, respectively. The intramolecular hydrogen bonding interactions of these amides still partially block the top of the pocket and partially constrain the rotation of the phenyl groups. The crystals for crystallography were grown from a mixture of CH_2Cl_2 and methanol. The use of the protic solvent could be the cause of the imperfection of the intramolecular hydrogen bonding. We believe that in nonprotic solvents better intramolecular hydrogen bonding interactions can be formed. This hypothesis seems to be borne out by the exceptionally high selectivity observed in the catalytic epoxidation reactions as discussed below.

Shape-Selective Epoxidation Reactions

The structures of the manganese porphyrins used for selective epoxidation are shown in Figure 3-5. The epoxidation reactions with the manganese porphyrins were performed in CH_2Cl_2 using iodosylbenzene as oxygen donor. To study the steric effects of our manganese porphyrins on the shape selective epoxidation of alkenes, both intra- and intermolecular selectivity tests were performed. In the first case, a series of non-conjugated dienes containing both internal and external C=C bonds were used to investigate the relative selectivity. In the second case, a series of 1:1 mixtures of *cis*-

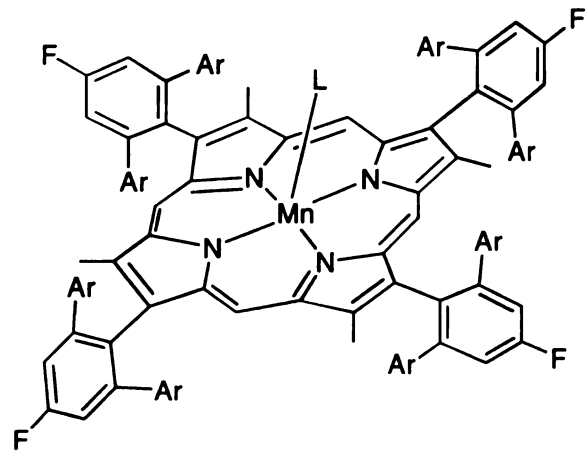

50 Ar = 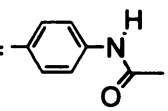 (Mn(TMTAP)(OMe))

51 Ar = 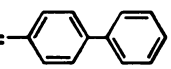 (Mn(TMTBPP)(Cl))

52 Ar = 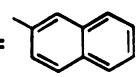 (Mn(TMTNP)(Cl))

53 Ar = 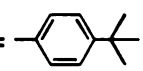 (Mn(TMTt-BP)(Cl))

54 Ar =  (Mn(TMTPP)(Cl))

Figure 3-5. Structures of the manganese complexes of β-substituted bis-pocket porphyrins.

cyclooctene and various alkenes with different sizes and shapes were employed for intermolecular selectivity. Control epoxidation reactions were carried out with Mn(TPP)(Cl). Figure 3-6 shows the data for the intramolecular epoxidation selectivity. The β-substituted bis-pocket porphyrins are more selective than Mn(TPP)(Cl) and Mn(T(2,4,6-OMeP)P)(OAc). Suslick et al. have reported the synthesis and shape selectivity of dendrimer porphyrins.[136] Our system exhibited selectivity similar to those dendrimer porphyrins. Among the β-substituted porphyrins, **50** (MnTMTAP) with intramolecular hydrogen bonding, shows the highest selectivity. Figure 3-7 shows the intermolecular selectivity for the various alkene mixtures with the β-substituted bis-pocket porphyrins. For unhindered catalysts, more preferential attack should occur at *cis*-cyclooctene than 1-alkenes. For hindered catalysts, one can expect that the relative reactivity of 1-alkenes increases. The intermolecular selectivity of β-substituted bis-pocket porphyrins is much higher than that of *meta*-substituted dendrimer porphyrins reported by Suslick.[136] Our system can be as much as thirty times more selective than Mn(TPP)(Cl), whereas *meso*-phenyl substituted dendrimer porphyrins, are only two to three times better than Mn(TPP)(Cl). Among these bis-pocket porphyrins, **50** shows the highest selectivity, indicating the intramolecular hydrogen bonds are doing their job in tying up the pockets above and below. Without intramolecular hydrogen bonding, **51** shows higher selectivity than the other porphyrins, indicating that the biphenyl groups hinder the pocket more effectively than *p-tert*-butylphenyl and 2-naphthyl groups.

Metalloporphyrins have a marked proclivity for self-destruction in oxidizing media. Generally, destructive oxidation occurs at the *meso*-carbon.[116] The oxidative stability of the metalloporphyrin can be increased by introducing steric hindered substituents at *meso*-positions and electron withdrawing groups at the periphery of the porphyrin. The system we studied here is *meso*-unsubstituted. One would expect that our system would show lower oxidative stability compared to *meso*-substituted porphyrins. The stability of

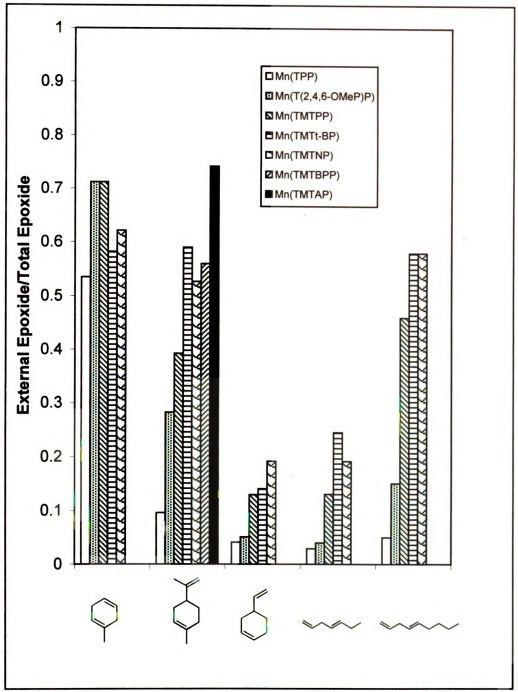

Figure 3-6. A plot of external epoxide to the total epoxide for intramolecular shape-selectivity of various Mn(III) porphyrin catalysts.

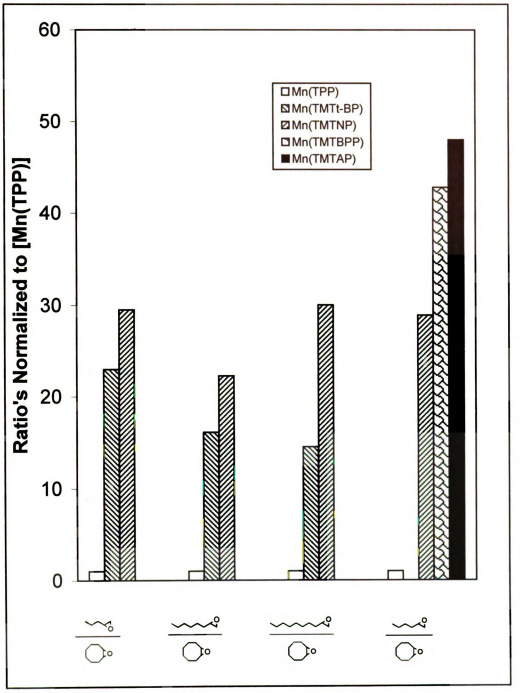

Figure 3-7. Epoxidation results for the intermolecular mixture of alkenes. The ratios of the epoxides were normalized to corresponding [Mn(TPP)(Cl)] values. Errors are estimated at 5% relative.

these β-substituted porphyrins was investigated in oxidizing media. The reactions were followed under pseudo-unimolecular conditions in dilute porphyrin solutions in benzene under argon. The stability of the porphyrin was monitored by the rate of bleaching of the Soret peak. Porphyrin concentrations were maintained around ~10 μM and ~10 mM in *m*-chloroperbenzoic acid. Mn(TPP)(Cl) shows an half-life of 5±0.5 min, while the porphyrins, **54**, **53** and **52** have half lives of 11 h, 13 h, and 15±0.5 h, respectively. Surprisingly, our system shows high oxidative stability comparable to that of the extremely hindered Mn(T(2,4,6-PhP)P)(OAc) (half-life, 25 h). We also carried out the reaction of the nickel complex of porphyrin **16** and Fe(F_{20}TPP)(Cl) in the presence of iodosybenzene in benzene under an argon atmosphere. Catabolic oxidation of the nickel porphyrin at *meso*-carbons was not observed. Instead, one of the methyl groups at β-positions was converted to aldehyde or carboxylic acid under the oxidative media. The results indicate that the steric protection of the metal center prevents self-destruction of the catalyst, and thus increases the oxidative stability of these β-substituted porphyrins. The reactivity of these β-substituted porphyrins are similar to that of unhindered catalyst, Mn(TPP)(Cl). Turnover numbers (i.e., mol product/mol metalloporphyrins/s) observed for the bis-pocket porphyrins studied here are in the range of 1 to 3 sec^{-1} comparable to 3 to 4 sec^{-1} of Mn(TPP)(Cl).

Figures 3-8, 3-9, and 3-10 show the computer-generated molecular models of the free base of bis-pocket porphyrins, **54**, **53**, and **50**. Porphyrin **54** has a ~0.5 nm pocket on both faces of the porphyrin while it is limited in the case of **50** and **53**. All of the bis-pocket porphyrins show negligible cavities along their sides. Furthermore, porphyrin **50** shows perfect intramolecular hydrogen bonding between the *para*-carboxamido groups, even though the X-ray crystal structure of the iron complex shows that one pair of the amide groups did not align perfectly. The intramolecular hydrogen bonding obviously can hold the substituents in position completely blocking top access and limiting sideway approach to the metal center. In contrast to the dendrimer porphyrins, the more crowded

Top View

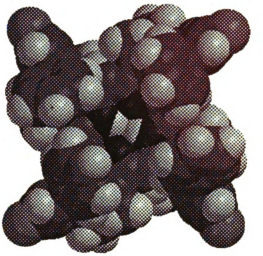

Side View

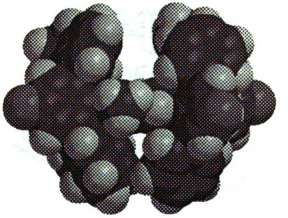

Figure 3-8. Computer-generated molecular models of the free base of **54**. The top view shows a cavity of around 5 Å on both faces of the porphyrin. The side view shows a negligible cavity.

Top View

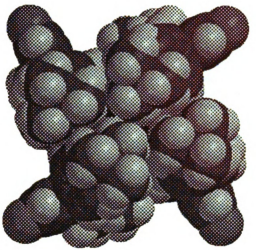

Side View

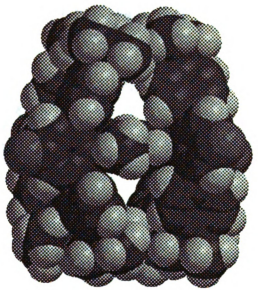

Figure 3-9. Computer-generated molecular models of the free base of **53**. The top and side views show the pockets are fully blocked

Top View

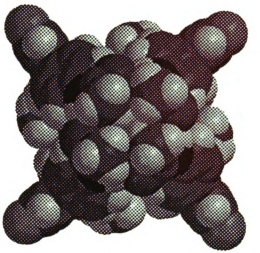

Side View

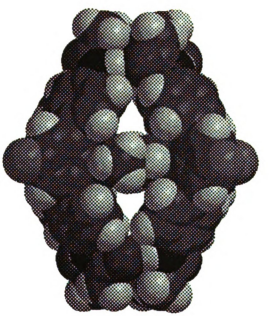

Figure 3-10. Computer-generated molecular models of the free base of **50**. The top view shows perfect intramolecular hydrogen bonding between amide groups. Both top and side views show the pockets are fully blocked.

porphyrins, **50**, **51**, **52**, and **53**, show reduced openings on both top and side ways. However, due to the higher flexibility in the β-substituents for these porphyrins, there are many conformations possible that would open up the pocket for the incoming alkene. The lower selectivity of **51**, **52**, and **53** relative to **50** indicates that free rotation of the substituents without hydrogen bonding would open up a bigger cavity than that of acetalinide groups with hydrogen bonding. These molecular modeling studies are consistent with the high shape-selectivity of these β-substituted porphyrins in the catalytic epoxidation reactions.

Shape-Selective Ligation

In the shape-selective ligation studies, we employed the zinc complexes of our β-substituted porphyrins as hosts since they are 5-coordinated in the presence of bases. The insertion of zinc was accomplished by the reaction of free bases with zinc salt in refluxing DMF. The structures of zinc porphyrins used for the shape-selective ligation are shown in Figure 3-11. Various substituted pyridines and primary amines were chosen to probe the shape-selectivity on ligation. As an example, Figure 3-12 shows the spectral changes of zinc porphyrin **58** at the Soret band at various 4-phenylpyridine concentrations in toluene. Upon addition of 4-phenylpyridine, the Soret band at 419 nm shifts to 431 nm with clean isosbestic points. The equilibrium constant (K_{eq}) can be obtained from the plot of [base]/ΔA versus [base] as shown in the inset of Figure 3-12.[175] In each case, the plot gave a straight line with an intercept equal to $1/K_{eq}$.

Figure 3-13 shows the binding constants of β-substituted zinc porphyrins and Zn(TPP) with various nitrogenous ligands. All zinc porphyrins bind *para*-substituted amines (e.g., 4-phenylpyridine) better than *meta*-substituted ones (e.g., 3-phenylpyridine) due to the steric interactions between the *meta*-substituent and the β-substitutents on the porphyrin. The decreased K_{eq}'s of the zinc porphyrins binding to 3-chloropyridine and 3-bromopyrindine can be ascribed to both steric interaction and electron defficiency on

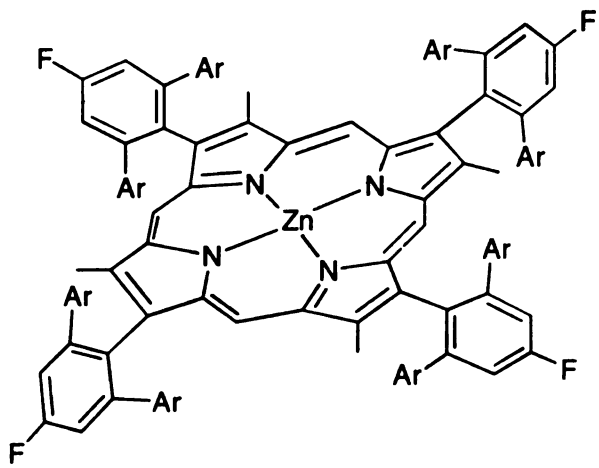

55 Ar =  (Zn(TMTPP))

56 Ar = 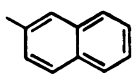 (Zn(TMTNP))

57 Ar = 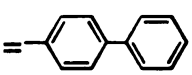 (Zn(TMTBPP))

58 Ar = 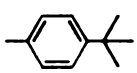 (Zn(TMTt-BP))

Figure 3-11. Structures of the zinc complexes of β-substituted porphyrins for shape-selective ligation.

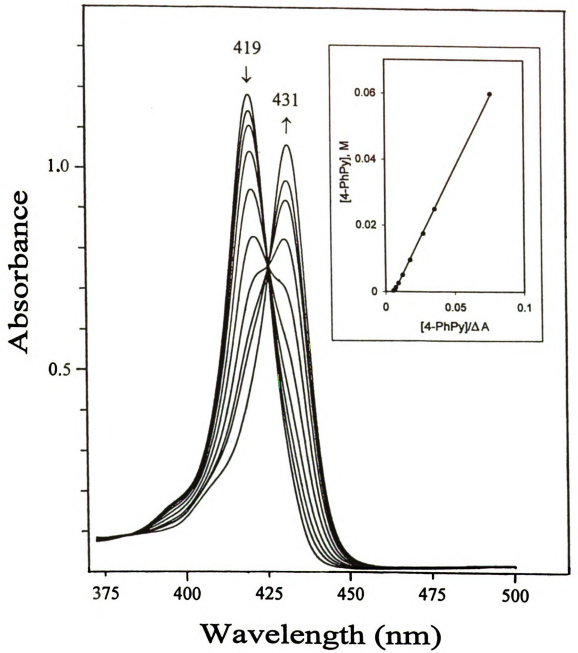

Figure 3-12. Spectral changes of **58** in the Soret band region in toluene upon titration with 4-phenylpyridine. Inset: Plot of 4-phenylpyridine concentration versus 4-phenylpyridine divided by absorbance changes at 431 nm.

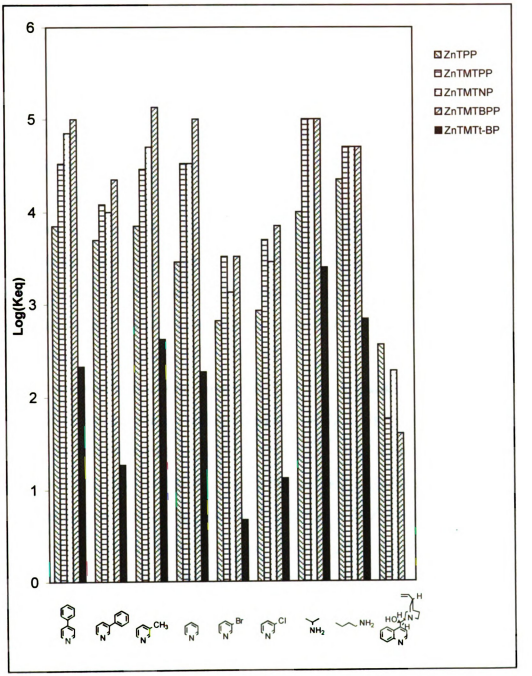

Figure 3-13. Ligand binding constants for β-substituted zinc porphyrins relative to Zn(TPP). Errors in Keq values are less than ±10%.

the pyridine ring. As expected, compared to Zn(TPP), zinc porphyrins **55**, **56**, and **57** exhibit higher affinities to both aromatic and alkyl amines due to the hydrophobic pockets, whereas the more closed-pocketed zinc porphyrin **58**, as the molecular models shown in Figures 3-9, exhibits a lower affinity to the bases. The computer-generated molecular models show the steric interactions between the phenyl group of the ligand and the *tert*-butyl groups of the porphyrin upon binding with 4-phenylpyridine (Figure 3-14). When a bigger ligand, cinchonidine, was used the β-substituted zinc porphyrins showed lower K_{eq}'s compared to Zn(TPP). Moreover, zinc porphyrin **58** does not bind cinchonidine at all as evidenced by the UV-vis spectrum, which did not change upon addition of cinchonidine. The discrimination between small and big ligands for these bis-pocket porphyrins is consistent with the difference in the pocket size and shape around the binding center. These results are also consistent with those of dendrimer-zinc porphyrins reported by Suslick.[175]

It is noteworthy that zinc porphyrin **57** shows the highest affinities to aromatic amines and about the same binding constants to alkyl amines as compared to zinc porphyrins **55** and **56**, even though the computer-generated molecular model of the free base shows much more restrictions on both top and side approaches (Figure 3-15). The high binding constants of zinc porphyrin **57** with substituted pyridine can be ascribed to π-π interactions. As an example, Figure 3-16 shows π-π interactions between the aromatic ring of the ligand and the aromatic substituents of the porphyrin. The presence of π-π interactions is further confirmed by the similar binding ability of **55**, **56**, and **57** to alkyl amines, which do not have aromatic rings for π-π interactions with the aromatic rings on porphyrins. Thus, the size of the pocket is not the only factor that influences the binding of amines to the porphyrins.

Top View

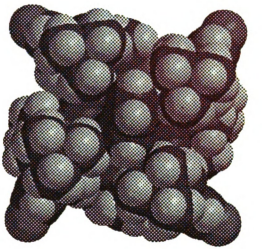

Side View

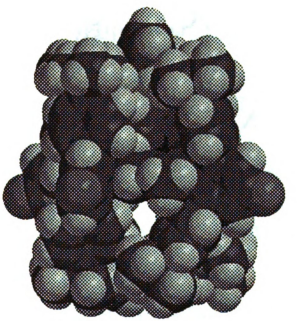

Figure 3-14. Computer-generated molecular models of the **58**-4-phenylpyridine complex. The models show the steric interactions between the phenyl group of the ligand and the *tert*-butyl groups of the porphyrin.

Top View

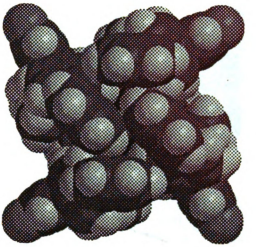

Side View

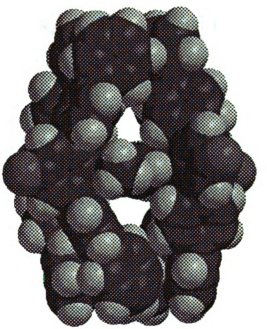

Figure 3-15. Computer-generated molecular models of **57**. The top and side views show the pockets are fully blocked.

Top View

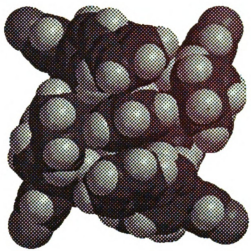

Side View

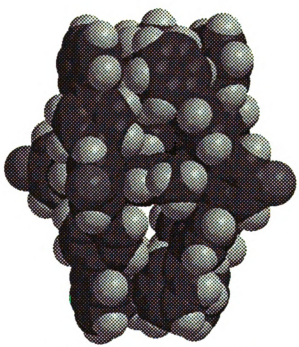

Figure 3-16. Computer-generated molecular models of the **57**-4-phenylpyridine complex. The model of the complex shows the π-π interactions between the phenyl group of the ligand and the phenyl groups of the porphyrin.

Conclusions

Shape-selective epoxidation of alkenes has been carried out by using sterically hindered manganese porphyrins as catalysts. The size of the shielding superstructures is responsible for the shape selectivity. The moderately hindered porphyrin, **54**, shows a cavity size of ~ 0.5 nm on the top, which allows the substrate to approach the reaction center. The more crowded porphyrins, **50**, **51**, **52**, and **53**, have more restricted access on both the top and sides. However, larger sideway openings created by conformational changes of the shielding wings may allow easier access to the reaction center. Higher selectivity is observed with the increase in steric crowding on both the face and sides of the porphyrins. Moreover, porphyrin **50** shows the highest shape-selectivity due to intramolecualr hydrogen bonding. In our system, the steric protection of the active site by substituents at β-positions also increases the stability of catalysts during the oxidation reacitons.

The β-substituted zinc porphyrins show shape-selectivity on ligation with various amines having different sizes and shapes. The hydrophobic pockets of the porphyrins can stabilize the coordinating ligand, thus showing higher binding constants than those of Zn(TPP). While the size of the pocket of the porphyrin reflects on the selectivity for ligation to small and bulky ligands, other interactions such as π-π stacking also play an important role in the shape selectivity of ligation.

Experimental

Materials

All reagents and solvents were obtained from commercial sources and were used without further purification unless otherwise noted. Dichloromethane was distilled over CaH_2 under N_2 atmosphere. THF was distilled over Na/benzophenone. All the 1-alkenes and dienes were purchased from Aldrich and were used as received. Silica gel was of 60-200 mesh, manufactured by Fisher Scientific. Analytical TLC was performed on

Eastman Kodak 13181 silica gel sheets. Compositions of solvent mixtures are quoted as ratios of volume.

Instrumentation

^{1}H NMR (300 MHz) spectra were recorded on a Varian Gemini spectrometer. Chemical shifts were reported in ppm relative to the residual proton in deuterated chloroform (7.24 ppm). Absorption spectra were recorded on a Shimadzu UV-160, or Varian Carry 219 spectrometer. Mass spetra were obtained on a benchtop VG Trio-1 mass spectrometer. FAB-MS mass spectra were obtained on a JEOL HX-110 HF double focusing spectrometer operating in the positive ion detection mode. The epoxidation products were analyzed using a Varian GL 3700 series capillary gas chromatograph and a Hewlett-Packard GCMS. Energy minimized structures of β-pyrrole substituted porphyrins were performed on an Indigo Silicon Graphics System using Spartan software packages.

Crystallography

Crystals of porphyrin **49** were grown from a mixture of CH_2Cl_2 and methanol by slow evaporation. To prevent solvent evaporation, the chosen crystal was coated with hydrocarbon oil and mounted on a Nonius CAD4 diffractometer with graphite-monochromated Mo Kα radiation. The crystal structure was solved by direct methods and refined by full matrix least-squares using the NRCVAX program. All non-hydrogen atoms were refined anisotropically, while hydrogen atoms were refined isotropically. Crystallographic details for the structure are given in Table 3-1.

Epoxidation Reactions

All epoxidation reactions were performed in CH_2Cl_2 under an argon atmosphere. Iodosylbenzene was employed as the oxygen donor. Standard epoxides were obtained

from Aldrich or synthesized from reported procedures. Epoxidation reactions were carried out in CH_2Cl_2 (1 ml) solution containing 1 μM of catalyst, 0.5 mM of alkene and 10-20 μM of iodosylbenzene. The reaction mixture was vigorously stirred at room temperature for 30 min under argon. To this solution an internal standard, *n*-decane or *n*-octane was added and the products were analyzed by GC and GCMS. Control epoxidation reactions were performed with Mn(TPP)(Cl) under similar conditions. In all cases, the yields of the epoxides were greater than 70% based on the amount of iodosylbenzene employed.

4-Bromo-N, N-dibenzylaniline (35)

To the solution of dibenzylaniline **34** (50.00 g, 0.183 mol) in 125 ml of $CHCl_3$ at 0 °C was added a solution of Br_2 (29.38 g, 0.183 mol) in 125 ml of $CHCl_3$ through an addition funnel. After the addition of Br_2 was completed, the solution was stirred at room temperature for 10 min. The reaction mixture was then washed with $Na_2CO_{3(aq)}$. The organic layer was separated and dried over anhydrous Na_2SO_4 and then the solvent was removed in *vacuo*. The crude product was recrystallized from CH_2Cl_2 and methanol to give 60.6 g (94%) of **35**. m.p. 125-126 °C; ^{1}H NMR (300 MHz, $CDCl_3$): δ 7.40-7.15 (12H, m, phenyl), 6.59 (2H, d, phenyl), 4.64 (8H, s, CH2); MS found m/e 351.1, cacld. 351.06 for $C_{20}H_{18}BrN$; Anal. found: C, 68.96; H, 5.03; N, 3.59. cacld: C, 68.18; H, 5.15; N, 3.98. for $C_{20}H_{18}BrN$.

4-(N, N-Dibenzylaminophenyl)boronic acid (37)

The arylboronic acid was prepared by standard Grignard techniques. Mg (39.50 g, 1.72 mol) was placed in a 500 ml three-necked round-bottomed flask equipped with a reflux condenser and mechanical stirrer. The system was flushed with nitrogen for 20 min while the Mg and flask were heated with a heating mantle. The apparatus was cooled and 4-bromo-N,N-dibenzylaniline **35** (60.60 g, 0.172 mol) was added to THF (250 ml) in the

reaction flask. The resulting mixture was refluxed for 4 hr and then transferred to an addition funnel. Under argon the Grignard reagent was slowly added to a solution of trimethyl borate (21.5 ml, 0.189 mol) in THF (250 ml) cooled at –78 °C. The solution was stirred overnight at room temperature. After acidification with 50 ml of 10% $HCl_{(aq)}$, the organic layer was separated from the mixture. THF was then removed in *vacuo*. The oily residue was dissolved in ether and washed with saturated $NaHCO_{3(aq)}$. The organic layer was collected and dried over anhydrous Na_2SO_4. After removal of the solvent, 100 ml of CH_2Cl_2 was added to the crude product and heated on steam bath. The precipitates were filtered to give 23.8 g (43.6%) of boronic acid **37**. ^1H NMR (300 MHz, $CDCl_3$): δ 8.00 (2H, d, phenyl), 7.40-7.30 (10H, m, phenyl), 6.82 (2H, d, phenyl), 4.73 (8H, s, CH_2); Anal. found: C, 78.69; H, 6.01; N, 4.18. cacld: C, 75.67; H, 6.36; N, 4.42 for $C_{20}H_{20}BNO_2$.

Ethyl 4-methyl-3-(2,6-bis(4-(N,N-dibenzylaminophenyl))-4-fluorophenyl)-2-pyrrole-carboxylate (38)

A mixture of pyrrole **5** (1.00 g, 2.47 mmol), boronic acid **37** (1.97 g, 6.2 mmol), and $Pd(PPh_3)_4$ (200 mg, 0.17 mmol) in 25 ml DMF containing 5 ml 2M $Na_2CO_{3(aq)}$ was purged with N_2 for 10 min. The solution was gently refluxed under N_2 for 2 d. The reaction mixture was then cooled to room temperature and the inorganic solids were removed by filtration. The filtrate was concentrated in *vacuo*, and then extracted with CH_2Cl_2. The solvent was dried over anhydrous Na_2SO_4 and removed under reduced pressure. The product was separated by column chromatography on silica gel eluting with CH_2Cl_2 and hexanes (4:6) to give 4.1g (70%) of pyrrole **38**. The product for analysis was recrystalized from CH_2Cl_2 and methanol. m.p. 197-198 °C; ^1H NMR (300 MHz, DMSO-d_6): δ 11.05 (1H,br d, NH), 7.35-7.10 (20H, m, phenyl), 6.93 (2H, d, phenyl), 6.75 (4H, d, phenyl), 6.51(1H, d, pyrryl), 6.45 (2H, d, phenyl), 4.58 (8H, s,

CH_2), 3.79 (2H, q, CH_2 of ethyl), 1.35 (3H, s, CH_3), 0.86 (3H, t, CH_3 of ethyl); MS found m/e 789.1, cacld. 790. for $C_{54}H_{48}FN_3O_2$.

Ethyl 4-methyl-3-(2,6-bis(4-aminophenyl)-4-fluorophenyl)-2-pyrrolecarboxylate 42.

To a solution of pyrrole **38** (790 mg, 1 mmol) in dried THF (30 ml) was added 10% palladium on charcoal (50 mg). The mixture was deaerated first and hydrogenated at room temperature under 1 atm of pressure. After stirring for 24 h, the reaction mixture was filtered, the solvent was removed in *vacuo* and the residue was chromatographed on silica gel eluting with CH_2Cl_2 and methanol (50:1). The crude product was recrystallized from CH_2Cl_2 and toluene to give 352 mg (82%) of **38**. m.p. 145-148 °C; ^{1}H NMR (300 MHz, $CDCl_3$): δ8.65 (1H,br s, NH), 6.99 (2H, d, phenyl), 6.85 (4H, d, phenyl), 6.45 (5H, m, pyrryl and phenyl), 3.99 (2H, q, CH_2 of ethyl), 3.55 (4H, br s, NH_2), 1.03 (3H, t, CH_3 of ethyl); MS: found m/e 429.2, cacld. 429.49 for $C_{26}H_{24}FN_3O_2$.

Ethyl 4-methyl-3-(2,6-bis(4-acetanilino)-4-fluorophenyl)-2-pyrrolecarboxylate (44)

Excess acetic anhydride was added to a solution of pyrrole **42** (430 mg, 1 mmol) in 5 ml of CH_2Cl_2. The resulting mixture was stirred at room temperature under nitrogen. After stirring for 20 min, the reaction mixture was filtered to give the product quantitaitvely. m.p. >260 °C; ^{1}H NMR (300 MHz, DMSO-d_6): δ 11.14 (1H,br s, NH of pyrrole), 9.86 (2H, br s, NH of amide), 7.37 (4H, d, phenyl), 7.10 (2H, d, phenyl), 6.95 (4H, d, phenyl), 6.52 (1H, d, pyrryl), 3.91 (2H, q, CH_2 of ethyl), 2.00 (6H, s, CH_3 of amide), 1.43 (3H, s, CH_3), 0.97 (3H, t, CH_3 of ethyl); MS: found m/e 513.1, cacld. 513.57 for $C_{30}H_{28}FN_3O_4$.

2,7,12,17-Tetramethyl-3,8,13,18-tetrakis(2,6-bis(4-acetanilino)-4-fluorophenyl)-porphyrin (29)

To a 30 ml THF solution of pyrrole **42** (430 mg, 1 mmol) was dropwise added Red-Al (6 ml, 65% in toluene, 20 mmol) at 0 °C under argon. When the addition of Red-Al was

complete, the mixture was returned to room temperature and stirred for 6 hr. To the resulting solution was added 40 ml of CH_2Cl_2. The excess Red-Al was destroyed by the addition of ice at 0 °C. The liquid layer was washed with water twice. The organic layer was separated, dried over Na_2SO_4, and concentrated under reduced pressure to give white solid. Without further purification, the white solid was added to 50 ml of CH_2Cl_2. To the solution was added acetic anhydride (0.51 g, 5 mmol) and the resulting solution was stirred at room temperature under nitrogen. After stirring for 10 min, acetic acid (10 ml) was added to the solution followed by the addition of dimethoxymethane (0.28 ml, 3 mmol) and trifluoroacetic acid (23 mg, 0.2 mmol). After stirring overnight under nitrogen, DDQ (227 mg, 1 mmol) was added and the solution was stirred for a further hour. The solvent was removed in *vacuo* to give a dark residue. The residue was chromatographed on silica gel eluting with a mixture of CH_2Cl_2, methanol, and trifluoroacetic acid (200:20:1). The purple fraction was collected and recrystallized from CH_2Cl_2, methanol and trifluroacetic acid to give 167 mg (37%) of porphyrin. IR: ν_{max} 3314 (N-H), 1674 (C=O) cm-1; UV-vis (0.2% TFA in CH_2Cl_2, λ_{max} nm (ε)): 605 (12,400), 564 (20,600), 412 (160,300); ^{1}H NMR (300 MHz, 1% TFA in $CDCl_3$): δ 10.02 (4H, s, *meso*), 8.04 (8H, s, NH of amide), 7.49 (8H, d, phenyl), 6.90 (16H, d, phenyl), 6.70 (16H, d, phenyl), 3.12 (12H, s, CH_3), 1.92 (24H, s, CH3 of amide), -3.70 - -4.2 (3H, 2 br s, N-H); MS (FAB): found m/e 1710.6, 1725.8, 1737.0, 1750.5, 1766.5, 1779.0, 1792.5, 1809.7 (M^++1), 1825.0, 1831.9, cacld. 1808.02. for $C_{112}H_{90}F_4N_{12}O_8$.

2,7,12,17-Tetramethyl-3,8,13,18-tetrakis(2,6-bis(4-aminophenyl)-4-fluorophenyl) porphyrin (41)

Porphyrin **29** (180 mg, 0.1 mmol) was added to a mixture of methanol, H_2SO_4, and water (90:12:1). After the solution was refluxed for 24 h under nitrogen, 2 ml of water was added and the resulting mixture was refluxed for 48 h. The solution was cooled in an ice bath and neutralized with NaOH(aq). The mixture was filtered and the solid was washed

with water to give the hydrolyzed porphyrin quantitatively. UV-vis (5% MeOH in CH_2Cl_2, λ_{max} nm (rel intens)): 636 (0.05), 581 (0.06), 551 (0.10), 515 (0.11), 421 (1.00); ^{1}H NMR (300 MHz, DMSO-d_6): δ 9.21 (4H, s, *meso*), 7.39 (8H, d, phenyl), 6.65 (16H, d, phenyl), 5.81 (16H, d, phenyl), 4.50 (16H, s, NH_2), 2.78 (12H, s, CH_3); MS (FAB): found m/e 1473.3, cacld. 1471.72 for $C_{96}H_{74}F_4N_{12}$.

Zn(II) 2,7,12,17-Tetramethyl-3,8,13,18-tetrakis(2,6-bis(4-acetanilino)-4-fluoro-phenyl)porphyrin (48)

Porphyrin **41** (30 mg, 0.02 mmol), $Zn(OAc)_2 \cdot 4H_2O$ (440 mg, 2.0 mmol), and 5 ml of pyridine were added to 10 ml of DMF and refluxed under nitrogen. After 2 h, the reaction was completed as monitored by the visible spectrum. The solution mixture was cooled to room temperature and then 2 ml of acetic anhydride was added to the reaction mixture. After stirring for 2 h at room temperaturen, the solution was concentrated in *vacuo*. Water was added to the residue, the mixture filtered, and the solid air-dried. The solid was chromatographed on Al_2O_3 eluting with CH_2Cl_2 and methanol (20:1). The product was recrystallized from CH_2Cl_2 and methanol to give 32 mg (86%) of Zinc porphyrin **48**. IR: ν_{max} 3314 (N-H), 1675 (C=O) cm^{-1}; UV-vis (5% MeOH in CH_2Cl_2, λ_{max} nm (ε)): 586 (16,900), 551 (15,800), 426 (177,600); ^{1}H NMR (300 MHz, 20% CD_3OD in CDCl3): δ 9.06 (4H, s, *meso*), 7.22 (8H, d, phenyl), 6.82 (16H, d, phenyl), 6.57 (16H, d, phenyl), 2.70 (12H, s, CH_3), 1.61 (24H, s, CH_3 of amide); MS (FAB): found m/e 1812.8, 1826.9, 1841.8, 1870.4 (M^++2), 1884.4, cacld. 1868.61 for $C_{112}H_{88}F_4N_{12}O_8Zn$.

Fe(III) 2,7,12,17-tetramethyl-3,8,13,18-tetrakis(2,6-bis(4-acetanilino)-4-fluoro-phenyl)porphyrin methoxide (49)

The free base **41** was treated with excess $FeBr_2$ employing a procedure similar to that used for the synthesis of **48** except that a longer reaction time was needed. The crude

product after chromatography was recrystallized from CH_2Cl_2 and methanol to give 85% of iron porphyrin **49**. IR: ν_{max} 3314 (N-H), 1676 (C=O) cm^{-1}; UV-vis (5% MeOH in CH_2Cl_2, λ_{max} nm (rel intens)): 599 (0.12), 412 (1.00); MS (FAB): found m/e 1805.6, 1819.9, 1833.9, 1847.6, 1862.5 (M^++2), 1877.4, cacld. 1860.61 for $C_{112}H_{88}F_4N_{12}O_8Fe$.

Mn(III) 2,7,12,17-tetramethyl-3,8,13,18-tetrakis(2,6-bis(4-acetanilino)-4-fluoro-phenyl)porphyrin methoxide (50)

The free base **41** was treated with excess $MnCl_2 \cdot 4H_2O$ employing a procedure similar to that used for the synthesis of **48** except that a longer reaction time was needed. The product after chromatography was recrystallized from CH_2Cl_2, methanol, and toluene to give 82% of maganese porphyrin **50**. IR: ν_{max} 3314 (N-H), 1673 (C=O) cm^{-1}; UV-vis (5% MeOH in CH_2Cl_2, λ_{max} nm (rel intens)): 704 (0.02), 590 (0.14), 557 (0.20), 469 (1.00), 377 (0.93); MS (FAB): found m/e 1804.6, 1819.9, 1832.9, 1847.7, 1861.5 (M^++2), 1877.32, cacld. 1859.62 for $C_{112}H_{88}F_4N_{12}O_8Mn$.

2-Naphthylboronic acid

The boronic acid was prepared by the standard Grignard method as described in Chapter 2. m.p. >260 °C; ^1H NMR (300 MHz, $CDCl_3$): δ 8.88 (1H, s), 8.32 (1H, dd), 8.08 (1H, dd), 7.99 (1H, d), 7.92 (1H, dd), 7.64-7.42 (2H, m).

Ethyl 4-methyl-3-(2,6-bis-(2-naphthyl)-4-fluorophenyl)-2-pyrrolecarboxylate

A procedure similar to that used for the synthesis of pyrrole **9** in Chater 2 was employed to give the product in 63% yield. m.p. 167-168 °C; ^1H NMR (300 MHz, $CDCl_3$): δ 8.48 (1H,br s, NH), 7.78-7.67 (4H, m, arryl), 7.66 (2H, d, arryl), 7.58 (2H, d, arryl), 7.46-7.36 (4H, m, arryl), 7.22 -7.15 (4H, m, arryl), 6.32 (1H, d, pyrryl), 4.04 (2H, q, CH_2), 1.56 (3H, s, CH_3), 1.08 (3H, t, CH_3); MS found m/e 499.4, cacld. 499.19 for $C_{34}H_{26}FNO_2$.

2,7,12,17-Tetramethyl-3,8,13,18-tetra(2,6-bis-(2-naphthyl)-4-fluorophenyl) porphyrin

A procedure similar to that used for the synthesis of porphyrin **15** in Chapter 2 was employed to give the product in 32% yield. ^{1}H NMR (300 MHz, $CDCl_3$): δ 9.21 (4H, s, *meso*), 7.90 (8H, s, arryl), 7.51 (8H, d, arryl), 7.49 (8H, d, arryl), 7.22-7.10 (24H, m, arryl), 6.46 (8H, d, arryl), 6.30 (8H, d, arryl), 2.86 (12H, s, CH_3), -4.46 (2H,br s, NH); UV-vis (Toluene, λ_{max} nm (ε)): 637 (6,100), 582 (7,700), 548 (13,100), 512 (16,500), 423 (158,200); MS (FAB): found m/e 1752.9, cacld. 1750.65 for $C_{128}H_{82}N_4F_4$.

Mn(III) 2,7,12,17-tetramethyl-3,8,13,18-tetrakis(2,6-diphenyl-4-fluorophenyl) porphyrin chloride (54)

Free base **15** (27 mg, 0.02 mmol), $MnCl_2 \cdot 4H_2O$ (198 mg, 1.0 mmol), and 0.5 ml of pyridine were added to 20 ml of DMF and refluxed under argon overnight. The solvent was evaporated in *vacuo* and the manganese porphyrin was purified on silica gel column eluting with CH_2Cl_2 and methanol (95:5). The collected product was washed with saturated $NaCl_{(aq)}$ and dried with Na_2SO_4, and the solvent was evaporated under reduced pressure, yielding 24 mg (87%) of manganese porphyrin **54**. UV-vis(toluene, λ_{max} nm (rel intens)): 780 (0.02), 577 (0.17), 483 (0.91), 373 (1.00); MS (FAB): found m/e 1404.6, cacld. 1403.44 for $C_{96}H_{64}F_4N_4Mn$.

Mn(III) 2,7,12,17-tetramethyl-3,8,13,18-tetrakis(2,6-bis(4-t-butylphenyl)-4-fluoro-phenyl)porphyrin chloride (53)

A procedure similar to that used for the synthesis of **54** was employed to give the product in 76% yield. UV-vis(toluene, λ_{max} nm (rel intens)): 783 (0.02), 576 (0.17), 482 (1.00), 375 (0.91); MS (FAB): found m/e 1853.2, cacld. 1851.95 for $C_{128}H_{128}F_4N_4Mn$.

Mn(III) 2,7,12,17-tetramethyl-3,8,13,18-tetrakis(2,6-bis(2-naphthyl)-4-fluorophenyl) porphyrin chloride (52)

A procedure similar to that used for the synthesis of **54** was employed to give the product in 88% yield. UV-vis (toluene, λ_{max} nm (rel intens)): 785 (0.02), 577 (0.18), 483 (1.00), 378 (0.81); MS (FAB): found m/e 1805.0, cacld. 1803.57 for $C_{128}H_{80}N_4F_4Mn$.

Mn(III) 2,7,12,17-Tetramethyl-3,8,13,18-tetra(2,6-bis-(4-biphenyl)-4-fluorophenyl) porphyrin chloride (51)

A procedure similar to that used for the synthesis of **54** was employed to give the product in 83% yield. UV-vis (toluene, λ_{max} nm (ε)): 786 (1,500), 604 (5,500), 576 (12,000), 483 (70,500), 375 (58,100); MS (FAB): found m/e 2012.8, cacld. 2011.70 for $C_{144}H_{96}F_4N_4Mn$

Zn(II) 2,7,12,17-Tetramethyl-3,8,13,18-tetrakis(2,6-diphenyl-4-fluorophenyl) porphyrin (55)

To a solution of free base **15** (27 mg, 0.02 mmol) in 10 ml of $CHCl_3$ and 10 ml of DMF was added a saturated solution of zinc acetate (0.5 ml). The solution was refluxed for 1 hr, and then concentrated in *vacuo*. Water was added to the residue and the solid was filtered. The solid was chromatographed on basic alumina eluting with CH_2Cl_2 to give 26 mg (94%) of zinc porphyrin **32**. ^{1}H NMR (300 MHz, $CDCl_3$): δ 8.86 (4H, s, *meso*), 7.12 (8H, d, phenyl), 6.74 (16H, d, phenyl), 6.40-6.20 (24H, m, phenyl), 2.59 (12H, s, CH3); UV-vis (toluene, λ_{max} nm (ε)): 582 (26,000), 546 (16,000), 422 (253,500); MS (FAB): found m/e1414.1, cacld. 1412.44 for $C_{96}H_{64}F_4N_4Zn$.

Zn(II) 2,7,12,17-Tetramethyl-3,8,13,18-tetrakis(2,6-bis(2-naphthyl)-4-fluorophenyl) porphyrin (56)

A procedure similar to that used for the synthesis of **55** was employed to give the product in 90% yield. ^{1}H NMR (300 MHz, $CDCl_3$): δ 9.20 (4H, s, *meso*), 7.85 (8H, s, naphthyl),

7.49 (8H, d, phenyl), 7.42 (8H, d, naphthyl), 7.20-7.00-6.20 (24H, m, naphthyl), 6.51 (8H, d, naphthyl), 6.29 (8H, d, naphthyl), 2.86 (12H, s, CH_3); UV-vis (toluene, λ_{max} nm (ε)): 588 (20,200), 552 (17,500), 432 (211,500); MS (FAB): found m/e 1814.5, cacld. 1812.56 for $C_{128}H_{80}N_4F_4Zn$.

Zn(II) 2,7,12,17-Tetramethyl-3,8,13,18-tetra(2,6-bis-(4-biphenyl)-4-fluorophenyl) porphyrin (57)

A procedure similar to that used for the synthesis of **55** was employed to give the product in 90% yield. ^1H NMR (300 MHz, $CDCl_3$): δ 9.29 (4H, s, *meso*), 7.47 (8H, d, phenyl), 7.03 (16H, d, phenyl), 6.97-6.73 (40H, m, phenyl), 6.67 (16H, d, phenyl), 2.90 (12H, s, CH_3); UV-vis (toluene, λ_{max} nm (rel intens)): 585 (0.16), 548 (0.14), 432 (1.00); MS (FAB): found m/e 2022.3, cacld. 2020.69 for $C_{144}H_{96}F_4N_4Zn$.

Zn(II) 2,7,12,17-tetramethyl-3,8,13,18-tetrakis(2,6-bis(4-t-butylphenyl)-4-fluorophenyl) porphyrin (58)

A procedure similar to that used for the synthesis of **55** was employed to give the product in 93% yield. ^1H NMR (300 MHz, $CDCl_3$): δ 9.25 (4H, s, *meso*), 7.39 (8H, d, phenyl), 6.89 (16H, d, phenyl), 6.55 (16H, s, phenyl), 2.83 (12H, s, CH_3), 0.72 (72H, s, CH_3); UV-vis (toluene, λ_{max} nm (rel intens)): 582 (0.11), 546 (0.06), 423 (1.00); MS (FAB): found m/e 1862.8, cacld. 1860.97 for $C_{128}H_{128}F_4N_4Zn$

Chapter 4

A STERICALLY HINDERED PORPHYRIN MADE WATER SOLUBLE

Introduction

Metalloporphyrins serve many functions in biological system. These functions include dioxygen transportation and storage,[169,179] electron transfer,[173,180] and biocatalysis.[129,181,182] These diverse biological functions of metalloporphyrins have spawned numerous studies involving model complexes. Most porphyrins are only sparingly soluble in organic solvents. Since water is a major component of many biological systems, it would be of great interest to study porphyrins in an aqueous environment. Furthermore, the advantages of an aqueous system are numerous. First, water is a bountiful source of active oxygen in electrocatalytic oxidation of water mediated by metalloporphyrins. Secondly, H_2O and OH^- as the axial ligands influence the reactivity of redox centers. Thirdly, redox reactions may be controlled by adjusting the pH of the solution.

Electrochemical and chemical redox reactions of water-soluble metalloporphyrins have been extensively studied to elucidate the catalytic properties and to understand the ligand effects and substituent effects.[183-185] However, compared to the voluminous studies carried out in organic solvents, water-soluble systems are less well studied. One of the reasons is that highly modified water-soluble porphyrins are much more difficult to synthesize. The other reason is that many simple water-soluble porphyrins can aggregate in solution, either through π-π interactions or through formation of μ-oxo dimers in alkaline aqueous solution.[186-188] These aggregates complicate the studies of these porphyrins because their properties are different from those of monomers. It is important to prevent the formation of dimer in the studies of iron porphyrins in aqueous solution. Therefore, some sterically hindered water-soluble porphyrins have been

synthesized.[186,189,190] Almost all synthetic water-soluble porphyrins available to date are *meso*-substituted. Only limited results have been reported for β-substituted water-soluble porphyrins.[191] We have now synthesized a highly hindered water-soluble porphyrin based on the β-substituted terphenyl wings as described in previous chapters. This porphyrin is highly water-soluble over the whole range of pH values and has no propensity to form μ-oxo dimer due to the steric hindrance of terphenyl groups.

The catalysis of dioxygen reduction by metalloporphyrins is a current topic.[192-194] Recent studies of O_2 reduction have shown that water soluble iron porphyrins catalyze the reduction of both dioxygen and hydrogen peroxide via an EC mechanism.[195,196]

(I) E step

$$Fe^{III}P + e^- \rightleftharpoons Fe^{II}P \qquad (4\text{-}1)$$

(II) C step

$$2\,Fe^{II}P + O_2 + 2\,H^+ \rightleftharpoons 2\,Fe^{III}P + H_2O_2 \qquad (4\text{-}2)$$

$$2\,Fe^{II}P + H_2O_2 + 2\,H^+ \rightleftharpoons 2\,Fe^{III}P + 2\,H_2O \qquad (4\text{-}3)$$

Iron(III) porphyrin is reduced electrochemically to iron(II) porphyrin, which reduces O_2 to H_2O_2 and then H_2O stepwise in aqueous solutions. We investigated O_2 reduction catalyzed by a sterically hindered β-substituted water-soluble iron porphyrin at various pH values.

The biological functions of metalloporphyrins are dependent on the protein residues surrounding them and the axial ligands. For example, the number and the nature of axial ligands,[197] the binding geometry of the axial ligands,[198,199] and the hydrogen bonding[64] between the protein and axial ligands appear to be of importance in regulating the biological functions of the active sites. It is known that the coordination properties of water-soluble porphyrins are influenced by the peripheral structure. Miskelly and coworker have shown that the perfluorinated water-soluble porphyrin they synthesized

has a hydrophobic environment about the metal center.[189,200] This behavior was examined by the binding of organic molecules. In water solutions of the porphyrin, addition of small amounts of organic solvents or water soluble organic molecules resulted in the displacement of axial water molecules from six-coordinate nickel porphyrin to form the square planar four-coordinate nickel species. Similar behavior for the iron(III) complex of methylated (nicotinamidophenyl) porphyrin was also observed.[187] The axial water molecules of the iron complex can not be replaced by anions such as Cl^-, Br^-, and NO^{3-}. Thus, it is of interest to learn what chemical and structural features of the porphyrin determine its coordination chemistry. Our water-soluble porphyrin having four substituted terphenyl groups at β-positions shows hydrophobic character about the binding site. The coordination chemistry of the iron complex has been investigated.

Results and Discussion

Synthesis

The synthesis of H_2TSPP and H_2TSDCPP has been reported.[85,201] The reactions were performed in hot sulfuric solution and hot fuming sulfuric acid solution, respectively. The structures of the β-substituted porphyrins used for sulfonation are shown in Scheme 1. The synthesis of the parent porphyrins has been described in Chapter 2. We started the sulfonation of the terphenylporphyrin **59** at various temperatures in sulfuric acid solutions. However, a mixture of sulfonated porphyrins was produced. The mixture could not be separated by typical methods such as chromatography. Attempts to solve this problem by substitution of hydrogen by fluorine to deactivate the phenyl group directly attached to the porphyrin ring (**15**) also did not prevent the formation of a mixture of sulfonated porphyrins. Our approach was then switched to the activation of the terminal phenyl groups by the introduction of methoxy groups (**16**), and this permitted us to obtain a single sulfonated porphyrin **60** under a mild reaction condition. It has been shown that unreacted starting material was detected in the

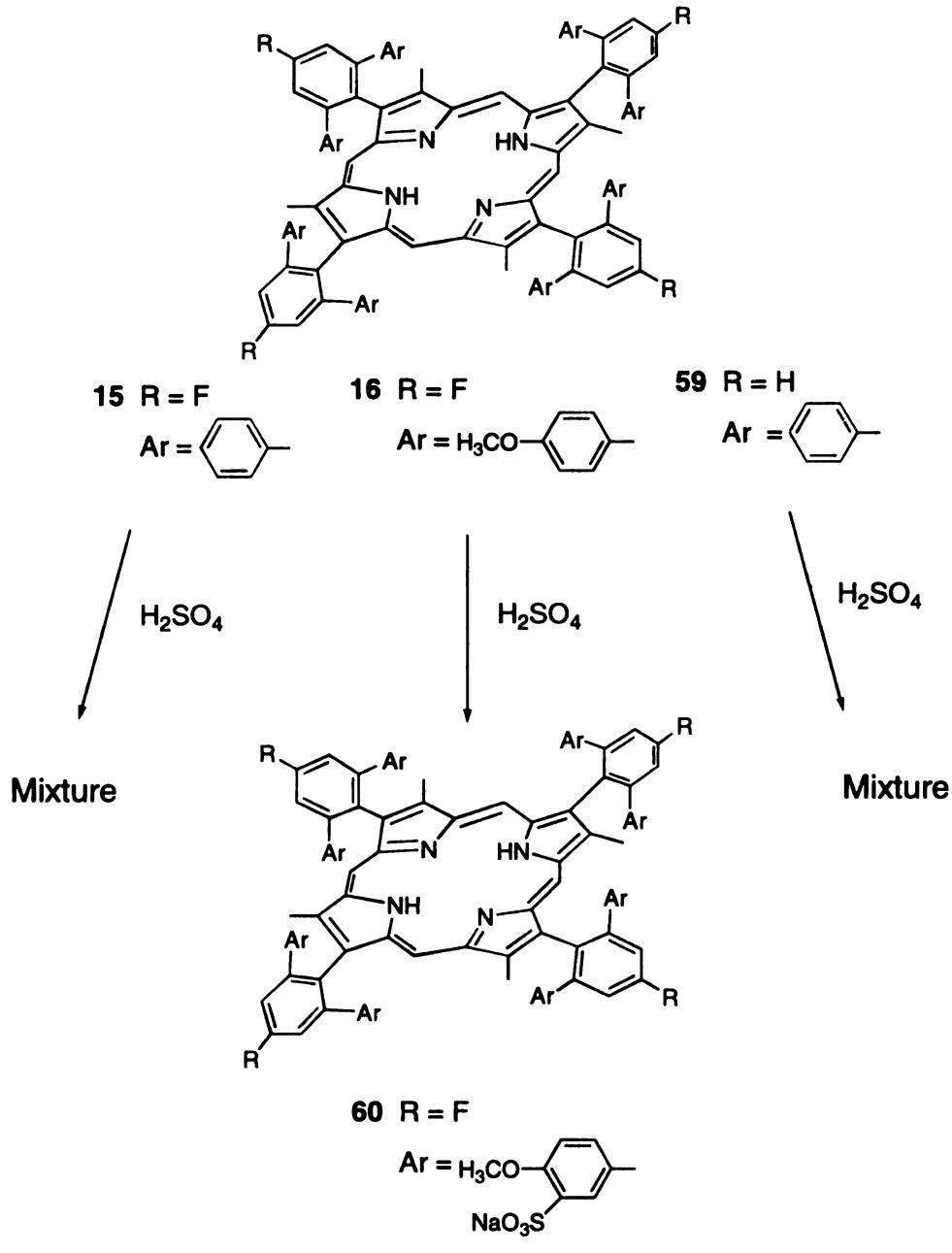

2,7,12,17-Tetramethyl-3,8,13,18-tetra(2,6-bis-(4-methoxy-3-sulfonatophenyl)-4-fluorophenyl)porphyrin (H_2TMTSPP)

Scheme 4-1

sulfonation reaction of TPP under the mild reaction condition.[186] A similar result was also observed in our system using the typical procedure of stirring the porphyrin in H_2SO_4 at room temperature. The porphyrin did not completely dissolve in H_2SO_4 during the course of the reaction. This problem can be solved by dissolving the porphyrin in CH_2Cl_2 followed by the addition of H_2SO_4. The porphyrin was protonated immediately and converted to its diacid form, thus dissolving in H_2SO_4. The sulfonation was carried out for 1 h at room temperature. The work-up of the reaction involved the addition of water and neutralization with alkaline solution. The crude product was precipitated from methanol and acetone several times to give 85% of sulfonated porphyrin **61** (H_2TMTSPP). The solubility of this porphyrin is good in the whole range (0-14) of pH of aqueous solution. It is also soluble in highly polar organic solvents such as MeOH, DMSO, and DMF.

The identification of the sulfonated porphyrin was based on the ^{1}H NMR spectra in D_2O and deuterated DMSO. The ^{1}H NMR of the sulfonated porphyrin in D_2O shows three peaks for the aromatic hydrogens of the sulfonated methoxyphenyl groups at 8.07, 6.27, and 5.84 ppm. The integrated area of the three peaks gave the expected 1:1:1 ratio. There is a singlet at 9.23 ppm due to the hydrogens at meso-positions, a doublet at 7.51 ppm due to the hydrogens on the phenyl groups attached to the β-positions, a singlet at 2.96 ppm due to methoxy groups, and a singlet at 2.71 ppm which arises from the methyl groups at β-positions. The integration of these peaks is consistent with the structure. There is no evidence for the demethylation of the methoxy groups under the sulfonation condition. The NMR spectrum gives definite evidence for sulfonation occurring at all the eight carbons *ortho* to the methoxyl group. In the mass spectrum, the molecular ion peak (M=2406) was absent. However, the largest peak at m/z 2369 was observed. This could be assigned to the species after loss of one CH_3 and one Na, and gain of one H (M - CH_3 - Na + H) from the molecular ion. Along with the largest peaks some other intense peaks observed are consistent with the consecutive loss of sodium ions. The insertion of iron

was accomplished by the typical method of refluxing an aqueous solution containing the sulfonated free base and excess $FeSO_4$ under argon for 1 h. The excess iron salt was precipated out as $Fe(OH)_3$ by adusting the pH of the solution mixture to the range of 12-13 by $NaOH_{(aq)}$. The iron porphyrin **61** (FeTMTSPP) was then precipitated from methanol and acetone several times to give 84% of iron porphyrin.

pKa of iron porphyrin 61 (FeTMTSPP)

The pKa of the water ligated FeTMTSPPP was determined by spectrophotometric titration. Figure 4-1 shows the Q band spectral change of FeTMTSPP as a function of pH. The absorption peaks at 504 and 624 nm in pH 6.83 solution shift to 486 and 606 nm in pH 9.90 solution with isosbestic points at 508, 518 and 636 nm. A pKa of 8.11 is calculated from spectrophotometric titration. The reaction thus involves a one-proton transfer between the acid and base forms.

$$(H_2O)Fe^{III}TMTSPP \rightleftharpoons (HO)Fe^{III}TMTSPP + H^+ \quad pKa = 8.11 \qquad (4\text{-}4)$$

The observed pKa is the higher than other sulfonated iron porphyrins. For example, iron(III) *meso*-tetrakis(3-sulfonatomesityl)porphyrin ($Fe^{III}TSMP$) and iron(III) *meso*-tetrakis(4-sulfonatophenyl) porphyrin ($Fe^{III}TSPP$) have pKa's at 6.6 and 7.0, respectively.[202] The higher pKa value for FeTMTSPP is probably due to the electron-donating groups at β-positions, which increase the electron density of porphyrin ring and iron center. In the pH range 1.0 - 6.0, the absorption spectra do not change significantly. No significant change in the absorption spectra was observed in the pH range 10.0 - 13.0 as well. As expected, there was no evidence for dimerization of FeTMTSPP.

Titration of Fe^{III}TMTSPP with anions

No significant spectral change was observed when the acid and base forms of FeTMTSPP were titrated with sulfate, perchlorate, and phosphate. The same was

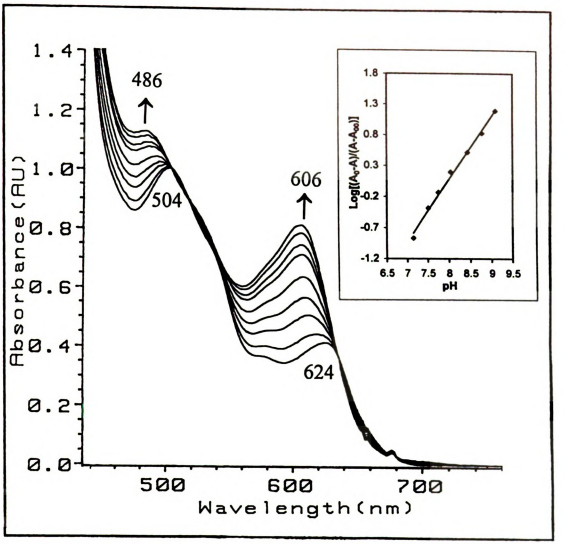

Figure 4-1. Spectral changes of Fe^{III}TMTSPP in 0.1M $NaClO_4$ at different pH. pH = 6.83 - 9.90. Inset: Plot of log $((A_0\text{-}A)/(A\text{-}A_\infty))$ vs. pH.

observed when titrated with nitrite at pH 10.0. Similar results were also observed in the systems in which the *meso*-phenyl groups have some bulky groups attached at the *ortho*-positions.[187] This is probably because the highly hindered substituents, terphenyl groups at the β-positions provide hydrophobic environment which impedes the ligation of anions to the metal. However, at pH 6.1, the spectra of **61** changed significantly when titrated with nitrite. Figure 4-2 shows the spectral changes of **61** at pH 6.1 in the presence of various nitrite concentrations. The bands at 414, 506 and 628 nm decrease while those at 430, 540, and 578 nm increase with isosbestic points at 422, 526, and 592 nm. The resulting spectrum is identical with that of Fe^{II}TMTSPP(NO) obtained by directly bubbling NO into Fe^{III}TMTSPP. In solutions, NO_2^- disproportionates to NO_3^- and NO according to the following equation.[203]

$$2\,NO + NO_3^- + 2\,OH^- \rightleftharpoons 3\,NO_2^- + H_2O \quad K = 1.1 \times 10^{20}\,M^{-2} \qquad (4\text{-}5)$$

Scheidt et al. have reported that the reactions between iron(III) porphyrin complexes and nitrite salts resulted only in the isolation of nitrosyl complexes rather than the expected nitrite complexes.[204] The proposed mechanism involves the formation of nitrite complexes that react with excess nitrite ions to produce the nitrosyl complexes. Based on the redox potentials of NO and (NO)$Fe^{III/II}$TPP, Su and coworkers have reported that NO is thermodynamically capable of reducing (NO)Fe^{III}(TMPyP).[203] Based on the observation that nitrite does not ligate to Fe^{III}TMTSPP at pH 10.0, we assume that the formation of Fe^{II}TMTSPP(NO) involves NO ligation to iron(III) followed by reduction of Fe^{III}TMTSPP(NO). The inset of Figure 4-2 demonstrates that the formation constant K_f is 2.1×10^6 M, and one NO coordinates to the iron center.

Titration of Fe^{III}TMTSPP with imidazole

Figure 4-3 shows the Q band spectral changes of Fe^{III}TMTSPP titrated with imidazole having concentrations ranged from 0 to 3×10^{-4} M in a pH 6.5 phosphate

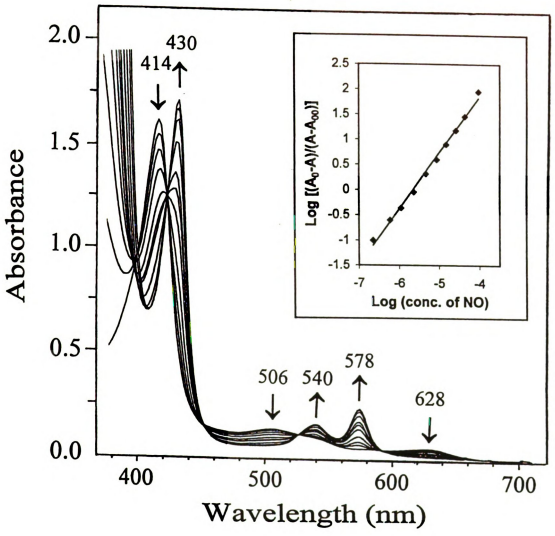

Figure 4-2. Spectral changes of Fe^{III}TMTSPP in pH 6.1 of 0.1 M phosphate solution in the presence of various concentrations of $NaNO_2$. $[NaNO_2] = 0 - 0.67$ M. Inset: Plot of log $((A_0\text{-}A)/(A\text{-}A_\infty))$ versus log (conc. of NO).

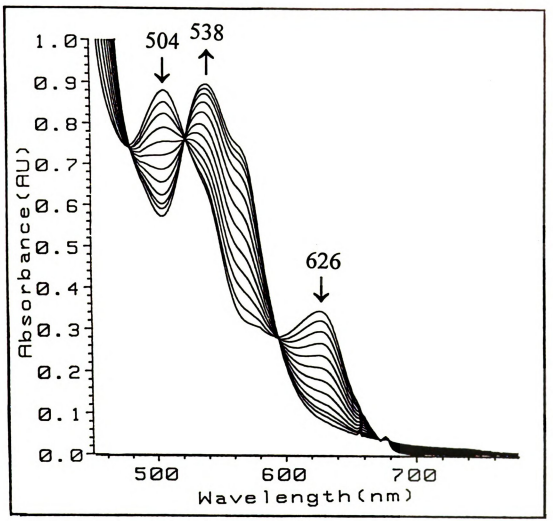

Figure 4-3. Spectral changes of Fe^{III}TMTSPP in pH 6.5 of 0.1 M phosphate solution in the presence of various concentration of imidazole. [ImH] = 0 – 3 x 10^{-4} M.

buffer solution. As the concentration of imidazole increases, the absorbances at 504 and 626 nm decrease while that at 538 nm increases with isosbestic points at 552 and 594 nm. The absorption spectra do not change as the imidazole amount is greater than two equivalents of Fe^{III}TMTSPP and remain unchanged as the imidazole concentration reaches 0.1 M. Thus, the total number of imidazole ligated to the iron porphyrin is two.

$$(H_2O)Fe^{III}TMTSPP + 2\ ImH \rightleftharpoons (ImH)_2Fe^{III}TMTSPP + H_2O \qquad (4\text{-}6)$$

Ashley and coworker reported the imidazole ligation of Cr(III)TSPP with distinct stages for the first and second ligations. The values of K_1 and K_2 were estimated to be 1.0×10^4 and 2.9×10^2 for the acid form, and 1.9×10^3 and 3.3 for the base form.[205] Su et al. reported the coordination properties of iron(III) *meso*-tetrakis(3-sulfonatomesityl)-porphyrin with imidazole.[203] They found that in the spectrophotometric titration of Fe^{III}TSMP with imidazole, distinct stages for the first and second imidazole ligation were not observed. Two imidazoles were coordinated to the iron center.

Titration of Fe^{II}TMTSPP with imidazole

The determination of the equilibrium constants for imidazole ligation was achieved by spectrophotometric titration at pH 6.5 using phosphate buffer. Fe^{III}TMTSPP was reduced to Fe^{II}TMTSPP by sodium dithionite and the measurements were made under nitrogen. Fig. 5-4 shows how the Q band spectra change of Fe^{II}TMTSPP in the presence of various imidazole concentrations. It is noteworthy that in the titration of Fe^{II}TMTSPP with imidazole, distinct stages for the first and second base ligations were observed. As the concentration of imidazole increases in the range of $0 - 2 \times 10^{-4}$ M, a broad band at 500 - 600 nm shifts to 528 and 558 nm with isosbestic points at 506, 540, 550 and 566 nm. Upon further titration with imidazole, the absorption bands at 528 and 558 nm shift to 532 and 562 nm. The isosbestic points are at 530, 542, 554 and 568 nm. No further

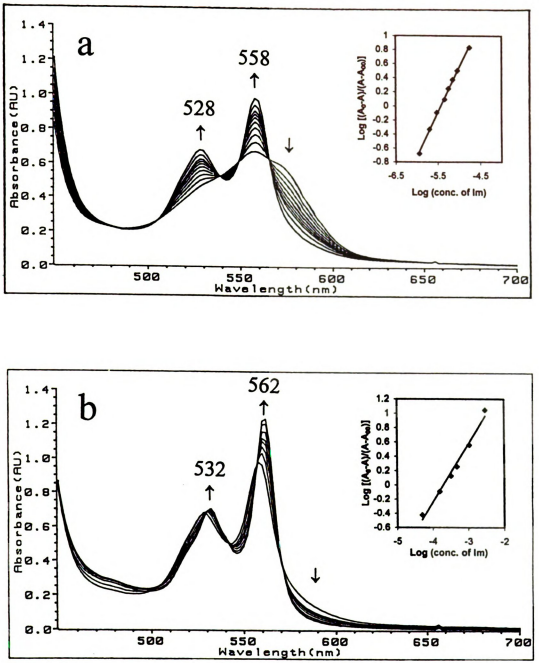

Figure 4-4. Spectral changes of Fe^{II}TMTSPP reduced by dithionite in pH 6.5 of 0.1 M phosphate solution in the presence of various concentrations of imidazole under N_2. [ImH] = (a) 0 – 2 x 10^{-4} M; (b) 2 x 10^{-4} M – 5 x 10^{-2} M. Inset: Plot of log $((A_0\text{-}A)/(A\text{-}A_\infty))$ versus log (conc. of imidazole).

change in absorbance was seen after reaching 0.05 M in imidazole concentration. The equilibria between iron(II) porphyrin and axial bases are expressed as follows:

$$Fe^{II}TMTSPP + ImH \rightleftharpoons Fe^{II}TMTSPP(ImH) \quad K_1 = 7.1 \times 10^6 \qquad (4\text{-}7)$$

$$Fe^{II}TMTSPP(ImH) + ImH \rightleftharpoons Fe^{II}TMTSPP(ImH)_2 \quad K_2 = 1.0 \times 10^3 \qquad (4\text{-}8)$$

The concentration of free imidazole ([ImH]) was calculated from the total imidazole concentration ($[ImH_2^+]$ + [ImH]), the pKa of imidazole (6.95), and the pH of the solution. The binding constants were calculated from plots of log $[(A - A_0)/(A_\infty - A)]$ vs. log [ImH], where A_0 is the absorbance of iron(III) porphyrin at a particular wavelength in the absence of imidazole, A_∞ the absorbance in the presence of a large excess imidazole, and A is the absorbance at a particular imidazole concentration. Both plots of log $[(A - A_0)/(A_\infty - A)]$ vs. log [ImH] shows a slope of 1 ± 0.1 indicating one imidazole ligation for each stage. The equilibrium constants, $K_1 = 7.1 \pm 0.1 \times 10^6$ and $1.0 \pm 0.1 \times 10^3$, were calculated from the intercepts of the plots. The binding behavior of Fe^{II}TMTSPP with imidazole is different from those of most other iron(II) porphyrins that bind the second axial ligand more strongly than the first for unhindered imidazole.[47,52] It should be noted, that the binding behavior is also different from those of the β-substituted porphyrins we used for O_2 binding studies.

The dioxygen binding to Fe^{II}TMTSPP in aqueous solution in the presence of imidazole was our goal. However, in the presence of O_2, iron(II) oxidized to iron(III) immediately. This is probably because the hydrophobic pockets can not impede the approach of water molecules, which act as proton sources to accelerate the oxidation of the iron(II) porphyrin-O_2 adduct.

Electrochemistry of FeTBMSPFPP

Figure 4-5 shows the cyclic voltammograms of FeTMTSPP in various pH solutions under N_2. An irreversible reduction wave of $Fe^{III/II}$TMTSPP at about -0.40 V was

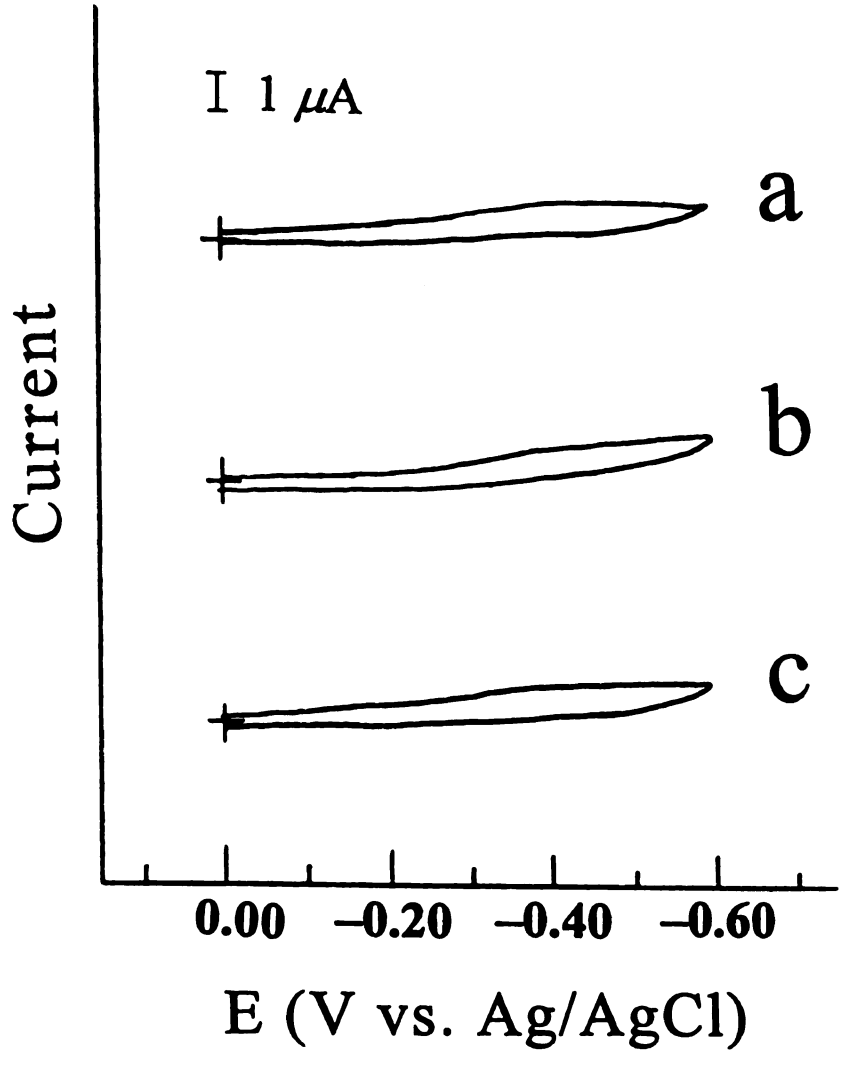

Figure 4-5. Cyclic voltammograms of $Fe^{III}TMTSPP$ in 0.1 M Na_2SO_4 solution at scan rate of 100 mV/s. (a) pH = 1.0; (b) pH = 6.4; (c) pH = 9.1.

observed, indicating an overpotential for the reduction or a chemical reaction following the reduction. Figure 4-6 shows thin layer spectra of FeTMTSPP in various pH solutions. When the pH is lower than 2, the bands at 414, 504 and 628 nm shift to 418, 574 and 616 nm upon reduction. The new spectrum is consistent with that of the diacid form, $H_4TMTSPP^{2+}$, in aqueous pH 1 solution. The results indicate that demetallation followed the reduction at pH < 2. In pH 4.0 solution, the absorption peaks at 414, 504 and 628 nm shift to 424 and 558 nm upon reduction. The OTTLE method has been used to determine the formal potentials. However, attempts to obtain the formal potential of $Fe^{III/II}TMTSPP$ could not be achieved. The spectrum of $Fe^{III}TMTSPP$ did not change at $E_{appl.}$ = -0.40 V at pH 4.0 but changed completely to $Fe^{II}TMTSPP$ when the applied potential was stepped to -0.50 V for 30 min. The new spectrum upon electroreduction is identical with that of $Fe^{II}TMTSPP$ obtained from chemical reduction of $Fe^{III}TMTSPP$ by sodium dithionite. The spectrum of $Fe^{III}TMTSPP$ could not be regenerated by stepping the potential to -0.40 V, but could be regenerated by stepping the potential to -0.30 V. These results suggest that there is an overpotential for the conversion between iron(III) and iron(II) with glassy carbon.[202] The overpotential and slow heterogeneous electron-transfer rate are probably due to the increased distance between iron center and the surface of the electrode caused by the negatively charged sulfonate groups and bulky terphenyl groups. As the pH increases, a more negative potential is needed to reduce the base form of $Fe^{III}TMTSPP$. The bands at 412, 486, and 606 nm shift to 424, and 558 nm upon reduction as shown in Figure 4-6. At pH 10.0, the spectrum of $Fe^{III}TMTSPP$ does not change at $E_{appl.}$ = -0.70 V, but changes completely to $Fe^{II}TMTSPP$ at -0.80 V. The spectrum of $Fe^{II}TMTSPP$ could not be regenerated even at -0.50 V, but could be regenerated by stepping the potential to -0.40 V. In alkaline solutions this overpotential is more pronounced since the surface of the glassy carbon electrode is covered by carboxylate groups which would repulse FeTMTSPP containing eight negatively charged sulfonate groups.

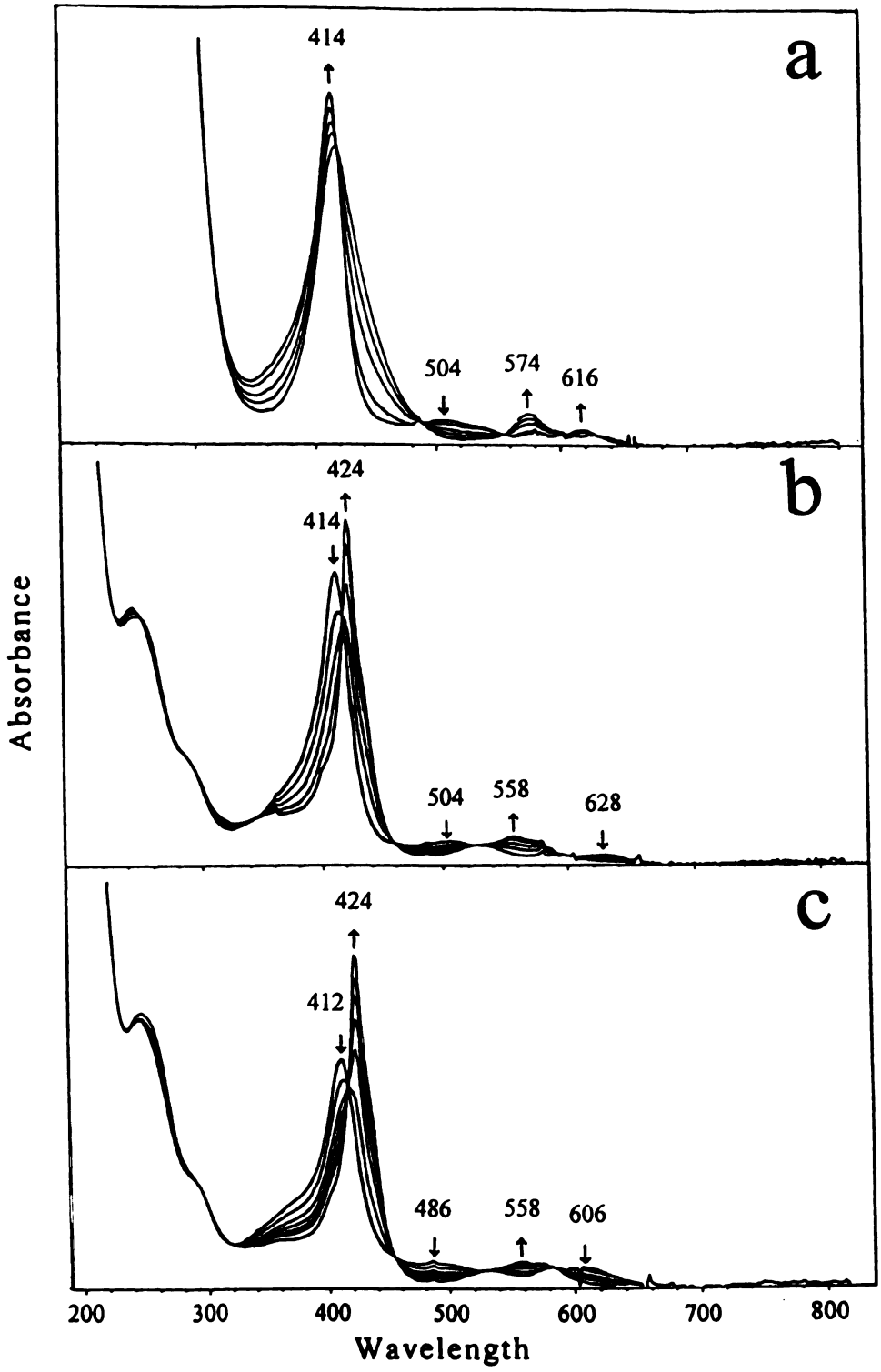

Figure 4-6. Time-resolved spectral changes of Fe^{III}TMTSPP reduction in various pH solutions under N_2. (a) pH = 1.0; (b) pH = 4.0; (c) pH = 10.0.

O_2 Reduction Catalyzed by FeTMTSPP

Numerous of studies on the O_2 reduction catalyzed by metalloporphyrins have been reported.[206,207] Kuwana et al. have shown that CoTMPyP catalyzed two-electron reduction of O_2 to H_2O_2 and FeTMPyP catalyzes four-electron reduction of O_2 to H_2O via H_2O_2.[196] Figure 4-7 shows the cyclic voltammograms of electrocatalytic O_2 reduction by FeTMTSPP in various pH solutions under O_2. As the pH increases, $E_{p,cat.}$ moves toward more negative potentials. This is due to the higher overpotential at higher pH as mentioned above, or the rate-determining step of the O_2 reduction involving protons. The electrocatalytic reduction of O_2 was studied with varying amounts of FeTMTSPP in O_2-saturated pH 2 solution. As the iron porphyrin concentration is increased from 0.2 to 1.0 mM. $E_{p,cat}$ and catalytic current do not change. These results indicate that the kinetic rate of C step is very fast. The electrochemistry of adsorbed FeTMTSPP in the absence and presence of O_2 was also investigated. The reduction is not significantly different from that of bulk FeTMTSPP. Adsorbed FeTMTSPP catalyzes the reduction of O_2 as well. As the scan number increases, $E_{p,cat.}$ shifts to nagative direction and $i_{p,cat.}$ decreases. This phenomenon was also observed in bulk FeTMTSPP solution. The possibility is that demetallation and/or decomposition of FeTMTSPP deactivates the electrode.

Dual catalysts: CoTPyP and FeTMTSPP.

Figure 4-8 shows the cyclic voltammograms of O_2 reduction by adsorbed CoTPyP and dissolved FeTMTSPP in 0.05 M H_2SO_4 solution. In the presence of adsorbed CoTPyP, a double wave was observed. The first wave corresponds to the reduction of O_2 to hydrogen peroxide catalyzed by CoTPyP. The hydrogen peroxide produced was then reduced to water by Fe^{II}TMTSPP. If Fe^{II}TMTSPP does not reduce H_2O_2 to H_2O, then the second catalytic wave would be absent. Thus, the results are consistent with the iron porphyrin reducing O_2 to H_2O via H_2O_2.

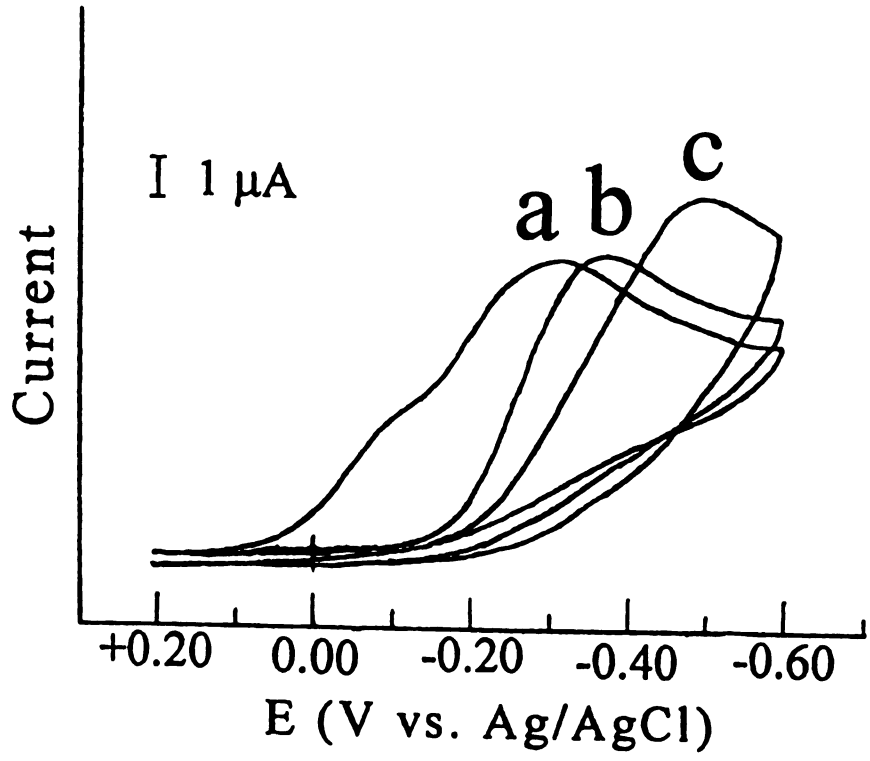

Figure 4-7. Cyclic voltammograms for O_2 reduction in O_2-saturated solutions containing 1.0×10^{-3} M $Fe^{III}TMTSPP$ in various pH solutions at a scan rate of 100 mV/s. (a) pH = 1.0; (b) pH = 6.4; (c) pH = 9.1.

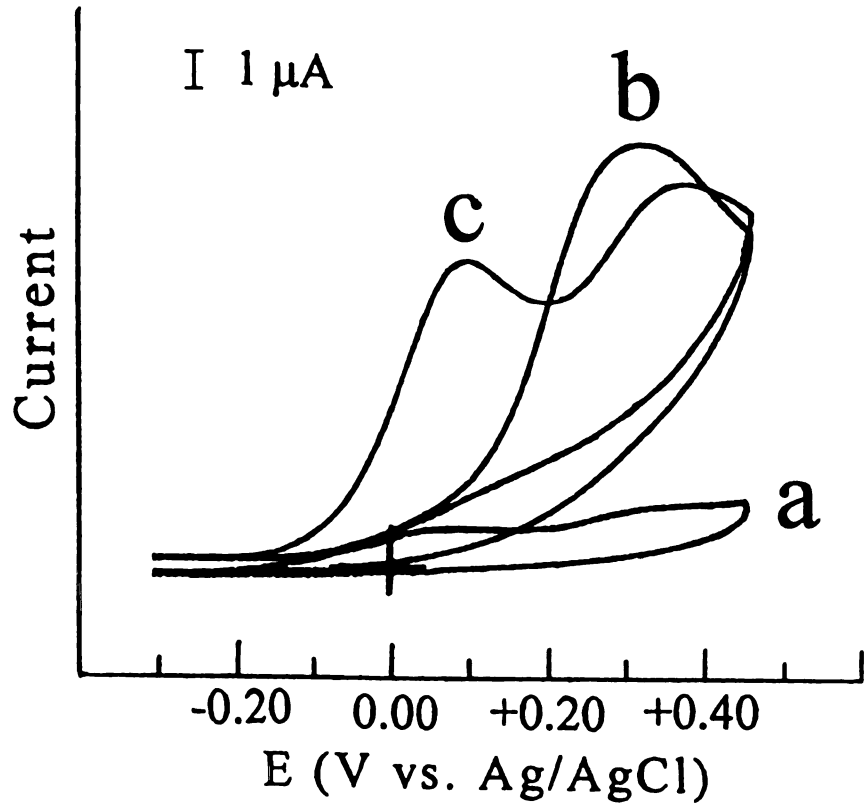

Figure 4-8. Cyclic voltammograms for O_2 reduction catalyzed by adsorbed CoTPyP and dissolved FeTMTSPP in pH 1 solution at a scan rate of 100 mV/s. (a) N_2-saturated, catalyst = adsorbed CoTPyP and solution FeTMTSPP; (b) O_2-saturated, catalyst = solution FeTMTSPP; (c) O_2-saturated, catalyst = CoTPyP and solution FeTMTSPP.

Oxidation of FeTMTSPP

Figure 4-9 shows the oxidation of FeTMTSPP in various pH solutions. At pH 1.0, there is a redox couple at $E^{o'}$ = +0.73 V. The peak-to-peak separation at the scan rate of 100 mV/sec is 60 mV. As pH increases, the $E_{p,a}$ does not change but waves become quasi-reversible. To further probe the number of electrons transfered and the reaction center, thin-layer spectroelectrochemistry was performed in different pH solutions. Figure 4-10 shows the thin-layer spectra of FeTMTSPP at pH 1.0. The band at 416 nm decreases dramatically upon oxidation. The broad band in the region of 500-800 nm is the typical pattern for a porphine ring radical cation. The plot of log[O]/[R] as a function of $E_{appl.}$ shows that the $E^{o'}$ of Fe^{III}TMTSPP/Fe^{III}TMTSPP$^{+\bullet}$ is +0.73 V and the oxidation involves one electron transfer (slope = 72 mV). Based on the above evidence, the redox reaction is then assigned as

$$(H_2O)Fe^{III}TMTSPP^{\ddagger\bullet} + e^- \rightleftharpoons (H_2O)Fe^{III}TMTSPP \quad E^{o'} = +0.73\ V \qquad (4\text{-}9)$$

The iron porphyrin radical cation is stable at pH < 2 on the OTTLE time scale and starts to decompose at pH > 3 upon oxidation. Numerous iron(IV) porphyrins and iron(IV) porphyrin radical cations have been used to catalyze the oxidation reactions of organic substrates.[201,208,209] It is well known that the redox potential of the metal center for water-soluble metalloporphyrins is dependent on pH values. The electrocatalytic properties of Fe^{IV}TMTSPP and Fe^{IV}TMTSPP$^{+\bullet}$ would be of particular interest. Our appoach was to perform the spectroelectrochemistry of FeTMTSPP in alkaline solutions, but unfortunately, we could not obtain Fe^{IV}TMTSPP or Fe^{IV}TMTSPP$^{+\bullet}$ at a potential negative of the formal potential of Fe^{III}TMTSPP/Fe^{III}TMTSPP$^{+\bullet}$ even at pH 13.0. As mentioned, there is an overpotential for the conversion between $Fe^{II/II}$TMTSPP. Therefore, an overpotential for the conversion of $Fe^{II/IV}$ is expected. When the potential was increased until oxidation occurred, decomposition was observed from the decrease in absorbances.

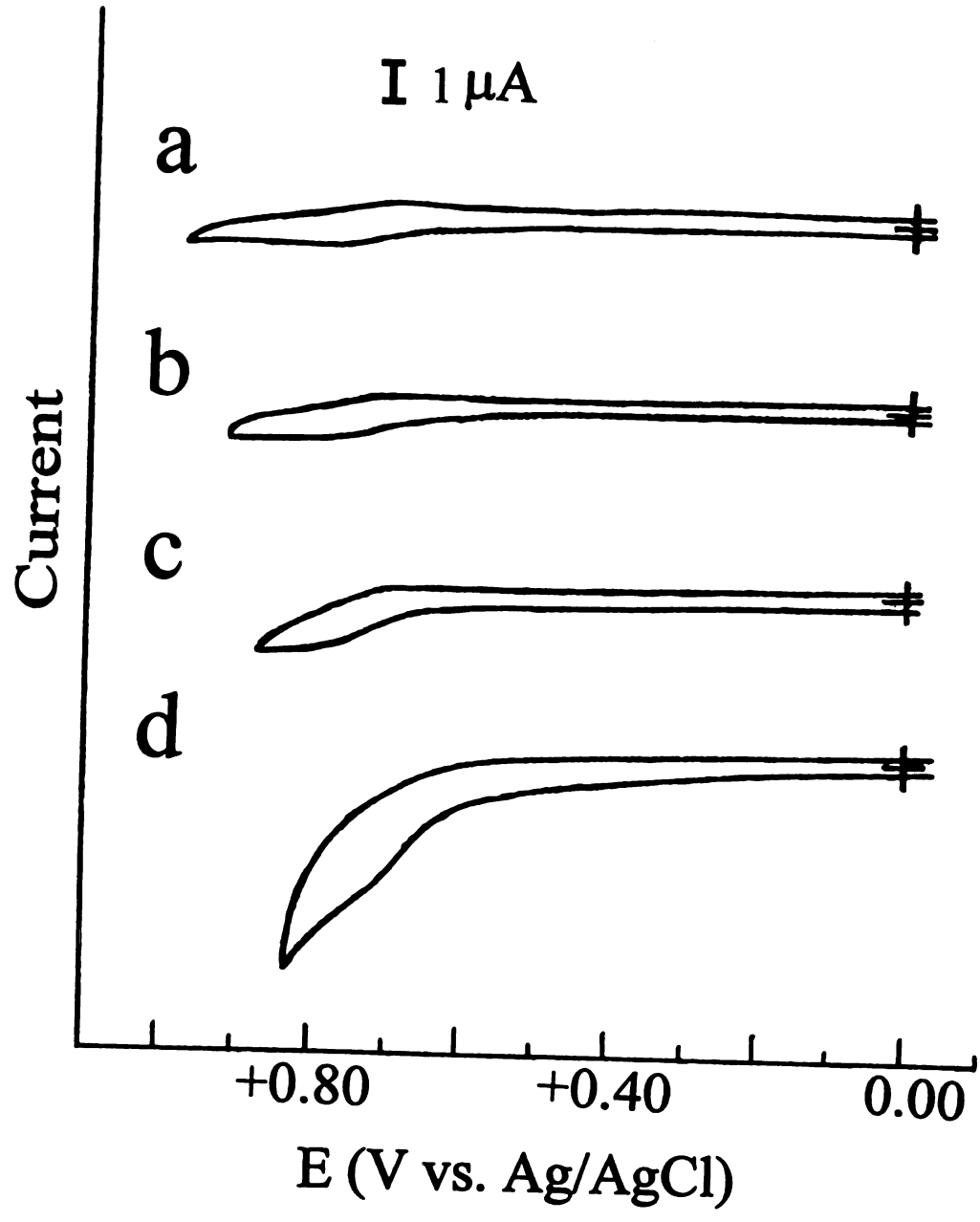

Figure 4-9. Cyclic voltammograms of Fe^{III}TMTSPP oxidation at various pH values. (a) pH = 1.0; (b) pH = 4.6; (c) pH = 6.4; (d) pH = 13.0.

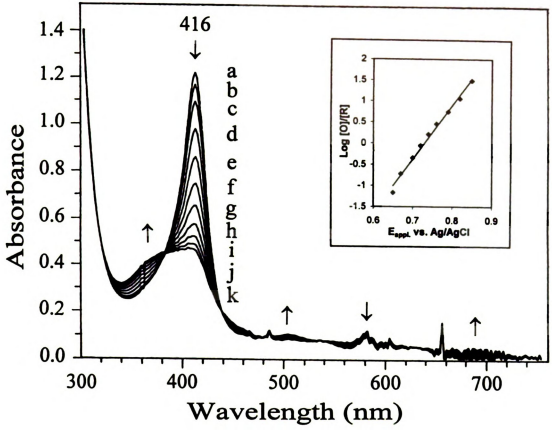

Figure 4-10. Thin-layer spectra of Fe^{III}TMTSPP at different applied potentials (vs. Ag/AgCl) in pH 1.0 solution. $E_{appl.}$ = (a) +0.60; (b) +0.65; (c) +0.67; (d) +0.70; (e) +0.72; (f) +0.74; (g) +0.76; (h) +0.79; (i) +0.82; (j) +0.85; (k) +0.90 V. Inset: Plot of log [O]/[R] vs. $E_{appl.}$.

Conclusions

We have successfully synthesized a new highly sterically crowded β-substituted water-soluble porphyrin (H_2TMTSPP) by the introdution of activating and deactivating groups into the terphenyl groups. The spectrophotometric data of the iron(III) complex (Fe^{III}TMTSPP) support the absence of μ-oxo dimeric species over the whole pH range due to the added sterically hindered substituents at β-positions. Similar to anionic water-soluble porphyrins, only a single pKa was observed whereas most of cationic water-soluble porphyrins show two pKa's. The pka of Fe^{III}TMTSPP(OH_2) was estimated to be 8.11 which is the highest among sulfonated iron porphyrins due to the electron-donating nature of the substituents at β-positions. It is unlikely that the ligated water molecules in FeTMTSPP(OH_2) can be replaced by anions such as SO_4^{2-}, NO_2^-, ClO_4^-, and PO_4^{3-} since the spectra did not change when titrated with these anions, whereas significant spectral changes did occur when titrated with imidazole. When titrated with NO_2^- in acidic solutions, the NO produced ligated to FeTMTSPP and converted iron(III) to iron(II). These coordination studies demonstrated that the hydrophobic pockets prohibited the coordination of anionic ligands.

The E°'of $Fe^{III/II}$TMTSPP can not be obtained with cyclic voltammetry and electrospectrophotometry due to the overpotential. When pH < 2, demetallation of FeTMTSPP occurred upon reduction. The mechanism of catalytic O_2 reduction by FeTMTSPP is consistent with the proposed '2+2' mechanism. The oxidation of FeTMTSPP was also investigated by cyclic voltammetry and electrospectrophotometry. The E°' of Fe^{III}TMTSPP/Fe^{III}TMTSPP$^{+\bullet}$ is +0.73 V obtained by cyclic voltammetry and electrophotospectrometry. Attempts to oxidize iron(III) to iron(IV) by electrochemical and chemical methods were unsuccessful.

Experimental

Materials

All pyrroles and porphyrins used were synthesized by the same procedure described in Chapter 2. All reagents and solvents were obtained from commercial sources and were used without further purification unless otherwise noted. Silica gel for chromatography was 60-200 mesh, manufactured by Fisher Scientific. Analytical TLC was performed on Eastman Kodak 13181 silica gel sheets. Compositions of solvent mixtures are quoted as ratios of volume.

Eletrochemical Measurements

All aqueous solutions used for electrochemistry were prepared with doubly distilled deionized water. Solutions were deoxygenated by purging with nitrogen gas. Buffer solutions ranging from pH 1 to pH 14 were prepared from H_2SO_4, potassium hydrogen phthalate (KHP), borate, carbonate, and NaOH. Dilute solutions of H_2SO_4 and NaOH were used for the adjustment of pH. The pH values of the solutions were measured before and after electrochemical experiments. The measured pH values were within ±0.05 pH units. All experiments were performed at room temperature. Metalloporphyrin concentrations ranged from 0.5 to 1.0 mM and contained 0.2 N Na_2SO_4 as electrolyte.

Instrumentation

^{1}H NMR (300 MHz) spectra were recorded on a Varian Gemini spectrometer. Chemical shifts were reported in ppm relative to the residual proton in deuterated chloroform (7.24 ppm), DMSO-d_6 (2.49 ppm), or D_2O (4.63 ppm). Absorption spectra were recorded on a Shimadzu UV-160, Varian Carry 219, or HP 8452A spectrometer. Mass spetra were obtained on a benchtop VG Trio-1 mass spectrometer. FAB-MS mass spectra were obtained on a JEOL HX-110 HF double focusing spetrometer operating in the positive ion detection mode. Electrochemistry was accomplished with a three-

electrode potentiostat (Bioanalytical Systems, Model CV-27) and a BAS X-Y recorder. Cyclic voltammetry was conducted with the use of a home-made three-electrode cell in which a BAS glassy carbon electrode (0.07 cm^2) was used as working electrode and a platinum wire as auxiliary electrode. All potentials taken were referenced to a home-made Ag/AgCl/KCl (sat.) electrode. The working electrode was polished with 0.03 μm aluminum on Buehler felt pads prior to each experiment. The reproducibility of individual potential values was within ±5 mV. The spectroelectrochemical experiments were accomplished with the use of a 1 mm cuvette, 100 mesh platinum gauze as the working electrode, a platinum wire as the auxiliary electrode, and a Ag/AgCl reference electrode. The design of cuvettes for spectroelectrochemical measurements has been described.[210]

2,7,12,17-Tetramethyl-3,8,13,18-tetra(2,6-bis-(4-methoxy-3-sulfonatophenyl)-4-fluorophenyl)porphyrin (60)

Porphyrin **16** (0.5 g) was added to 20 ml of CH_2Cl_2 and stirred for 5 min. The mixture was then cooled to 0 °C and 20 ml of concentrated H_2SO_4 was added. After the porphyrin was protonated and completely dissolved, the CH_2Cl_2 was removed by a pipette. The solution was stirred at room temperature for 1 h and then was cautiously diluted with two volumes of water at 0 °C. The resulting solution was neutralized with $NaOH_{(aq)}$ to a pH of 7-8. Methanol was added to the solution to precipitate Na_2SO_4,and the mixture was filtered through a sintered glass frit to remove the salt. The solvent was removed and the solid containing a small amount of Na_2SO_4 was then dissolved in a minimum amount of methanol. The mixture was filtered to remove the Na_2SO_4. The sulfonated porphyrin was precipitated from methanol and acetone three times, air dried, and yielded 85% of sulfonated porphyrin. ^1H NMR (300 MHz, D_2O): δ 9.32 (4H, s, *meso*), 7.38 (8H, d, phenyl), 6.92 (16H, d, phenyl), 6.15 (16H, d, phenyl), 3.31 (24H, t, CH_3), 2.87 (12H, s, CH_3), -4.21 (2H,br s, NH); UV-vis(H_2O (pH 8), λ_{max} nm (rel intens)):

628 (0.04), 575 (0.06), 552 (0.09), 514 (0.08), 417 (1.00); MS: found m/e 2175.4, 2201.3, 2223.9, 2247.2, 2269.3, 2288.0, 2312.1, 2335.0, 2348.6, 2371.2, 2391.2, 2412.9, 2435.0 cacld. 2406.12. for $C_{104}H_{74}F_4N_4O_{32}S_8Na_8$. Anal. found: C, 43.73; H, 4.55; N, 1.70. calcd.: C, 43.43; H, 4.42; N, 1.95 for $C_{104}H_{74}F_4N_4O_{32}S_8Na_8$ x 26 H_2O

Fe(III) 2,7,12,17-Tetramethyl-3,8,13,18-tetra(2,6-bis-(4-methoxy-3-sulfonatophenyl)-4-fluorophenyl)porphyrin (61)

The free base was metallated by refluxing with an excess of $FeSO_4$ in water between pH 5 and 8 for 1 h, at which time there was no longer any spectrophotometric evidence for the unreacted free base. The solution was cooled and the pH was adjusted between 12 and 13 to precipitate excess iron(III) as $Fe(OH)_3$. The mixture was filtered through a sintered glass frit to remove the salt. The solvent was then removed and the solid was purified by precipitation from methanol and acetone three times, and air dried to yield 83% of the iron porphyrin. UV-vis(H_2O (pH 4), λ_{max} nm (rel intens)): 627 (0.04), 506 (0.09), 413 (1.00); Anal. found: C, 40.95; H, 5.04; N, 1.60. calcd.: C, 40.16; H, 4.67; N, 1.80 for $C_{104}H_{72}F_4N_4O_{32}S_8Na_8Fe$ x 32 H_2O

Chapter 5

CHIRAL NONPLANAR PORPHYRINS

Introduction

The distortion of tetrapyrrole macrocycles has been observed in biological systems such as the bacterial photosynthetic reaction centers,[211] vitamin B_{12}-dependent enzymes,[212] cofactor F430 of methylreductase,[213,214] and photosynthetic antenna complexes.[215] The distortion is presumably caused by the protein environments surrounding the macrocycle.[216] In particular, the axial ligands coordinated to the metal center, substituents covalently attached to the macrocycle, and the amino acid residues in the vicinity of the active site are undoubtedly important. The presumption of protein induced distortion is based on the fact that the isolated macrocycles are nearly planar in solution and nonplanar in proteins. It has been suggested that the nonplanar distortions of the macrocycles play an important role in their biological function. For examples, recent structural data for photosynthetic centers showed that the chromophores have multiple nonplanar conformations.[217] The conformational variations have been believed to shift the energy of the highest occupied (HOMO) and lowest unoccupied (LUMO) molecular orbitals of the chromophores, thus modulating their optical properties, and redox potentials, with consequent effects on the electron-transfer rates of the reaction centers. For cytochromes c, high resolution X-ray structures have shown that the iron porphyrin is distorted from planarity by a significant degree.[218] The distortions are believed to be related to the modification of redox properties of the hemes. Additional evidence is the observation that the nonplanar distortions are conserved for proteins belonging to the same functional class. For example, the ruffling distortion is highly conserved for mitochondrial cytochromes c isolated from diverse species.[219] These conserved distorted structures are most likely to influence enzymatic functions.

The investigation of nonplanar porphyrins has been an active area due to the significant relationship between macrocycle distortion and physiochemical properties in biological systems.[220,221] In the past years, a number of nonplanar porphyrins have been synthesized and their physical and chemical properties have been demonstrated. Studies on nonplanar model compounds have contributed to the better understanding the origin of porphyrin nonplanar distortions. These model compounds also provided information about the effects of the distortions on the porphyrins. Numerous X-ray structural data of highly substituted nonplanar porphyrins have elucidated various conformations for the macrocycles.[222-224] In general, these conformations can be classified into four types, the saddled, ruffled, waved, and domed conformations as shown in Figure 5-1.[225] Among these four conformations, saddled and ruffled are the most common observed in nonplanar porphyrins. For the saddled conformation, the porphyrin *meso* carbons are in the porphyrin mean plane whereas the pyrrole units are alternatively above and below the mean plane of the porphyrin. NiOETPP and ZnOETPP are specific examples for the porphyrins with the saddled conformation.[223,226] The X-ray crystal structure shows that NiOETPP is severely nonplanar and adopts an S_4 saddle conformation. The *meso* carbons lie nearly in the plane of the macrocycle with the average displacement of the C_β atoms from the mean plane of the molecule is 1.23 Å. The angles for the adjacent pyrrole planes are 34.5° and for opposite pyrroles 58.0°.

The ruffled conformation is quite different from the saddled conformation. In the ruffled conformation the pyrrole nitrogens are in the mean plane whereas the *meso* carbons are alternatively above and below the porphyrin mean plane. The β carbons in the same pyrrolic unit for the ruffled conformation are on the opposite sides of the porphyrin mean plane since the pyrrolic units are twisted whereas in the saddled conformation the β carbons in the same pyrrolic unit are on the same side of the mean plane. The crystal structure of NiDPP, in which there are twelve phenyl groups at *meso*- and β-positions, shows a well-defined ruffled conformation.[227,228] The pyrrolic units

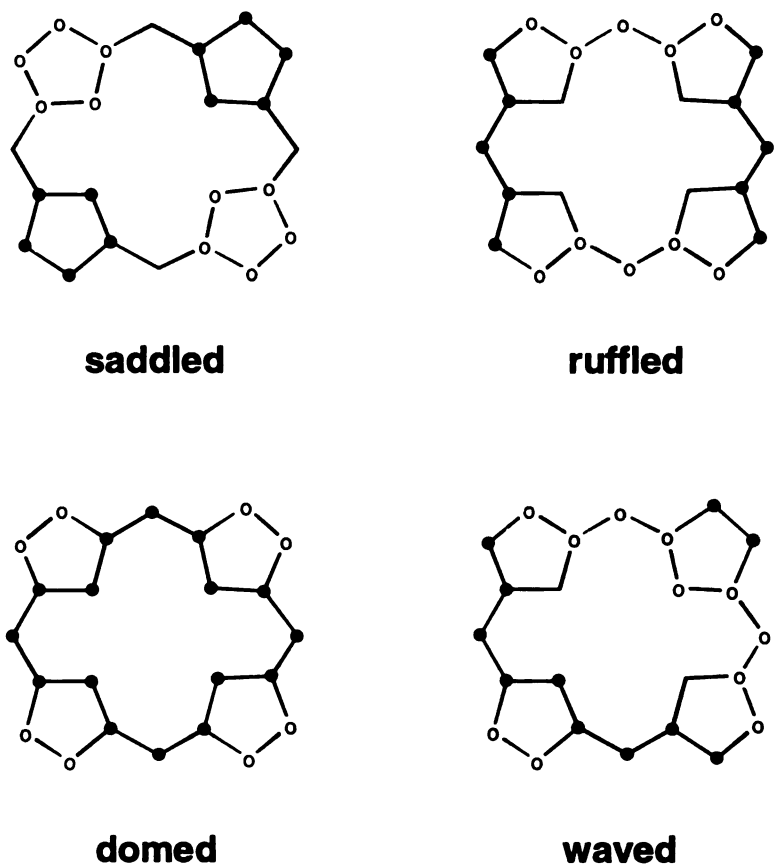

Figure 5-1. The saddled, ruffled, waved, and domed nonplanar porphyrin conformations. Filled circles represent atoms above the least-squares plane, and open circles correspond to atoms below the plane; atoms not circled are in the plane.

exhibit twist angles of 22.81° with respect to the porphyrin mean plane. A maximum displacement of 0.885 Å for the *meso* carbons and an average diplacement of 0.430 Å of the core atoms from the porphyrin mean plane have been observed. Waved and domed conformations are less often reported than are ruffled and saddled. The waved conformations exhibit smaller deviations from the porphyrin mean plane than do saddled and ruffled conformations. The domed conformations are only observed when a porphyrin is ligated to a large metal ion, usually having one or more ligands coordinated.

Because there is a significant relationship between nonplanarity and functions of tetrapyrrole complexes in biological systems, it is important to know the factors that control the nonplanar structure of the macrocycle. Numerous X-ray structures of synthetic nonplanr porphyrins point to four factors that relate to the conformation of the macrocycle have been found.[229-235] These factors include peripheral substituents, the central metal, the axial ligand, and the environment of the macrocycle. Peripheral substituent efftects include the number, size, orientation, and electronic properties. When the porphyrin has bulky groups at *meso*- and β-positions there are steric interactions between the *meso*-substituents and the adjacent β carbons. There are additional steric interactions between the *meso*- and β-substituents. X-ray crystal structures show that the bulkier the substituents are, the more distorted the porphyrin will be. The nature of the metal center in the macrocycle is integral in determining the degree of distortion. A shorter M-N bond results in a decrease in the porphyrin core size, thus distorting the macrocycle. In the case of NiOETPP and ZnOETPP, the Ni-N bond (1.906 Å) is shorter than Zn-N (2.063 Å), and therefore a more non-planar structure was observed in NiOETPP.[223,226,227] Structural and theoretical studies show that the axial ligand is also a factor that influences the conformation of the porphyrin.[236,237] Numerous crystal structures of Fe(TMP) complexes with various axial ligands suggest that the bulky planar axial ligands are capable of interacting with the peripheral substituents and induce strong ruffling in the porphyrin core.[238,239] The environment of the macrocycle can be

considered as solvents in synthetic model compounds and proteins in biological systems.

Both chemical and physical properties of non-planar porphyrins, which are different from those of planar porphyrins, have been demonstrated. The most common spectroscopic features of non-planar porphyrins are the red shifts at the Soret and Q bands in the UV-vis spectrum.[220,240] Shelnutt and coworkers have synthesized and studied the spectroscopic properties of a series of *meso*-tetrasubstituted porphyrins.[220] The porphyrin with simple linear alkane substituents have the Soret band near 430 nm and Q bands near 540 and 580 nm, whereas the porphyrin with bulky adamantyl groups give greatly red-shifted spectra with the Soret band near 470 nm and Q bands near 600 and 650 nm.

Resonance Raman spectroscopy has been proved to be a powerful technique for quantifying the conformational equilibrium between non-planar and planar conformers of porphyrins.[226,241-243] It has been shown that there is a relationship between the core size of the porphyrin and the resonance Raman frequencies between 1300 and 1500 cm^{-1} which are called core-size marker lines. The studies on synthetic model compounds have demonstrated a correlation between the frequencies of structure-sensitive lines and the degree of distortion of the macrocycle.

The distortion of the porphyrin shifts the energy levels of the frontier orbitals, HOMO and LUMO. Fajer et al. have reported that non-planar porphyrins are easier to oxidize and harder to reduce compared to planar porphyrins.[219] Based on the electrochemistry of nonplanar σ-bonded iron(III) porphyrins, Kadish and coworkers have shown how the nonplanarity of the porphyrin influences the electron transfer site and demonstrated that the facile oxidation of OETPP derivatives compared to their OEP analogs can be explained by the distortion of the porphyrin macrocycle.[244,245] In a series of brominated tetraphenylporphyrins, the porphyrin is initially harder to oxidize due to the electron-withdrawing ability of the added bromine groups and subsequently becomes easier to oxidize since the addition of more bromine substituents result in the

nonplanarity of the macrocycle. Some other chemical and physical properties of nonplanar porphyrins have also been investigated. These studies include NMR and EPR spectra, axial ligand affinity, and basicity.[232,246-249]

The chemistry of chiral porphyrins has attracted much attention because of the interest in the development of new chiral ligands and receptors for asymmetric catalysis and the modeling of biologically important reactions.[145,250,251] The chiralities of hemes in biological systems are induced by the protein pocket, while in synthetic planar porphyrins, they are often derived from chiral auxiliaries. Nonplanar porphyrins, however, may have intrinsic chirality associated with the nonequivalent up-and-down pyrrole quadrons.[252,253] Typically, nonplanar porphyrins in solution are capable of undergoing flip-flop of the two enantiomeric saddle forms giving rise to racemization. The racemization results in the difficulty to isolate the enantiomer from each other.[254]

Inoue and coworkers reported the photoinduced conformational ruffling of a "single-armed" porphyrin, derived from etioporphyrin, with a single pivaloylamino group at one of *meso*-positions.[252] The mono-substituted porphyrin is achiral when planar since its mirror images can be superimposed by C_2 rotation. However, the pivalamide substituent at the *meso* position is located on either side of the porphyrin plane due to the steric interactions with the adjacent substituents, thus making the porphyrin chiral. The enantiomers of the porphyrin were isolated by chiral chromatography. The ^{1}H NMR spectra of the enantiomers were both the same, whereas the circular dichroism spectra were perfect mirror images of each other. The enantiomers racemized slowly at room temperature and no racemization was observed below 0 °C. The factors that influence the racemization process were also demonstrated. These factors include the size of the substituents, temperature, the nature of the central metals, bases, and photoirradiation. Recently, Aida and coworkers used a D_2-symmetic fully substituted porphyrin that has a nonplanar structure as a conceptually new chirality sensor.[253] The chirality sensor can recognize chiral carboxylic acids through self-assembly and memorizes the acquired

information within its skeleton even after the assembly is broken as evidenced by CD spectroscopy. In the presence of a chiral carboxylic acid one of the two conformers was preferred. The CD spectra of the (R)- and (S)-mandelate porphyrin complexes were perfect mirror images of each other. However, the absolute porphyrin conformations of the enantiomers have not been determined.

We have synthesized a series of fully substituted chiral porphyrins by the introduction of either one or two chiral auxiliaries into the porphyrins as shown in Figure 6-2. Thus, a chiral environment around the metal center was created. The nonplanar chiral porphyrins we synthesized can be used for asymmetric epoxidation of alkenes and hydroxylation of alkanes. As noted above, the absolute conformation of the nonplanar chiral porphyrin has not been well established. In our system, one of the two conformations was preferred when a chiral auxiliary was attached to the nonplanar porphyrin. This has been observed by CD spectroscopy. The CD spectra of the (R) and (S) nonplanar porphyrins are mirror images of each other. The absolute conformations of single armed fully substituted porphyrins were determined by CD and X-ray spectroscopies, thus their correlation with CD profiles was established.

Results and Discussion

Synthesis

The key feature in our preparation of chiral nonplanar porphyrins was to develop an efficient route for the introduction of various chiral auxiliaries into the porphyrins. To attach the chiral auxiliary to the porphyrin, we chose xanthene as the rigid spacer group to bridge the porphyrin macrocycle and the chiral auxiliary. The intermediate, diformyl xanthene **64**, was prepared from xanthene **63** by treatment with butyl lithium in the presence of TMEDA and DMF, followed by hydrolysis as shown in Scheme 5-1.[255] Xanthene **63** was prepared from commercially available xanthone **62** and trimethyl aluminum in toluene.[256]

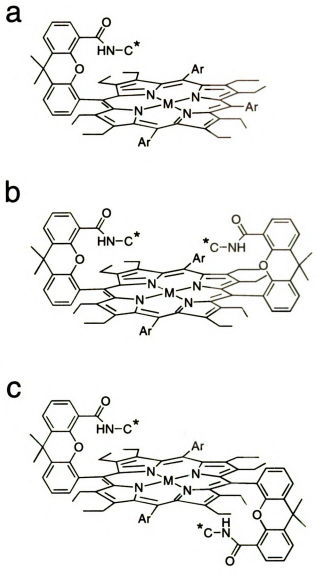

Figure 5-2. Structures of nonplanar porphyrins with (a) one chiral auxiliary; (b) two chiral auxiliaries on the same side; (c) two chiral auxiliaries on the opposite side.

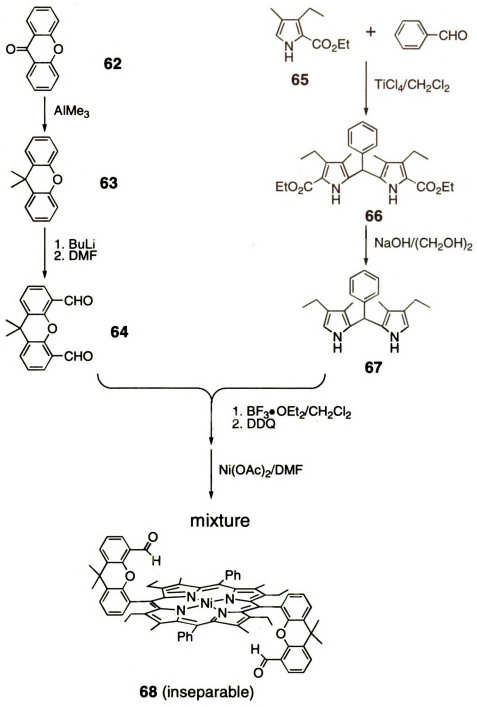
62
AlMe3
63
1. BuLi
2. DMF
CHO
64
CHO
65
CO2Et
+
CHO
TiCl4/CH2Cl2
EtO2C
CO2Et
66
NaOH/(CH2OH)2
67
1. BF3•OEt2/CH2Cl2
2. DDQ
Ni(OAc)2/DMF
mixture
Ph
Ni
Ph
68 (inseparable)

Scheme 5-1

We started the synthesis of the porphyrins with two xanthene bridges (Scheme 5-1). Initially, porphyrin **68** was chosen as the key intermediate, in which the formyl group on xanthene can be modified to create a chiral environment. Dipyrrylmethane **66** was obtained in 90% yield by the reaction of 2 equivalents of pyrrole **65** and benzaldehyde. Dipyrrylmethane **66** was decarboxylated in refluxing ethylene glycol containing NaOH to give dipyrrylmethane **67**, which was then immediately coupled with diformylxanthene **64** in the presence of $BF_3 \cdot OEt_2$ followed by oxidation with DDQ to give a mixture of porphyrins.[253] The use of *p*-chloranil resulted in incomplete oxidation even after refluxing the reaction overnight. Attempts to isolate the desired products, *cis*- and *trans*-porphyrin **68**, were unsuccessful due to the scrambling of the porphyrin during the cyclization.[257] It has been reported that the scambling can be suppressed by the use of solid catalysts such as silica gel[258] or montmorillonite clay K-10,[259] or of a dehydrating agent such as molecular sieves.[253] However, attempts to minimize the scrambling during cyclization step using either solid catalysts or molecular sieves failed.

Since it was impossible to isolate porphyrin **68** we employed diethylpyrrole **69** instead of ethylmethyl pyrrole **65** as the starting material. The use of diethylpyrrole **69** allowed us to reduce the number of porphyrin isomers even if severe scrambling of porphyrins occurred. A procedure similar to that of porphyrin **68** was empolyed as shown in Scheme 6-2. Dipyrrylmethane **70** can be prepared from pyrrole **69** and benzaldehyde either in CH_2Cl_2 catalyzed by $TiCl_4$[260] or in ethanol in the presence of $HClO_4$(aq) in higher than 90% yield. Decarboxylation of dipyrrylmethane **70** gave dipyrrolemethane **71**, which was then treated with diformylxanthene **64** followed by oxidation with DDQ to give a mixture of protonated porphyrins. Since the protonated porphyrins were inseparable with chromatography we inserted nickel into the porphyrins by treating with excess $Ni(OAc)_2$ in refluxing DMF. This allowed us to use chromatography to separate some of porphyrins from the mixture. The first band was identified as NiOETPP, which was formed due to scrambling during cyclization. The

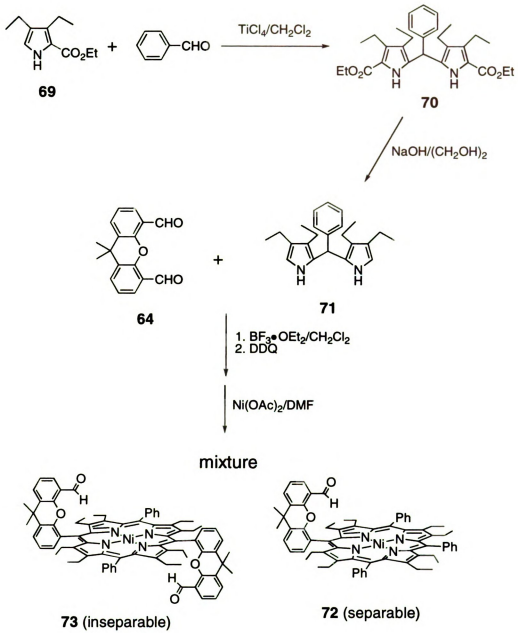
TiCl4/CH2Cl2
CHO
CO2Et
69
EtO2C
CO2Et
70
NaOH/(CH2OH)2
CHO
CHO
64
71
1. BF3•OEt2/CH2Cl2
2. DDQ
Ni(OAc)2/DMF
mixture
Ph
Ph
Ph
Ph
73 (inseparable)
72 (separable)

Scheme 5-2

second band, which was the major product, was separated in 9% yield and identified as porphyrin **72**. We expected that the third band was the *trans* form of porphyrin **73**. Unfortunately, this band contains two porphyrins and they could not be separated.

As noted, the use of silica gel, montmorillonite clay K-10, or molecular sieves could not minimize the scrambling. Our approach was then switched to the introduction of hindered substituents to the phenyl groups at *meso*-positions. Dipyrrylmethane **74** was obtained in 72% yield from the reaction of pyrrole **69** and mesitaldehyde in CH_2Cl_2 in the presence of $TiCl_4$ as shown in Scheme 5-3. Reactions using ethanol as solvent and $HClO_4$ as catalyst gave a lower yield and resulted in incomplete reaction. Decarboxylation of dipyrrylmethane **74** followed by reaction with diformylxanthene **64**, oxidation with DDQ and nickel insertion afforded a mixture of nickel porphyrins. As expected, the introduction of hindered substituents into the phenyl groups at *meso*-positions minimized the scrambling. The major product was the expected *trans* form of porphyrin **76** isolated with chromatography in 18% yield. It was hoped that the minor product was the *cis* form of porphyrin **74**. However, the *cis* porphyrin could not be separated from the mixture, presumably due to scrambling. We also tried the preparation of porphyrin **79** using dichlorobenzaldehyde instead of mesitaldehyde as shown in Scheme 6-4. In this case, both the *trans* and *cis* forms of porphyrin **79** were separated with chromatography in 22% and 17% yields, respectively.

We were able to anchor chiral auxiliaries to the xanthene bridge of porphyrin **76** and **79**, which have two xanthyl groups at the opposite *meso*-positions. The synthetic strategy for the synthesis of chiral porphyrins was shown in Scheme 5-4. The aldehyde on xanthyl group was converted to the nitrile by treating with hydroxylamine hydrochloride in refluxing 98% formic acid for 24 hr under argon. We could not convert the nitrile to the carboxylate group using an alkaline solution of ethylene glycol. Thus, acidic conditions were employed. The nitrile was converted to the acid in a refluxing mixture of acetic acid, water, and concentrated sulfuric acid. The carboxylic acid was

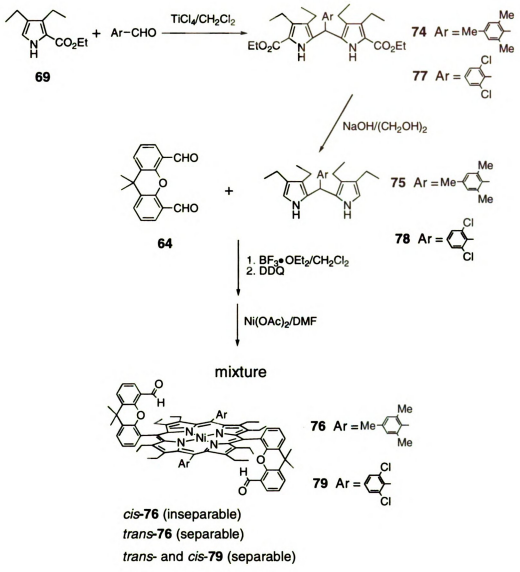
TiCl4/CH2Cl2
Ar–CHO
69
74 Ar = Me
77 Ar =
NaOH/(CH2OH)2
64
75 Ar = Me
78 Ar =
1. BF3•OEt2/CH2Cl2
2. DDQ
Ni(OAc)2/DMF
mixture
76 Ar = Me
79 Ar =
cis-76 (inseparable)
trans-76 (separable)
trans- and cis-79 (separable)

Scheme 5-3

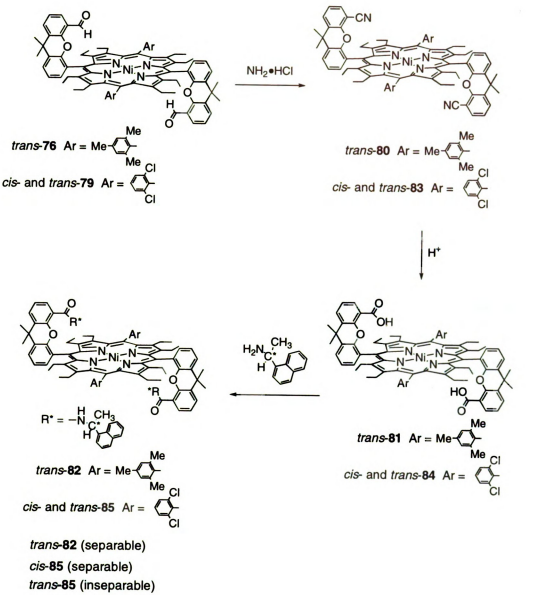
NH2•HCl
trans-76 Ar = Me
cis- and trans-79 Ar =
trans-80 Ar = Me
cis- and trans-83 Ar =
H+
trans-81 Ar = Me
cis- and trans-84 Ar =
trans-82 Ar = Me
cis- and trans-85 Ar =
trans-82 (separable)
cis-85 (separable)
trans-85 (inseparable)

Scheme 5-4

converted to the acid chloride by treating with thionyl chloride in refluxing CH_2Cl_2. After the solvent was removed *in vacuo*, chiral amines such as the (R) and (S) forms of 1-(1-naphthyl)ethylamine were coupled with the acid chloride of the porphyrin. However, a mixture of porphyrins was obtained for the preparation of *trans*-**85** and isolation using chromatography was not successful. The yields for *cis*-**85** and *trans*-**82** were 20% and 13%, respectively. Obviously, the low yield for *cis*-**85** was due to the steric interactions between the chiral auxiliaries on the same side of the porphyrin mean plane. The low yield for *trans*-**82** could be explained by the increased steric interactions between the coming nucleophile and the porphyrin. In our system, one of the two conformations was preferred as the first chiral auxiliary was anchored to the xanthene. Once the conformation was fixed, the porphyrin lost flexibility and the steric hindrance between the incoming auxiliary and the pyrrole unit increases during the coupling, thus resulting in low yields. In Scheme 5-4, most of conditions used were acidic and dematallation occurred during the reaction. To facilitate the purification of the porphyrins, it is necessary to metallate the porphyrin with $Ni(OAc)_2$ in each step.

To improve the yields of the chiral porphyrins, the effects of steric interactions during the reaction must be circumvented. Therefore, we switched to the synthesis of the chiral porphyrins with only one xanthene bridge. Two synthetic strategies, shown in scheme 5-5 and 5-6, were used for the preparation of the porphyrins anchored one xanthyl group. The first strategy shown in Scheme 5-5 was similar to that of TPP proposed by Lindsey.[261] A 4:3:1 mixture of diethylpyrrole **86**, benzaldehyde or pentafluoro-benzaldehyde, and diformylxanthene **64** was condensed in CH_2Cl_2 in the presence of $BF3{\cdot}OEt_2$ to give a mixture of porphyrins. After nickel insertion, the mixture was separated by chromatography to afford the porphyrins **72** and **87**, in 11% and 10% yields, respectively. To improve the yield of the xanthene-anchored porphyrins, we also tried "2 + 2" condensation (Scheme 5-6).[253] For the preparation of porphyrin **72**, a 2:1:1 mixture of di-α-free dipyrrylmethane **71**, bezaldehyde, and diformylxanthene **64**

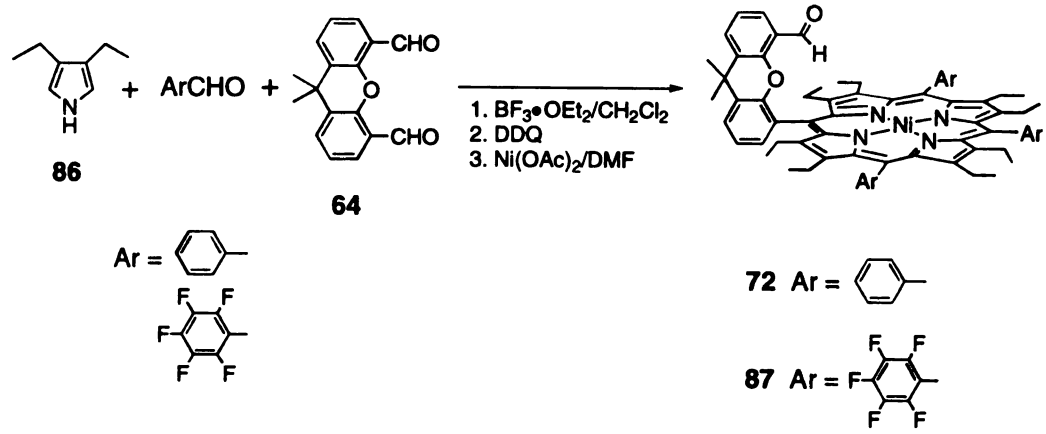

Scheme 5-5

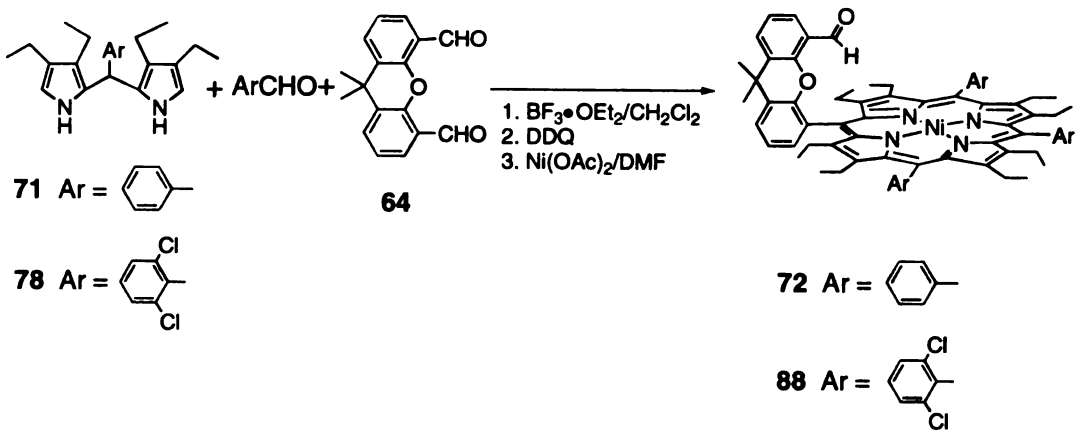

Scheme 5-6

were condensed in CH_2Cl_2 at room temperature in the presence of $BF_3{\cdot}OEt_2$. After oxidation with DDQ and nickel insertion, the desired porphyrin, **72**, was separated from the mixture of porphyrins by chromatography in 21% yield. A procedure similar to that of **72** was employed for the preparation of porphyrin **88** in 18% yield.

We have described the synthesis of bis-faced porphyrins having chiral auxiliaries on both sides of the porphyrin mean plane. Using a similar route, we were able to make the single-faced porphyrins having only one chiral auxiliary attached to the xanthyl group (Scheme 5-7). Porphyrin **72** was first converted to porphyrin nitrile **89** by treating with hydroxyamine hydrochloride in refluxing formic acid under argon. Nitrile **89** was hydrolyzed under acidic conditions to give porphyrin acid **90**, which was then transformed to acid chloride by reacting with thionyl chloride. The acid chloride was immediately coupled with 1-(1-naphthylethyl)amine to give single-faced chiral porphyrin **95** (Figure 5-3) in 70% yield. With this synthetic strategy, we successfully introduced various chiral amines into the single-faced porphyrins. The structures of the single-faced chiral porphyrins were shown in Figure 5-3. They have been characterized by ^1H NMR, MASS, and UV-vis spectroscopies. The general physical data for the (R) and (S) forms of the chiral porphyrins were identical. The UV-vis spectra of these porphyrins showed that both the Soret and Q bands were red-shifted. The ^1H NMR spectra of these chiral porphyrins shifted upfield for the chiral auxiliaries anchored on the xanthene bridge, due to the strong magnetic shielding by the porphyrin ring current.

The chiral manganese porphyrins were obtained after removal of nickel by washing several times with concentrated $HCl_{(aq)}$ and insertion of manganese by treating with $Mn(II)Cl_2$ in refluxing DMF. These chiral catalysts can be used for epoxidations of alkenes and hydroxylations of alkanes.

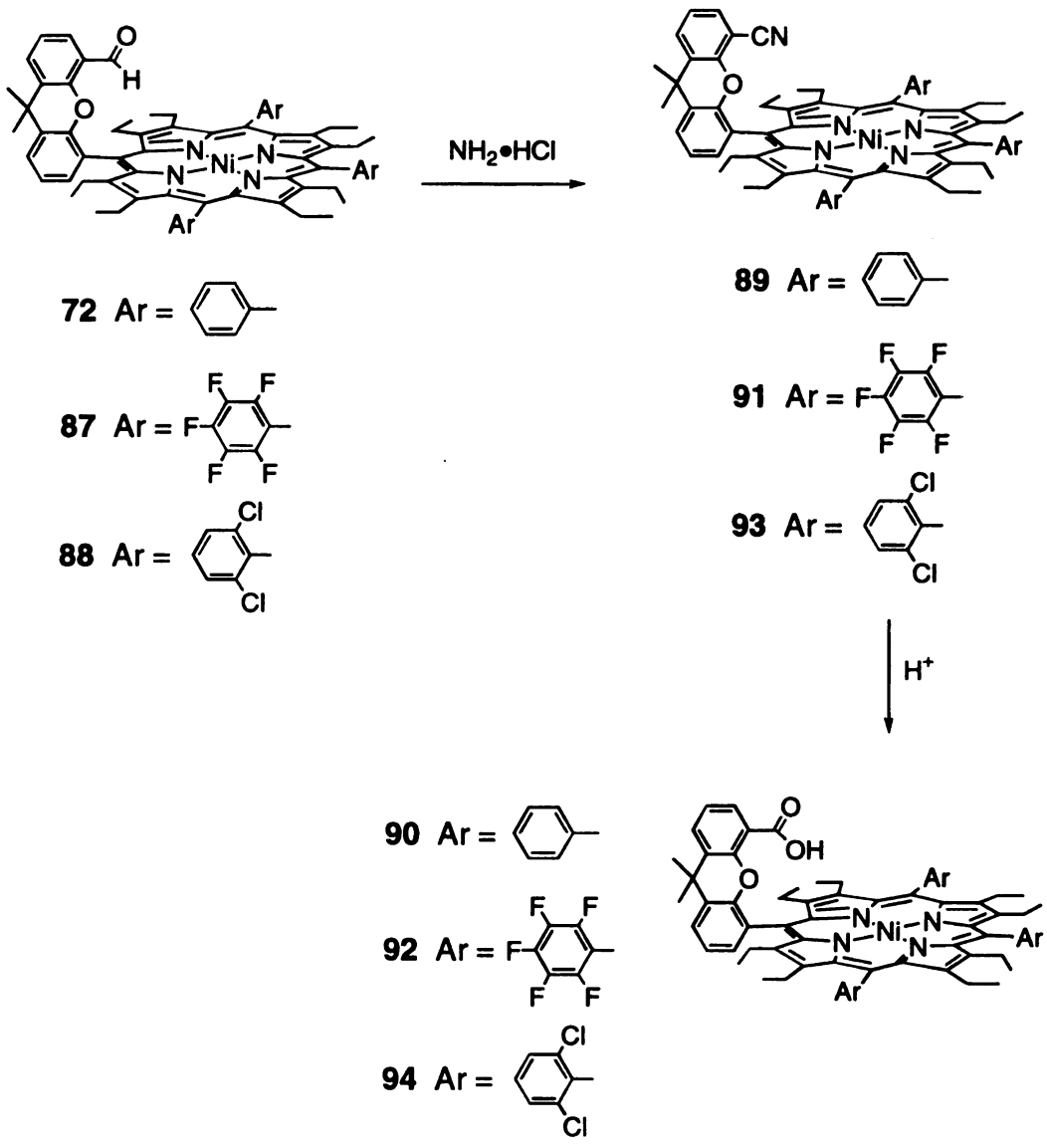

Scheme 5-7

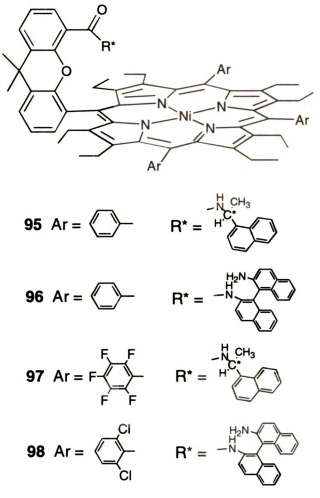

Figure 5-3. Structures of single armed chiral nonplanar porphyrins.

X-ray Crystal Structure of (R)-95 and CD Spectra

The X-ray crystal structure of (R)-**95** is shown in Figure 5-4. The crystal data and refinement parameters are given in Table 5-1. Table 5-2 lists the average out of plane displacements, bond lengths, and bond angles. The porphyrin ring indeed is a ruffled structure in which the pyrrole units bend alternately above and below the mean plane and the phenyl groups tilt into the macrocycle plane to minimize steric interactions with the substituents. The distance of N5-O1 is 2.932 Å, well within the range of H-bonding. However, the amide group tilts away from the xanthyl plane by 53.4°, presumably, due to steric interactions with the porphyrin ring and lies almost parallel to the C_{meso} plane (5.0°). As expected, the naphthyl group, being the largest on the chiral center moves away from the porphyrin plane to reduce steric interactions with the macrocycle. The dihedral angle between the naphthyl and C_{meso} planes is 88.4°. The methyl group (C72) is positioned right above the porphyrin ring (δ -1.29 ppm) and points into the quadron that bends down below the mean plane. This particular arrangement of the saddle shape in relation to the size of the substituents at the chiral center is almost intuitively predictable, and represents the most stable conformation by molecular mechanics (MMFF).

CD spectroscopy is a useful tool for determining the absolute configuration of molecules with chirality.[262-264] CD spectra of all our chiral porphyrins showed a mirror image relationship between their respective enantiomers. As an example, Figure 5-5 gives the CD spectra of porphyrin **95** in CH_2Cl_2 at room temperature, with a split Cotton effect near the Soret band showing that the (R) and (S) forms are perfect mirror images of each other. These results indicate that one of the two nonplanar enantiomers is stabilized when a particular chiral auxiliary is introduced to the porphyrin. The Δε values of CD spectra at low temperature (-78 °C) are not significantly different from those at room temperature, indicating that the chiral induction is effective even at room temperature. Ogoshi et al. reported the mechanism of induced CD of an amino acid ester-porphyrin

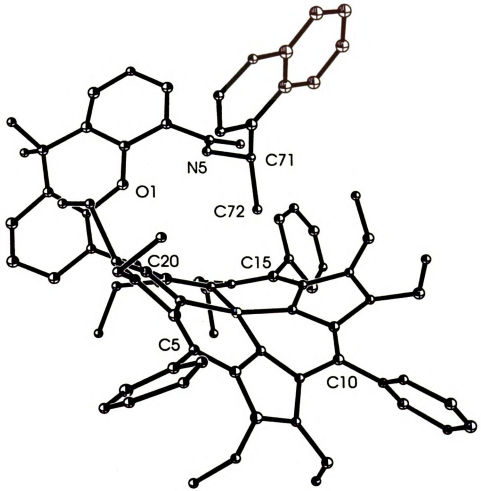

Figure 5-4. X-ray crystal structure of the (R) form of porphyrin **95**. Hydrogen atoms have been omitted for clarity.

Table 5-1. Crystal data, Intensity Measurements, and Refinement parameters for Porphyrin (R)-**95**.

Formula	$NiO_4N_5C_{90}H_{99}$
Formula Weight	1373.5
Crystal System	Monoclinic
Space Group	$P2_1$
Temperature, K	298
a, Å	13.430(6)
b, Å	22.081(6)
c, Å	13.77(1)
β, deg	108.30(6)
V, Å^3	3,877(4)
Z	2
Crystal Dimensions, mm	0.05 x 0.10 x 0.20
D_{calcd}, g cm^{-1}	1.176
μ, cm^{-1}	8.28
Radiation	CuKα
F(000)	1468
2θ range, deg	40.2 - 69.4
Scan Type	ω
Scan Width, deg	(0.94 + 0.3 tan θ)
Transm Range	0.7081 – 0.9821
No. of Unique Reflections	5948
No. of Reflections Observed	3224
Structure Solution	Direct Method
No. of Parameters	854
R; Rw[a]	0.094; 0.100
S	2.66

[a] $R = \Sigma||Fo|-|Fc||/\Sigma|Fo|$, $Rw = [\Sigma w (||Fo|-|Fc||)^2/\Sigma wFo^2]^{1/2}$.

Table 5-2. Average Out-of-Plane Displacements, Bond Lengths, and Bond Angles for Porphyrin (R)-**95**.

		Displacement (Å)[a]	
N	0.210	C_m	0.025
C_α	0.490	C_β	1.214
		Bond Length (Å)	
Ni-N	1.916	N- C_α	1.380
C_α- C_β	1.472	C_β- C_β	1.389
C_α- C_m	1.381		
		Bond Angle (deg)	
N- C_α- C_β	108.1	N- C_α- C_m	123.8
C_α- N- C_α	108.7	C_α- C_β - C_β	106.6
C_m- C_α- C_β	127.4	C_α- C_m - C_α	119.9

[a] From the least-square plane of the 4 C_{meso} atoms.

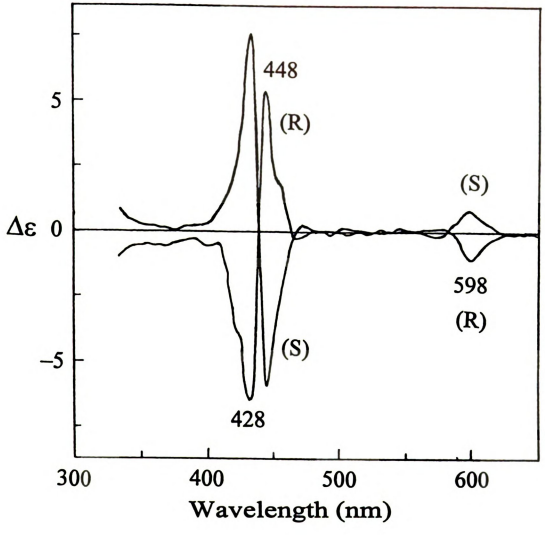

Figure 5-5. Circular dichroism (CD) spectra of (R)-**95** and (S)-**95** in CH_2Cl_2 at 20 °C.

complexation system.[265,266] The splitting in the CD spectra observed in the Soret region were ascribed to the coupling of the C=O group of the amino acid esters and the porphyrin. The splitting seen in CD spectra of our chiral porphyrins can also be ascribed to the coupling of the C=O and the porphyrin macrocylcle. As observed in the X-ray structure of (R)-**95**, the C=O on xanthyl group lies parallel to the porphyrin mean plane, which would have maximum coupling with the macrocycle. The coupling of the naphthyl group and the porphyrin can be excluded since they are nearly perpendicular to each other. The fact that no aggregation was observed in the concentration range used for UV-vis spectroscopy also rules out possible inter-porphyrin couplings. The ruffling of the porphyrin plane also could result in the Cotton effects.[265] Whether ring deformation alone could account for the observed splitting in the CD spectra, however, cannot be determined unambiguously with the present system.

Conclusions

We have described here the synthesis of xanthene-bridged chiral porphyrins and their circular dichroism profiles. The (R) and (S) forms of this series of chiral porphyrins exhibit positive and negative split Cotton effects at longer wavelengths in the Soret region, respectively. The CD spectra of the (R) and (S) forms are perfect mirror images of each other. The x-ray crystal structure of chiral porphyrin (R)-**95** shows that the macrocycle is strongly ruffled with the pyrrole units alternately positioned above and below the mean porphyrin plane. One of the two macrocyle conformations is favored due to the chiral auxiliary attached to xanthyl group. While the first crystallographic determination of the absolute configuration of a chiral N-substituted porphyrin and correlation with its CD spectrum was reported by Inoue and coworkers,[267] our study is the first to determine the CD behavior of a saddle-shaped nonplanar porphyrin with a well-defined structure. The simplicity in the synthesis to obtain chiral porphyrin ligands should render this approach quite attractive at providing useful metalloporphyrin catalysts

for asymmetric reactions.

Experimental

Materials

All reagents and solvents were obtained from commercial sources and were used without further purification unless otherwise noted. Dry dichloromethane and were obtained by refluxing and distilling over CaH_2. Silica gel for chromatography was 60-200 mesh, manufactured by Fisher Scientific. Analytical TLC was performed on Eastman Kodak 13181 silica gel sheets. Preparative TLC was performed on Analtech silica gel plates. Compositions of solvent mixtures are quoted as ratios of volume.

Instrumentation

^1H NMR (300 MHz) spectra were recorded on a Varian Gemini spectrometer. Chemical shifts are reported in ppm relative to the residual proton in deuterated chloroform (7.24 ppm). Absorption spectra were recorded on a Shimadzu UV-160 or Varian Carry 219 spectrometer. Mass spectra were obtained on a benchtop VG Trio-1 mass spectrometer. FAB-MS mass spectra were obtained on a JEOL HX-110 HF double focusing spetrometer operating in the positive ion detection mode. Circular dichroism spectra were recorded in CH_2Cl_2 on a JASCO Type J-720 spectropolarimeter.

Crystallography

Crystals of porphyrin (R)-**95** were grown from ether by slow evaporation. To prevent solvent evaporation, the chosen crystal was coated with hydrocarbon oil and mounted on a glass fiber of a Rigaku AFC5R diffractometer with graphite-monochromated Cu Kα radiation. The crystal structure was solved by direct methods and refined by full matrix least-squares using Fourier techniques. Some non-hydrogen atoms were refined anisotropically, while the rest were refined isotropically. Hydrogen

atoms were not refined. Crystallographic details for the structure are given in Table 5-1.

4,5-Diformyl-9,9-dimethylxanthene (64)

9,9-Dimethylxanthene **63** (3.00 g, 14 mmol) and tetramethylethylenediamine (5.7 ml, 35 mmol) in dry heptane (150 ml) was purged with argon for 5 min. To this solution was added dropwise butyl lithium (21.5 ml, 1.6 M in hexane) in a 30 min period. The resulting solution was refluxed for 10 min and cooled to 0 °C. After dry DMF (6 ml) was added, the solution was slowly warmed up to room temperature and stirred for 15 min. The solution was poured into water (500 ml), and the mixture was filtered and dried to give 2.98 g of the product (80%). m.p. 180-182 °C; ^{1}HNMR (300 MHz, $CDCl_3$): δ 10.69 (2H, s, aldehyde), 7.82 (2H, d, aryl), 7.71 (2H, d, aryl), 7.21 (2H, dd, aryl), 1.71 (2H, d, CH_3); MS found m/e 266.0, cacld. 266.09 for $C_{17}H_{14}O_3$.

Bis(3,4-diethyl-5-ethoxycarbonyl-2-pyrryl)phenylmethane (70)

A solution of pyrrole **69** (780 mg, 4 mmol) and benzaldehyde (212 mg, 2 mmol) in 10 ml CH_2Cl_2 was cooled in an ice bath under argon. To the solution was added $TiCl_4$ (240 µl, 2.2 mmol). The resulting solution was stirred at room temperature for 2 h. The mixture was then extracted with CH_2Cl_2 and washed several times with water. The organic layer was dried over anhydrous Na_2SO_4 and the solvent was removed in *vacuo*. The residue was then chromatographed on silica gel eluting with CH_2Cl_2 to give 880 mg of the product (92%). m.p. 138-140 °C; ^{1}HNMR (300 MHz, $CDCl_3$): δ 8.66 (2H, br s, NH), 7.34-7.22 (3H, m, phenyl), 7.07 (2H, d, phenyl), 5.58 (1H, s, CH), 4.17 (4H, q, CH_2), 2.71 (4H, q, CH_2), 2.32 (4H, q, CH_2), 1.26 (6H, t, CH_3), 1.15 (6H, t, CH_3), 0.92 (6H, t, CH_3); MS found m/e 478.4, cacld. 478.28 for $C_{29}H_{38}N_2O_4$.

Bis(3,4-diethyl-5-ethoxycarbonyl-2-pyrryl)(mesityl)methane (74)

A procedure similar to that used for the synthesis of **70** was employed to give a 72% yield

of the product. ^{1}HNMR (300 MHz, $CDCl_3$): δ 8.17 (2H, br s, NH), 7.26 (2H, s, phenyl), 5.82 (1H, s, CH), 4.25 (4H, q, CH_2), 2.71 (4H, q, CH_2), 2.26 (3H, s, CH_3), 2.18 (4H, q, CH_2), 1.99 (6H, s, CH_3), 1.31 (6H, t, CH_3), 1.15 (6H, t, CH_3), 0.88 (6H, t, CH_3); MS found m/e 520.4, cacld. 520.33 for $C_{32}H_{44}N_2O_4$.

Bis(3,4-diethyl-5-ethoxycarbonyl-2-pyrryl)(2,6-dichlorophenyl)methane (77)

A procedure similar to that used for the synthesis of **70** was employed to give a 90% yield of the product. m.p. 134-136 °C; ^{1}HNMR (300 MHz, $CDCl_3$): δ 8.57 (2H, br s, NH), 7.36 (2H, d, phenyl), 7.19 (1H, t, phenyl), 6.40 (1H, s, CH), 4.27 (4H, q, CH_2), 2.71 (4H, q, CH_2), 2.24 (4H, q, CH_2), 1.32 (6H, t, CH_3), 1.15 (6H, t, CH_3), 0.86 (6H, t, CH_3); MS found m/e 546.0, cacld. 546.21 for $C_{29}H_{36}Cl_2N_2O_4$.

Ni(II) *trans*-5,15-bis[5-carbonyl-4-(9,9-dimethyl)xanthyl]-10,20-dimesityl-2,3,7,8,12, 13,17,18-octaethylporphyrin (76)

Diester dipyrrylmethane **74** (1.04 g, 2 mmol) was decarboxylated by gently refluxing in ethylene glycol (10 ml) containing NaOH (1 g) for 4 h under argon to give quantitative yield of dipyrrylmethane **75** after extraction with CH_2Cl_2 and removal of solvent in *vacuo*. Without further purification, **75** was condensed with an equimolar amount of diformyldimethylxanthene **3** in CH_2Cl_2 (25 ml) at room temperature for 2h in the presence of $BF_3{\cdot}OEt_2$ (0.2 eq), followed by oxidation with DDQ (0.9 g, 4 mmol) for 30 min. The solvent was removed under reduced pressure and the residue was chromatographed on silica gel eluting with CH_2Cl_2 and methanol (30:1). The green band was collected and the solvent was removed under reduced pressure. The protonated porphyrins were dissovled in DMF (50 ml). Excess $Ni(OAc)_2$ was added to the solution and the mixture was refluxed until metallation was complete as evidenced by UV-vis (ca. 30 min). The solvent was removed in *vacuo* and the residue was extracted with CH_2Cl_2. The organic layer was collected and dried over Na_2SO_4. The solvent was removed under

reduced pressure. The mixture was chromatographed on silca gel eluting with CH_2Cl_2 and hexane (3:7) to give 233 mg (18%) of the *trans* product. The *cis*-porphyrin is inseparable from the mixture. UV-vis (CH_2Cl_2, λ_{max} nm (ε)): 595 (13,100), 555 (14,800), 438 (178,200); ^{1}HNMR (300 MHz, $CDCl_3$): δ 8.70 (2H, s, CHO), 7.76 (2H, dd, xanthyl), 7.68 (2H, dd, xanthyl), 7.66 (2H, dd, xanthyl), 7.48 (2H, dd, xanthyl), 7.38 (2H, t, xanthyl), 7.08 (2H, t, xanthyl), 7.03 (4H, s, mesityl), 2.50 (6H, s, CH_3 of mesityl), 2.5-2.0 (16H, b, CH_2 of ethyl), 1.95 (12H, s, CH_3 of mesityl), 1.85 (12H, s, CH_3 of xanthyl), 0.54 (24H, t, CH_3 of ethyl); MS (FAB) found m/e 1299.7, cacld. 1298.62 for $C_{86}H_{88}N_4O_4Ni$.

Ni(II) *trans*-5,15-bis[5-cyano-4-(9,9-dimethyl)xanthyl]-10,20-dimesityl-2,3,7,8,12,13, 17,18–octaethylporphyrin (80)

Porphyrin **76** (130 mg, 0.1 mmol) was demetallated by washing with conc. $HCl_{(aq)}$. The diacid form was dissolved in formic acid (20 ml) and $NH_2OH^{\cdot}HCl$ (17.4 mg, 0.25 mmol) was added to the solution. The mixture was refluxed for 2 d under argon atmosphere before the solvent was removed in *vacuo*. The residue was dissolved in CH_2Cl_2 and washed with 10% $HCl_{(aq)}$. The organic layer was dried over anhydrous Na_2SO_4 and the solvent was removed in *vacuo*. The residue was then dissolved in DMF (20 ml) and excess $Ni(OAc)_2$ was added to the solution. After the metallation was complete as evidenced by UV-vis (ca. 30 min), DMF was removed under reduced pressure. The solid was extracted with CH_2Cl_2. After removal of the solvent, the solid residue was chromatiographed on silica gel eluting with CH_2Cl_2 and hexane (3:7) to give 118 mg of the product (91%). IR ν_{max} 2236 (C≡N) cm^{-1}; UV-vis (CH_2Cl_2, λmax nm (ε)): 595 (13,200), 559 (14,600), 438 (191,500); ^{1}HNMR (300 MHz, $CDCl_3$): δ 7.69 (2H, dd, xanthyl), 7.64 (2H, dd, xanthyl), 7.55 (2H, dd, xanthyl), 7.33 (2H, t, xanthyl), 7.22 (2H, dd, xanthyl), 7.05 (2H, t, xanthyl), 7.05 (4H, s, mesityl), 2.47 (6H, s, CH_3 of mesityl), 2.5-2.0 (16H, b, CH_2 of ethyl), 2.00 (12H, s, CH_3 of mesityl), 1.83 (12H, s, CH_3 of

xanthyl), 0.53 (24H, t, CH_3 of ethyl); MS (FAB) found m/e 1293.7, cacld. 1292.61 for $C_{86}H_{86}N_6O_2Ni$.

Ni(II) *trans*-5,15-bis[5-hydroxylcarbonyl-4-(9,9-dimethyl)xanthyl]-10,20-dimesityl-2,3,7,8,12,13,17,18-octaethylporphyrin (81)

Porphyrin **80** (130 mg, 0.1 mmol) was demetallated by washing with conc. $HCl_{(aq)}$. The diacid form of the porphyrin was hydrolyzed for 5 d in the refluxing mixture of H_2SO_4 (6 ml), acetic acid (20 ml), and water (10 ml) under argon. The residue was dissolved in CH_2Cl_2 and washed with water. The organic layer was dried over anhydrous Na_2SO_4 and the solvent was removed in *vacuo*. The residue was then dissolved in DMF (20 ml) and excess $Ni(OAc)_2$ was added to the solution. After the metallation was complete as evidenced by UV-vis (ca. 30 min), DMF was removed under reduced pressure. The solid was extracted with CH_2Cl_2. After removal of the solvent, the solid residue was chromatographed on silica gel eluting with CH_2Cl_2 and hexane (7:3) to give 118 mg of the product (82%). IR ν_{max} 3403 (O-H), 1740 (C=O) cm^{-1}; UV-vis (CH_2Cl_2, λmax nm (ε)): 594 (14,100), 555 (14,700), 436 (178,800); ^{1}HNMR (300 MHz, $CDCl_3$): δ8.40 (2H, br s, OH), 7.86 (2H, dd, xanthyl), 7.78 (2H, dd, xanthyl), 7.73 (2H, dd, xanthyl), 7.69 (2H, dd, xanthyl), 7.46 (2H, t, xanthyl), 7.16 (2H, t, xanthyl), 7.05 (4H, s, mesityl), 2.47 (6H, s, CH_3 of mesityl), 2.5-2.0 (16H, b, CH_2 of ethyl), 2.03 (12H, s, CH_3 of mesityl), 1.83 (12H, s, CH_3 of xanthyl), 0.56 (12H, t, CH_3 of ethyl), 0.49 (12H, br s, CH_3 of ethyl); MS (FAB) found m/e 1331.7, cacld. 1330.61 for $C_{86}H_{88}N_4O_6Ni$.

Ni(II) *trans*-5,15-bis{5-[1-(1-naphthyl)ethylcarboxamide]-4-(9,9-dimethyl)xanthyl}-10,20-dimesityl-2,3,7,8,12,13,17,18-octaethylporphyrin (82)

To a solution of porphyrin **81** (27 mg, 0.02 mmol) in CH_2Cl_2 (10 ml) was added $SOCl_2$ (0.5 ml) and the solution was refluxed for 1h under argon atmosphere before the solvent was removed in *vacuo*. The residue was then dissolved in CH_2Cl_2 (10 ml) and (R or S) 1-naphthylethylamine (34 mg, 0.2 mmol) was added to the solution. The resulting mixture

was stirred at room temperature overnight under argon before the solvent was removed. The residue was then dissolved in DMF (20 ml) and excess $Ni(OAc)_2$ was added to the solution. After the metallation was complete as evidenced by UV-vis (ca. 30 min), DMF was removed under reduced pressure. The solid was extracted with CH_2Cl_2. After removal of the solvent, the solid residue was chromatographed on silica gel eluting with CH_2Cl_2 and methanol (100:1). After removal of the solvent, the solid was futher purified with preparative TLC plate to give 4.3 mg (13%) of the product. IR ν_{max} 3415 (N-H), 1664 (C=O) cm^{-1}; UV-vis (CH_2Cl_2, λmax nm (rel intens)): 599 (0.08), 559 (0.08), 438 (1.00); ^{1}HNMR (300 MHz, $CDCl_3$): δ8.06 (2H, dd, xanthyl), 7.74 (2H, dd, xanthyl), 7.67 (2H, dd, xanthyl), 7.40 (2H, dd, xanthyl), 7.18 (2H, t, xanthyl), 7.14-7.00 (6H, m, xanthyl and naphthyl), 6.93 (2H, t, naphthyl), 6.63 (2H, d, naphthyl), 6.18 (2H, t, naphthyl), 6.08 (2H, d, naphthyl), 4.68 (2H, t, naphthyl), 2.84 (2H, q, CH), 2.6-1.8 (16H, several m, CH_2 of ethyl), 2.48 (6H, s, CH_3 of mesityl), 2.14 (6H, s, CH_3 of mesityl), 2.00 (6H, s, CH_3 of xanthyl), 1.97 (6H, s, CH_3 of xanthyl), 1.79 (6H, s, CH_3 of mesityl), 0.56 (12H, t, CH_3 of ethyl), 0.43 (6H, t, CH_3 of ethyl), 0.24 (6H, t, CH_3 of ethyl), -1.56 (6H, d, CH_3); MS (FAB) found m/e 1637.9, cacld. 1636.79 for $C_{110}H_{110}N_6O_4Ni$.

Ni(II) 5,15-bis[5-carbonyl-4-(9,9-dimethyl)xanthyl]-10, 20-bis(2,6-dichlorophenyl)-2, 3, 7, 8, 12, 13, 17, 18- octaethylporphyrin (79)

A procedure similar to that used for the synthesis of **76** was employed to give the *trans*-porphyrin in 22 % yield and the *cis*-porphyrin in 17% yield.

Trans-**79**: UV-vis (CH_2Cl_2, λ_{max} nm (ε)): 600 (16,300), 560 (12,800), 436 (173,500); ^{1}HNMR (300 MHz, $CDCl_3$): δ8.75 (2H, s, CHO), 7.78 (2H, dd, xanthyl), 7.69 (2H, dd, xanthyl), 7.68 (2H, dd, xanthyl), 7.62-7.44 (6H, m, phenyl), 7.52 (2H, d, xanthyl), 7.40 (2H, t, xanthyl), 7.09 (2H, t, xanthyl), 2.80-1.90 (16H, br s, CH_2 of ethyl), 1.87 (6H, s, CH_3 of xanthyl), 0.72 (12H, t, CH_3 of ethyl), 0.50 (12H, br s, CH_3 of ethyl); MS (FAB) found m/e 1352.4, cacld. 1350.37 for $C_{80}H_{72}Cl_4N_4O_4Ni$.

Cis-**79**: UV-vis (CH_2Cl_2, λmax nm (ε)): 600 (15,700), 560 (12,700), 436 (171,800); ^{1}HNMR (300 MHz, $CDCl_3$): δ 9.09 (2H, s, CHO), 7.78 (2H, dd, xanthyl), 7.72 (2H, dd, xanthyl), 7.66-7.54 (6H, m, xanthyl and phenyl), 7.54-7.44 (4H, m, xanthyl and phenyl), 7.36 (2H, t, xanthyl), 7.12 (2H, t, xanthyl), 2.60-2.00 (16H, 2 br s, CH_2 of ethyl), 1.88 (6H, s, CH_3 of xanthyl), 0.70 (12H, t, CH_3 of ethyl), 0.52 (12H, t, CH_3 of ethyl); MS (FAB) found m/e 1352.3, cacld. 1350.37 for $C_{80}H_{72}Cl_4N_4O_4Ni$.

Ni(II) 5,15-bis[5-cyano-4-(9,9-dimethyl)xanthyl]-10,20-bis(2,6-dichlorophenyl)-2,3,7,8,12,13,17,18-octaethylporphyrin (83)

A produre similar to that used for the synthesis of **80** was employed to give 89% yield of *trans*-**83** and 86% yield of *cis*-**83**.

Trans-**83**: IR ν_{max} 2237 (C≡N) cm^{-1}; UV-vis (CH_2Cl_2, λ_{max} nm (ε)): 601 (16,500), 561 (12,900), 437 (173,800); ^{1}HNMR (300 MHz, $CDCl_3$): δ 7.70 (2H, dd, xanthyl), 7.64 (2H, dd, xanthyl), 7.60-7.40 (6H, m, phenyl, 7.53 (2H, dd, xanthyl), 7.32 (2H, t, xanthyl), 7.23 (2H, dd, xanthyl), 7.05 (2H, t, xanthyl), 2.60-1.90 (16H,br s, CH_2 of ethyl), 1.83 (12H, s, CH_3 of xanthyl), 0.67 (12H, t, CH_3 of ethyl), 0.53 (12H, t, CH_3 of ethyl); MS (FAB) found m/e 1346.3, cacld. 1344.37 for $C_{80}H_{70}Cl_4N_6O_2Ni$.

Cis-**83**: IR ν_{max} 2236 (C≡N) cm^{-1}; UV-vis (CH_2Cl_2, λ_{max} nm (ε)): 601 (15,800), 561 (12,400), 437 (168,900); ^{1}HNMR (300 MHz, $CDCl_3$): δ 7.70 (2H, dd, xanthyl), 7.67 (2H, dd, xanthyl), 7.59 (2H, dd, xanthyl), 7.56 (2H, dd, phenyl), 7.46 (2H, t, xanthyl), 7.33 (2H, dd, xanthyl), 7.31-7.25 (4H, m, phenyl), 2.60-2.10 (16H, br m, CH_2 of ethyl), 1.84 (12H, s, CH_3 of xanthyl), 0.67 (12H, t, CH_3 of ethyl), 0.53 (12H, t, CH_3 of ethyl); MS (FAB) found m/e 1346.3, cacld. 1344.37 for $C_{80}H_{70}Cl_4N_6O_2Ni$.

Ni(II) 5,15-bis[5-hydroxycarbonyl-4-(9,9-dimethyl)xanthyl]-10,20-bis(2,6-dichlorophenyl)-2,3,7,8,12,13,17,18-octaethylporphyrin (84)

A procedure similar to that used for the synthesis of **81** was employed to give 85 % yield of *trans*-**84** and 81% yield of *cis*-**84**.

Trans-**84**: IR ν_{max} 3409 (O-H), 1736 (C=O) cm^{-1}; UV-vis (CH_2Cl_2, λ_{max} nm (ε)): 598 (17,200), 559 (13,300), 435 (167,500); ^{1}HNMR (300 MHz, $CDCl_3$): δ 8.20-8.00 (2H, br s, CO_2H), 7.84 (2H, dd, xanthyl), 7.78 (2H, dd, xanthyl), 7.72 (2H, dd, xanthyl), 7.70 (2H, dd, xanthyl), 7.60-7.4 (6H, m, phenyl), 7.49 (2H, dd, xanthyl), 7.14 (2H, t, xanthyl), 2.5-2.0 (16H, s, CH_2 of ethyl), 1.85 (12H, s, CH_3 of xanthyl), 0.68 (12H, t, CH_3 of ethyl), 0.47 (12H, br s, CH_3 of ethyl); MS (FAB) found m/e 1384.2, cacld. 1382.36 for $C_{80}H_{72}Cl_4N_4O_6Ni$.

Cis-**84**: IR ν_{max} 3414 (O-H), 1740 (C=O) cm^{-1}; UV-vis (CH_2Cl_2, λ_{max} nm (ε)): 598 (17,100), 559 (13,500), 435 (174,800); ^{1}HNMR (300 MHz, $CDCl_3$): δ 8.40-8.00 (2H, br s, CO_2H), 7.93 (2H, dd, xanthyl), 7.79 (2H, dd, xanthyl), 7.73 (2H, dd, xanthyl), 7.61 (2H, dd, xanthyl), 7.60-7.45 (6H, m, phenyl), 7.39 (2H, dd, xanthyl), 7.19 (2H, t, xanthyl), 2.50-2.10 (16H,2 br s, CH_2 of ethyl), 1.88 (12H, s, CH_3 of xanthyl), 0.70 (12H, t, CH_3 of ethyl), 0.49 (12H, br s, CH_3 of ethyl); MS (FAB) found m/e 1384.2, cacld. 1382.36 for $C_{80}H_{72}Cl_4N_4O_6Ni$.

Ni(II) *cis*-5,15-bis{5-[1-(1-naphthyl)ethylcarboxamide]-4-(9,9-dimethyl)xanthyl}-10,20- bis(2,6-dichlorophenyl) -2,3,7,8,12,13,17,18-octaethylporphyrin (85)

A procedure similar to that used for the synthesis of **82** was employed to give the product in 15 % yield. IR ν_{max} 3422 (N-H), 1657 (C=O) cm^{-1}; UV-vis (CH_2Cl_2, λ_{max} nm (ε)): 605 (16,100), 561 (11,000), 439 (151,100); 1HNMR (300 MHz, CDCl3): δ 7.88 (2H, dd, xanthyl), 7.74 (2H, dd, xanthyl), 7.68 (2H, dd, xanthyl), 7.60 (4H, d, phenyl), 7.52 (2H, dd, xanthyl), 7.30-7.18 (2H, m, phenyl), 7.23 (2H, t, xanthyl), 7.12 (2H, t, xanthyl), 7.02 (2H, d, naphthyl), 6.85 (2H, t, naphthyl), 6.73 (2H, d, naphthyl), 6.65 (2H, d, naphthyl), 6.51(2H, t, naphthyl), 6.14 (2H, d, naphthyl), 4.74 (2H, t, naphthyl), 3.02 (2H, q, CH),

2.8-1.7 (16H, several m, CH_2 of ethyl), 1.96 (6H, s, CH_3 of xanthyl), 1.73 (6H, s, CH_3 of xanthyl), 0.96-0.30 (24H, m, CH_3 of ethyl), -1.77 (6H, d, CH_3); MS (FAB) found m/e 1692.54, cacld. 1688.54 for $C_{104}H_{94}Cl_4N_6O_4Ni$.

Ni(II) 5-[5-carbonyl-4-(9,9-dimethyl)xanthyl]-10,15,20-triphenyl-2,3,7,8,12,13,17,18-octaethylporphyrin (72)

Method **a**: Diformylxanthene **64** (0.67 g, 2.5 mmol), benzaldehyde (0.80 g, 7.5 mmol), and 3,4-diethylpyrrole (1.23 g, 10 mmol) were added to 1 L of freshly distilled dichloromethane, and the solution was stirred and purged with nitrogen. After 20 min, 0.1 equivalent of $BF_3{\cdot}OEt_2$ was added, and the reaction flask was shielded with aluminum foil. After the mixture was stirred for 1 h at room temperature under nitrogen, DDQ (2.27 g, 10 mmol) was added. The reaction mixture was refluxed for 30 min to give a green solution. The solution was then concentrated and chromatographed on silica gel eluting with CH_2Cl_2 and methanol (30:1). The green band was collected and the solvent was evaporated under reduced pressure. The protonated porphyrins were metallated with $Ni(OAc)_2$ in refluxing DMF using the typical procedure described. The mixture was chromatographed on silica gel eluting with CH_2Cl_2 and hexane (3:7). The first band was NiOETPP and the second band was the expected porphyrin. The second band was collected and the solvent was removed in *vacuo* to give 290 mg of the product (11%). UV-vis (CH_2Cl_2, λ_{max} nm (ε)): 590 (11,600), 553 (13,800), 435 (188,500); ^{1}HNMR (300 MHz, $CDCl_3$): δ 8.84 (1H, s, CHO), 8.20-8.00 (6H, m, phenyl), 7.84 (1H, dd, xanthyl), 7.79 (1H, dd, xanthyl), 7.72 (1H, dd, xanthyl), 7.67 (1H, dd, xanthyl), 7.64-7.52 (9H, m, phenyl), 7.42 (1H, t, xanthyl), 7.15 (1H, t, xanthyl), 2.80-1.70 (16H, br, CH_2 of ethyl), 1.85 (12H, s, CH_3 of xanthyl), 0.70-0.35 (24H, m, CH_3 of ethyl); MS (FAB) found m/e 1055.4, cacld. 1054.47 for $C_{70}H_{68}N_4O_2Ni$.

Method **b**: The diester dipyrrylmethane **70** (1.04 g, 2 mmol) was decarboxylated by

gently refluxing in ethylene glycol (10 ml) containing NaOH (1 g) for 4 h under argon to give dipyrrylmethane **71** in quantitative yield after extraction with CH_2Cl_2 and removal of solvent. Without further purification, dipyrrylmethane **71** was condensed with diformylxanthene **64** (0.27 g, 1 mmol) and benzaldehyde (0.11 g, 1 mmol) in CH_2Cl_2 (25 ml) at room temperature for 2h in the presence of $BF_3{\cdot}OEt_2$ (0.2 eq), followed by oxidation with DDQ (0.9 g, 4 mmol) for 30 min. The solvent was removed under reduced pressure and the residue was chromatographed on silica gel eluting with CH_2Cl_2 and methanol (30:1). The green band was collected and the solvent was removed under reduced pressure. The protonated porphyrins were metallated with $Ni(OAc)_2$ in refluxing DMF. The mixture was chromatographed on silica gel eluting with CH_2Cl_2 and hexane (3:7). The first band was NiOETPP and the second band was the expected porphyrin. The second band was collected and the solvent was removed in *vacuo* to give 111 mg of porphyrin **72** (21%).

Ni(II) 5-[5-cyano-4-(9,9-dimethyl)xanthyl]-10,15,20-triphenyl-2,3,7,8,12,13,17,18-octaethylporphyrin (89)

A procedure similar to that used for the synthesis of **80** was employed to give porphyrin **89** in 92% yield. IR ν_{max} 2232 (C≡N) cm^{-1}; UV-vis (CH_2Cl_2, λ_{max} nm (ε)): 592 (10,500), 554 (12,500), 435 (169,600); ^{1}HNMR (300 MHz, $CDCl_3$): δ 8.26-7.98 (6H, m, phenyl), 7.80 (1H, dd, xanthyl), 7.73 (1H, dd, xanthyl), 7.65 (1H, dd, xanthyl), 7.66-7.50 (9H, m, phenyl), 7.39 (1H, t, xanthyl), 7.37 (1H, dd, xanthyl), 7.09 (1H, t, xanthyl), 2.85-1.50 (16H, br, CH_2 of ethyl), 1.81 (12H, s, CH_3 of xanthyl), 0.70-0.35 (24H, m, CH_3 of ethyl); MS (FAB) found m/e 1052.4, cacld. 1051.47 for $C_{70}H_{67}N_5ONi$.

Ni(II) 5-[5-hydroxycarbonyl-4-(9,9-dimethyl)xanthyl]-10,15,20-triphenyl-2,3,7,8,12,13,17,18-octaethylporphyrinato)nickel (90)

A procedure similar to that used for the synthesis of **81** was employed to give porphyrin

90 in 92% yield. IR ν_{max} 3405 (O-H), 1738 (C=O) cm^{-1}; UV-vis (CH_2Cl_2, λ_{max} nm (ε)): 590 (11,000), 554 (13,000), 435 (161,000); ^{1}HNMR (300 MHz, $CDCl_3$): δ8.39 (1H, br s, CO_2H), 8.24-8.02 (6H, m, phenyl), 8.00 (1H, dd, xanthyl), 7.86 (1H, dd, xanthyl), 7.81 (1H, dd, xanthyl), 7.74 (1H, dd, xanthyl), 7.70-7.52 (9H, m, phenyl), 7.47 (1H, t, xanthyl), 7.22 (1H, t, xanthyl), 2.85-1.60 (16H, br, CH_2 of ethyl), 1.87 (6H, s, CH_3 of xanthyl), 0.65-0.30 (24H, m, CH_3 of ethyl); MS (FAB) found m/e 1071.2, cacld. 1070.46 for $C_{70}H_{68}N_4O_3Ni$.

Ni(II) 5-{5-[1-(1-naphthyl)ethylcarboxamide]-4-(9,9-dimethyl)xanthyl}-10,15,20-triphenyl-2,3,7,8,12,13,17,18-octaethylporphyrin (95)

A procedure similar to that used for the synthesis of **82** was employed to give porphyrin **95** in 71% yield. IR ν_{max} 3420 (N-H), 1661 (C=O) cm^{-1}; UV-vis (CH_2Cl_2, λ_{max} nm (ε)): 590 (10,600), 552 (12,800), 435 (164,900); ^{1}HNMR (300 MHz, $CDCl_3$): δ8.21 (2H, br, phenyl), 8.06 (2H, d, phenyl), 8.01 (1H, dd, xanthyl), 7.74 (1H, dd, xanthyl), 7.61 (1H, dd, xanthyl), 7.66-7.50 (12H, m, phenyl and xanthyl), 7.37 (1H, d, naphthyl), 7.28 (1H, t, xanthyl), 7.18 (1H, t, xanthyl), 7.10-7.00 (3H, m, naphthyl), 6.46 (1H, d, naphthyl), 6.10 (1H, t, naphthyl), 5.98 (1H, d, naphthyl), 4.50-4.20 (1H, br s, CH), 2.85-1.80 (16H, m, CH_2 of ethyl), 2.00 (3H, s, CH_3 of xanthyl), 1.73 (3H, s, CH_3 of xanthyl), 0.60-0.20 (24H, m, CH_3 of ethyl), -1.22 (3H, d, CH_3); MS (FAB) found m/e 1224.3, cacld. 1223.56 for $C_{82}H_{79}N_5O_2Ni$.

Ni(II) 5-{5-[2-(1-(2-aminonaphthyl)naphthyl)carboxamide]-4-(9,9-dimethyl)xanthyl} -10,15,20-triphenyl-2,3,7,8,12,13,17,18-octaethylporphyrin (96)

A procedure similar to that used for the synthesis of **82** was employed to give porphyrin **96** in 66% yield. IR ν_{max} 3478, 3395 (N-H), 1697 (C=O) cm^{-1}; UV-vis (CH_2Cl_2, λ_{max} nm (ε)): 590 (11,000), 554 (13,100), 436 (159,500); ^{1}HNMR (300 MHz, $CDCl_3$): δ8.38-8.02 (5H, m, arryl), 7.76-7.44 (13H, m, arryl), 7.39 (1H, dd, xanthyl), 7.29 (1H, t, xanthyl),

6.97 (1H, t, xanthyl), 6.92-6.61 (7H, m, binaphthyl), 6.49 (1H, br s, binaphthyl), 6.31 (1H, s, binaphthyl), 6.18 (1H, s, binaphthyl), 4.81 (1H, br s, binaphthyl), 4.41 (1H, br s, binaphthyl), 3.12(2H, br s, NH_2), 2.60-1.90 (16H, br s, CH_2 of ethyl), 1.82 (3H, s, CH_3 of xanthyl), 1.70 (3H, s, CH_3 of xanthyl), 0.90-0.00 (24H, m, CH_3 of ethyl); MS (FAB) found m/e 1337.1, cacld. 1336.59 for $C_{90}H_{82}N_6O_2Ni$.

Ni(II) 5-[5-carbonyl-4-(9,9-dimethyl)xanthyl]-10,15,20-tris-(pentafluorophenyl)-2,3,7,8,12,13,17,18-octaethylporphyrin (87)

A procedure similar to method **a** used for the synthesis of **72** was employed to give porphyrin **87** in 10% yield. UV-vis (CH_2Cl_2, λ_{max} nm (ε)): 599 (14,700), 558 (9,100), 430 (126,500); ^{1}HNMR (300 MHz, $CDCl_3$): δ8.33 (1H, s, CHO), 7.87 (1H, dd, xanthyl), 7.81 (1H, dd, xanthyl), 7.65 (1H, dd, xanthyl), 7.48 (1H, dd, xanthyl), 7.45 (1H, t, xanthyl), 7.07 (1H, t, xanthyl), 2.80-2.00 (16H, br s, CH_2 of ethyl), 1.84 (6H, s, CH_3 of xanthyl), 0.70-0.30 (24H, m, CH_3 of ethyl); MS (FAB) found m/e 1325.54, cacld. 1324.33 for $C_{70}H_{53}F_{15}N_4O_2Ni$.

Ni(II) 5-[5-cyano-4-(9,9-dimethyl)xanthyl]-10,15,20-tris-(pentafluorophenyl)-2,3,7,8,12,13,17,18-octaethylporphyrin (91)

A procedure similar to that used for the synthesis of **80** was employed to give porphyrin **91** in 87% yield. IR ν_{max} 2234 (C≡N) cm^{-1}; UV-vis (CH_2Cl_2, λ_{max} nm (ε)): 599 (19,800), 558 (11,800), 431 (156,900); ^{1}HNMR (300 MHz, $CDCl_3$): δ7.86 (1H, dd, xanthyl), 7.78 (1H, dd, xanthyl), 7.61 (1H, dd, xanthyl), 7.43 (1H, t, xanthyl), 7.22 (1H, dd, xanthyl), 7.04 (1H, t, xanthyl), 2.80-2.00 (16H, br s, CH_2 of ethyl), 1.82 (6H, s, CH_3 of xanthyl), 0.80-0.40 (24H, m, CH_3 of ethyl); MS (FAB) found m/e 1321.33, cacld. 1321.33 for $C_{70}H_{52}F_{15}N_5ONi$.

Ni(II) 5-[5-hydroxycarbonyl-4-(9,9-dimethyl)xanthyl]-10,15,20-tris-(pentafluorophenyl)-2,3,7,8,12,13,17,18-octaethylporphyrin (92)

A procedure similar to that used for the synthesis of **81** was employed to give porphyrin **92** in 81% yield. IR ν_{max} 3422 (O-H), 1742 (C=O) cm^{-1}; UV-vis (CH_2Cl_2, λ_{max} nm (ε)): 597 (19,600), 558 (11,500), 428 (158,500); ^{1}HNMR (300 MHz, $CDCl_3$): δ 7.88 (1H, dd, xanthyl), 7.85 (1H, dd, xanthyl), 7.84 (1H, dd, xanthyl), 7.68 (1H, dd, xanthyl), 7.49(1H, t, xanthyl), 7.15 (1H, t, xanthyl), 2.80-2.00 (16H, br s, CH_2 of ethyl), 1.86 (6H, s, CH_3 of xanthyl), 0.85-0.30 (24H, m, CH_3 of ethyl); MS (FAB) found m/e 1341.5, cacld. 1340.32 for $C_{70}H_{53}F_{15}N_4O_3Ni$.

Ni(II) 5-{5-[1-(1-naphthyl)ethylcarboxamide]-4-(9,9-dimethyl)xanthyl}-10,15,20-tris-(pentafluorophenyl)-2,3,7,8,12,13,17,18-octaethylporphyrin (97)

A procedure similar to that used for the synthesis of **82** was employed to give porphyrin **97** in 62% yield. IR ν_{max} 3418 (N-H), 1647 (C=O) cm^{-1}; UV-vis (CH_2Cl_2, λmax nm (ε)): 598 (19,300), 558 (11,400), 430 (154,700); ^{1}HNMR (300 MHz, $CDCl_3$): δ 8.12 (1H, dd, xanthyl), 7.79 (1H, dd, xanthyl), 7.66 (1H, dd, xanthyl), 7.48 (1H, dd, xanthyl), 7.32 (1H, t, xanthyl), 7.25 (1H, d, naphthyl), 7.22 (1H, t, xanthyl), 7.02-6.86 (2H, m, naphthyl), 6.37 (1H, d, naphthyl), 6.20 (1H, br s, naphthyl), 3.57 (1H, br s, CH), 2.80-2.00 (16H, br s, CH_2 of ethyl), 1.92 (3H, s, CH3 of xanthyl), 1.82 (3H, s, CH_3 of xanthyl), 0.90--0.10 (24H, m, CH_3 of ethyl), -0.95 (3H, d, CH_3); MS (FAB) found m/e 1494.5, cacld. 1493.42 for $C_{82}H_{64}F_{15}N_5O_2Ni$.

Ni(II) 5-[5-carbonyl-4-(9,9-dimethyl)xanthyl]-10,15,20-tris-(2,6-dichlorophenyl)-2,3, 7, 8,12,13,17,18-octaethylporphyrin (88)

A procedure similar to method **b** used for the synthesis of **72** was employed to give porphyrin **88** in 18% yield. IR ν_{max} 1690 (C=O) cm^{-1}; UV-vis (CH_2Cl_2, λ_{max} nm (ε)): 605 (15,500), 562 (11,500), 438 (161,700); ^{1}HNMR (300 MHz, $CDCl_3$): δ 8.82 (1H, s, CHO),

7.76 (1H, dd, xanthyl), 7.67 (1H, dd, xanthyl), 7.65-7.44 (11H, m, xanthyl and phenyl), 7.37 (1H, t, xanthyl), 7.08 (1H, t, xanthyl), 2.90-1.90 (16H, br s, CH_2 of ethyl), 1.85 (6H, s, CH_3 of xanthyl), 1.00-0.70 (24H, m, CH_3 of ethyl); MS (FAB) found m/e 1261.7, cacld. 1258.24 for $C_{70}H_{62}Cl_6N_4O_2Ni$.

Ni(II) 5-(5-cyano-4-(9,9-dimethyl)xanthyl)-10,15,20-tris-(2,6-dichlorophenyl)-2,3,7, 8,12,13,17,18-octaethylporphyrin (93)

A procedure similar to that used for the synthesis of **80** was employed to give porphyrin **93** in 82% yield. IR ν_{max} 2234 (C≡N) cm^{-1}; UV-vis (CH_2Cl_2, λ_{max} nm (ε)): 604 (16,600), 562 (12,200), 438 (163,300); ^{1}HNMR (300 MHz, $CDCl_3$): δ7.73 (1H, dd, xanthyl), 7.66 (1H, dd, xanthyl), 7.66-7.45 (10H, m, xanthyl and phenyl), 7.35 (1H, t, xanthyl), 7.27 (1H, dd, xanthyl), 7.08 (1H, t, xanthyl), 2.70-2.00 (16H, br s, CH_2 of ethyl), 1.85 (6H, s, CH_3 of xanthyl), 0.80-0.40 (24H, m, CH_3 of ethyl); MS (FAB) found m/e 1258.9, cacld. 1255.24 for $C_{70}H_{61}Cl_6N_5ONi$.

Ni(II) 5-[5-hydroxycarbonyl-4-(9,9-dimethyl)xanthyl]-10,15,20-tris-(2,6-dichloro-phenyl)-2,3,7,8,12,13,17,18-octaethylporphyrin (94)

A procedure similar to that used for the synthesis of **81** was employed to give porphyrin **94** in 78% yield. IR ν_{max} 3412 (O-H), 1740 (C=O) cm^{-1}; UV-vis (CH_2Cl_2, λ_{max} nm (rel intens)): 602 (0.10), 561 (0.07), 437 (1.00); ^{1}HNMR (300 MHz, $CDCl_3$): δ8.14 (1H, br s, acid), 7.89 (1H, dd, xanthyl), 7.78 (1H, dd, xanthyl), 7.74-7.46 (11H, m, xanthyl and phenyl), 7.43 (1H, t, xanthyl), 7.16 (1H, t, xanthyl), 2.70-2.00 (16H, br s, CH_2 of ethyl), 1.85 (6H, s, CH_3 of xanthyl), 0.90-0.30 (24H, m, CH_3 of ethyl); MS (FAB) found m/e 1277., cacld. 1274.23 for $C_{70}H_{62}Cl_6N_4O_3Ni$.

Ni(II) 5-{5-[2-(1-(2-aminonaphthyl)naphthyl)carboxamide]-4-(9,9-dimethyl)-xanthyl}-10,15,20-tris-(2,6-dichlorophenyl)-2,3,7,8,12,13,17,18-octaethylporphyrin (98)

A procedure similar to that used for the synthesis of **82** was employed to give porphyrin **98** in 48% yield. IR ν_{max} 3474, 3384 (N-H), 1688 (C=O) cm^{-1}; UV-vis (CH_2Cl_2, λ_{max} nm (ε)): 603 (15,900), 562 (12,200), 438 (151,300); ^{1}HNMR (300 MHz, $CDCl_3$): δ7.71 (1H, dd, xanthyl), 7.69 (1H, dd, xanthyl), 7.66 (1H, dd, xanthyl), 7.63-7.36 (9H, m, phenyl), 7.24 (1H, t, xanthyl), 6.96 (1H, t, xanthyl), 6.92-6.56 (9H, m, binaphthyl), 6.21 (1H, d, binaphthyl), 4.93 (1H, d, binaphthyl), 4.36 (1H, d, binaphthyl), 3.36 (2H, br s, NH_2), 2.70-1.94 (16H, br m, CH_2 of ethyl), 1.82 (3H, s, CH_3 of xanthyl), 1.72 (3H, s, CH_3 of xanthyl), 0.98-0.15 (24H, m, CH_3 of ethyl); MS (FAB) found m/e 1544.2, cacld. 1540.35 for $C_{90}H_{76}Cl_6N_6O_2Ni$.

General procedure for manganese insertion

The Ni porphyrin was demetallated by washing with concentrated $HCl_{(aq)}$ several times until the demetallation was complete as evidenced by UV-vis spectra. The protonated porphyrin was metallated with excess $MnCl_2 \cdot 4H_2O$ in gently refluxing DMF under nitrogen. After the reaction was complete (ca. 30 min), the solvent was concentrated under reduced pressure. Water was added to the mixture and the solid was filtered. The solid was dried and chromatographed on silica gel eluting with CH_2Cl_2 and methanol. The solvent was removed and the product was washed with 5-10% HCl(aq) to give the manganese porphyrin in 70-80% yield.

Mn(III) 5-{5-[1-(1-naphthyl)ethylcarboxamide]-4-(9,9-dimethyl)xanthyl}-10,15,20-triphenyl-2,3,7,8,12,13,17,18-octaethylporphyrin chloride

IR ν_{max} 3424 (N-H), 1670 (C=O) cm^{-1}; UV-vis (CH_2Cl_2, λmax nm (rel intens)): 597 (0.15), 496 (1.00), 378 (0.73); MS (FAB) found m/e 1220.2, cacld. 1220.56 for

$C_{82}H_{79}N_5O_2Mn$

Mn(III) 5-{5-[2-(1-(2-aminonaphthyl)naphthyl)carboxamide]-4-(9,9-dimethyl) xanthyl}-10,15,20-triphenyl-2,3,7,8,12,13,17,18-octaethylporphyrin chloride

IR ν_{max} 3478, 3395, 3503, 3199, 1697 (C=O) cm^{-1}; UV-vis (CH_2Cl_2, λ_{max} nm (rel intens)): 594 (0.15), 497 (1.00), 375 (0.67); MS (FAB) found m/e 1333.4, cacld. 1333.59 for $C_{90}H_{82}N_6O_2Mn$.

Mn(III) 5-{5-[2-(1-(2-aminonaphthyl)naphthyl)carboxamide]-4-(9,9-dimethyl) xanthyl}-10,15,20-tris-(2,6-dichlorophenyl)-2,3,7,8,12,13,17,18-octaethylporphyrin chloride

IR ν_{max} 3464, 3395, 3320, 3202, 1695 (C=O) cm^{-1}; UV-vis (CH_2Cl_2, λ_{max} nm (rel intens)): 604 (0.18), 502 (1.00), 379 (0.79); MS (FAB) found m/e 1541.0, cacld. 1537.35 for $C_{90}H_{76}Cl_6N_6O_2Mn$.

Mn(III) 5-{5-[1-(1-naphthyl)ethylcarboxamide]-4-(9,9-dimethyl)xanthyl}-10,15,20-tris-(pentafluorophenyl)-2,3,7,8,12, 3,17,18-octaethylporphyrin chloride

IR ν_{max} 3424 (N-H), 1647 (C=O) cm^{-1}; UV-vis (CH_2Cl_2, λ_{max} nm (rel intens)): 578 (0.20), 497 (0.99), 378 (1.00); MS (FAB) found m/e 1490.1, cacld. 1490.42 for $C_{82}H_{64}F_{15}N_5O_2Mn$.

The preparation, characterization and the general physical data for the (R) and (S) forms of chiral porphyrins were identical.

References

1. Ellerton, H. D.; Ellerton, N. F.; Robinson, H. A. *Prog. Biophys. Mol. Biol.* **1983**, *41*, 143.

2. Wilkins, P. C.; Wilkins, R. G. *Coor. Chem. Rev.* **1987**, *79*, 195.

3. Perutz, M. F. *nature* **1970**, *228*, 726.

4. Dickerson, R. E. G., I. *Hemoglobin: Structure, Function, Evolution, and Pathology*; Benjamin/Cummings: Califonia, 1983.

5. Kendrew, J. C.; Dickerson, R. E.; Stangdberg, B E.; Hart, R. G.; Davies, D. R.; Phillips, D. C.; Shore, V. C. *Nature* **1960**, *185*, 422.

6. Cohen, I. A.; Caughey, W. S. *Biochemistry* **1968**, *7*, 624.

7. Weschler, C. J.; Anderson, D. L.; Basolo, F. *J. Am. Chem. Soc.* **1975**, *97*, 6707.

8. Phelps, C. F.; Antonimi, E.; Brunori, M.; Kellett, G. *Biochem. J.* **1972**, *129*, 891.

9. Spiro, T. G. *Metal Ion Activation of Dioxygen*; John Wiley & Sons: New York, 1980.

10. Perutz, M. F.; Fermi, G.; Luisi, B.; Shaanan, B.; Liddington, R. C. *Acc. Chem. Res.* **1987**, *20*, 309.

11. Monod, J.; Wyman, J.; Changeux, J. P. *J. Mol. Biol.* **1965**, *12*, 88.

12. Wittenberg, J. B.; Appleby, C. A.; Wittenberg, B. A. *J. Biol. Chem.* **1972**, *247*, 527.

13. Imamura, T.; Riggs, A.; Gibson, Q. *J. Biol. Chem.* **1972**, *247*, 521.

14. O'carra, P. *Porphyrins and metalloporphyrins*; Elsevier: Amsterdam, 1975.

15. Traylor, T. G.; Koga, N.; Deardurff, L. A. *J. Am. Chem. Soc.* **1985**, *107*, 6504.

16. Collman, J. P.; Brauman, J. I.; Collins, T. J.; Iverson, B.; Sessler, J. L.; Morris, R. M.; Gibson, Q. H. **1983**, *79*, 101.

17. Chang, C. K.; Traylor, T. G. *J. Am. Chem. Soc.* **1973**, *95*, 5810.

18. Chang, C. K.; Traylor, T. G. *J. Am. Chem. Soc.* **1973**, *95*, 8477.

19. Tsuchida, E.; Komatsu, T.; Arai, K.; Nishide, H. *J. Chem. Soc.-Chem. Commun.* **1993**, 730.

20. Chen, X. S.; Nishide, H.; Tsuchida, E. *Bull. Chem. Soc. Jpn.* **1996**, *69*, 255.

21. Ward, B.; Wang, C. B.; Chang, C. K. *J. Am. Chem. Soc.* **1981**, *103*, 5236.

22. Collman, J. P.; Brauman, J. I.; Doxsee, K. M.; Halbert, T. R.; Suslick, K. S. *Proc. Natl. Acad. Sci. U. S. A.* **1978**, *75*, 564.

23. Jiang, D. L.; Aida, T. *Chem. Commun.* **1996**, 1523.

24. Anderson, D. L.; Weschler, C. J.; Basolo, F. *J. Am. Chem. Soc.* **1974**, *96*, 5599.

25. Almag, J.; Baldwin, J. E.; Dyer, R. L.; Huff, J.; Wilkerson, C. J. *J. Am. Chem. Soc.* **1974**, *96*, 5600.

26. Chang, C. K.; Brinigar, W. S. *J. Am. Chem. Soc.* **1974**, *96*, 5595.

27. Wang, J. H. *Acc. Chem. Res.* **1970**, *3*, 90.

28. Chang, C. K.; Traylor, T. G. *Proc. Natl. Acad. Sci. U.S.A.* **1973**, *70*, 2647.

29. Leal, O.; Anderson, D. L.; Bowman, R. G.; Basolo, F.; Burwell, R. L. *J. Am. Chem. Soc.* **1975**, *97*, 5125.

30. Fuhrhop, J. H.; Besecke, S.; Vogt, W.; Ernst, J.; Subramanian, J. *Makromol. Chem.* **1977**, *178*, 1621.

31. Tsuchida, E.; Hasegawa, E.; Kanayama, T. *Macromolecules* **1978**, *11*, 947.

32. Kawai, N.; Komatsu, T.; Yanagimoto, T.; Nishide, H.; Tsuchida, E. *Chem. Lett.* **1995**, 477.

33. Diekmann, H.; Chang, C. K.; Traylor, T. G. *J. Am. Chem. Soc.* **1971**, *93*, 4068.

34. Collman, J. P.; Gagne, R. R.; Reed, C. A.; Robinson, W. T.; Rodley, C. A. *Proc. Natl. Acad. Sci. U.S.A.* **1974**, *71*, 1326.

35. Collman, J. P.; gagne, R. R.; Reed, C. A.; Halbert, T. R.; Lang, G.; Robinson, W. T. *J. Am. Chem. Soc.* **1975**, *97*, 1427.

36. Collman, J. P.; Brauman, J. I.; Iverson, B. L.; Sessler, J. L.; Morris, R. M.; Gibson, Q. H. *J. Am. Chem. Soc.* **1983**, *105*, 3052.

37. Collman, J. P.; Brauman, J. I.; Doxsee, K. M.; Sessler, J. L.; Morris, R. M.; Gibson, Q. H. *Inorg. Chem.* **1983**, *22*, 1427.

38. Tsuchida, E.; Komatsu, T.; Kumamoto, S.; Ando, K.; Nishide, H. *J. Chem. Soc.-Perkin Trans. 2* **1995**, 747.

39. Elkasmi, D.; Tetreau, C.; Lavalette, D.; Momenteau, M. *J. Chem. Soc.-Perkin Trans. 2* **1993**, 1799.

40. Baldwin, J. E.; Cameron, J. H.; Crossley, M. J.; Dagley, I. J.; Hall, S. R.; Klose, T. *J. Chem. Soc.-Dalton Trans.* **1984**, 1739.

41. Johnson, M. R.; Seok, W. K.; Ibers, J. A. *J. Am. Chem. Soc.* **1991**, *113*, 3998.

42. Johnson, M. R.; Seok, W. K.; Ma, W. P.; Slebodnick, C.; Wilcoxen, K. M.; Ibers, J. A. *J. Org. Chem.* **1996**, *61*, 3298.

43. Collman, J. P.; Brauman, J. I.; Collins, T. J.; Iverson, B. L.; Lang, G.; Pettman, R. B.; Sessler, J. L.; Walters, M. A. *J. Am. Chem. Soc.* **1983**, *105*, 3038.

44. Collman, J. P.; Brauman, J. I.; Fitzgerald, J. P.; Sparapany, J. W.; Ibers, J. A. *J. Am. Chem. Soc.* **1988**, *110*, 3486.

45. Chang, C. K. *J. Am. Chem. Soc.* **1977**, *99*, 2819.

46. Momenteau, M.; Loock, B.; Tetreau, C.; Lavalette, D.; Croisy, A.; Schaeffer, C.; Huel, C.; Lhoste, J. M. *J. Chem. Soc.-Perkin Trans. 2* **1987**, 249.

47. Suslick, K. S.; Fox, M. M. *J. Am. Chem. Soc.* **1983**, *105*, 3507.

48. Tsuchida, E.; Hasegawa, E.; Komatsu, T.; Nakata, T.; Nakao, K.; Nishide, H. *Bull. Chem. Soc. Jpn.* **1991**, *64*, 888.

49. Rose, E.; Boitrel, B.; Quelquejeu, M.; Kossanyi, A. *Tetrahedron Lett.* **1993**, *34*, 7267.

50. Richard, P.; Rose, E.; Boitrel, B. *Inorg. Chem.* **1998**, *37*, 6532.

51. Battersby, A. R.; Bartholomew, S. A. J.; Nitta, T. *J. Chem. Soc.-Chem. Commun.* **1983**, 1291.

52. Tsuchida, E.; Komatsu, T.; Hasegawa. E.; Nishide, H. *J. Chem. Soc.-Dalton Trans.* **1990**, 2713.

53. Momenteau, M.; Mispelter, J.; Loock, B.; Lhoste, J. M. *J. Chem. Soc.-Perkin Trans. 1* **1985**, 221.

54. Traylor, T. G. *Accounts Chem. Res.* **1981**, *14*, 102.

55. Traylor, T. G.; Popovitzbiro, R. *J. Am. Chem. Soc.* **1988**, *110*, 239.

56. Collman, J. P.; Zhang, X. M.; Wong, K.; Brauman, J. I. *J. Am. Chem. Soc.* **1994**, *116*, 6245.

57. Chang, C. K.; Ward, B.; Young, R.; Kondylis, M. P. **1988**, *A25*, 1307.

58. Tsuchida, E.; Komatsu, T.; Arai, K.; Nishide, H. *J. Chem. Soc.-Dalton Trans.* **1993**, 2465.

59. Komatsu, T.; Kumamoto, S.; Nishide, H.; Tsuchida, E. *Bull. Chem. Soc. Jpn.* **1993**, *66*, 1640.

60. Momenteau, M.; Loock, B.; Lavalette, D.; Tetreau, C.; Mispelter, J. *J. Chem. Soc.-Chem. Commun.* **1983**, 962.

61. Chang, C. K.; Kondylis, M. P. *J. Chem. Soc.-Chem. Commun.* **1986**, 316.

62. Wuenschell, G. E.; Tetreau, C.; Lavalette, D.; Reed, C. A. *J. Am. Chem. Soc.* **1992**, *114*, 3346.

63. Chang, C. K.; Liang, Y.; Aviles, G. *J. Am. Chem. Soc.* **1995**, *117*, 4191.

64. Cheng, X. D.; Schoenborn, B. P. *J. Mol. Biol.* **1991**, *220*, 381.

65. Hanson, J. C.; Schoenborn, B. P. *J. Mol. Biol.* **1981**, *153*, 117.

66. Kuriyan, J.; Wilz, S.; Karplus, M.; Petsko, G. A. *J. Mol. Biol.* **1986**, *192*, 133.

67. Peng, S. M.; Ibers, J. A. *J. Am. Chem. Soc.* **1976**, *98*, 8032.

68. Li, X. Y.; Spiro, T. G. *J. Am. Chem. Soc.* **1988**, *110*, 6024.

69. Schlichting, I.; Berendzen, J.; Phillips, G. N.; Sweet, R. M. *Nature* **1994**, *371*, 808.

70. Quillin, M. L.; Arduini, R. M.; Olson, J. S.; Phillips, G. N. *J. Mol. Biol.* **1993**, *234*, 140.

71. Ray, G. B.; Li, X. Y.; Ibers, J. A.; Sessler, J. L.; Spiro, T. G. *J. Am. Chem. Soc.* **1994**, *116*, 162.

72. David, S.; James, B. R.; Dolphin, D.; Traylor, T. G.; Lopez, M. A. *J. Am. Chem. Soc.* **1994**, *116*, 6.

73. Traylor, T. G.; Tsuchiya, S.; Campbell, D.; Mitchell, M.; Stynes, D.; Koga, N. *J. Am. Chem. Soc.* **1985**, *107*, 604.

74. Collman, J. P.; Brauman, J. I.; Collins, T. J.; Iverson, B.; Sessler, J. L. *J. Am. Chem. Soc.* **1981**, *103*, 2450.

75. Collman, J. P.; Herrmann, P. C.; Fu, L.; Eberspacher, T. A.; Eubanks, M.; Boitrel, B.; Hayoz, P.; Zhang, X. M.; Brauman, J. I.; Day, V. W. *J. Am. Chem. Soc.* **1997**, *119*, 3481.

76. Slebodnick, C.; Ibers, J. A. *J. Biol. Inorg. Chem.* **1997**, *2*, 521.

77. Slebodnick, C.; Duval, M. L.; Ibers, J. A. *Inorg. Chem.* **1996**, *35*, 3607.

78. Collman, J. P.; Eberspacher, T.; Fu, L.; Herrmann, P. C. *J. Mol. Catal. A-Chem.* **1997**, *117*, 9.

79. Sono, M.; Roach, M. P.; Coulter, E. D.; Dawson, J. H. *Chem. Rev.* **1996**, *96*, 2841.

80. Bertini, I.; Gray, H. B.; Lippard, S. J.; Valentine, J. S. *Bioinorganic Chemistry*; University Science Books: Sausalito, 1994.

81. Ullrich, V. *Top. Curr. Chem.* **1979**, *83*, 67.

82. Garfinkel, D. *Arch. Biochem. Biophys.* **1958**, *77*, 493.

83. Estabrook, R. W.; Cooper, D. Y.; Rosenthal, O. Z. *Biochemistry* **1963**, *338*, 741.

84. Omura, T.; Sato, R. *J. Biol. Chem.* **1964**, *239*, 2370.

85. Sheldon, R. A. *Metalloporphyrins in Catalytic Oxidation*; Marcel Dekker: New York, 1994.

86. Yu, C.; Gunsalus, I. C. *Biochem. Biophys. Res. Commun.* **1970**, *40*, 524.

87. Poulos, T. L.; Finzel, B. C.; Gunsalus, I. C.; Wagner, G. C.; Kraut, J. *J. Biol. Chem.* **1985**, *260*, 6122.

88. Poulos, T. L.; Finzel, B. C.; Howard, A. J. *Biochemistry* **1986**, *25*, 5314.

89. Fisher, M. T.; Sligar, S. G. *J. Am. Chem. Soc.* **1985**, *107*, 5018.

90. Sligar, S. G.; Lipscomb, J. D.; Debrunner, I. D.; Gunsalus, I. C. *Biochem. Biophys. Res. Commun.* **1974**, *61*, 290.

91. White, R. E.; Coon, M. J. *Annu. Rev. Biochem.* **1980**, *49*, 315.

92. Groves, J. T.; Quinn, R.; McMurry, T. J.; Lang, G.; Boso, B. *J. Chem. Soc.-Chem. Commun.* **1984**, 1455.

93. Sundaramoorthy, M.; Terner, J.; Poulos, T. L. *Chem. Biol.* **1998**, *5*, 461.

94. Sundaramoorthy, M.; Terner, J.; Poulos, T. L. *Structure* **1995**, *3*, 1367.

95. Palcic, M. M.; Rutter, R.; Araiso, T.; Hager, L. P.; Dunford, H. B. *Biochem. Biophys. Res. Commun.* **1980**, *94*, 1123.

96. Egawa, T.; Shimada, H.; Ishimura, Y. *Biochem. Biophys. Res. Commun.* **1994**, *201*, 1464.

97. Groves, J. T. *J. Chem. Educ.* **1985**, *62*, 928.

98. Groves, J. T.; McClusky, G. A.; White, R. E.; Coon, M. J. *Biochem. Biophys. Res. Commun.* **1978**, *81*, 154.

99. Hjelmeland, L. M.; Aronow, L.; Trudell, J. R. *Biochem. Biophys. Res. Commun.* **1977**, *76*, 541.

100. Atkinson, J. K.; Hollenberg, P. F.; Ingold, K. U.; Johnson, C. C.; Letadic, M. H.; Newcomb, M.; Putt, D. A. *Biochemistry* **1994**, *33*, 10630.

101. Bowry, V. W.; Ingold, K. U. *J. Am. Chem. Soc.* **1991**, *113*, 5699.

102. Demontellano, P. R. O.; Stearns, R. A. *J. Am. Chem. Soc.* **1987**, *109*, 3415.

103. Toy, P. H.; Newcomb, M.; Coon, M. J.; Vaz, A. D. N. *J. Am. Chem. Soc.* **1998**, *120*, 9718.

104. Toy, P. H.; Newcomb, M.; Hollenberg, P. F. *J. Am. Chem. Soc.* **1998**, *120*, 7719.

105. Newcomb, M.; Letadicbiadatti, F. H.; Chestney, D. L.; Roberts, E. S.; Hollenberg, P. F. *J. Am. Chem. Soc.* **1995**, *117*, 12085.

106. Collman, J. P.; Chien, A. S.; Eberspacher, T. A.; Brauman, J. I. *J. Am. Chem. Soc.* **1998**, *120*, 425.

107. Ostovic, D.; Bruice, T. C. *Accounts Chem. Res.* **1992**, *25*, 314.

108. Ostovic, D.; Bruice, T. C. *J. Am. Chem. Soc.* **1989**, *111*, 6511.

109. Groves, J. T.; Nemo, T. E.; Myers, R. S. *J. Am. Chem. Soc.* **1979**, *101*, 1032.

110. Groves, J. T.; Kruper, W. J.; Haushalter, R. C. *J. Am. Chem. Soc.* **1980**, *102*, 6375.

111. Groves, J. T.; Kruper, W. J. *J. Am. Chem. Soc.* **1979**, *101*, 7613.

112. Traylor, T. G.; Miksztal, A. R. *J. Am. Chem. Soc.* **1989**, *111*, 7443.

113. Groves, J. T.; Nemo, T. E. *J. Am. Chem. Soc.* **1983**, *105*, 5786.

114. Bortolini, O.; Meunier, B. *J. Chem. Soc.-Chem. Commun.* **1983**, 1364.

115. Chang, C. K.; Ebina, F. *J. Chem. Soc.-Chem. Commun.* **1981**, 778.

116. Traylor, P. S.; Dolphin, D.; Traylor, T. G. *J. Chem. Soc.-Chem. Commun.* **1984**, 279.

117. Traylor, T. G.; Tsuchiya, S. *Inorg. Chem.* **1987**, *26*, 1338.

118. Battioni, P.; Brigaud, O.; Desvaux, H.; Mansuy, D.; Traylor, T. G. *Tetrahedron Lett.* **1991**, *32*, 2893.

119. Bartoli, J. F.; Brigaud, O.; Battioni, P.; Mansuy, D. *J. Chem. Soc.-Chem. Commun.* **1991**, 440.

120. Gonsalves, A.; Johnstone, R. A. W.; Pereira, M. M.; Shaw, J.; Sobral, A. *Tetrahedron Lett.* **1991**, *32*, 1355.

121. Chen, H. L.; Ellis, P. E.; Wijesekera, T.; Hagan, T. E.; Groh, S. E.; Lyons, J. E.; Ridge, D. P. *J. Am. Chem. Soc.* **1994**, *116*, 1086.

122. Gonsalves, A.; Pereira, M. M.; Serra, A. C.; Johnstone, R. A. W.; Nunes, M. *J. Chem. Soc.-Perkin Trans. 1* **1994**, 2053.

123. Tsuchiya, S.; Seno, M. *Chem. Lett.* **1989**, 263.

124. Woller, E. K.; DiMagno, S. G. *J. Org. Chem.* **1997**, *62*, 1588.

125. Lindsey, J. S.; Schreiman, I. C.; Hsu, H. C.; Kearney, P. C.; Marguerettaz, A. M. *J. Org. Chem.* **1987**, *52*, 827.

126. Porhiel, E.; Bondon, A.; Leroy, J. *Tetrahedron Lett.* **1998**, *39*, 4829.

127. Bartoli, J. F.; Battioni, P.; Defoor, W. R.; Mansuy, D. *J. Chem. Soc.-Chem. Commun.* **1994**, 23.

128. Ozette, K.; Battioni, P.; Leduc, P.; Bartoli, J. F.; Mansuy, D. *Inorg. Chim. Acta* **1998**, *272*, 4.

129. Mansuy, D. *Pure Appl. Chem.* **1994**, *66*, 737-744.

130. Fu, H.; Newcomb, M.; Wong, C. H. *J. Am. Chem. Soc.* **1991**, *113*, 5878.

131. Groves, J. T.; Neumann, R. *J. Org. Chem.* **1988**, *53*, 3891.

132. Collman, J. P.; Zhang, X. M.; Hembre, R. T.; Brauman, J. I. *J. Am. Chem. Soc.* **1990**, *112*, 5356.

133. He, G. X.; Mei, H. Y.; Bruice, T. C. *J. Am. Chem. Soc.* **1991**, *113*, 5644.

134. Cook, B. R.; Reinert, T. J.; Suslick, K. S. *J. Am. Chem. Soc.* **1986**, *108*, 7281.

135. Collman, J. P.; Brauman, J. I.; Fitzgerald, J. P.; Hampton, P. D.; Naruta, Y.; Michida, T. *Bull. Chem. Soc. Jpn.* **1988**, *61*, 47.

136. Bhyrappa, P.; Young, J. K.; Moore, J. S.; Suslick, K. S. *J. Mol. Catal. A-Chem.* **1996**, *113*, 109.

137. Bhyrappa, P.; Young, J. K.; Moore, J. S.; Suslick, K. S. *J. Am. Chem. Soc.* **1996**, *118*, 5708.

138. Mansuy, D.; Battioni, P.; Battioni, J. P. *Eur. J. Biochem.* **1989**, *184*, 267.

139. Collman, J. P.; Zhang, X. M.; Lee, V. J.; Uffelman, E. S.; Brauman, J. I. *Science* **1993**, *261*, 1404.

140. Groves, J. T.; Myers, R. S. *J. Am. Chem. Soc.* **1983**, *105*, 5791.

141. Groves, J. T.; Viski, P. *J. Org. Chem.* **1990**, *55*, 3628.

142 Naruta, Y.; Ishihara, N.; Tani, F.; Maruyama, K. *Bull. Chem. Soc. Jpn.* **1993**, *66*, 158.

143. Naruta, Y.; Tani, F.; Ishihara, N.; Maruyama, K. *J. Am. Chem. Soc.* **1991**, *113*, 6865.

144. Halterman, R. L.; Jan, S. T.; Abdulwali, A. H.; Standlee, D. J. *Tetrahedron* **1997**, *53*, 11277.

145. Campbell, L. A.; Kodadek, T. *J. Mol. Catal. A-Chem.* **1996**, *113*, 293.

146. Collman, J. P.; Schwenninger, R.; Rapta, M.; Broring, M.; Fu, L. *Chem. Commun.* **1999**, 137.

147. Collman, J. P.; Fu, L.; Zingg, A.; Diederich, F. *Chem. Commun.* **1997**, 193.

148. Elkasmi, D.; Tetreau, C.; Lavalette, D.; Momenteau, M. *J. Am. Chem. Soc.* **1995**, *117*, 6041.

149. Rose, E.; Lecas, A.; Quelquejeu, M.; Kossanyi, A.; Boitrel, B. *Coord. Chem. Rev.* **1998**, *180*, 1407.

150. Maillard, P.; Vilain, S.; Huel, C.; Momenteau, M. *J. Org. Chem.* **1994**, *59*, 2887.

151. Traylor, T. G.; Chang, C. K.; Geibel, J.; Berzinis, A.; Mincey, T.; Cannon, J. *J. Am. Chem. Soc.* **1979**, *101*, 6716.

152. Barton, D. H. R.; Kervagoret, J.; Zard, S. Z. *Tetrahedron* **1990**, *46*, 7587.

153. Ono, N.; Wada, H. *J. Synth. Org. Chem. Jpn.* **1993**, *51*, 826.

154. Miyaura, N.; Suzuki, A. *Chem. Rev.* **1995**, *95*, 2457.

155. Beachell, H. C.; Deistel, D. W. *Inorg. Chem.* **1964**, *3*, 1028.

156. Bag, N.; Chern, S. S.; Peng, S. M.; Chang, C. K. *Tetrahedron Lett.* **1995**, *36*, 6409.

157. Ono, N.; Kawamura, H.; Bougauchi, M.; Maruyama, K. *Tetrahedron* **1990**, *46*, 7483.

158. Smith, K. M.; Eivazi, F. *J. Org. Chem.* **1979**, *44*, 2591.

159. David, S.; James, B. R.; Dolphin, D. *J. Inorg. Biochem.* **1986**, *28*, 125.

160. Linard, J. E.; Ellis, P. E.; Budge, J. R.; Jones, R. D.; Basolo, F. *J. Am. Chem. Soc.* **1980**, *102*, 1896.

161. Hashimoto, T.; Dyer, R. L.; Crossley, M. J.; Baldwin, J. E.; Basolo, F. *J. Am. Chem. Soc.* **1982**, *104*, 2101.

162. Geibel, J.; Cannon, J.; Campbell, D.; Traylor, T. G. **1978**, *100*, 3575.

163. Mispelter, J.; Momenteau, M.; Lavalette, D.; Lhoste, J. M. *J. Am. Chem. Soc.* **1983**, *105*, 5165.

164. Portela, C. F.; Magde, D.; Traylor, T. G. *Inorg. Chem.* **1993**, *32*, 1313.

165. Medforth, C. J.; Senge, M. O.; Forsyth, T. P.; Hobbs, J. D.; Shelnutt, J. A.; Smith, K. M. *Inorg. Chem.* **1994**, *33*, 3865.

166. Bonarlaw, R. P.; Mackay, L. G.; Walter, C. J.; Marvaud, V.; Sanders, J. K. M. *Pure Appl. Chem.* **1994**, *66*, 803.

167. Barry, J. F.; Campbell, L.; Smith, D. W.; Kodadek, T. *Tetrahedron* **1997**, *53*, 7753.

168. Halterman, R. L.; Jan, S. T.; Nimmons, H. L.; Standlee, D. J.; Khan, M. A. *Tetrahedron* **1997**, *53*, 11257.

169. Hamachi, I.; Tajiri, Y.; Nagase, T.; Shinkai, S. *Chem.-Eur. J.* **1997**, *3*, 1025.

170. Kuroda, Y.; Kato, Y.; Higashioji, T.; Ogoshi, H. *Angew. Chem.-Int. Edit. Engl.* **1993**, *32*, 723.

171. Kuroda, Y.; Kato, Y.; Higashioji, T.; Hasegawa, J.; Kawanami, S.; Takahashi, M.; Shiraishi, N.; Tanabe, K.; Ogoshi, H. *J. Am. Chem. Soc.* **1995**, *117*, 10950.

172. Zheng, J. Y.; Konishi, K.; Aida, T. *Tetrahedron* **1997**, *53*, 9115.

173. Hayashi, T.; Miyahara, T.; Kumazaki, S.; Ogoshi, H.; Yoshihara, K. *Angew. Chem.-Int. Edit. Engl.* **1996**, *35*, 1964.

174. Hayashi, T.; Miyahara, T.; Aoyama, Y.; Kobayashi, M.; Ogoshi, H. *Pure Appl. Chem.* **1994**, *66*, 797.

175. Bhyrappa, P.; Vaijayanthimala, G.; Suslick, K. S. *J. Am. Chem. Soc.* **1999**, *121*, 262.

176. Tomoyose, Y.; Jiang, D. L.; Jin, R. H.; Aida, T.; Yamashita, T.; Horie, K.; Yashima, E.; Okamoto, Y. *Macromolecules* **1996**, *29*, 5236.

177. Ishiyama, T.; Murata, M.; Miyaura, N. *J. Org. Chem.* **1995**, *60*, 7508.

178. Giroux, A.; Han, Y. X.; Prasit, P. *Tetrahedron Lett.* **1997**, *38*, 3841.

179. Momenteau, M.; Reed, C. A. *Chem. Rev.* **1994**, *94*, 659.

180. Wittung-Stafshede, P.; Malmstrom, B. G.; Winkler, J. R.; Gray, H. B. *J. Phys. Chem. A* **1998**, *102*, 5599.

181. Aissaoui, H.; Ghirlanda, S.; Gmur, C.; Woggon, W. D. *J. Mol. Catal. A-Chem.* **1996**, *113*, 393.

182. Mansuy, D.; Leclaire, J.; Fontecave, M.; Momenteau, M. *Biochem. Biophys. Res. Commun.* **1984**, *119*, 319.

183. Chang, C. H.; Cheng, S. H.; Su, Y. O. *J. Chin. Chem. Soc.* **1999**, *46*, 221.

184. Lu, Y. H.; Su, Y. O. *Chem. Commun.* **1997**, 753.

185. Forshey, P. A.; Kuwana, T. *Inorg. Chem.* **1981**, *20*, 693.

186. Fleischer, E. B.; Palmer, J. M.; Srivastava, T. S.; Chatterjee, A. *J. Am. Chem. Soc.* **1971**, *92*, 3162.

187. Miskelly, G. M.; Webley, W. S.; Clark, C. R.; Buckingham, D. A. *Inorg. Chem.* **1988**, *27*, 3773.

188. Ivanca, M. A.; Lappin, A. G.; Scheidt, W. R. *Inorg. Chem.* **1991**, *30*, 711.

189. La, T.; Richards, R.; Miskelly, G. M. *Inorg. Chem.* **1994**, *33*, 3159.

190. Balasubramanian, P. N.; Smith, J. R. L.; Davies, M. J.; Kaaret, T. W.; Bruice, T. C. *J. Am. Chem. Soc.* **1989**, *111*, 1477.

191. Ono, N.; Bougauchi, M.; Maruyama, K. *Tetrahedron Lett.* **1992**, *33*, 1629.

192. Shi, C. N.; Anson, F. C. *Inorg. Chem.* **1998**, *37*, 1037.

193. Dong, S. J.; Kuwana, T. *Electrochim. Acta* **1988**, *33*, 667.

194. Hutchison, J. E.; Postlethwaite, T. A.; Chen, C. H.; Hathcock, K. W.; Ingram, R. S.; Ou, W.; Linton, R. W.; Murray, R. W.; Tyvoll, D. A.; Chng, L. L.; Collman, J. P. *Langmuir* **1997**, *13*, 2143.

195. Su, Y. O.; Kuwana, T.; Chen, S. M. *J. Electroanal. Chem.* **1990**, *288*, 177.

196. Forshey, P. A.; Kuwana, T. *Inorg. Chem.* **1983**, *22*, 699.

197. Green, M. T. *J. Am. Chem. Soc.* **1998**, *120*, 10772.

198. Ellison, M. K.; Scheidt, W. R. *J. Am. Chem. Soc.* **1997**, *119*, 7404.

199. Hatano, K.; Safo, M. K.; Walker, F. A.; Scheidt, W. R. *Inorg. Chem.* **1991**, *30*, 1643.

200. La, T.; Richards, R. A.; Lu, R. S.; Bau, R.; Miskelly, G. M. *Inorg. Chem.* **1995**, *34*, 5632.

201. Zipplies, M. F.; Lee, W. A.; Bruice, T. C. *J. Am. Chem. Soc.* **1986**, *108*, 4433.

202. Cheng, S. H.; Chen, Y. S.; Su, Y. O. *J. Chin. Chem. Soc.* **1991**, *38*, 15.

203. Yu, C. H.; Su, Y. O. *J. Electroanal. Chem.* **1994**, *368*, 323.

204. Finnegan, M. G.; Lappin, A. G.; Scheidt, W. R. *Inorg. Chem.* **1990**, *29*, 181.

205. Ashley, K. R.; Kuo, J. *Inorg. Chem.* **1988**, *27*, 3556.

206. Yu, H. Z.; Baskin, J. S.; Steiger, B.; Anson, F. C.; Zewail, A. H. *J. Am. Chem. Soc.* **1999**, *121*, 484.

207. Anson, F. C.; Shi, C. N.; Steiger, B. *Accounts Chem. Res.* **1997**, *30*, 437.

208. Lu, Y. H.; Su, Y. O. *J. Electroanal. Chem.* **1998**, *446*, 25.

209. Liu, M. H.; Su, Y. O. *J. Electroanal. Chem.* **1998**, *452*, 113.

210. Mu, X. H.; Kadish, K. M. *Inorg. Chem.* **1988**, *27*, 4720.

211. Deisenhofer, J.; Michel, H. *Science* **1989**, *245*, 1463.

212. Geno, M. K.; Halpern, J. *J. Am. Chem. Soc.* **1987**, *109*, 1238.

213. Shelnutt, J. A. *J. Phys. Chem.* **1989**, *93*, 6283-6290.

214. Shelnutt, J. A. *J. Am. Chem. Soc.* **1987**, *109*, 4169.

215. Tronrud, D. E.; Schmid, M. F.; Matthews, B. W. *J. Mol. Biol.* **1986**, *188*, 443.

216. Ma, J. G.; Laberge, M.; Song, X. Z.; Jentzen, W.; Jia, S. L.; Zhang, J.; Vanderkooi, J. M.; Shelnutt, J. A. *Biochemistry* **1998**, *37*, 5118.

217. Alden, R. G.; Ondrias, M. R.; Shelnutt, J. A. *Biophys. J.* **1990**, *57*, 236.

218. Hobbs, J. D.; Shelnutt, J. A. *J. Protein Chem.* **1995**, *14*, 19.

219. Barkigia, K. M.; Chantranupong, L.; Smith, K. M.; Fajer, J. *J. Am. Chem. Soc.* **1988**, *110*, 7566.

220. Jentzen, W.; Simpson, M. C.; Hobbs, J. D.; Song, X.; Ema, T.; Nelson, N. Y.; Medforth, C. J.; Smith, K. M.; Veyrat, M.; Mazzanti, M.; Ramasseul, R.; Marchon, J. C.; Takeuchi, T.; Goddard, W. A.; Shelnutt, J. A. *J. Am. Chem. Soc.* **1995**, *117*, 11085.

221. Barkigia, K. M.; Renner, M. W.; Furenlid, L. R.; Medforth, C. J.; Smith, K. M.; Fajer, J. *J. Am. Chem. Soc.* **1993**, *115*, 3627.

222. Jia, S. L.; Zhang, J.; Ema, T.; Nelson, N. Y.; Ma, J. G.; Jentzen, W.; Song, X. Z.; Medforth, C. J.; Smith, K. M.; Shelnutt, J. A. *Biophys. J.* **1998**, *74*, 81.

223. Barkigia, K. M.; Berber, M. D.; Fajer, J.; Medforth, C. J.; Renner, M. W.; Smith, K. M. *J. Am. Chem. Soc.* **1990**, *112*, 8851.

224. Fajer, J.; Barkigia, K. M.; Melamed, D.; Sweet, R. M.; Kurreck, H.; vonGersdorff, J.; Plato, M.; Rohland, H. C.; Elger, G.; Mobius, K. *J. Phys. Chem.* **1996**, *100*, 14236.

225. Shelnutt, J. A.; Song, X. Z.; Ma, J. G.; Jia, S. L.; Jentzen, W.; Medforth, C J. *Chem. Soc. Rev.* **1998**, *27*, 31.

226. Shelnutt, J. A.; Medforth, C. J.; Berber, M. D.; Barkigia, K. M.; Smith, K. M. *J. Am. Chem. Soc.* **1991**, *113*, 4077.

227. Medforth, C. J.; Senge, M. O.; Smith, K. M.; Sparks, L. D.; Shelnutt, J. A. *J. Am. Chem. Soc.* **1992**, *114*, 9859.

228. Nurco, D. J.; Medforth, C. J.; Forsyth, T. P.; Olmstead, M. M.; Smith, K. M. *J. Am. Chem. Soc.* **1996**, *118*, 10918.

229. Anderson, K. K.; Hobbs, J. D.; Luo, L. A.; Stanley, K. D.; Quirke, J. M. E.; Shelnutt, J. A. *J. Am. Chem. Soc.* **1993**, *115*, 12346.

230. Gentemann, S.; Medforth, C. J.; Forsyth, T. P.; Nurco, D. J.; Smith, K. M.; Fajer, J.; Holten, D. *J. Am. Chem. Soc.* **1994**, *116*, 7363.

231. Hodge, J. A.; Hill, M. G.; Gray, H. B. *Inorg. Chem.* **1995**, *34*, 809.

232. Jia, S. L.; Jentzen, W.; Shang, M.; Song, X. Z.; Ma, J. G.; Scheidt, W. R.; Shelnutt, J. A. *Inorg. Chem.* **1998**, *37*, 4402.

233. Medforth, C. J.; Muzzi, C. M.; Smith, K. M.; Abraham, R. J.; Hobbs, J. D.; Shelnutt, J. A. *J. Chem. Soc.-Chem. Commun.* **1994**, 1843.

234. Renner, M. W.; Barkigia, K. M.; Fajer, J. *Inorg. Chim. Acta* **1997**, *263*, 181.

235. Sibilia, S. A.; Hu, S. Z.; Piffat, C.; Melamed, D.; Spiro, T. G. *Inorg. Chem.* **1997**, *36*, 1013.

236. Safo, M. K.; Gupta, G. P.; Walker, F. A.; Scheidt, W. R. *J. Am. Chem. Soc.* **1991**, *113*, 5497.

237. Safo, M. K.; Nesset, M. J. M.; Walker, F. A.; Debrunner, P. G.; Scheidt, W. R. *J. Am. Chem. Soc.* **1997**, *119*, 9438.

238. Safo, M. K.; Gupta, G. P.; Watson, C. T.; Simonis, U.; Walker, F. A.; Scheidt, W. R. *J. Am. Chem. Soc.* **1992**, *114*, 7066.

239. Munro, O. Q.; Marques, H. M.; Debrunner, P. G.; Mohanrao, K.; Scheidt, W. R. *J. Am. Chem. Soc.* **1995**, *117*, 935.

240. Song, X. Z.; Jentzen, W.; Jia, S. L.; Jaquinod, L.; Nurco, D. J.; Medforth, C. J.; Smith, K. M.; Shelnutt, J. A. *J. Am. Chem. Soc.* **1996**, *118*, 12975.

241. Piffat, C.; Melamed, D.; Spiro, T. G. *J. Phys. Chem.* **1993**, *97*, 7441.

242. Blackwood, M. E.; Rush, T. S.; Medlock, A.; Dailey, H. A.; Spiro, T. G. *J. Am. Chem. Soc.* **1997**, *119*, 12170.

243. Jentzen, W.; Unger, E.; Song, X. Z.; Jia, S. L.; TurowskaTyrk, I.; SchweitzerStenner, R.; Dreybrodt, W.; Scheidt, W. R.; Shelnutt, J. A. *J. Phys. Chem. A* **1997**, *101*, 5789.

244. D'Souza, F.; Zandler, M. E.; Tagliatesta, P.; Ou, Z. P.; Shao, J. G.; Van Caemelbecke, E.; Kadish, K. M. *Inorg. Chem.* **1998**, *37*, 4567.

245. Tagliatesta, P.; Li, J.; Autret, M.; VanCaemelbecke, E.; Villard, A.; Dsouza, F.; Kadish, K. M. *Inorg. Chem.* **1996**, *35*, 5570.

246. Othman, S.; Fitch, J.; Cusanovich, M. A.; Desbois, A. *Biochemistry* **1997**, *36*, 5499.

247. Renner, M. W.; Barkigia, K. M.; Zhang, Y.; Medforth, C. J.; Smith, K. M.; Fajer, J. *J. Am. Chem. Soc.* **1994**, *116*, 8582.

248. Medforth, C. J.; Muzzi, C. M.; Shea, K. M.; Smith, K. M.; Abraham, R. J.; Jia, S. L.; Shelnutt, J. A. *J. Chem. Soc.-Perkin Trans. 2* **1997**, 833.

249. Jentzen, W.; Song, X. Z.; Shelnutt, J. A. *J. Phys. Chem. B* **1997**, *101*, 1684.

250. Gross, Z.; Ini, S. *J. Org. Chem.* **1997**, *62*, 5514.

251. Collman, J. P.; Wang, Z.; Straumanis, A.; Quelquejeu, M.; Rose, E. *J. Am. Chem. Soc.* **1999**, *121*, 460.

252. Konishi, K.; Miyazaki, K.; Aida, T.; Inoue, S. *J. Am. Chem. Soc.* **1990**, *112*, 5639.

253. Furusho, Y.; Kimura, T.; Mizuno, Y.; Aida, T. *J. Am. Chem. Soc.* **1997**, *119*, 5267.

254. Medforth, C. J.; Muzzi, C. M.; Shea, K. M.; Smith, K. M.; Abraham, R. J.; Jia, S. L.; Shelnutt, J. A. *J. Chem. Soc.-Perkin Trans. 2* **1997**, 839.

255. Hillebrand, S.; Bruckmann, J.; Kruger, C.; Haenel, M. W. *Tetrahedron Lett.* **1995**, *36*, 75.

256. Nowick, J. S.; Ballester, P.; Ebmeyer, F.; Rebek, J. *J. Am. Chem. Soc.* **1990**, *112*, 8902.

257. Ono, N.; Hironaga, H.; Ono, K.; Kaneko, S.; Murashima, T.; Ueda, T.; Tsukamura, C.; Ogawa, T. *J. Chem. Soc.-Perkin Trans. 1* **1996**, 417.

258. Ono, N.; Maruyama, K. *Chem. Lett.* **1989**, 1237.

259. Pichon, C.; Scott, A. I. *Tetrahedron Lett.* **1994**, *35*, 4497.

260. Setsune, J.; Hashimoto, M. *J. Chem. Soc.-Chem. Commun.* **1994**, 657.

261. Lindsey, J. S.; Wagner, R. W. *J. Org. Chem.* **1989**, *54*, 828.

262. Nakanishi, K.; Berova, N.; Woody, R. W. *Circular Dichroism - Principles and Applications*; VCH: New York, NY, 1994.

263. Harada, N.; Nakanishi, K. *Circular Dichroic Spectroscopy - Exciton Coupling in Organic Stereochemistry*; University Science Books: Mill Valley, CA, 1983.

264. Matile, S.; Berova, N.; Nakanishi, K.; Fleischhauer, J.; Woody, R. W. *J. Am. Chem. Soc.* **1996**, *118*, 5198.

265. Mizutani, T.; Ema, T.; Yoshida, T.; Kuroda, Y.; Ogoshi, H. *Inorg. Chem.* **1993**, *32*, 2072.

266. Mizutani, T.; Ema, T.; Yoshida, T.; Renne, T.; Ogoshi, H. *Inorg. Chem.* **1994**, *33*, 3558.

267. Konishi, K.; Takahata, Y.; Aida, T.; Inoue, S.; Kuroda, R. *J. Am. Chem. Soc.* **1993**, *115*, 1169.